

AD-A150 007

JTIC FILE COPY

**RADC-TR-84-186**  
**Final Technical Report**  
**September 1984**

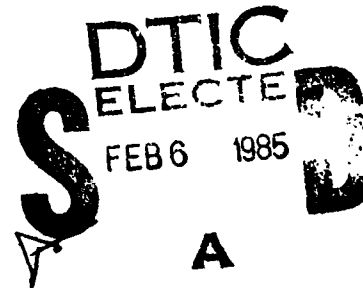


# ***ACROSS SEVENTEEN (ACTIVE CONTROL OF SPACE STRUCTURES)***

**Control Dynamics Company**

**Sponsored by**  
**Defense Advanced Research Projects Agency (DOD)**  
**ARPA Order No. 3654**

**APPROVED FOR PUBLIC RELEASE; DISTRIBUTION UNLIMITED**



**The views and conclusions contained in this document are those of the authors and should not be interpreted as necessarily representing the official policies, either expressed or implied, of the Defense Advanced Research Projects Agency or the U.S. Government.**

**ROME AIR DEVELOPMENT CENTER**  
**Air Force Systems Command**  
**Griffiss Air Force Base, NY 13441**

**85 01 28 103**

This report has been reviewed by the RADC Public Affairs Office (PA) and is releasable to the National Technical Information Service (NTIS). At NTIS it will be releasable to the general public, including foreign nations.

RADC-TR-84-186 has been reviewed and is approved for publication.

APPROVED:



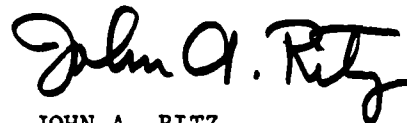
RICHARD W. CARMAN  
Project Engineer

APPROVED:



LAWRENCE J. HILLEBRAND, Colonel, USAF  
Chief, Surveillance Division

FOR THE COMMANDER:



JOHN A. RITZ  
Acting Chief, Plans Office

If your address has changed or if you wish to be removed from the RADC mailing list, or if the addressee is no longer employed by your organization, please notify RADC (OCSP) Griffiss AFB NY 13441-5700. This will assist us in maintaining a current mailing list.

Do not return copies of this report unless contractual obligations or notices on a specific document requires that it be returned.

ACOSS SEVENTEEN (ACTIVE CONTROL OF  
SPACE STRUCTURES)

Sherman M. Seltzer  
H. Eugene Worley  
John R. Glaese  
Marlow L. Butler  
Victoria L. Jones  
Danny K. Tollison

Contractor: Control Dynamics Company  
Contract Number: F30602-82-C-0053  
Effective Date of Contract: 1 February 1982  
Contract Expiration Date: 1 February 1984  
Short Title of Work: ACOSS SEVENTEEN (ACTIVE CONTROL OF  
SPACE STRUCTURES)  
Program Code Number: 2E20  
Period of Work Covered: 1 Feb 82 - 31 Jan 84  
  
Principal Investigator: Dr. Sherman Seltzer  
Phone: 205-837-8510  
  
Project Engineer: Richard W. Carman  
Phone: 315-330-4481

Approved for public release; distribution unlimited

This research was supported by the Defense Advanced Research  
Projects Agency of the Department of Defense and was monitored  
by Richard W. Carman (OCSP), Griffiss AFB NY 13441-5700, under  
Contract F30602-82-C-0053.

UNCLASSIFIED

SECURITY CLASSIFICATION OF THIS PAGE

## REPORT DOCUMENTATION PAGE

1a. REPORT SECURITY CLASSIFICATION UNCLASSIFIED			1b. RESTRICTIVE MARKINGS N/A	
2a. SECURITY CLASSIFICATION AUTHORITY N/A			3. DISTRIBUTION/AVAILABILITY OF REPORT Approved for public release; distribution unlimited	
2b. DECLASSIFICATION/DOWNGRADING SCHEDULE N/A			5. MONITORING ORGANIZATION REPORT NUMBER(S) RADC-TR-84-186	
4. PERFORMING ORGANIZATION REPORT NUMBER(S) 0330284TR-DA09-AC004			7a. NAME OF MONITORING ORGANIZATION Rome Air Development Center (OCSP)	
6a. NAME OF PERFORMING ORGANIZATION Control Dynamics Company		6b. OFFICE SYMBOL (If applicable)	7b. ADDRESS (City, State and ZIP Code) Griffiss AFB NY 13441-5700	
6c. ADDRESS (City, State and ZIP Code) 555 Sparkman Drive, Suite 1414 Huntsville AL 35805		8. PROCUREMENT INSTRUMENT IDENTIFICATION NUMBER F30602-82-C-0053		
6d. NAME OF FUNDING/SPONSORING ORGANIZATION Defense Advanced Research Projects Agency		6e. OFFICE SYMBOL (If applicable) STO	10. SOURCE OF FUNDING NOS.	
6f. ADDRESS (City, State and ZIP Code) 1400 Wilson Blvd Arlington VA 22209		PROGRAM ELEMENT NO. 62301E	PROJECT NO. 3654	TASK NO. 01
			WORK UNIT NO. 17	
11. TITLE (Include Security Classification) ACROSS SEVENTEEN (ACTIVE CONTROL OF SPACE STRUCTURES)				
12. PERSONAL AUTHOR(S) Sherman M. Seltzer, H. Eugene Worley, John R. Glaese, Marlow L. Butler. (Cont'd on reverse)				
13a. TYPE OF REPORT Final		13b. TIME COVERED FROM 01Feb82 TO 31Jan84		14. DATE OF REPORT (Yr., Mo., Day) September 1984
				15. PAGE COUNT 278
16. SUPPLEMENTARY NOTATION N/A				
17. COSATI CODES			18. SUBJECT TERMS (Continue on reverse if necessary and identify by block number)	
FIELD	GROUP	SUB. GR.		
17	8	5	Stability Optimal	
22	2	5	Modeling Digital Control	
			Evaluation Large Space Structures	
19. ABSTRACT (Continue on reverse if necessary and identify by block number) This is the Control Dynamics Company final technical report on extended analysis and evaluation of the Control Techniques of Large Space Structures. The research effort was primarily aimed at mathematical model development and control system analysis and design tool development. <i>Additional keywords: Spacecraft structural mechanics, experimental design, control theory, stability, damping, cost analysis, line of sight, computations, flow charting, computer aided design.</i>				
20. DISTRIBUTION/AVAILABILITY OF ABSTRACT UNCLASSIFIED/UNLIMITED <input checked="" type="checkbox"/> SAME AS RPT. <input type="checkbox"/> DTIC USERS <input type="checkbox"/>			21. ABSTRACT SECURITY CLASSIFICATION UNCLASSIFIED	
22a. NAME OF RESPONSIBLE INDIVIDUAL Richard W. Carman			22b. TELEPHONE NUMBER (Include Area Code) 315-330-4481	22c. OFFICE SYMBOL RADC (OCSP)

DD FORM 1473, 83 APR

EDITION OF 1 JAN 73 IS OBSOLETE.

UNCLASSIFIED  
SECURITY CLASSIFICATION OF THIS PAGE

UNCLASSIFIED

SECURITY CLASSIFICATION OF THIS PAGE

Block 12. Personal Authors (Cont'd)

Victoria L. Jones, Danny K. Tollison

UNCLASSIFIED

SECURITY CLASSIFICATION OF THIS PAGE

## ACKNOWLEDGEMENT

The work reported upon in this report was performed by the Control Dynamics Company in Huntsville, Alabama under Contract No. F30602-82-C-0053. It was supported by the Department of Defense Advanced Research Projects Agency (DARPA) and monitored by Rome Air Development Center. The DARPA Program Manager is LTC Allen F. Herzberg, USAF, and the Rome Air Development Center Project Engineer is Mr. Richard Carman.

The Program Manager and Principal Investigator is Dr. Sherman M. Seltzer, and the Co-Investigator is Dr. H. Eugene Worley. Primary contributors to the accomplishment of the work and the preparation of this report are:

Task 1: Mr. Marlon L. Butler  
Mr. Danny K. Tollison

Task 2: Dr. John R. Glaese

Task 3: Ms. Victoria L. Jones

Task 4: Mr. Marlon L. Butler  
Mr. Danny K. Tollison

Task 5: Dr. John R. Glaese

Task 6: Dr. Robert E. Skelton (Dynamic Systems Research, Inc.)  
Dr. John R. Glaese

Accession For	
GRA&I	<input checked="checked" type="checkbox"/>
TAB	<input type="checkbox"/>
Unannounced	<input type="checkbox"/>
Justification	
Distribution/	
Availability Codes	
Dist	Special

A-1



# TABLE OF CONTENTS

SECTION	PAGE
1. INTRODUCTION . . . . .	1
1.1 BACKGROUND . . . . .	1
1.2 ACROSS SEVENTEEN OBJECTIVE . . . . .	1
2. ACHIEVEMENTS . . . . .	2
2.1 TASK 1 - DIGITAL IMPLEMENTATION OF CONTROL TECHNIQUES . .	2
2.2 TASK 2 - EXTENSIONS OF MODELING TECHNIQUES . . . . .	14
2.3 TASK 3 - EVALUATION OF ACROSS CONTROL METHODOLOGIES . . .	19
2.4 TASK 4 - DETERMINATION OF OPTIMAL FORM FOR ACROSS CONTROLLER . . . . .	62
2.5 TASK 5 - INVESTIGATION OF STRUCTURAL DAMPING MODELS . . .	77
2.6 TASK 6 - IMPLEMENTATION OF COMPONENT COST ANALYSIS . . .	78
3. CONCLUSIONS . . . . .	87
APPENDICES . . . . .	89
A. Paper presented at 1982 AIAA Guidance and Control Confer- ence, San Diego, California, August 1982; "Extensions of the Parameter Space Method to Large Flexible Structures."	90
B. Derivation of Modal Cost Function . . . . .	105
C. Derivation of $OT^2$ Modal Peak Function . . . . .	111
D. A Tutorial Example of Modal Cost Analysis . . . . .	112
E. Case Studies of Model Reduction of Flexible Structures by Modal Cost Analysis	115

## 1. INTRODUCTION

1.1 Background. Several spaceborne surveillance and weapon system concepts for the USAF and DARPA require precision line-of-sight (LOS) and figure control in order to achieve their missions. To date four major system concepts have been identified: High Altitude Large Optics (HALO), Advanced Optical Technology (ADOPT), Large Beam Expander Technology (LBET), and Large Optics Demonstration (LODE). Each of these systems has common features in terms of its large size, extreme complexity, low mass, low stiffness and precision structural tolerances. Each concept also is required to maintain stringent LOS and figure stability despite the fact that isolation, damping, and control technology required to achieve the desired performance is beyond the state-of-the-art practiced today. New control techniques must be developed and demonstrated which have broad application to Large Space Structures (LSS) of the type described above.

1.2 ACOSS SEVENTEEN Objective. The objective of this contract is to extend the work and results developed under Contract No. F30602-81-C-0179 (ACOSS FIFTEEN) and specifically to study active structural control technology as applied to Large Space Structures (LSS). In particular,

1.2.1 To provide analysis and design tools that can be readily applied by practicing dynamicists and control system engineers in their investigations and design of future Large Space Structures; and

1.2.2 To provide an evaluation of new control techniques that have been developed for application to Large Space Structures. This objective is in support of the overall ACOSS objective which is to develop and understand a generic, unified structural dynamics and control technology base for LSS with stringent line-of-sight (LOS) and figure performance requirements that must be maintained in the presence of onboard and natural disturbances.

1.2.3 To develop highly accurate, computationally-efficient dynamics and control models of future ACOSS-type LSS systems.

## 2. ACHIEVEMENTS

### 2.1 Task 1 - Digital Implementation of Control Technologies

2.1.1 Introduction. The recent advances in the area of digital computing have made possible new and innovative approaches to control system analysis and design. As far as the analysis is concerned, computers have reduced the computational burdens associated with this process and thus allowed the designer to use his intuition and skills to concentrate on the control problem.

This section discusses two approaches to the design of digital controllers for the ACOSS structure. The first approach uses classical sampled-data frequency domain techniques to design digital filters that exclude dynamic effects of high frequency bending modes (with respect to control system bandwidth). The second approach is an extension of Seltzer's Digital Parameter Space Method to large scale systems [1]. The method permits the analytical and graphical portrayal of stability conditions as a function of closed-loop damping and natural frequency.

A paper, entitled "Extensions of the Parameter Space Method to Large Flexible Structures" (AIAA Paper No. AIAA-82-1437), was prepared by Drs. Seltzer, Worley, and York. It was approved by RADC for presentation at the 1982 AIAA Guidance and Control Conference in San Diego in August 1982. A copy of the paper is provided as Appendix A.

#### 2.1.2. Computer-Aided Design.

2.1.2.1. Frequency Response Analysis. The frequency response method of control system analysis and design has several advantages over time-domain techniques. The main advantage is that it is possible to take a simplistic approach to design in the frequency domain, whereas time-domain or optimal control techniques often result in designs that are either extremely complicated and expensive to implement or physically unrealizable. By cleverly using a common data base, the frequency-domain method lends itself well to the analysis of very high order systems.

The philosophy used here is to develop one program that could be used to generate the sampled-data frequency responses of each transfer function in the system. With the common data base a second program could then be used to access the response data previously generated and algebraically manipulate it in any manner the designer chooses.

- 
1. S. M. Seltzer, H. E. Worley, and R. J. York, "Extension of the Parameter Space Method to Large Flexible Structures," AIAA/AAS Astrodynamics Conference, San Diego, California, August 1982.

(a). Frequency Response Generation. The frequency response generation (FRGEN) code is used at the start of the analysis to create a workspace (data base) where all response data will be stored. The user specifies the total number of responses to be stored in the workspace, the total number of points per response, the frequency range, and the sampling rate for the digital control system. FRGEN provides the user with a menu of options for data generation, cataloging, printing, and plotting.

The computation of sampled-data frequency responses is accomplished using the infinite series technique, i.e.,

$$G^*(s) = \frac{1}{T} \sum_{n=-\infty}^{\infty} G(j\omega + jn\omega_s) + \frac{g(0+)}{2} \quad (1-1)$$

where  $\omega$  is frequency,  $G(j\omega)$  is the frequency response of a continuous transfer function,  $G^*(j\omega)$  is the sampled-data frequency response,  $T$  is the sampling period,  $\omega_s$  is the sample rate in rad/sec, and  $g(0+)$  is the value of the impulse response of  $G(s)$  evaluated at  $t = 0+$  [2]. The series will converge if the transfer function  $G(s)$  has at least one more pole than zero. Practical use of Equation (1-1) is obtained by truncating the series after a specified number of terms. The program was written so that the user need only specify a tolerance for this computation, and the number of terms necessary for convergence is automatically selected. Furthermore, the code naturally assumes that the continuous system is preceded by a zero order hold whose transfer function is given by

$$G_{ho}(s) = \frac{1 - e^{-Ts}}{s} \quad (1-2)$$

The program also has the capability of generating the discrete frequency response of a z-domain transfer function by making the substitution

$$z = e^{j\omega T} \quad (1-3)$$

in the z-transfer function.

(b). Frequency Response Manipulation. The algebraic manipulation method of analyzing sampled-data systems has been avoided to a large extent

---

2. B. C. Kuo, Digital Control Systems, Holt, Rhinehart, and Winston, New York, New York, 1980.

due to the fact that it is tedious, and somewhat unrealistic for complex systems, and hence, signal-flow-graph techniques were indeed preferable. However the signal-flow-graph technique while being more systematic, can be extremely involved and is not easily implemented on a digital computer.

The frequency response manipulation (FRMAN) program was written to provide the user with the routines necessary to make the algebraic analysis as simple as calculator arithmetic. Thus, by using Seltzer's Systematic Analytical Method (SAM) [3], or some equivalent technique to determine the loop transfer functions, FRMAN can then be used to perform the mathematical operations needed to generate a desired response. Again, the common data base makes it possible for FRMAN and FRGEN to share the same workspace.

The menu provided with the FRMAN program includes options for cataloging, printing, and plotting of response data and is identical to the FRGEN menu. The algebraic routines provided with the code include the addition of a constant and a response, the sum of two responses, the product of a constant and a response, the product of two responses, the division of one response by another, and finally the negation of a response. It should be readily obvious that very complex control systems can be analyzed using the generation and manipulation programs.

#### 2.1.2.2 Digital Filter Design Methods.

(a) Direct z-domain Compensator Design. A technique for designing digital controllers directly in the z-plane has been developed by Mitchell and Tollison [4] and implemented on Control Dynamic's computing systems. In the past, digital controller design was accomplished by first producing a w-plane design using classical techniques such as Wakeland [5], and then by transforming to the z-plane using the bilinear transformation

$$w = \frac{z - 1}{z + 1}, \quad (1-4)$$

- 
3. S. M. Seltzer, "SAM: An Alternative to Sampled-Data Signal Flow Graphs," Technical Report T-79-49, US Army Missile Research and Development Command, May 1979.
  4. J. R. Mitchell, and D. K. Tollison, "A New Approach to the Analytical Design of Compensators," Proceedings of the 1982 Southeastern Symposium on System Theory, Virginia Polytechnic Institute and State University, Blacksburg, Va., April 1982.
  5. W. R. Wakeland, "Bode Compensator Design," IEEE Transactions on Automatic Control, Vol. AC-22, No. 5, October 1977.

the corresponding z-domain compensator was derived. However, because of nonlinear frequency scaling and the z-plane transformation this method becomes extremely cumbersome for higher order controllers. Mitchell and Tollison developed an analytical technique that bypasses the inherent difficulties of nonlinear frequency scaling associated with the w-plane method and permits the z-domain compensator to be determined directly in terms of a gain and phase at a desired frequency. The technique can be used to design various types of digital filters including lead, lag, lead-lag, and dominant pole networks. The discussion that follows will show how the design equations are developed for a simple first order compensator.

The transfer function for a first order digital controller can be written in the form

$$G_C(z) = \frac{a_0 + a_1 z}{1 + b_1 z} \quad (1-5)$$

where the coefficients  $a_0$ ,  $a_1$ , and  $b_1$  will be determined such that the compensator is stable, minimum phase, has unity gain in steady-state, and satisfies a set of design specifications.

Suppose the compensator is to be designed to produce a gain  $M_1$  and a phase  $\theta_1$  at some frequency  $\omega_1$ , i.e.,

$$G_C(e^{j\omega_1 T}) = M_1 / \theta_1 \quad (1-6)$$

or in rectangular form

$$G_C(e^{j\omega_1 T}) = x_1 + jy_1 \quad (1-7)$$

where  $T$  is the sampling period of the digital controller. The substitution

$$z = e^{j\omega_1 T} \quad (1-8)$$

is made in Equation (1-5) and equated to (1-7) to produce

$$\frac{a_0 + a_1 e^{j\omega_1 T}}{1 + b_1 e^{j\omega_1 T}} = x_1 + jy_1. \quad (1-9)$$

Using Euler's identity Equation (1-9) can be written as

$$\frac{a_0 + a_1 (\cos \omega_1 T + j \sin \omega_1 T)}{1 + b_1 (\cos \omega_1 T + j \sin \omega_1 T)} = x_1 + jy_1, \quad (1-10)$$

Cross multiplying in Equation (1-10) yields

$$\begin{aligned} x_1 + (x_1 \cos \omega_1 T) b_1 - (y_1 \sin \omega_1 T) b_1 \\ + j[y_1 + (y_1 \cos \omega_1 T) b_1 + (x_1 \sin \omega_1 T) b_1] \\ = a_0 + (\cos \omega_1 T) a_1 + j (\sin \omega_1 T) a_1 \end{aligned} \quad (1-11)$$

Equating real and imaginary parts on both sides gives

$$a_0 + (\cos \omega_1 T) a_1 - (x_1 \cos \omega_1 T - y_1 \sin \omega_1 T) b_1 = x_1 \quad (1-12)$$

$$(\sin \omega_1 T) a_1 - (y_1 \cos \omega_1 T + x_1 \sin \omega_1 T) b_1 = y_1 \quad (1-13)$$

At this point the observation can be made that Equations (1-12) and (1-13) represent a system of algebraic linear equations in terms of the compensator coefficients. However, there are only two equations and three unknowns. The third equation that can be imposed on this system is the unity d.c. gain requirement. In the z-domain "d.c.," or steady-state, corresponds to  $z = 1$ . Using this assertion in Equation (1-5) gives

$$G_C(1) = \frac{a_0 + a_1}{1 + b_1} = 1 \quad (1-14)$$

which produces the equation,

$$a_0 + a_1 - b_1 = 1. \quad (1-15)$$

In matrix form the design equations for the first order digital controller can be written as

$$\begin{bmatrix} 1 & \cos \omega_1 T & (y_1 \sin \omega_1 T - x_1 \cos \omega_1 T) \\ 0 & \sin \omega_1 T & -(y_1 \cos \omega_1 T - x_1 \sin \omega_1 T) \\ 1 & 1 & -1 \end{bmatrix} \begin{bmatrix} a_0 \\ a_1 \\ b_1 \end{bmatrix} = \begin{bmatrix} x_1 \\ y_1 \\ 1 \end{bmatrix} \quad (1-16)$$

These equations can now be solved for the compensator coefficients. However, some consideration must be given to the stability of the compensator in terms of the design specifications. Mitchell and Tollison have shown that

the following requirements must be satisfied in order for the resulting compensator to be both stable and minimum phase:

#### Stability Requirements.

$$\text{Lead } (\theta_1 > 0) \text{ and } x_1 > 1 \quad (1-17a)$$

$$\text{Lag } (\theta_1 < 0) \text{ and } x_1 < 1 \quad (1-17b)$$

#### Minimum Phase Requirements.

$$\text{Lead } (\theta_1 > 0) \text{ and } M_1 > x_1 \quad (1-18a)$$

$$\text{Lag } (\theta_1 < 0) \text{ and } M_1 < x_1 \quad (1-18b)$$

This technique has been implemented on Control Dynamics' HP-9000 system. The user inputs the magnitude and phase contribution of the compensator and the frequency at which he wants to achieve these specifications. The program then computes the required compensator coefficients, assuming the specifications are realistically achievable. The routine has been used along with FRGEN and FRMAN to perform frequency domain design directly in the z-plane for a wide variety of control problems.

#### (b) Digital Controller Design Using the Parameter Space Technique.

(1). Background. The Parameter Space technique has been extended to the application of digital controller design for large scale systems. The method being presented here permits the application of the technique to control problems associated with digital control of large flexible structures characterized by a rigid body mode and an arbitrary number of bending modes. Based upon stability considerations and the desired damping and bandwidth, values for the compensator coefficients can be determined using this technique. The major contribution of the work presented is the ability to design digital controllers using the Parameter Space technique in the presence of an arbitrary number of bending modes. Furthermore, the method discussed here has been automated on Control Dynamics' digital computers.

The Parameter Space method assumes that the characteristic equation of the closed loop system can be expressed as a linear function of the parameters defining the parameter space, i.e.,

$$\Delta(z) = P_1(z) a + P_2(z) b + P_3(z) \quad (1-19)$$

where  $a$  and  $b$  are the two arbitrary parameters. The polynomials  $P_1(z)$ ,  $P_2(z)$ , and  $P_3(z)$  are of the form,

$$P_i(z) = \sum_{k=0}^n C_{ki} z^k, \quad i = 1, 2, 3. \quad (1-20)$$

where  $n$  is the order of the system. The characteristic equation in (1-19) requires that the overall system be expressed in the  $z$ -domain. This aspect of the problem becomes significantly difficult for  $n > 2$ . Therefore, some method must be devised for automating the  $z$ -transform process. The work that follows will be devoted to determining the polynomials  $P_1(z)$ ,  $P_2(z)$ , and  $P_3(z)$  given by Equation (1-20).

(2) Plant Representation. It is assumed that the plant is expressed in modal coordinates, i.e.,

$$[m]\ddot{\underline{X}} + [k]\underline{X} = \underline{F} \quad (1-21)$$

where

$[m]$  is the system mass matrix,  
 $[k]$  is the system stiffness matrix,  
 $\underline{F}$  is a vector force or torque,  
 $\underline{X}$  is a vector of system states

Using the transformation

$$\underline{X} = Q \underline{n} \quad (1-22)$$

where  $Q$  is the modal matrix composed of the normalized eigenvectors, and  $\underline{n}$  is a set of generalized coordinates, the desired representation

$$\ddot{\underline{n}} + [c]\underline{\dot{n}} + [\omega^2]\underline{n} = \underline{I}c \quad (1-23)$$

is produced. The matrices  $[c]$  and  $[\omega^2]$  are the diagonal damping and frequency matrices, respectively.

Using the Laplace transform technique the transfer function for the plant is given by

$$G_p(s) = \sum_{i=1}^N \frac{\phi_i \gamma_i}{s^2 + 2\zeta\omega_{ni}s + \omega_{ni}^2} \quad (1-24)$$

where

$\zeta$  is the damping ratio for each mode,  
 $\omega_{ni}$  is the undamped natural frequency  
of the  $i$ th bending mode,  
 $\phi_i$  and  $\gamma_i$  denote the slope of the  $i$ th  
mode at the sensor, torquer, respectively.

The block diagram representation of Equation (1-24) is shown below in Figure 1-1.

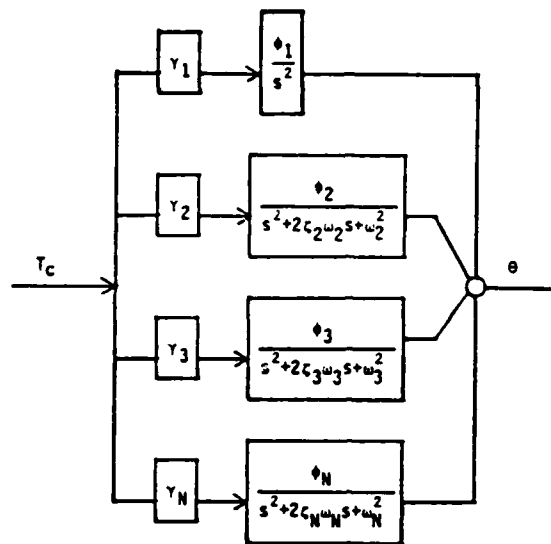


Figure 1-1. Block diagram of the plant for the modal representation.

(3) Control Algorithm Development. Now suppose it is desired to design a digital controller to stabilize a system of the form shown in Figure 1-1. (The block diagram in Figure 1-2 showing a digital controller in the forward path will be used for the sake of illustrating the design technique).

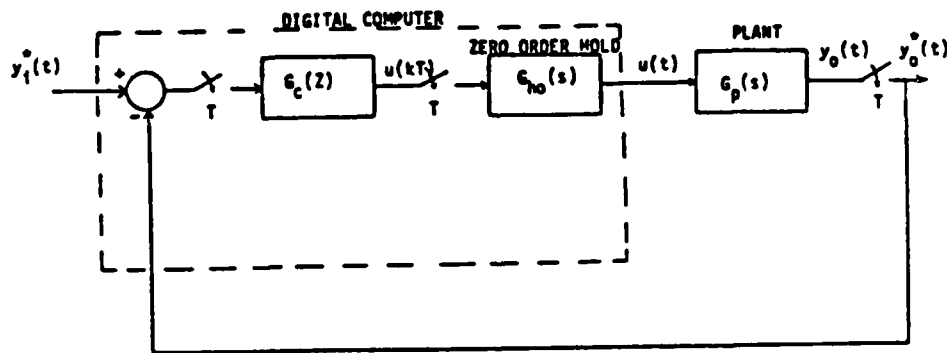


Figure 1-2. Block diagram of the digital control system.

Since the characteristic equation must be expressed in the z-domain, it is necessary to obtain the z-transform of the plant,  $G_p(s)$ , where  $G_p(s)$  is

given by Equation (1-24). The process of computing the z-transform directly for systems of order higher than two is extremely difficult, if not impossible. An alternate approach for obtaining the z-transform is to first cast the continuous system in state variable form, i.e.

$$\begin{aligned}\dot{\underline{x}}(t) &= A \underline{x}(t) + B u(t) \\ y_0(t) &= C \underline{x}(t)\end{aligned}\tag{1-25}$$

where

A is the  $2N \times 2N$  system matrix,

B is the  $2N \times 1$  input matrix,

C is the  $1 \times 2N$  output matrix,

$\underline{x}$  is the  $2N \times 1$  state vector,

$y_0$  is the system output,

and

N is the number of modes, including the rigid body mode.

It is now possible to transform the continuous state equations in Equation (1-25) to an equivalent set of discrete state equations. Kuo has shown that the following procedure can be used to compute the discrete state equations:

#### Discrete state equations

$$\begin{aligned}\underline{x}[(k+1)T] &= \phi(T) \underline{x}(kT) + \theta(T) u(kT) \\ y_0(kT) &= C \underline{x}(kT), \quad k=0, 1, 2, \dots \\ \phi(T) &= e^{AT}\end{aligned}\tag{1-26}$$

$$\theta(T) = \int_0^T \phi(\tau) B d\tau\tag{1-27}$$

Where A and B are defined in Equation (1-25). The following steps can now be used to compute the z-transform of the plant:

- (1) Convert discrete state equations to the z-domain

$$z\underline{X}(z) = \phi(T) \underline{X}(z) + \theta(T) U(z)\tag{1-28}$$

- (2) Solve for  $\underline{X}(z)$

$$\underline{X}(z) = [zI - \phi(T)]^{-1} \theta(T) U(z)\tag{1-29}$$

- (3) Use the output equation to compute the z-transfer function of the plant,

$$\begin{aligned} Y(z) &= CX(z) \\ &= C [zI - \Phi(T)]^{-1} \Theta(T) U(z) \end{aligned}$$

Then 
$$\frac{Y(z)}{U(z)} = C[zI - \Phi(T)]^{-1} \Theta(T) \quad (1-30)$$

Equation (1-30) represents the z-transfer function for the open loop plant in Equation (1-24). Now assume that

$$\frac{Y(z)}{U(z)} = \frac{N_p(z)}{D_p(z)} \quad (1-31)$$

and also assume the digital controller is of the form

$$G_C(z) = \frac{N_C(z)}{D_C(z)} = \frac{(1 + a)z + (1 - a)}{(1 + b)z + (1 - b)} \quad (1-32)$$

Note that the form of the compensator in (1-32) results in only two arbitrary coefficients, which is ideal for the Parameter Plane, and also produces unity gain in steady-state ( $z=1$ ).

Using Equations (1-31) and (1-32), and the block diagram in Figure 1-2, the closed loop characteristic equation can be written as

$$\Delta(z) = 1 + \frac{N_C(z)}{D_C(z)} \cdot \frac{N_p(z)}{D_p(z)} = 0$$

or

$$\Delta(z) = N_C(z) N_p(z) + D_C(z) D_p(z) = 0.$$

Substituting the numerator and denominator of the digital compensator for  $N_C(z)$  and  $D_C(z)$  yields

$$\begin{aligned} \Delta(z) &= [(1 + a)z + (1 - a)] N_p(z) \\ &\quad + [(1 + b)z + (1 - b)] D_p(z) = 0 \end{aligned} \quad (1-33)$$

Equation (1-33) can now be written in the form required for the Parameter Plane calculations,

$$[(z - 1) N_p(z)]a + [(z - 1) D_p(z)] b + (z + 1) [N_p(z) + D_p(z)] = 0 \quad (1-34)$$

Comparison of Equations (1-34) and (1-19) shows that the polynomials necessary to generate a parameter space in terms of the compensator coefficients  $a$  and  $b$  are:

$$P_1(z) = (z - 1) N_p(z)$$

$$P_2(z) = (z - 1) D_p(z) \quad (1-35a,b,c)$$

$$P_3(z) = (z + 1) [N_p(z) + D_p(z)]$$

and

where  $N_p(z)$  and  $D_p(z)$  are the numerator and denominator polynomials, respectively, of the  $z$ -transfer function of the open-loop plant defined by the substitutions implied by Equations (1-30) and (1-31).

Equations (1-35a,b,c) contain the polynomial coefficients necessary to use Seltzer's Digital Parameter Space Program. This technique has been applied successfully on large space structure controller design. The following is a summary of the steps involved in using this design technique:

- Step 1: Assuming plant is characterized by modal coordinates, cast in state variable form,
- Step 2: Compute the discrete state equations by discretizing the continuous equations in Step 1,
- Step 3: Generate the  $z$ -transfer function of the open loop plant using Equation (1-30),
- Step 4: Generate the  $z$ -domain characteristic equation of the closed loop system including the digital controller coefficients (unspecified),
- Step 5: Identify the polynomials needed to run the Parameter Plane Program.

Each of these steps has been automated on Control Dynamics' computer system. The only approximation used in the design process is the computation of the discrete state equations. However, if the system is basically low-pass, convergence of the series is not a problem, assuming the proper choice of the sampling rate has been made.

### 2.1.3. Conclusions.

Software routines have been written that allow systems of the DARPA type to be analyzed quickly and efficiently. Frequency domain design programs have been developed that allow digital compensators to be designed rather simply. A design technique has also been developed that extends the application of Seltzer's Digital Parameter Space technique to the design of digital controllers for large flexible structures characterized by an arbitrary number of bending modes.

## 2.2 Task 2 - Extensions of Modeling Techniques.

2.2.1 Ground Test Facility. Control Dynamics modeled the NASA MSFC Large Space Structure Ground Test Verification Facility (LSS/GTV) which is shown in Figure 2-1. The test article is the ASTROMAST beam which is placed atop the Advanced Gimbal System Engineering (EAGS) model. The EAGS, along with a torque actuator about the vertical axis, provides three torques which may be used both for control and excitation. The base of the test apparatus provides two translational degrees of freedom in the horizontal, producing a five degree of freedom (DOF) system.

The ASTROMAST is gravity unloaded by a constant tension cable from the mast Tip Instrument Package (TIP) to a tripod mounted on air bearings. Measurements of translation and rotation of the TIP are provided by gyros and accelerometers in the instrument package. An additional set of gyros is mounted on the EAGS faceplate. An accelerometer package is mounted on the movable base.

Signals from the instrument packages and to the effectors are handled by the COSMEC I data and control system at a rate of 50 samples per second. This AIM 65 based system carries out an inertial strapdown algorithm to remove the effects of gravity and earth rotation from the measurements, exercises a system control law and utilizes the HP 9845C desktop computer as a data storage, output and post analysis device.

The model of the LSS/GTV is based on rigid body models of the base, EAGS and TIP. The ASTROMAST consists of three small (.1" x .14") rectangular fiberglass longerons running the length of the ASTROMAST that are laced together in an equilateral triangle configuration by .045" diameter fiberglass diagonals which are maintained in tension by transverse battens. The diagonals provide the lateral stiffness of the ASTROMAST which is designed to be deployable from a cannister into which it can also be retracted manually. The ASTROMAST consists of 92 identical levels with battens at each level and diagonal lacework between. The diagonals are cords of fiberglass which are held in tension by the battens. A model of the ASTROMAST beam was also developed and coupled analytically to the rest of the LSS/GTV model. The energy dissipation within the beam structure has previously been shown to be on the order of 1% or less of critical damping and distributed around the structure. Thus, detailed analysis of the damping of this structure has not proved to be necessary, so that proportional, modal damping has been used for this model.

The modes and frequencies of the composite model are presented in Table 2-1. To be conservative, we have assumed the structural modal damping is 0.5%. All modes of our structural model are assumed to be damped at 0.5% of critical. The inertial displacements are listed for base translation in X and Y; and gimbal rotations in X, Y, and Z. Motion in six degrees of freedom is also given for both ends of the beam.

The first five modes are rigid body modes. It can be seen in Table 2-1 that modes one and two are pure base translations in X and Y. The next three modes are combinations of base translation in X and Y, and gimbal rotations in X, Y, and Z. The first bending mode of the structure is at 5.91 rad/sec.

2.2.2 Conclusions. The modeling techniques developed for the LSS/GTV were given important corroboration by modal testing done on the ASTROMAST beam at MSFC. These results indicated accuracies in the lower modes of 11% or better. Thus, a dynamic model was developed of the LSS/GTV and it has been verified, to the extent it can be currently, with the data available. The modeling techniques, therefore, adequately represent the structures. Because the work on Tasks 2 and 5 was so closely related, the results and conclusions reported in this section serve to describe the accomplishment of the objective of both tasks.

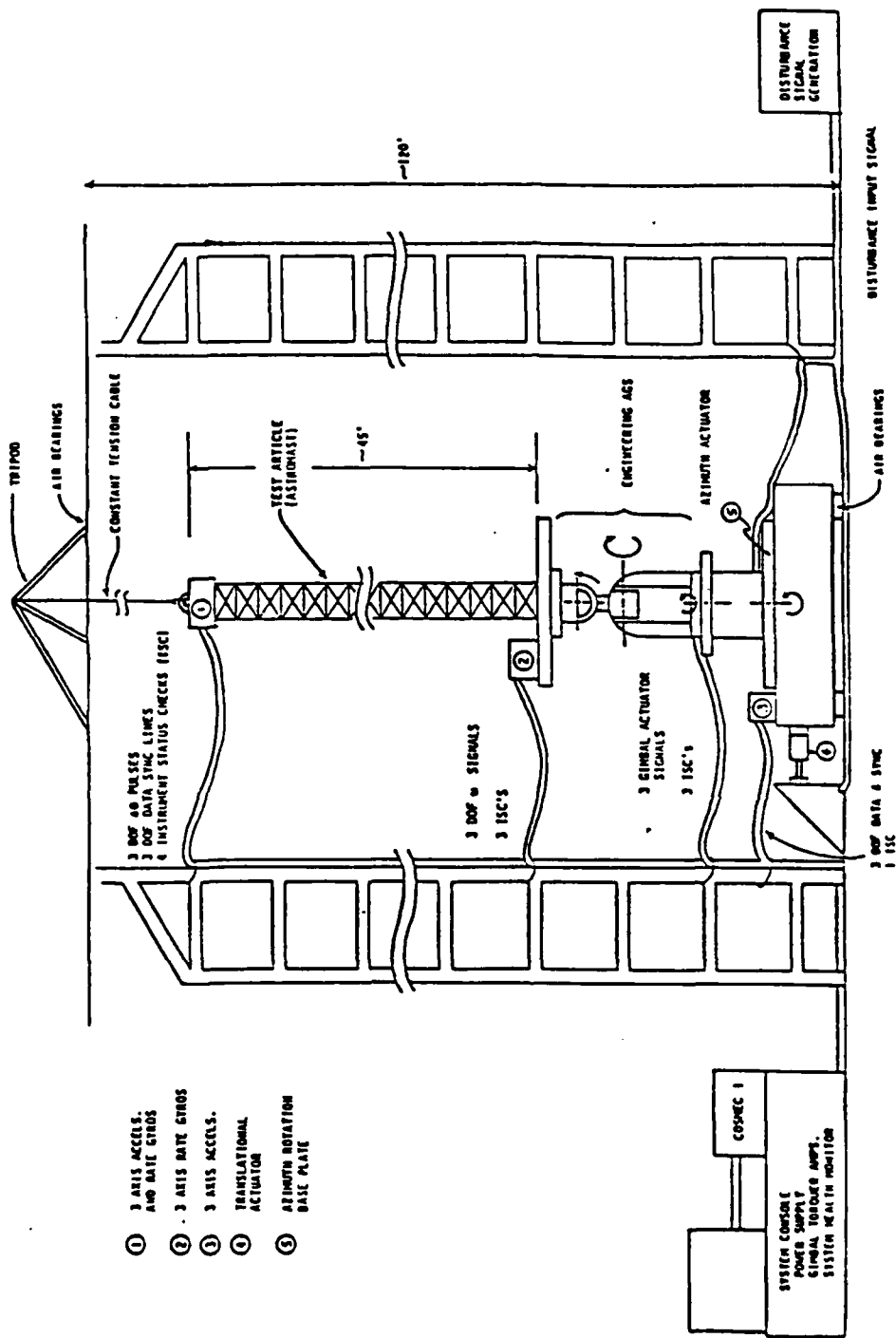


Figure 2-1. NASA MSFC Large Space Structure Ground Test Verification Experiment.

TABLE 2-1.  
Mode and Frequencies of Composite Model.

MODAL FREQUENCY	0.0000000	RAD/SEC	X	Y	Z
BASE TRANSLATION		0.7208357		0.0000000	0.0000000
ROLL GIMBAL ROTATION		0.0000000			
AZIMUTH GIMBAL ROTATION		0.0000000			
ELEVATION GIMBAL ROTATION		0.0000000			
BEAM BASE TRANSLATION		0.7208357		0.0000000	0.0000000
BEAM BASE ROTATION		0.0000000		0.0000000	0.0000000
TIP INSTRUMENT PACKAGE TRANSLATION		0.7208357		0.0000000	0.0000000
TIP INSTRUMENT PACKAGE ROTATION		0.0000000		0.0000000	0.0000000
MODAL FREQUENCY	0.0000000	RAD/SEC			
BASE TRANSLATION		0.0000000		0.7208357	0.0000000
ROLL GIMBAL ROTATION		0.0000000			
AZIMUTH GIMBAL ROTATION		0.0000000			
ELEVATION GIMBAL ROTATION		0.0000000			
BEAM BASE TRANSLATION		0.0000000		0.7208357	0.0000000
BEAM BASE ROTATION		0.0000000		0.0000000	0.0000000
TIP INSTRUMENT PACKAGE TRANSLATION		0.0000000		0.7208357	0.0000000
TIP INSTRUMENT PACKAGE ROTATION		0.0000000		0.0000000	0.0000000
MODAL FREQUENCY	0.0000000	RAD/SEC			
BASE TRANSLATION		0.0101980		-0.0012932	0.0000000
ROLL GIMBAL ROTATION		0.1187835			
AZIMUTH GIMBAL ROTATION		0.0000000			
ELEVATION GIMBAL ROTATION		0.0000000			
BEAM BASE TRANSLATION		0.0101980		-0.0012932	0.0000000
BEAM BASE ROTATION		0.0000000		0.0000000	0.1187835
TIP INSTRUMENT PACKAGE TRANSLATION		-0.2215391		0.0280927	0.0000000
TIP INSTRUMENT PACKAGE ROTATION		0.0000000		0.0000000	0.1187835
MODAL FREQUENCY	0.0000000	RAD/SEC			
BASE TRANSLATION		-0.2126753		-0.0000823	0.0000000
ROLL GIMBAL ROTATION		0.0075818			
AZIMUTH GIMBAL ROTATION		0.0063638			
ELEVATION GIMBAL ROTATION		0.0000000			
BEAM BASE TRANSLATION		-0.0791444		-0.0000823	0.0000000
BEAM BASE ROTATION		0.0000000		0.0063638	0.0075818
TIP INSTRUMENT PACKAGE TRANSLATION		3.2468774		0.0017931	-0.0015743
TIP INSTRUMENT PACKAGE ROTATION		0.0000000		0.0063638	0.0075818
MODAL FREQUENCY	0.0000000	RAD/SEC			
BASE TRANSLATION		-0.0000439		0.2133059	0.0000000
ROLL GIMBAL ROTATION		0.0009661			
AZIMUTH GIMBAL ROTATION		0.0000033			
ELEVATION GIMBAL ROTATION		0.0064128			
BEAM BASE TRANSLATION		0.0000413		0.1025569	0.0000000
BEAM BASE ROTATION		0.0064128		0.0000033	0.0009661
TIP INSTRUMENT PACKAGE TRANSLATION		-0.0001019		-3.2637730	0.0125100
TIP INSTRUMENT PACKAGE ROTATION		0.0064128		0.0000033	0.0009661
MODAL FREQUENCY	5.913205	RAD/SEC			
BASE TRANSLATION		0.6340323		0.0000961	0.0000000
ROLL GIMBAL ROTATION		0.0017399			
AZIMUTH GIMBAL ROTATION		-0.0497098			
ELEVATION GIMBAL ROTATION		0.0000120			

TABLE 2-1. (CONT.)

	X	Y	Z
BEAM BASE TRANSLATION	-0.4432107	-0.0001104	0.0000000
BEAM BASE ROTATION	0.0000120	-0.0497098	0.0017399
TIP INSTRUMENT PACKAGE TRANSLATION	0.5983857	-0.0000565	-0.0005947
TIP INSTRUMENT PACKAGE ROTATION	-0.0000228	0.0345617	-0.0163021
MODAL FREQUENCY 7.293426 RAD/SEC			
BASE TRANSLATION	-0.0003125	0.4891170	0.0000000
ROLL GIMBAL ROTATION	-0.0001548		
AZIMUTH GIMBAL ROTATION	0.0000250		
ELEVATION GIMBAL ROTATION	0.0602246		
BEAM BASE TRANSLATION	0.0003297	-0.3509624	0.0000000
BEAM BASE ROTATION	0.0602246	0.0000250	-0.0001548
TIP INSTRUMENT PACKAGE TRANSLATION	-0.0003338	0.5674684	-0.0884927
TIP INSTRUMENT PACKAGE ROTATION	-0.0453606	-0.0000090	0.0000523
MODAL FREQUENCY 11.29450 RAD/SEC			
BASE TRANSLATION	-0.0302741	-0.0009661	0.0000000
ROLL GIMBAL ROTATION	0.0184101		
AZIMUTH GIMBAL ROTATION	0.0024533		
ELEVATION GIMBAL ROTATION	-0.0000814		
BEAM BASE TRANSLATION	0.0327604	0.0004400	0.0000000
BEAM BASE ROTATION	-0.0000814	0.0024533	0.0184101
TIP INSTRUMENT PACKAGE TRANSLATION	0.0370206	-0.0081332	0.0009380
TIP INSTRUMENT PACKAGE ROTATION	-0.0000700	-0.0043433	-0.7151111
MODAL FREQUENCY 20.44361 RAD/SEC			
BASE TRANSLATION	-0.4059115	-0.0021554	0.0000000
ROLL GIMBAL ROTATION	-0.0001958		
AZIMUTH GIMBAL ROTATION	0.0339763		
ELEVATION GIMBAL ROTATION	-0.0002847		
BEAM BASE TRANSLATION	0.4670748	0.0027617	0.0000000
BEAM BASE ROTATION	-0.0002847	0.0339763	-0.0001958
TIP INSTRUMENT PACKAGE TRANSLATION	0.3724887	0.0012984	-0.0236142
TIP INSTRUMENT PACKAGE ROTATION	-0.0003839	0.0924256	0.0305842
MODAL FREQUENCY 23.29484 RAD/SEC			
BASE TRANSLATION	0.0019001	-0.4684157	0.0000000
ROLL GIMBAL ROTATION	0.0001902		
AZIMUTH GIMBAL ROTATION	-0.0001598		
ELEVATION GIMBAL ROTATION	-0.0616555		
BEAM BASE TRANSLATION	-0.0022049	0.5943746	0.0000000
BEAM BASE ROTATION	-0.0616555	-0.0001598	0.0001902
TIP INSTRUMENT PACKAGE TRANSLATION	-0.0018192	0.3291788	-0.1791701
TIP INSTRUMENT PACKAGE ROTATION	-0.0919095	-0.0005578	-0.0098476
MODAL FREQUENCY 57.86488 RAD/SEC			
BASE TRANSLATION	-0.1169710	-0.0530800	0.0000000
ROLL GIMBAL ROTATION	0.0000152		
AZIMUTH GIMBAL ROTATION	0.0105723		
ELEVATION GIMBAL ROTATION	-0.0074173		
BEAM BASE TRANSLATION	0.1546738	0.0730166	0.0000000
BEAM BASE ROTATION	-0.0074173	0.0105723	0.0000152
TIP INSTRUMENT PACKAGE TRANSLATION	-0.1921388	-0.0510709	0.1028474
TIP INSTRUMENT PACKAGE ROTATION	0.0371458	-0.1227977	-0.0027129
MODAL FREQUENCY 58.02358 RAD/SEC			
BASE TRANSLATION	0.0377894	-0.1626017	0.0000000
ROLL GIMBAL ROTATION	0.0000524		
AZIMUTH GIMBAL ROTATION	-0.0034170		
ELEVATION GIMBAL ROTATION	-0.0227311		
BEAM BASE TRANSLATION	-0.0500081	0.2294638	0.0000000
BEAM BASE ROTATION	-0.0227311	-0.0034170	0.0000524
TIP INSTRUMENT PACKAGE TRANSLATION	0.0637058	-0.1613539	0.2150347
TIP INSTRUMENT PACKAGE ROTATION	0.1153053	0.0400853	-0.0013618

## 2.3 Task 3 - Evaluation of ACOSS Control Methodologies.

2.3.1 Introduction. Recent technological advances in active damping control techniques applied to Large Space Structures (LSS) include Lockheed's Low Authority Control/High Authority Control (LAC/HAC), TRW's Positivity, and General Dynamic's Model Error Sensitivity Suppression (MESS). Each of these techniques, developed under the DARPA ACOSS program, incorporates a different approach to the control problem.

Each of these techniques is described in a similar format in an attempt to enhance understanding and to aid in comparison. A flowchart form of each technique's control law design procedure has been developed by Control Dynamics and is presented. This form will provide an orderly, methodical approach to understanding the development of an active control scheme. This approach is useful when first learning to apply these seemingly complicated, multi-faceted design tools. It provides a means of comparison of the various techniques in that the complexity of implementation, ease of understanding, and practicality can be readily observed. Each of these qualities is of considerable importance, especially when contemplating their application to control of complex, high order space structures.

The numerous problems inherent in LSS control system design include the following:

Inaccurate structural models.

- (a) modal truncation - approximation of an infinite dimensional system by a finite dimensional model
- (b) inaccurate knowledge of modal frequencies and mode shapes, especially high frequency modes
- (c) poor knowledge of structural damping

Effects of including non-collocated actuators and sensors.

Spillover - effects of unknown high frequency modes on the system control and observation.

Effects of including accurate sensor and actuator dynamic models.

Each technique incorporates a variety of distinctive concepts to solve these numerous problems associated with LSS control.

### 2.3.2 TRW's positivity design.[6]

2.3.2.1 Objective. Assure stability of control system designs based on inaccurate structural models. Design a robust control system with respect to the following model errors - modal truncation and poor knowledge of modal frequencies, mode shapes, and structural damping.

#### 2.3.2.2 Properties of technique.

- (a) No assumptions are made concerning dimensionality or linearity of systems involved
- (b) Low sensitivity to model errors
- (c) Conservative design.

2.3.2.3 Overall approach. Design is augmented by pre-flight and on-orbit data. All preflight information is incorporated in the initial positivity design. The key parameters are identified using on-orbit performance. Improved knowledge of model parameters is used to "fine tune" the system for optimum performance.

#### 2.3.2.4 Positivity results.

- (a) A negative feedback connection of a positive system with a strictly positive system is stable.
- (b) A LSS with colocated, ideal actuators and rate sensors is a positive system.
- (c) Embedding operations permit the treatment of non-positive systems.

2.3.2.5 Basic theory. Positivity is a design method which has low sensitivities to model errors.

#### 2.3.2.6 Definitions.

- (a) Positive real: the real part of a transfer function as a function of frequency is always greater than or equal to zero.
- (b) Strictly positive real: the real part of a transfer function as a function of frequency is always greater than zero.

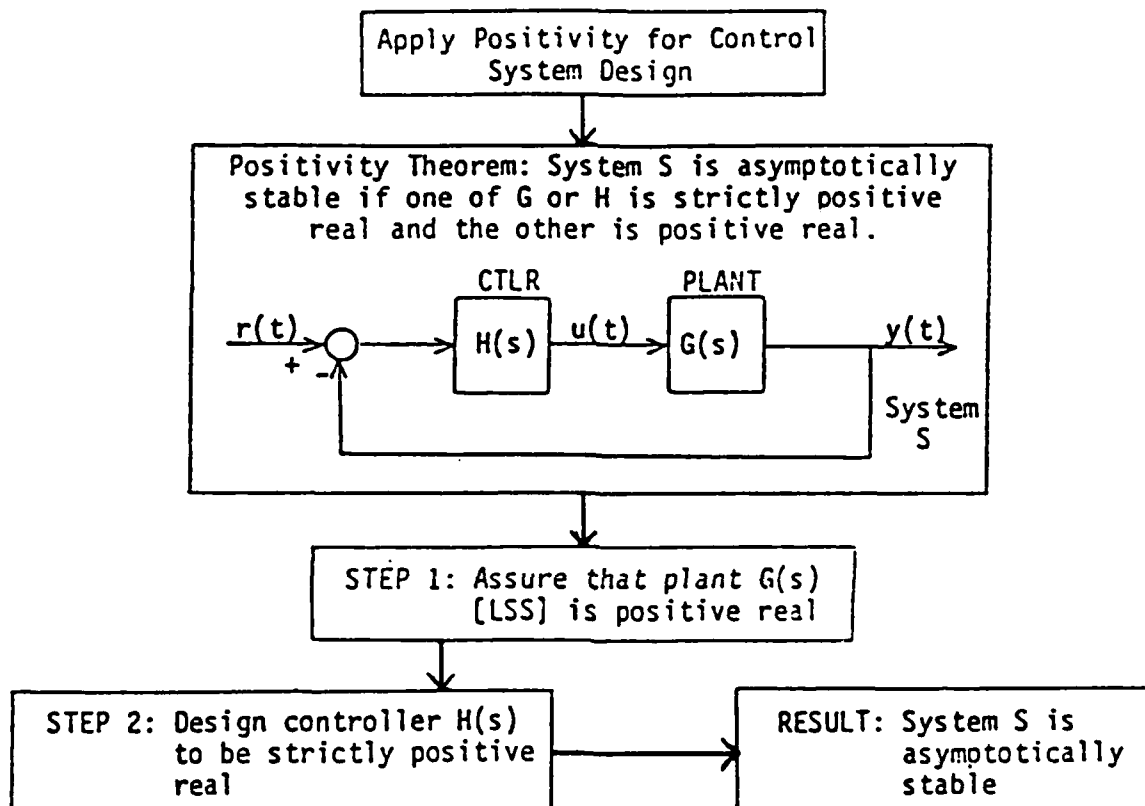
---

6. "ACOSS Eight (Active Control of Space Structures) Phase II," TRW, Sponsored by Defense Advanced Research Projects Agency, Report No. RADC-TR-81-242, September 1981.

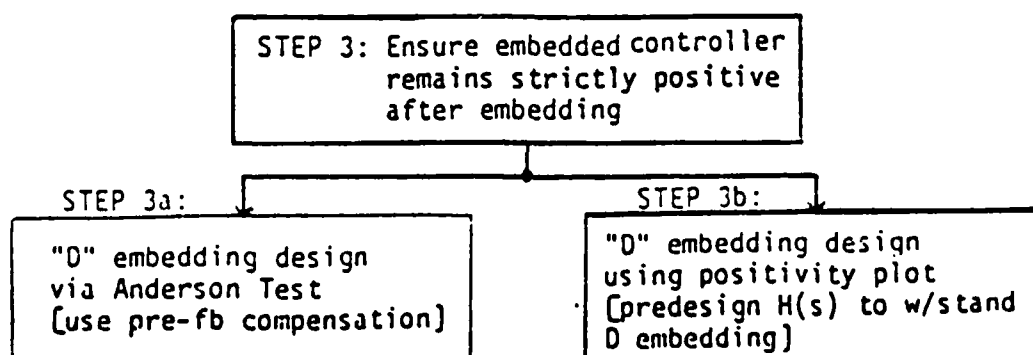
2.3.2.7 The TRW positivity design procedure applies the positivity theorem to LSS control system design. The theorem imposes restrictions of positive realness and strict positive realness on the plant and controller, and this guarantees an asymptotically stable system.

The two basic design steps are:

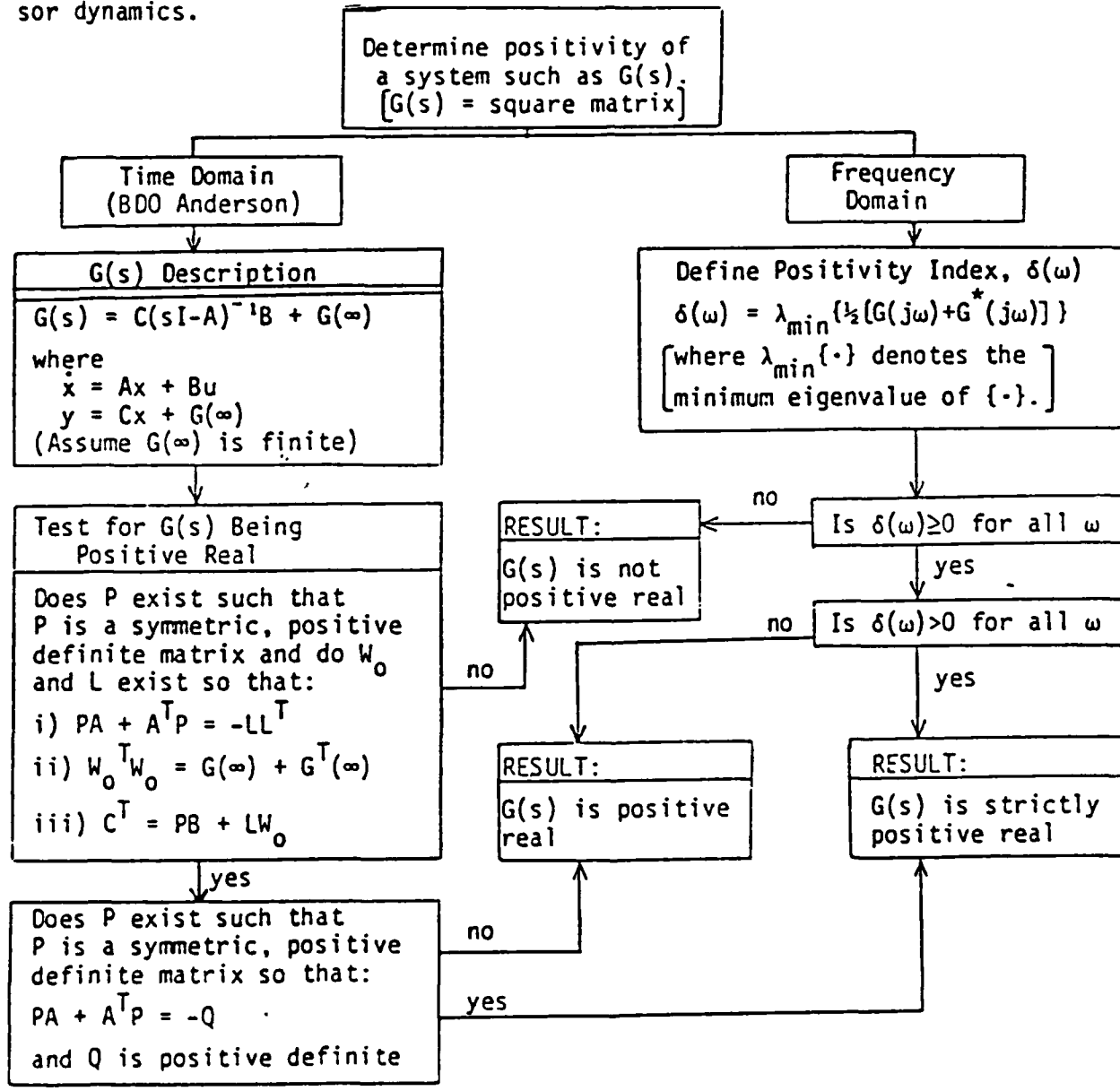
- Step 1 Assure plant (LSS) is positive real.
- Step 2 Design controller that is strictly positive real.



note: STEP 3 is added if embedding is used



The positivity of a system is determined either in the time or frequency domain. Of course, knowledge of the plant is necessary to calculate its positivity. The time domain test uses B.D.O. Anderson's positivity criterion. [7] Application of this test results in the observation that the transfer matrix of the LSS is positive real if ideal, colocated actuators and rate sensors are used. A disadvantage of this test is that inclusion of the actuator and sensor dynamics with the LSS makes it difficult to apply. The frequency domain test incorporates a positivity index - a measure of positive realness of a system. The frequency domain test has the advantages of obtaining experimental frequency response data and of easily including actuator and sensor dynamics.

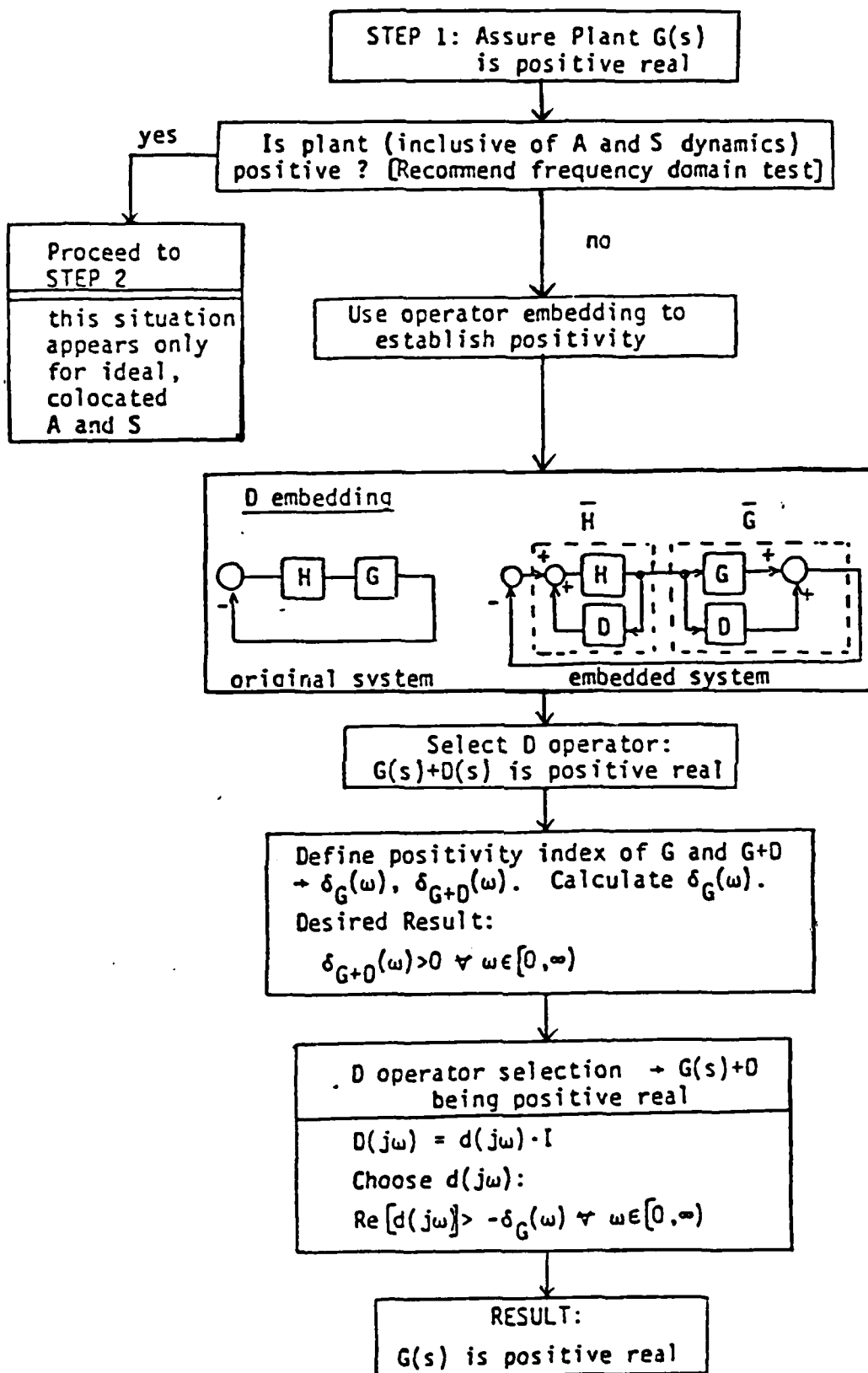


7. Anderson, B.D.O, "A System Theory Criterion For Positive Real Matrices," SIAM J. of Control, Vol. 5, No. 2, pp 171-182, May 1967.

An apparent shortcoming of the positivity approach is realized if the plant is determined to be non-positive, since the theorem requires a positive plant. However, a design tool found instrumental in establishing the positivity of a non-positive system is operator embedding. Through selection of an appropriate embedding operator, the embedded plant becomes positive, and thus satisfies the requirement of the first step.

Step 1 in positivity design.

If the plant  $G(s)$  is not positive, use D (parallel) embedding theory to obtain a positive  $G(s)+D(s)$ . The embedding transformation is purely mathematical and is not implemented in a physical sense, but it may impose conditions on the controller which are implemented. The effect of D embedding is to decrease the gain of the controller. Therefore, the controller  $H(s)$  must be very stable and positive initially so that the D positive feedback loop does not destabilize it. (Note: another embedding technique, F (cascade) embedding, also exists, but is not used in this case)

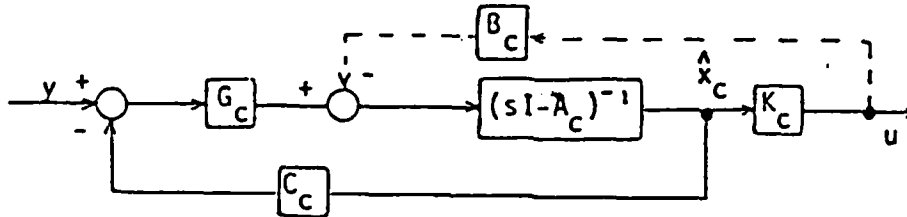


Step 2 in positivity design.

The controller is designed using Linear Quadratic Gaussian (LQG) controller topology and by applying optimal control and estimation techniques. In addition, the positivity criterion is applied to produce a strictly positive real controller.

STEP 2: Design Controller  $H(s)$   
to be strictly positive real

Use LQG controller topology



State equations: w/o  $B_C$  loop

$$\dot{\hat{x}}_C = (A_C - G_C C_C) \hat{x}_C + G_C y$$

$$u = K_C \hat{x}_C$$

$$\frac{u(s)}{\hat{x}_C(s)} = K_C$$

$$\frac{\hat{x}_C(s)}{y(s)} = (sI - \Gamma)^{-1} G_C \quad \Gamma \triangleq A_C - G_C C_C$$

$$H(s) = \frac{u(s)}{y(s)} = K_C (sI - \Gamma)^{-1} G_C$$

Solve for estimator gain matrix,  $G_C$ .  
(use steady state Kalman filter gain solution). \*

Apply Anderson's positivity criterion  
so that  $H(s)$  of controller is strictly  
positive real:

1) Solve for  $P$ :

$$P\Gamma + \Gamma^T P = -Q$$

[ $Q$  is any positive, definite,  
symmetric matrix]

2) Solve for  $K_C$ :

$$K_C^T = P G_C$$

3) Add  $B_C$  Loop

$$B_C = G_C$$

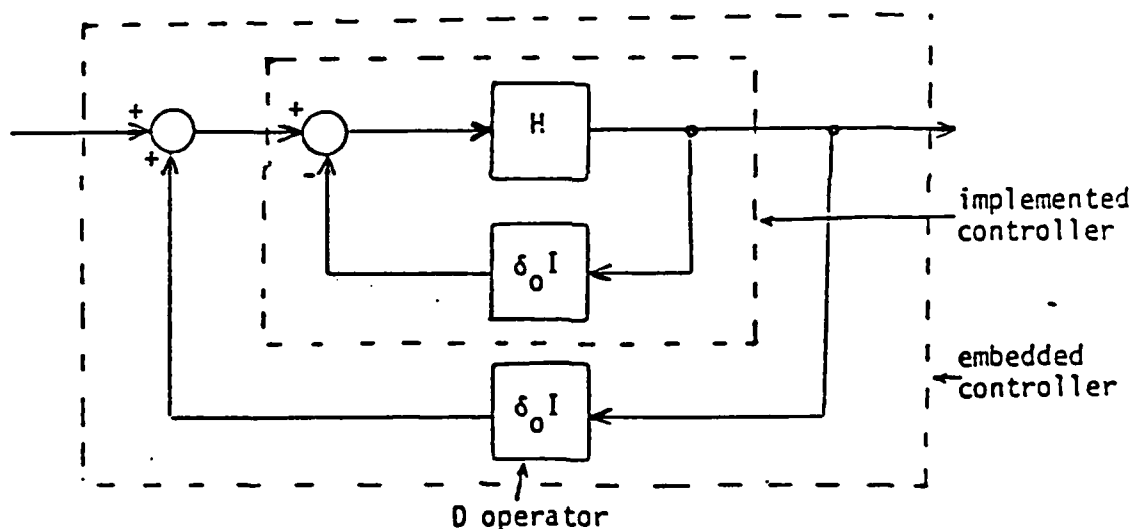
RESULT:  $H(s)$  is strictly positive real

# Step 3a in positivity design.

If embedding is used to assure a positive plant, it is necessary to compensate for the effect of embedding on the controller. While contributing positively to the plant, the embedding operation contributes negatively to the controller. Implementation of a pre-feedback loop around the controller eliminates the negative effect of the embedding operator on the controller. (i.e. the pre-feedback ensures that the controller remains strictly positive even after embedding).

## STEP 3a: D embedding design via the Anderson Test

Implement pre-feedback to create new controller that is positive even after D embedding wraps a  $+\delta_0 I$  feedback around it.



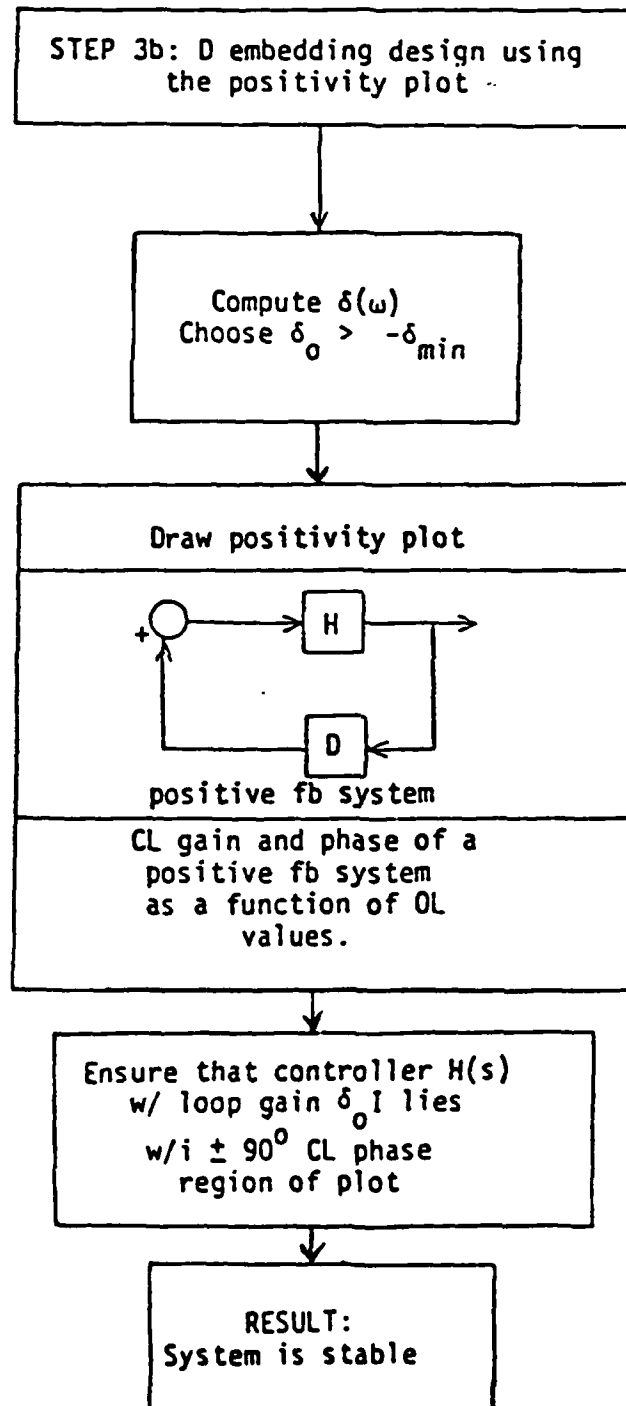
Define  $\delta_0 > -\delta_{\min} > 0$   
 Implement pre-feedback:  
 Wrap  $-\delta_0 I$  feedback around  
 positive controller.

RESULT:

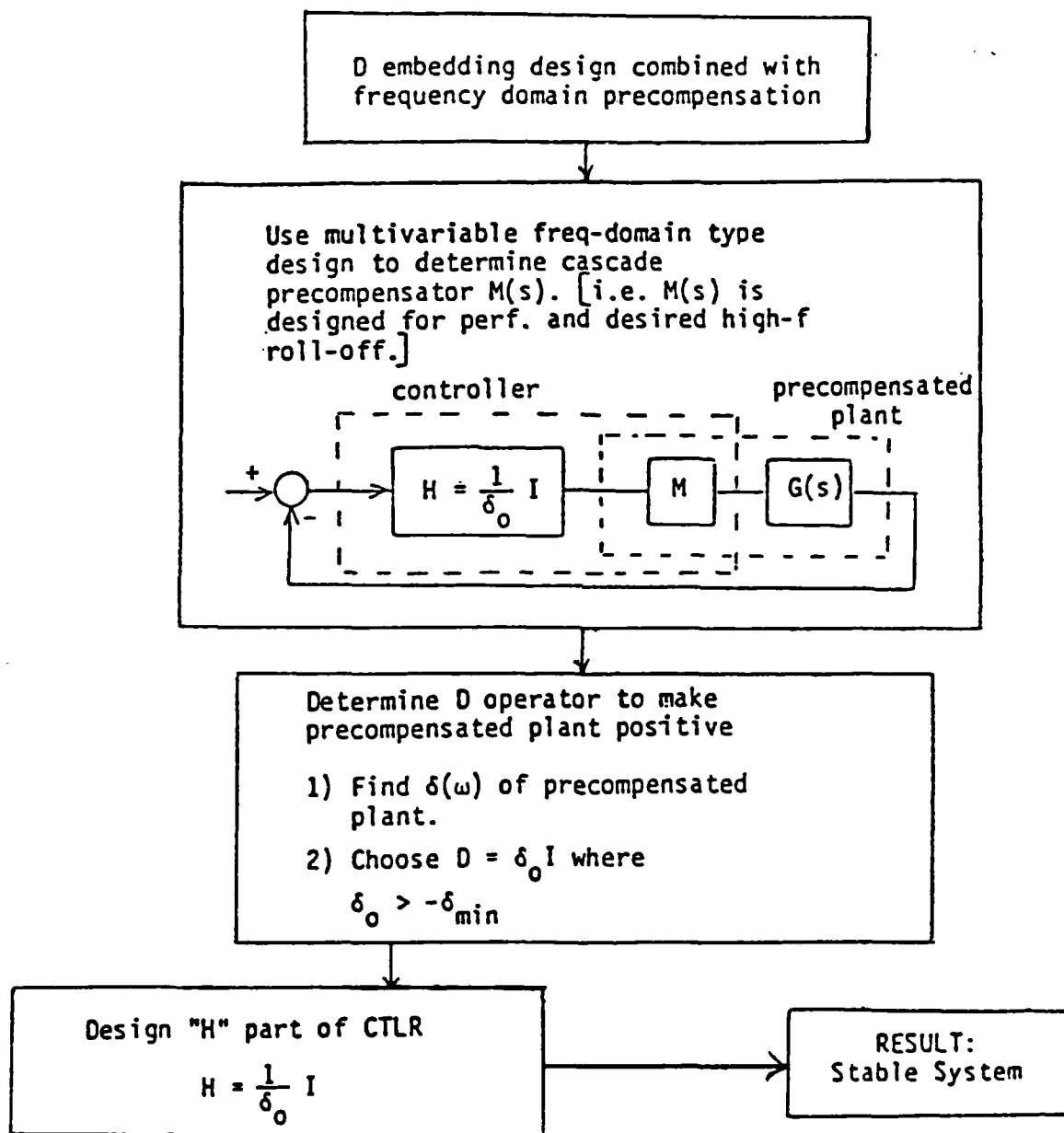
System is asymptotically stable.

Step 3b in positivity design.

Determine the positivity index  $\delta(\omega)$  and choose  $\delta_0$  for D operator. Using the positivity plot, predesign the controller such that the controller with loop gain remains strictly positive. The positivity plot is a plot of closed loop gain and phase as a function of open loop gain and phase.



Another method of applying positivity to the design of control systems is "D embedding with frequency domain precompensation." To apply this method, a full multivariable linear frequency-type design is performed to determine the precompensator  $M(s)$ . The design involves extension of the classical Nyquist/ Bode approach to the multivariable case. [8] It incorporates the examination of the characteristic gains of the open loop plant (or precompensated plant) transfer matrix. Then, D embedding is applied to ensure positivity of the precompensated plant.



8. MacFarlane, et. al., "Complex Variable Methods for Multivariable Feedback Systems Analysis and Design," in Alternatives For Linear Multivariable Control, NEC, Chicago, Ill., 1978.

### 2.3.3 TRW's positivity design for non-colocated systems.[9]

2.3.3.1 Objective. Extend the positivity approach to enable control design of non-colocated systems. The theoretical efforts are:

- (a) Find design conditions for a non-square plant which, when imposed, result in a stable system.
- (b) Develop a procedure to make a non-square plant square (i.e. squaring filter).

Non-colocated is defined as being non-positive and/or non-square (an unequal number of inputs and outputs). The property of non-positivity is handled as it were in colocated control (through operator embedding) and is not a limitation of the positivity approach. However, the property of being non-square is not considered in the initial positivity design approach (ACOSS 8), and was investigated later (ACOSS 14). The resulting approach to non-colocated control is twofold; it may be handled via a squaring procedure or via a stability ensuring design condition for non-square systems.

---

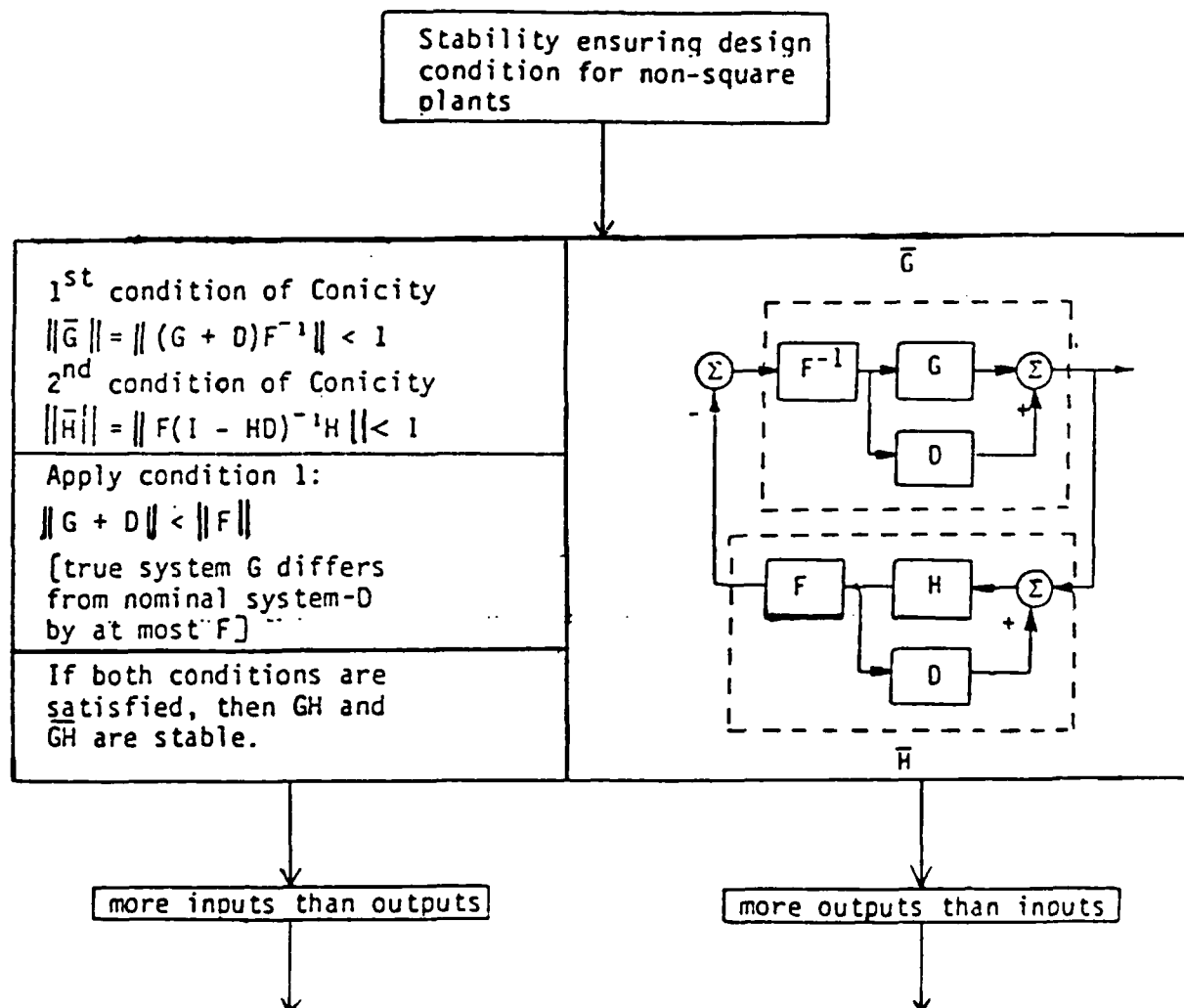
9. "ACOSS Fourteen (Active Control of Space Structures)," TRW, Sponsored by Defense Advanced Research Projects Agency, Contract No. F30602-81-C-0194, November 1982.

- (a) Find conditions required for non-square plant to ascertain stability.

The conicity theorem is applied to the system to provide a stability ensuring design condition for a non-square system. The positivity theorem is found to be a special case of the conicity theorem, which has no limitations to square systems. Two types of operator embedding, parallel (D) and cascade (F), are employed in the derivation of the design condition. The condition is then applied to a non-square system to generate the control law.

Conicity theorem: if the open loop gain of  $GH < 1$ , then the closed loop system is stable

Applying conicity results in the imposition of two design conditions on each of the possibilities inherent in non-square plants (i.e. # outputs > # inputs or # inputs > # outputs).

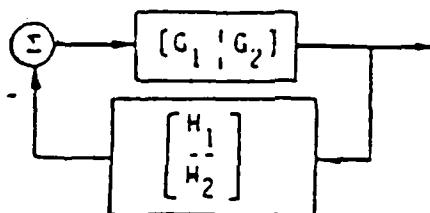


more inputs than outputs

Partition plant  $G$  and controller  $H$  into collocated and noncollocated parts.

$$G = \begin{bmatrix} G_1 & G_2 \end{bmatrix} \quad \begin{array}{l} G_1 = \text{collocated} \\ G_2 = \text{noncollocated} \end{array}$$

$$H = \begin{bmatrix} H_1 \\ H_2 \end{bmatrix} \quad \begin{array}{l} H_1 = \text{collocated} \\ H_2 = \text{noncollocated} \end{array}$$



Apply 2<sup>nd</sup> condition of Conicity:

$$G = \begin{bmatrix} G_1 & G_2 \end{bmatrix} \quad F = \begin{bmatrix} F_1 & F_2 \end{bmatrix}$$

$$D = \begin{bmatrix} D_1 & D_2 \end{bmatrix} \quad H = \begin{bmatrix} H_1 \\ H_2 \end{bmatrix}$$

Substitute into:

$$\| F(I - HD)^{-1}H \| < 1$$

Use  $\ell_2$  norm to evaluate expression.

Apply Parseval's theorem.

Resulting condition:

$$\lambda_{\max} \{ (F_1 H_1 + F_2 H_2)^* (F_1 H_1 + F_2 H_2) \} <$$

$$\lambda_{\min} \{ (I + H_1 D_1 + H_2 D_2)^* (I + H_1 D_1 + H_2 D_2) \}$$

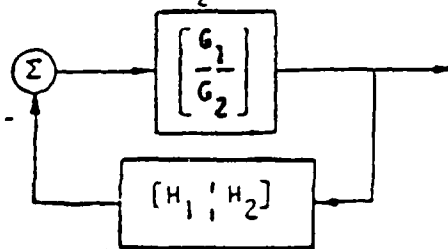
RESULT: Stability  
ensuring design  
condition

more outputs than inputs

Partition plant  $G$  and controller  $H$  into collocated and noncollocated parts.

$$G = \begin{bmatrix} G_1 \\ -G_2 \end{bmatrix} \quad \begin{array}{l} G_1 = \text{collocated} \\ G_2 = \text{noncollocated} \end{array}$$

$$H = \begin{bmatrix} H_1 & H_2 \end{bmatrix} \quad \begin{array}{l} H_1 = \text{collocated} \\ H_2 = \text{noncollocated} \end{array}$$



Apply 2<sup>nd</sup> condition of Conicity

$$G = \begin{bmatrix} G_1 \\ -G_2 \end{bmatrix} \quad F = \begin{bmatrix} F_1 \\ -F_2 \end{bmatrix}$$

$$D = \begin{bmatrix} D_1 \\ -D_2 \end{bmatrix} \quad H = \begin{bmatrix} H_1 & H_2 \end{bmatrix}$$

Substitute into:

$$\| F(I - HD)^{-1}H \| < 1$$

Use  $\ell_2$  norm to evaluate expression.

Apply Parseval's theorem.

Resulting condition:

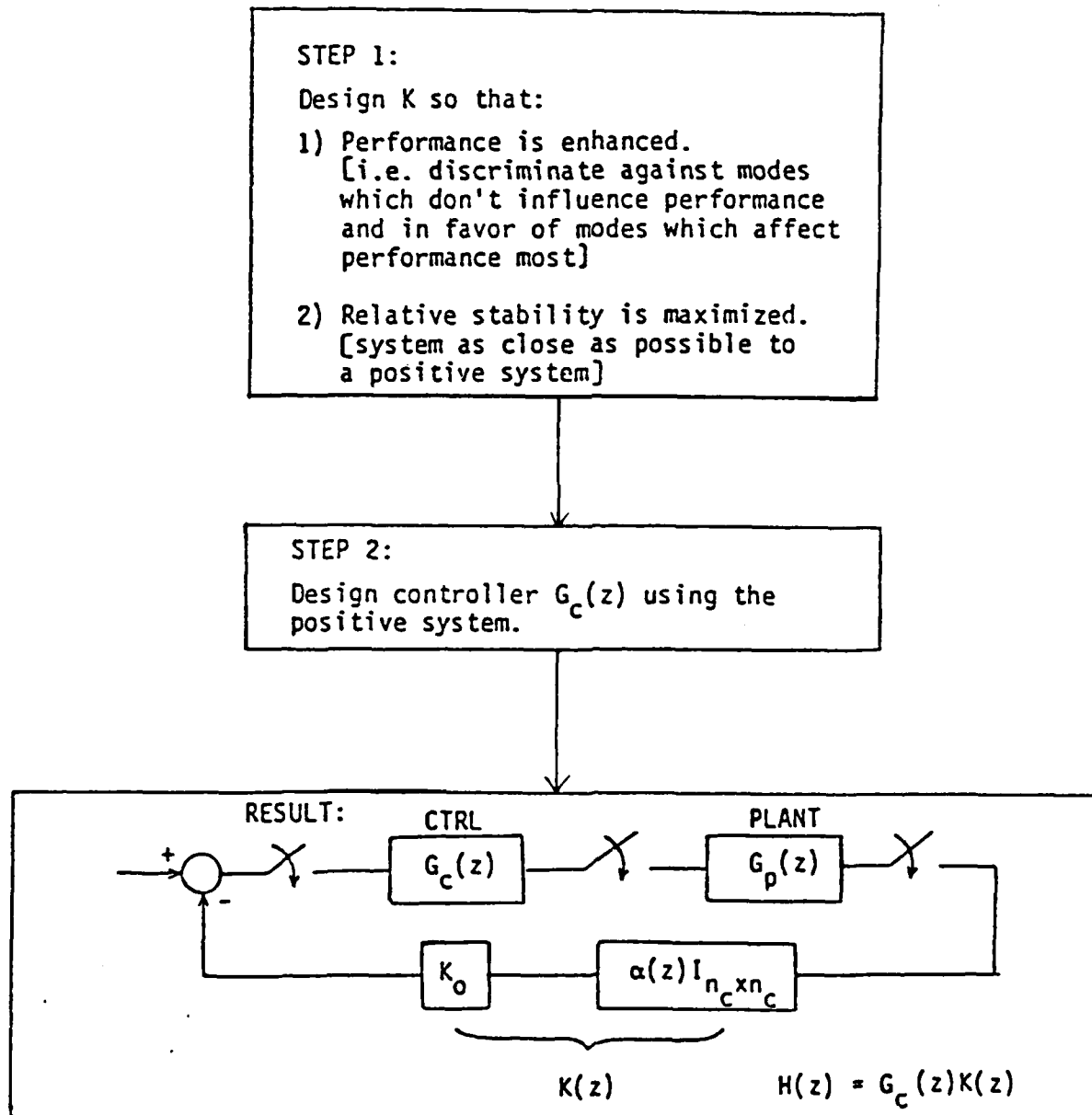
$$\lambda_{\max} \left\{ \begin{bmatrix} F_1 H_1 & F_1 H_2 \\ F_2 H_1 & F_2 H_2 \end{bmatrix}^* \begin{bmatrix} F_1 H_1 & F_1 H_2 \\ F_2 H_1 & F_2 H_2 \end{bmatrix} \right\} <$$

$$\lambda_{\min} \left\{ \begin{bmatrix} I + H_1 D_1 & H_1 D_2 \\ -H_2 D_1 & I + H_2 D_2 \end{bmatrix}^* \begin{bmatrix} I + H_1 D_1 & H_1 D_2 \\ -H_2 D_1 & I + H_2 D_2 \end{bmatrix} \right\}$$

SULT: Stability ensuring design condition

- (b) Basic outline for control of non-colocated systems using squaring filter.

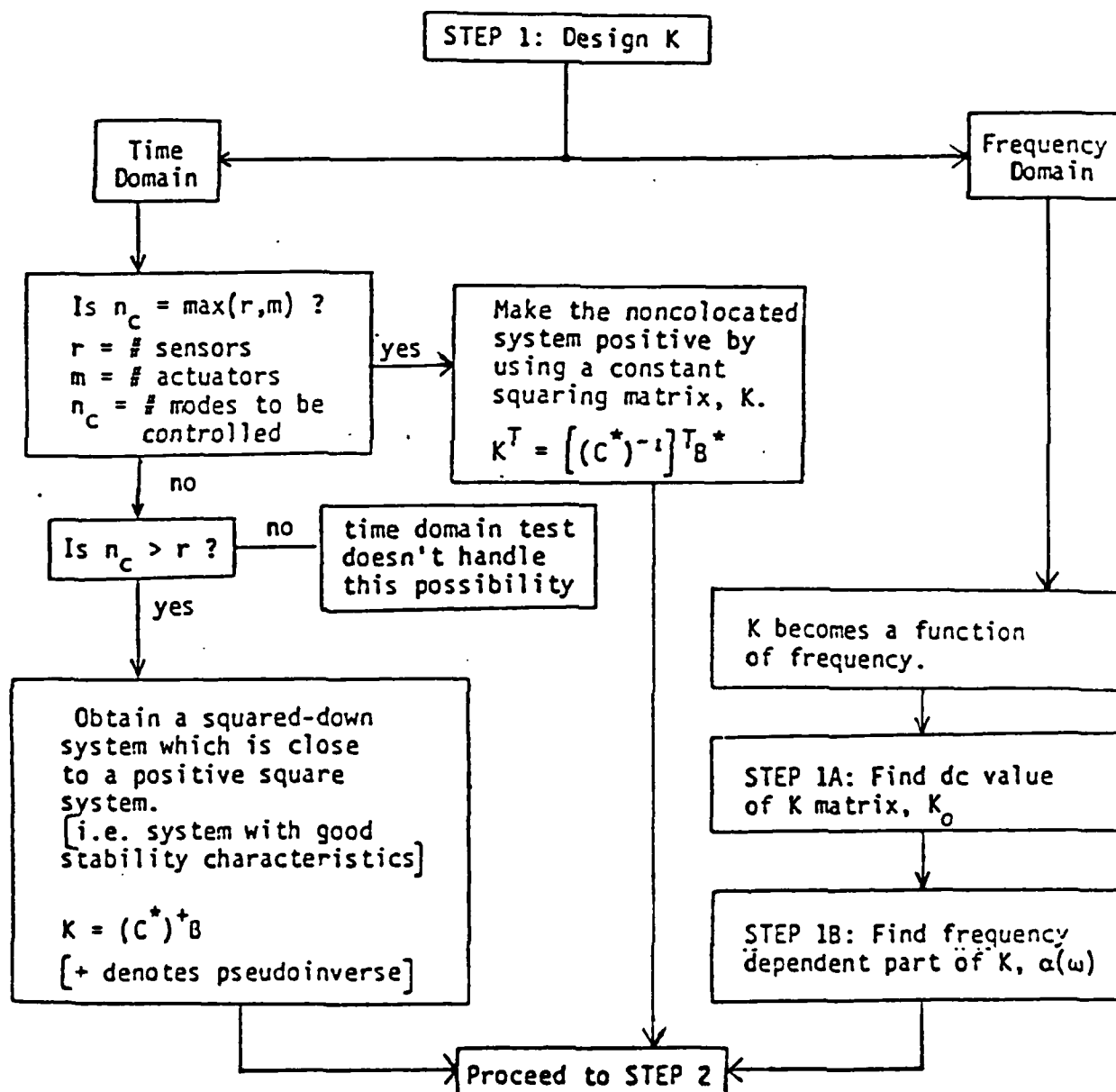
The squaring procedure involves design of a squaring filter through which a non-square plant is made square. After establishing a square plant, the design procedure continues as colocated positivity design.



The squaring filter can be designed in either the time or frequency domain. In the time domain, a constant squaring matrix is determined. A disadvantage is the procedure may require a high number of sensors if many modes are to be controlled. In the frequency domain, the squaring procedure is separated into three steps:

1. Design the d.c. gain of the filter,  $K_0$
2. Design the frequency dependent portion of the filter,  $\alpha(\omega)$
3. Approximate resultant filter by realizable discrete-time filter  $\alpha(z)$

In many frequency domain cases, a constant  $K=K_0$  gives reasonable results and no filter is required.



Step 1a) Find  $K_0$

STEP 1A: Find  $K_0$

$$K_0 = K(0)$$

$$K_0 = \frac{R_0}{G(0)}$$

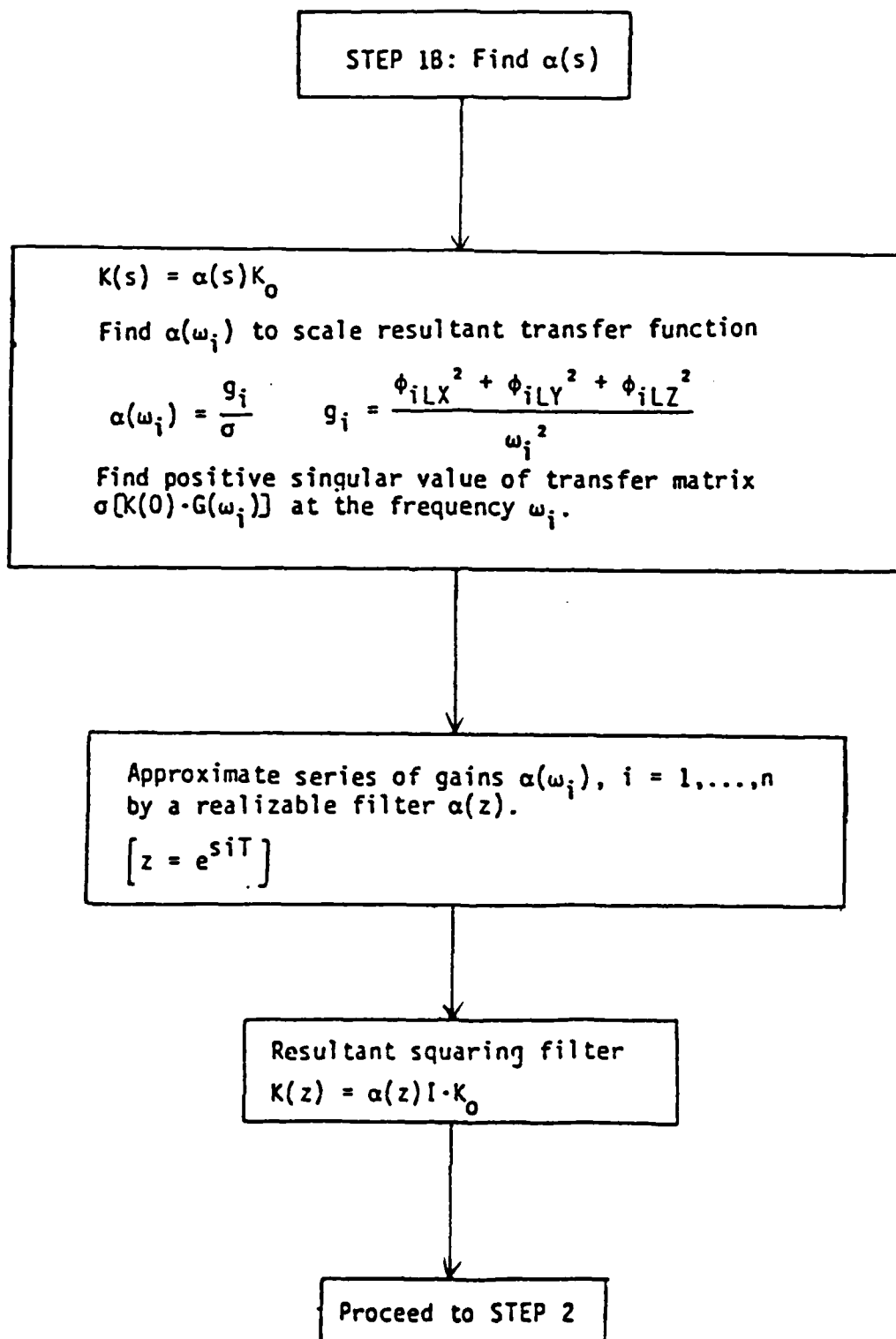
$$G_{ij}(0) = \sum_{K=1}^n \frac{\phi_K(s_i) \phi_K(a_j)}{\omega_K^2} \quad \begin{matrix} i = 1, 2, \dots, r \\ j = 1, 2, \dots, m \end{matrix}$$

$$r_{jj} = \sum_{K=1}^n \frac{\sqrt{\phi_{KLX}^2 + \phi_{KLY}^2 + \phi_{KLZ}^2}}{\omega_K^2} \cdot \phi_K(a_j)$$

$$R_0 = \text{diag} [r_{jj}]$$

This equation has many solutions. Choose solution with minimum norm using singular value decomposition.

Step 1b) Find  $K(z)$



#### 2.3.4 Lockheed's LAC/HAC design.[10]

2.3.4.1 Objective. Develop a technique that eliminates instabilities created by spillover. Summarily stated, spillover is the interaction of the controller with unmodeled modes. The control design must cope with poorly known high frequency modes by not destabilizing them while controlling the low frequency modes.

#### 2.3.4.2 Properties of technique.

- (a) Robust performance
- (b) Suppression of spillover

#### 2.3.4.3 LAC/HAC approach.

- (a) HAC - modify the structural mode shapes and modal damping with the HAC estimator and control law.
- (b) LAC - incorporate LAC control law to reduce spillover instability created by HAC controller.  
LAC design is based on a higher order model than HAC design.

#### 2.3.4.4 Theory: LAC/HAC is a design method which meets the objective.

#### 2.3.4.5 Definition.

- (a) Spillover: interaction of the controller with unmodeled modes

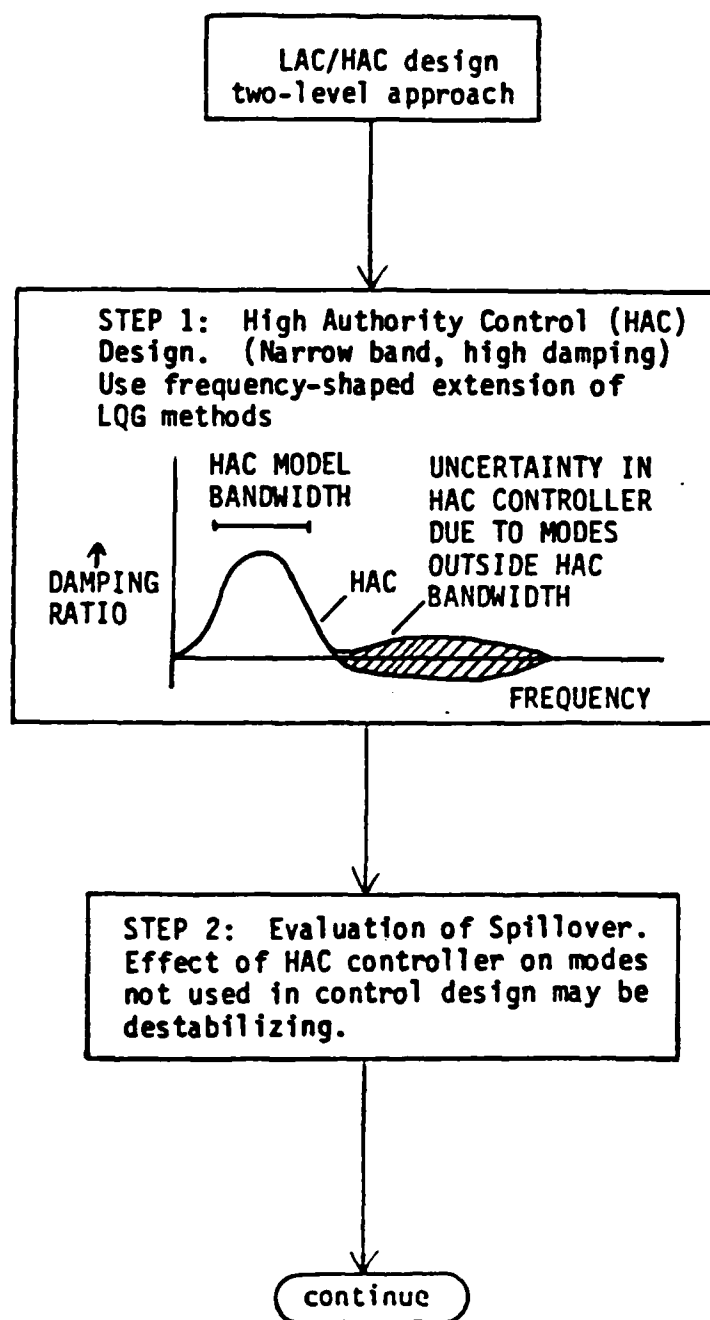
2.3.4.6 Lockheed's Low Authority Control/High Authority Control (LAC/HAC) design procedure applies a two-level approach to LSS control system design. The first level involves HAC design, which incorporates a narrow band and high damping to meet performance requirements. The concept of using a frequency-shaped extension of the LQG method is presented. The second level involves LAC design, which incorporates a wide band and low damping to eliminate spillover induced instabilities.

---

10. "ACOSS Five (Active Control of Space Structures) Phase IA," Lockheed Missiles and Space Company, Inc., Sponsored by Defense Advanced Research Projects Agency, Report No. RADC-TR-82-21, March 1982.

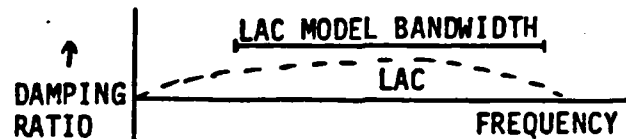
Implement the following four steps to design a LAC/HAC controller:

- 1) HAC design
- 2) Spillover evaluation
- 3) LAC design
- 4) Stability, performance evaluation



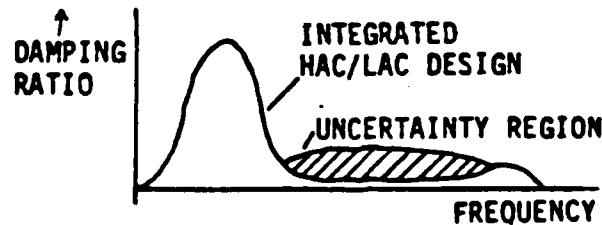
continue

STEP 3: Low Authority Control (LAC) Design. (Wide band, low damping) solves destabilization problems created by HAC.



STEP 4: Stability and Performance Evaluation

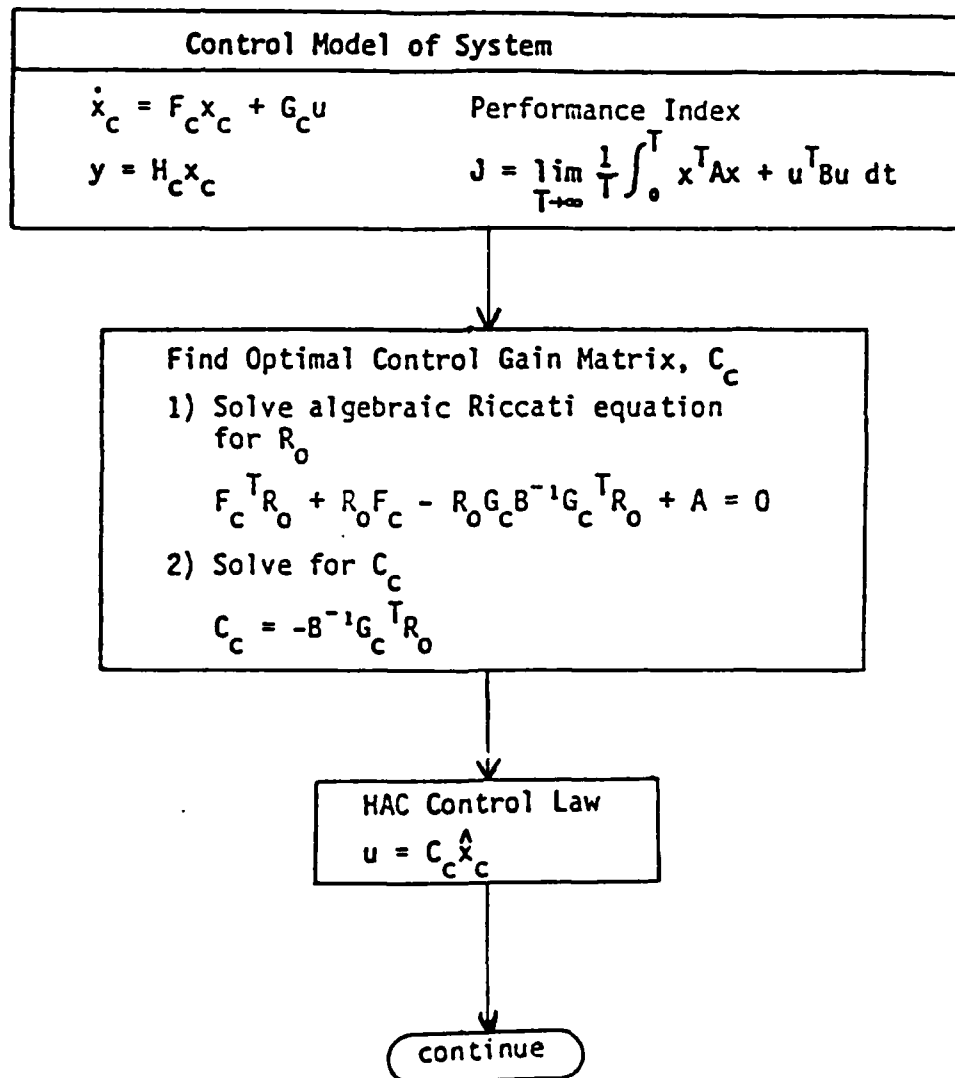
Result: Stable system which handles Spillover (i.e. interaction of the controller with unmodeled modes)



Step 1 in LAC/HAC design.

The HAC design uses a standard LQG controller and applies optimal control and estimation techniques to develop the HAC control law. The concept of frequency shaping the performance index (PI) may be applied to:

- i) Avoid spillover - high frequency spillover, in the case of LSS
- ii) State estimation - minimize the problem of interaction of unmodeled high frequency modes with the estimation of low frequency states
- iii) Disturbance rejection - minimize the effect of a disturbance at a particular frequency



continue

Find State Estimator Gain Matrix, K.  
(Use steady state Kalman filter sol'n)  
State Estimator Equations:

$$\dot{\hat{x}}_C = F_C \hat{x}_C + G_C u + K(y - H_C \hat{x}_C)$$

1) Find P, Q

v = input noise vector

w = measurement noise vector

$$E\{v(t)v^T(t+\tau)\} = Q\delta(\tau)$$

$$E\{w(t)w^T(t+\tau)\} = P\delta(\tau)$$

2) Solve algebraic Riccati equation

$$0 = F_C^T R + R F_C - R H_C^T P^{-1} H_C R + G_C Q G_C^T$$

3) Solve for K

$$K = R H_C^T P^{-1}$$

Apply frequency-shaping methods  
in the following three areas as  
necessary:

1) Spillover Avoidance

2) State Estimation

3) Disturbance Rejection

Spillover Avoidance  
in HAC design

10

State Estimation  
in HAC design

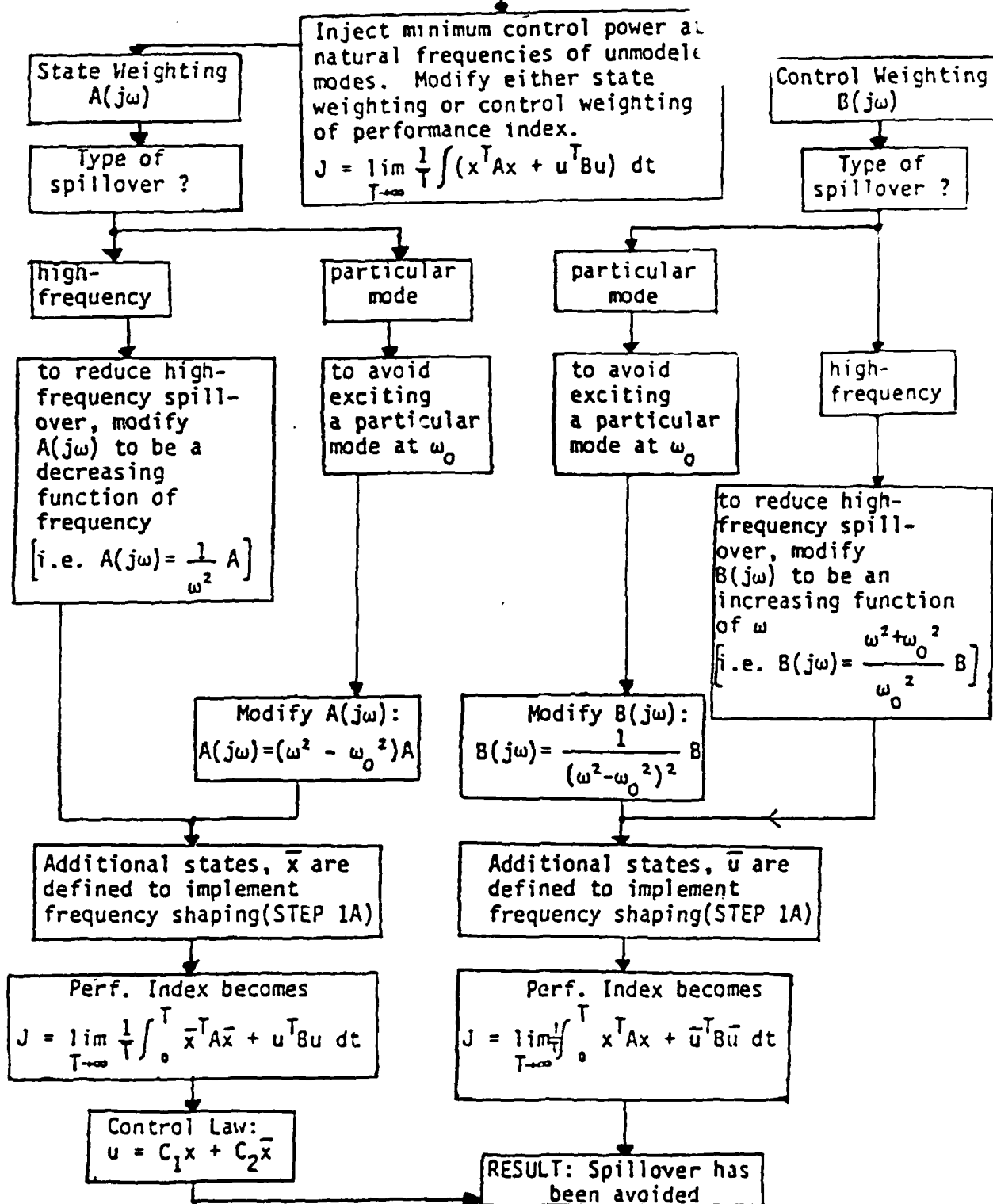
20

Disturbance Rejection  
in HAC design

30

Frequency shaping the performance index to avoid spillover.

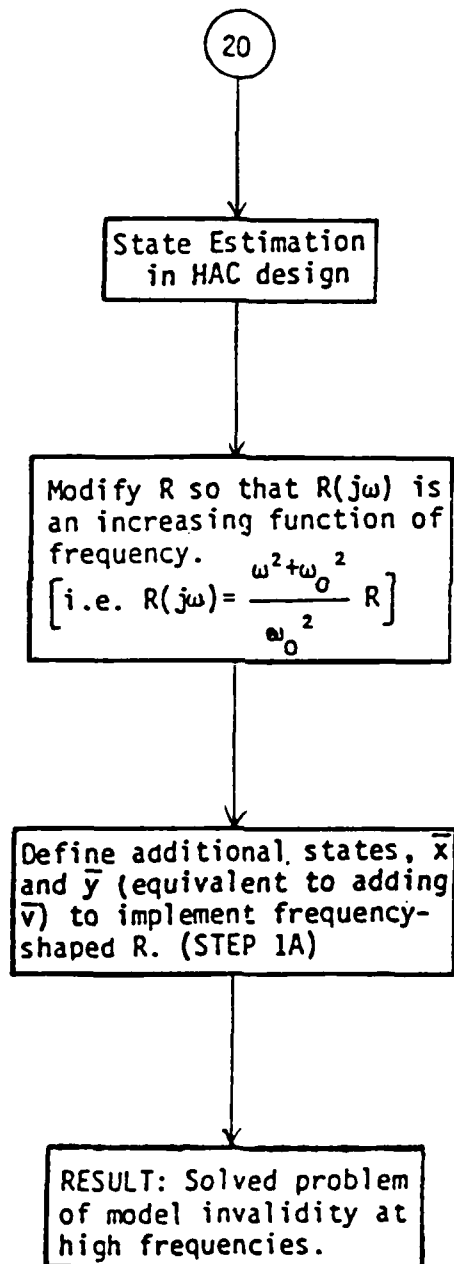
The fundamental idea of frequency shaping is to provide minimum control authority at the unmodeled modal frequencies. The state and/or control weighting of the performance index are modified to be appropriate functions of frequency. An increased penalty in the LQG cost functional is placed where less response is desired. For example, to reduce high frequency spillover, the state weighting is modified to be a decreasing function of frequency and/or the control weighting is modified to be an increasing function of frequency. The objective is to penalize the low frequency states (to impose limitations on state magnitude) and/or to penalize high frequency control power (to avoid placing controller energy at high frequencies). Additional states must then be defined to implement the frequency shaping and are included in both the control law and performance index.



## State estimation in HAC design.

Problem: Estimation of low frequency states when high frequency modes are not modeled.

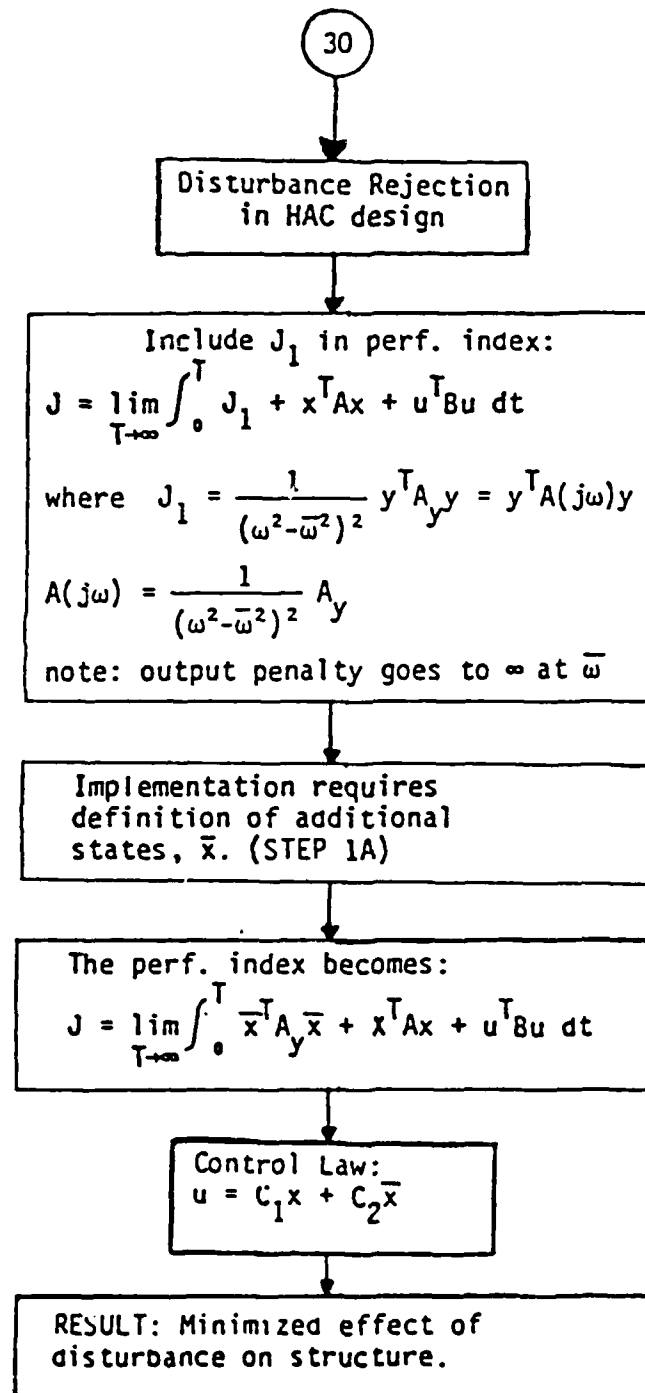
Frequency shape R (while Q remains unchanged), since all errors associated with modal truncation are incorporated in measurements.



Disturbance rejection in HAC design.

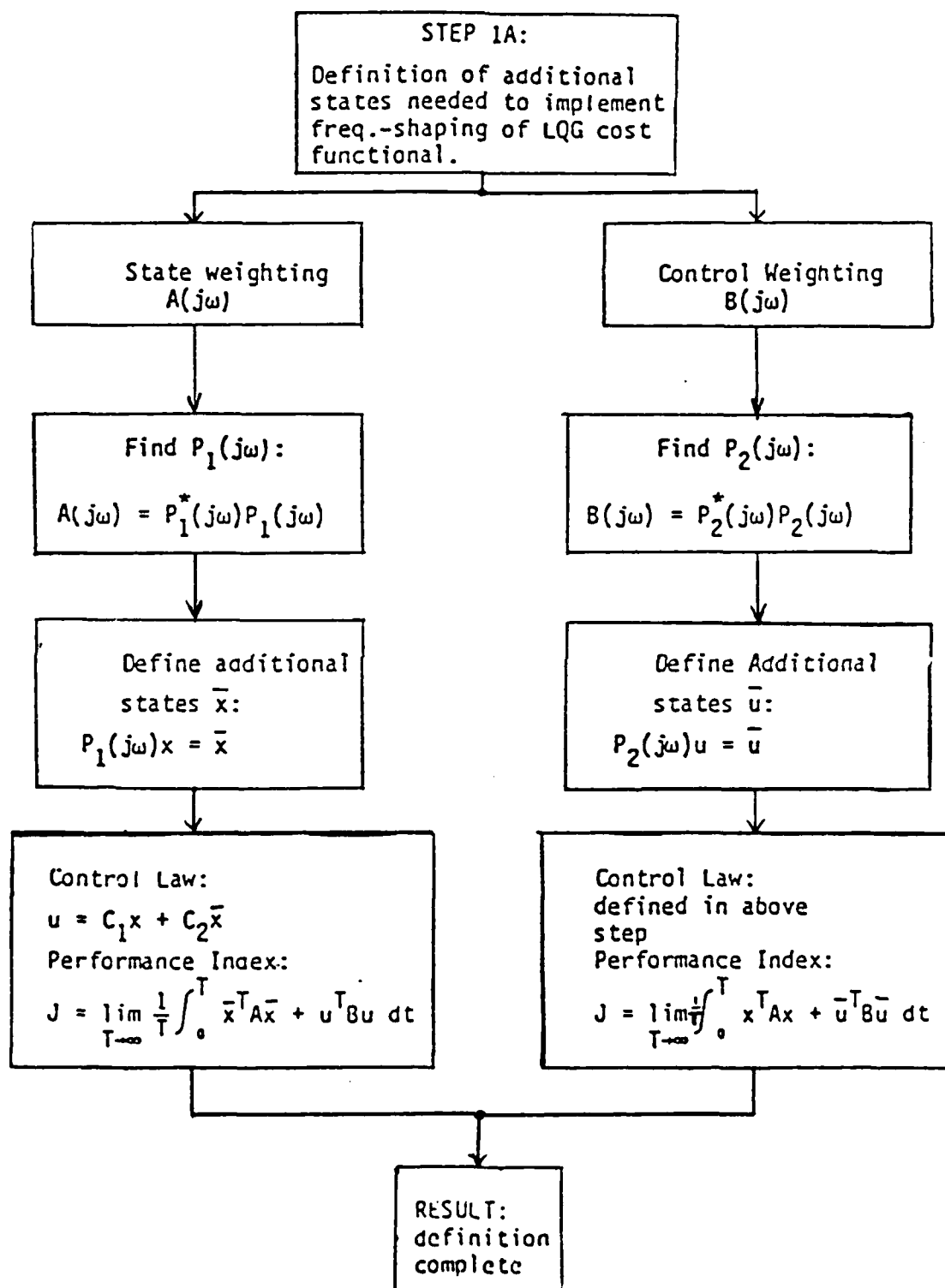
Problem: Minimize effect of disturbance on output  $y$ . The disturbances attenuated in this type of disturbance rejection include disturbances at a particular frequency,  $\omega_0$ .

Include additional term in performance index,  $J_1$ .



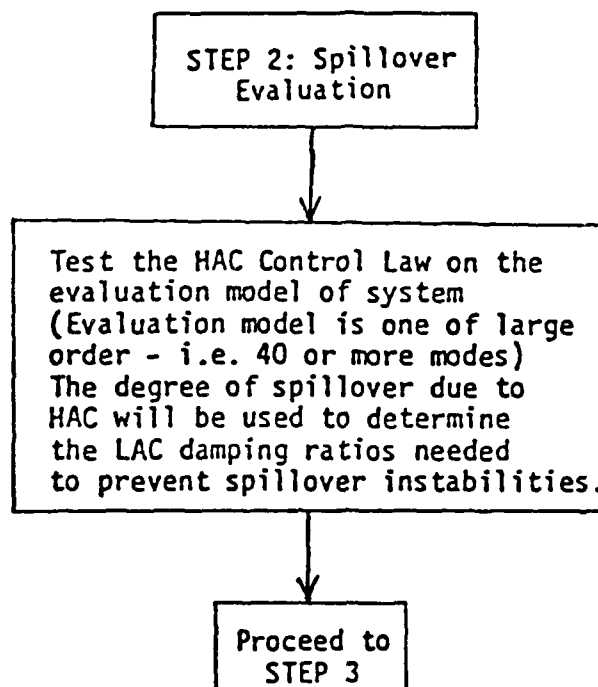
Step 1a in LAC/HAC design.

Define additional states required to implement frequency shaped performance index.



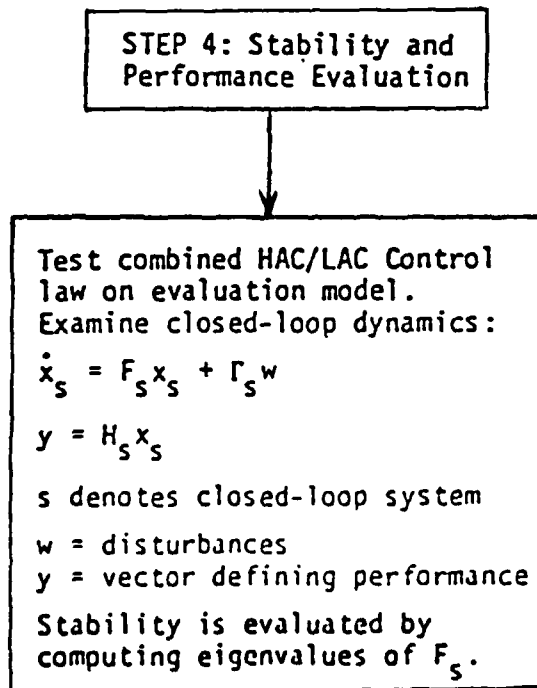
Step 2 in LAC/HAC design: Spillover evaluation.

Test HAC control law on large order model.



Step 4 in LAC/HAC design: Stability and performance evaluation.

Test HAC/LAC control law on large order model and examine output.



Step 3 in LAC/HAC design: LAC design.

The LAC design procedure develops a LAC control law which generates closed loop system root shifts. The introduction of the LAC control system produces root shifts into the stability domain. The root shifts, which can be predicted algebraically, are used to derive the fundamental root shift formula of LAC design. A cost function involving predicted root shifts and desired root shifts is minimized to determine the LAC control law.

STEP 3:

LAC Design

The determination of the matrix of the damping gains,  $C_L$  (where  $u = C_L y$ ) is the synthesis of LAC systems.  $C_L = [C_{ar}]$

Find  $(d\lambda_n)_p$  - predicted root shift

Derivation of LAC formula to algebraically predict root shifts produced by introducing the LAC Control System.

System Equations:

Dynamics :	$\dot{x} = Fx + Gu$	Closed Loop Dynamics
Sensors :	$y = Hx$	$\dot{x} = (F + GC_L H)x$
Controls :	$u = C_L y$	

For small controls,  $C_L$

$$GC_L H = dF$$

The dynamics become:

$$\dot{x} = (F + dF)x$$

\*Fundamental Root Shift Formula\*

$$d\lambda_n \cong \frac{1}{2} \sum_{a,r} C_{ar} \phi_{an}^A \phi_{rn}^R$$

$\lambda_n = n^{\text{th}}$  root of  $F$

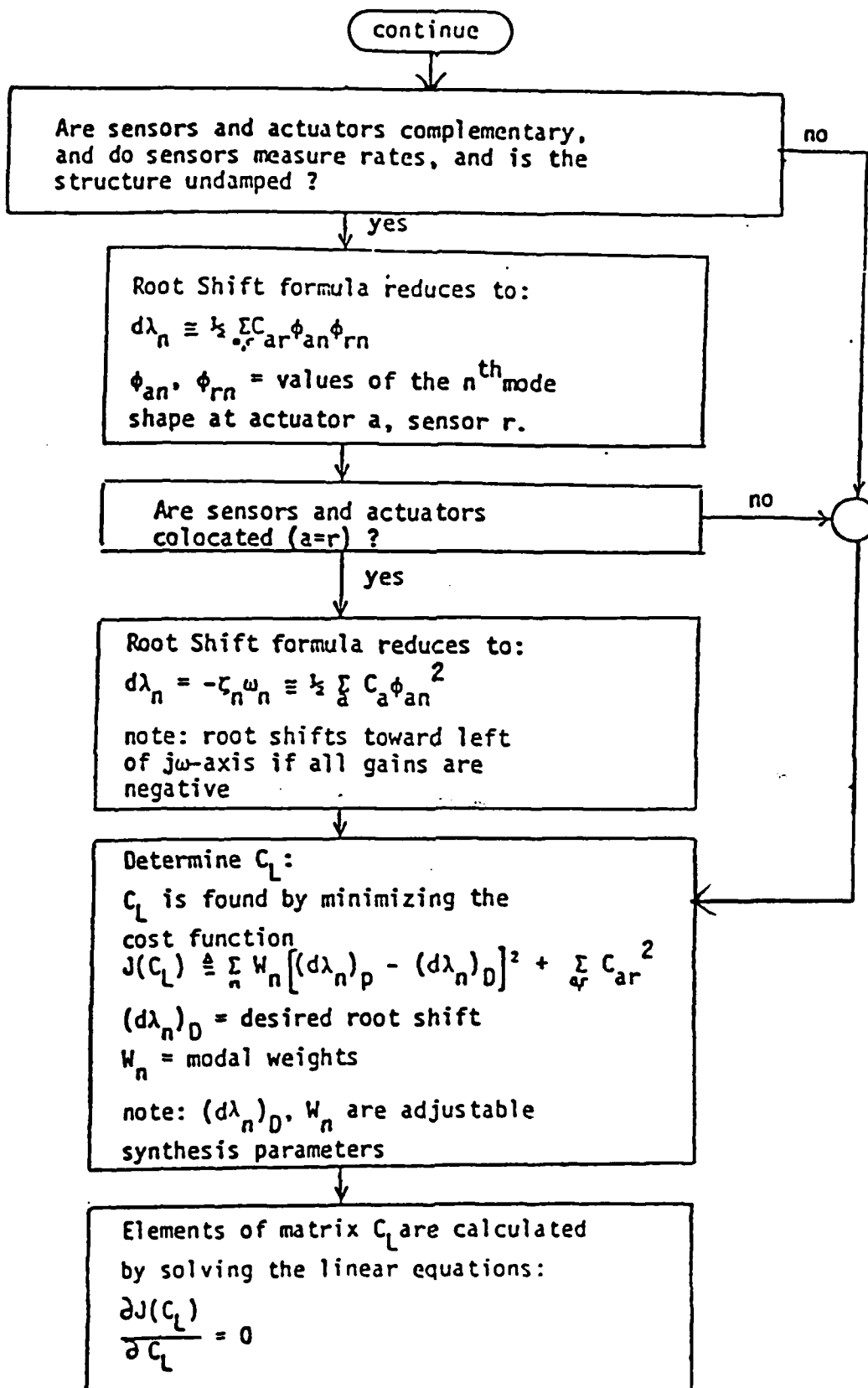
$d\lambda_n$  = root shift corresponding to  $dF$

$L_n, R_n$  = corresponding left, right eigenvectors of  $F$

$$[ \text{i.e. } F^T L_n = \lambda_n L_n, F R_n = \lambda_n R_n ]$$

$$\phi_n^A \triangleq G^T L_n \quad \phi_n^R \triangleq H R_n$$

continue



### 2.3.5 General Dynamic MESS design.[11]

2.3.5.1 Objective. Stabilization of control model, attenuating effects of control and observation spillover, and model errors caused by truncation of known high frequency residual modes.

2.3.5.2 Overall approach. General Dynamic's Model Error Sensitivity Suppression (MESS) design procedure involves an extension of optimal control theory with standard LQG controller topology. MESS uses the performance index to constrain sensitivity to modeling errors.

#### 2.3.5.3 Properties.

- (a) Algorithm only provides solution to the problem of known model truncation
- (b) Low sensitivity to modeling errors

#### 2.3.5.4 Definitions.

- (a) Control spillover: excitation of uncontrolled modes by controller
- (b) Observation spillover: sensing of uncontrolled modal responses by observer

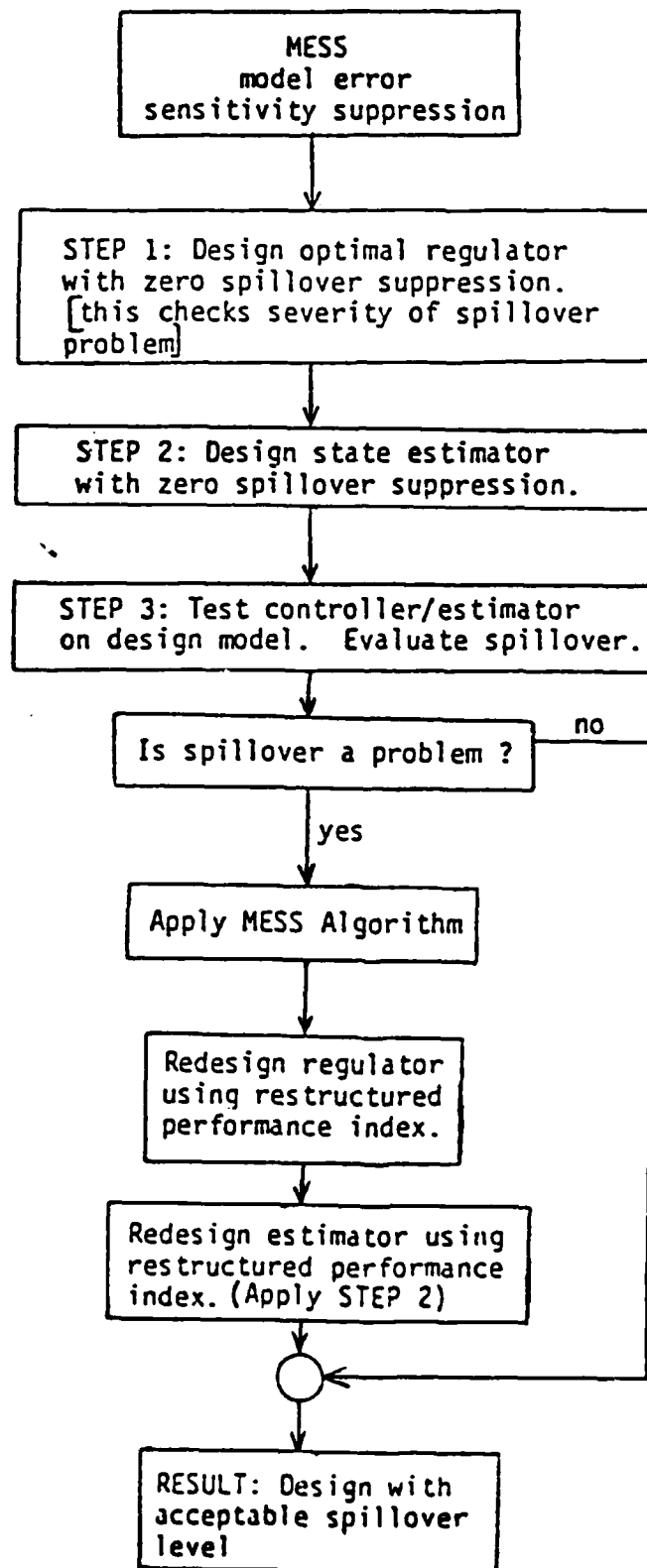
---

11. "ACOSS One (Active Control of Space Structures) Phase I," General Dynamics, Sponsored by Defense Advanced Research Projects Agency, Report No. RADC-TR-80-79, March 1980.

## Model Error Sensitivity Suppression.

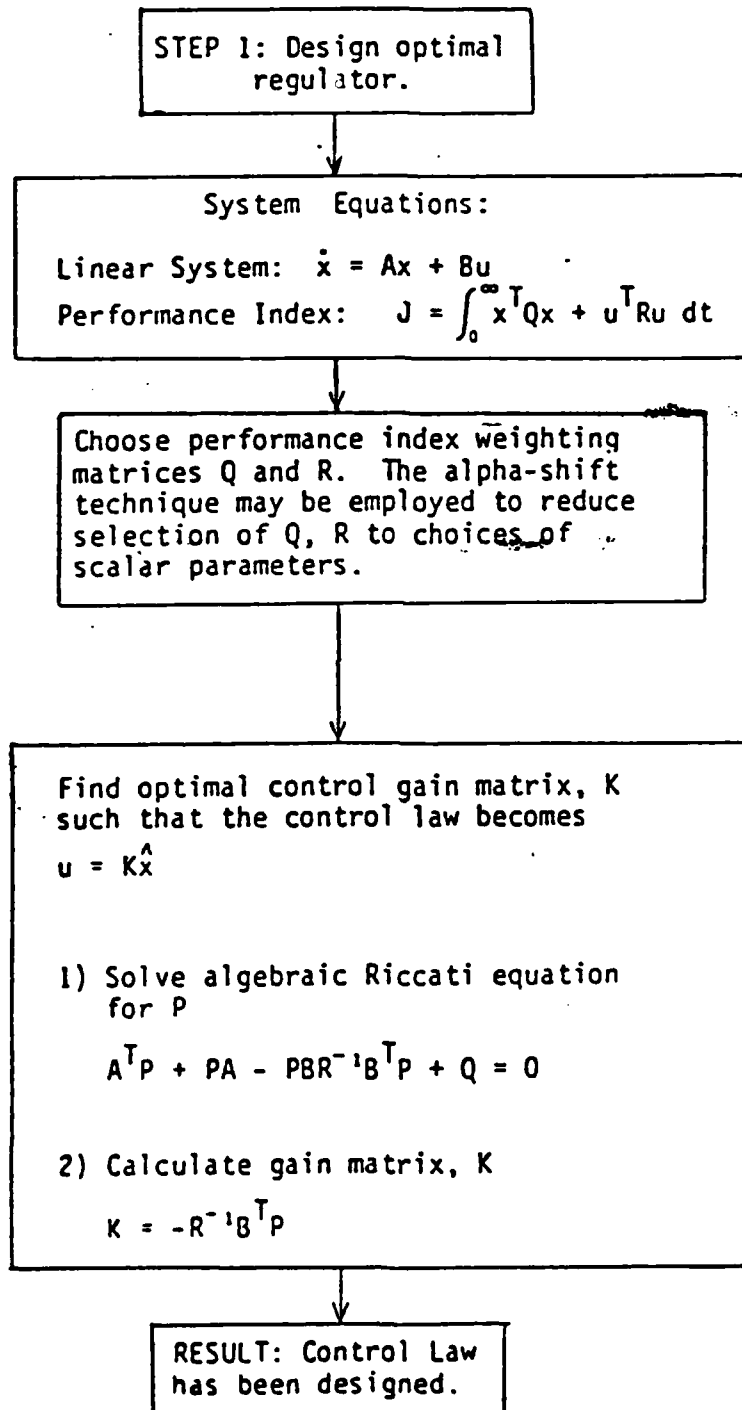
The design procedure consists basically of the 4 following steps:

- 1) Design optimal regulator
- 2) Design state estimator
- 3) Evaluate spillover
- 4) Apply MESS algorithm and redesign regulator, estimator



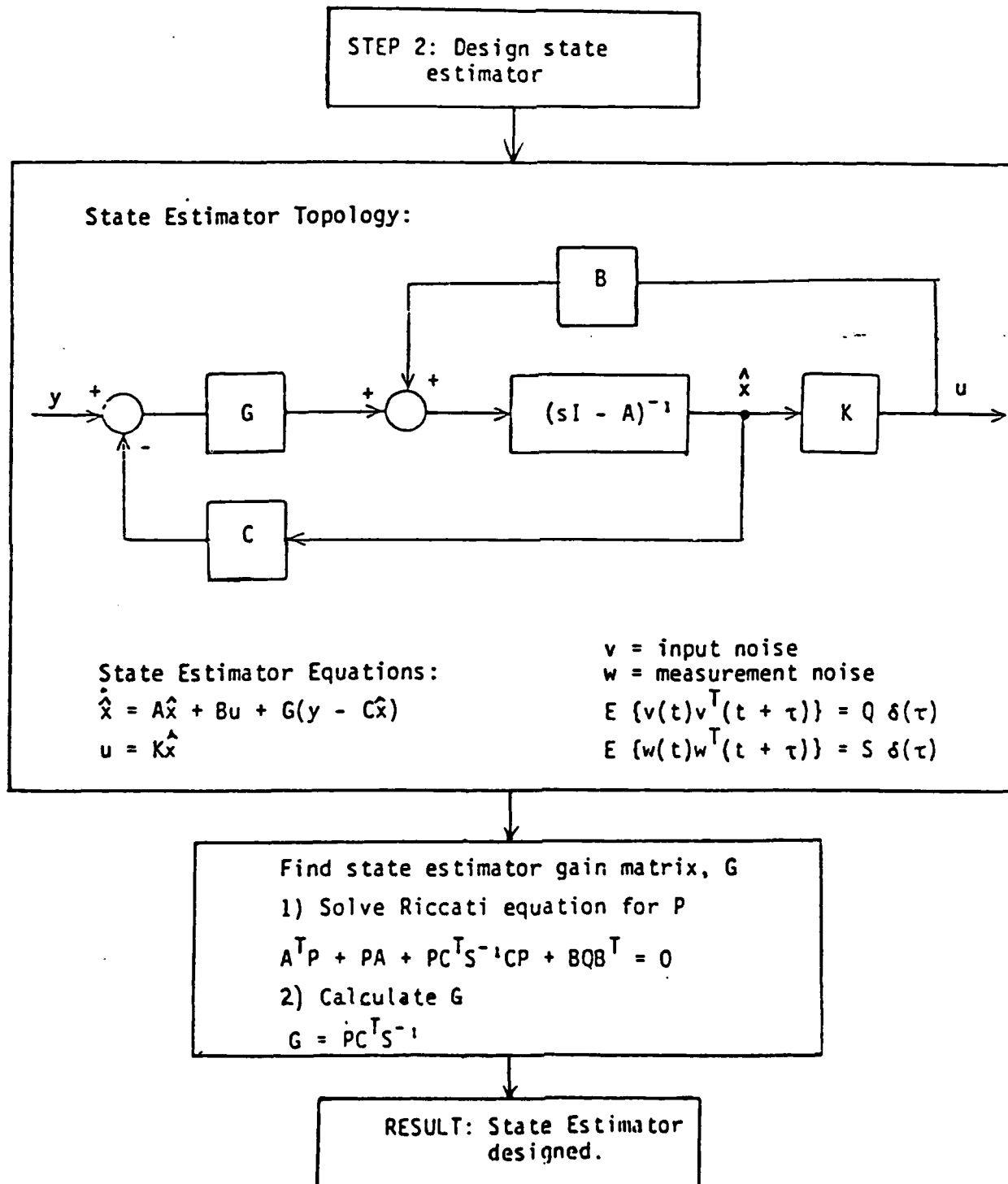
### Step 1 Design optimal regulator.

Standard LQG control methods are used to design the optimal regulator and state estimator. Using the alpha-shift technique, the selection of PI weighting matrices is reduced to a choice of scalar parameters.

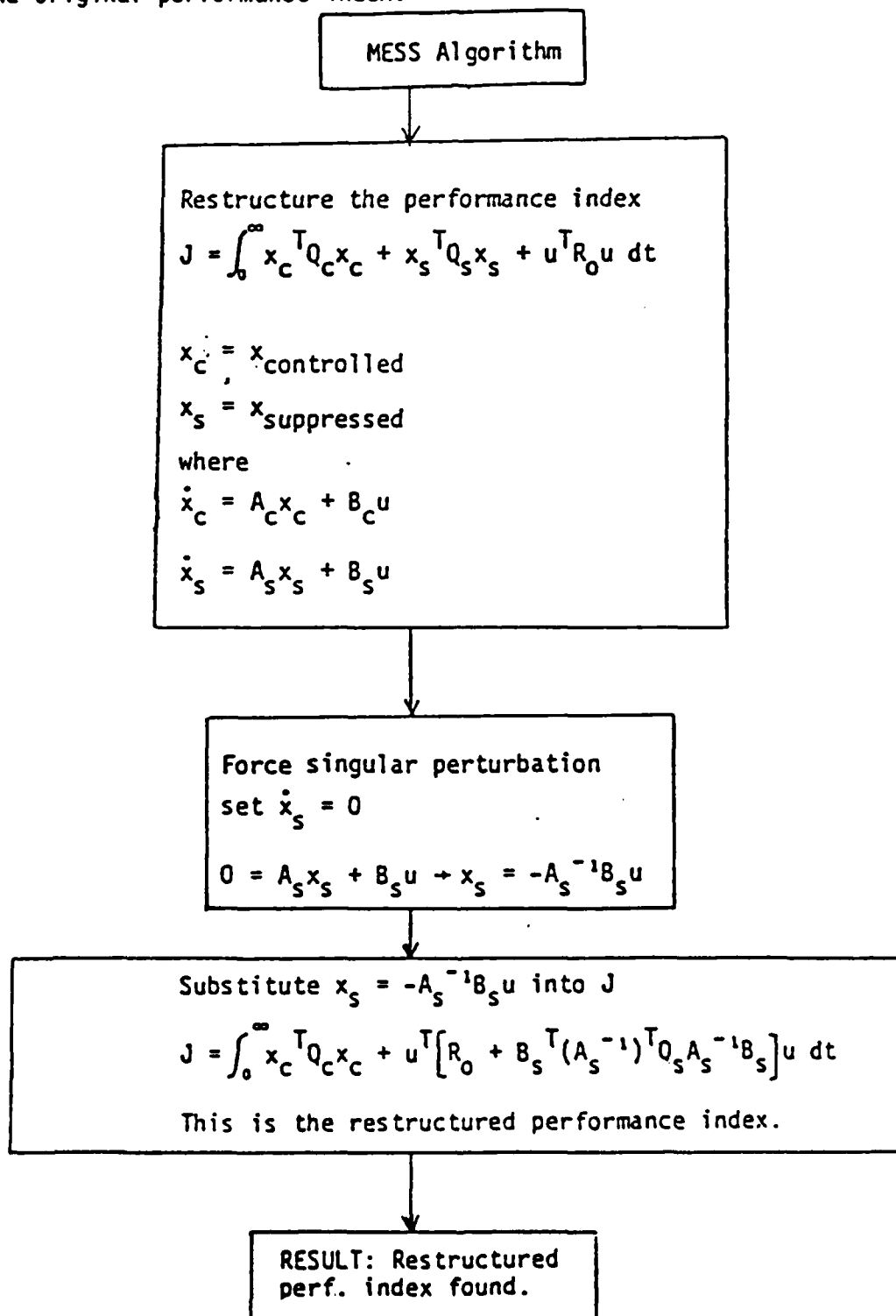


## Step 2 Design state estimator.

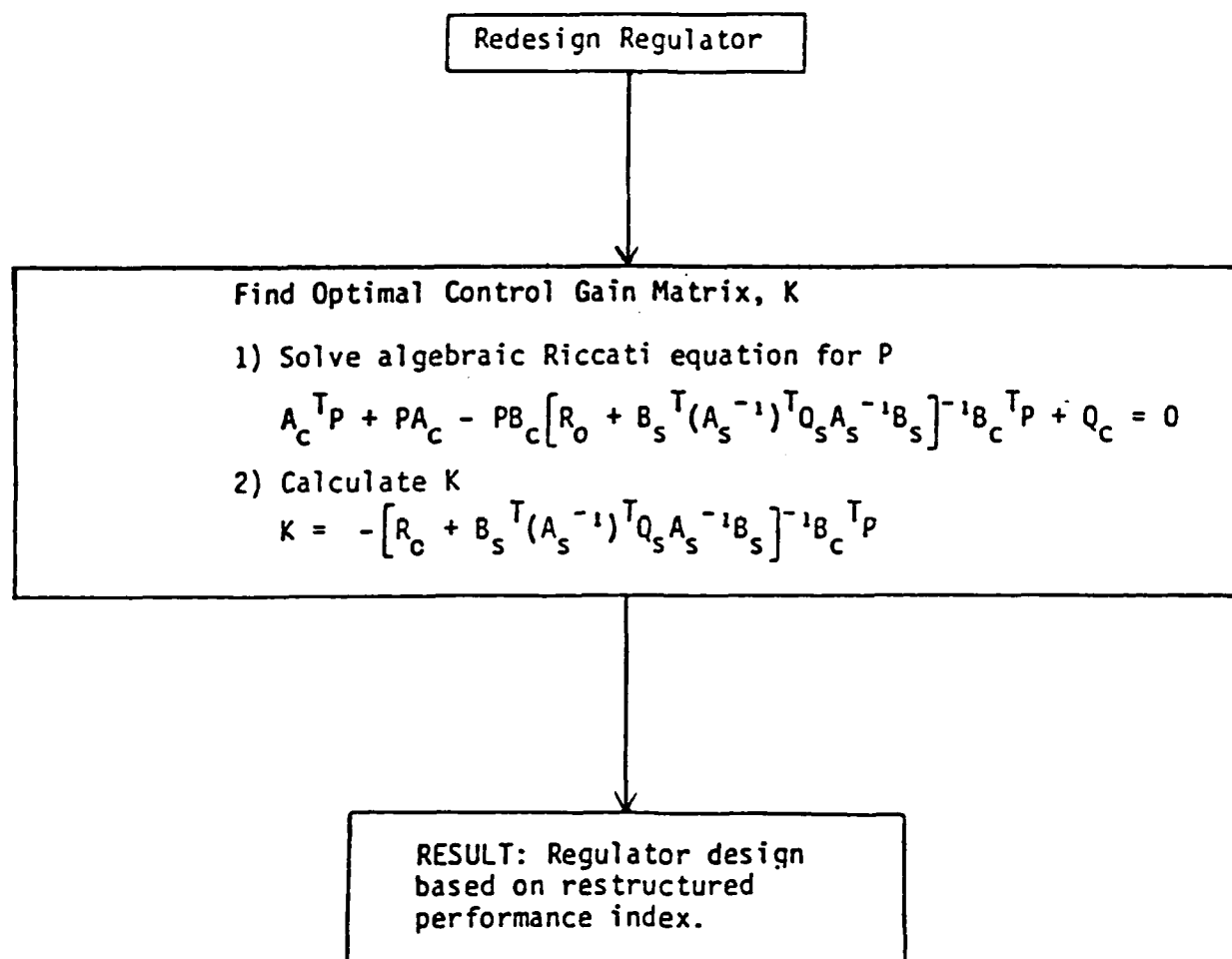
Standard LQG control methods are applied to design the state estimator. The system model is then tested for spillover and if spillover is a problem, the MESS algorithm is applied.



A fundamental concept behind the MESS algorithm is to restructure the performance index (PI). Initially, the PI is a function of controlled and suppressed states, and the control vector. Singular perturbation is forced in the suppressed state model, and the resulting expression is substituted into the original performance index.



The restructured PI is now used with optimal control techniques to redesign the regulator and to determine the modified control law.



### 2.3.6 Conclusion.

2.3.6.1 The LSS control techniques discussed include Lockheed's LAC/HAC, TRW's Positivity, and General Dynamic's MESS. Although each approach is observedly different, each technique employs the same objective, optimal performance when presented with an inaccurate plant model. Each technique addressed the problem of the destabilizing effect of uncontrolled modes on the system. TRW concludes that application of the positivity theorem to LSS assures stability (i.e. system will not become unstable due to observation and control spillover effects.). In addition, positivity more indepthly (than LAC/HAC or MESS) examines the problem of non-colocation and inclusion of actuator and sensor dynamics. Lockheed concludes that the LAC/HAC algorithm eliminates spillover instabilities through the application of frequency shaping. General Dynamics concludes that MESS solves the problem of known modal truncation through restructuring of the performance index.

2.3.6.2 An orderly flowchart format of each technique's control law design procedure is extremely helpful when comparing and considering development of the control schemes. The flowchart helps one draw conclusions about the practicality of each technique in the situation of LSS.

2.3.7 Activities Participated In and Conducted Relative to the Evaluation of ACOSS Control Methodologies. During the February 1982 - February 1984 period, Control Dynamics senior personnel collaborated with counterparts of other organizations at the meetings and conferences listed. Their active participation contributed measurably to the objective, in-depth evaluation of control methodologies presented in this section.

	<u>Meeting Topic  . Organization</u>	<u>Date</u>	<u>Location</u>	<u>Control Dynamics Participants</u>
1.	Power Spectral Density Model . Draper Laboratory	March 15, 1982	Cambridge, MA	Dr. Seltzer Dr. Doane
2.	Stochastic Approach to Model Development . Lincoln Laboratory	March 16, 1982	Lexington, MA	"
3.	JOSIE Program . Draper Laboratory and ITEK	March 16, 1982	"	"
4.	Large Space Structures Program . Marshall Space Flight Center	April 30, 1982	MSFC, AL	Dr. Seltzer
5.	ACOSS Methodology . TRW . Draper Laboratory	June 2, 1982	Riverside Research Arlington, VA	Dr. Seltzer
6.	VCOSS Methodology . Lockheed - Palo Alto	June 16, 1982	Wright- Patterson AFB, OH	Dr. Seltzer
7.	VCOSS Methodology . TRW	June 17, 1982	"	"
8.	ACOSS Methodology . Minneapolis - Honeywell	June 29, 1982	Riverside Research Arlington, VA	Dr. Seltzer Dr. Doane
9.	Power Spectral Density Model . Draper Laboratory	June 29, 1982	Riverside Research Arlington, VA	Dr. Seltzer Dr. Doane
10.	Spacecraft Disturbances . Control Dynamics	June 29, 1982	"	"

<u>Meeting Topic • Organization</u>	<u>Date</u>	<u>Location</u>	<u>Control Dynamics Participants</u>
11. Workshop on "Application of Distributed Systems Theory to the Control of Large Space Structures" • JPL	July 14-16, 1982	Pasadena, CA	Dr. Doane
12. Guidance, Control, and Dynamics Conference • AIAA	August 9-11, 1982	San Diego, CA	Dr. Seltzer Dr. York
13. ACOSS Phase II Final Technical Review • Lockheed	September 23, 1982	Palo Alto and Sunnyvale, CA	Dr. Seltzer
14. ACOSS Final Technical Review • TRW	December 16, 1982	Los Angeles, CA	Dr. Seltzer
15. LAMP • ITEK	December 20, 1982	Lexington, MA	Dr. Seltzer
16. LAMP • Perkin-Elmer	December 21, 1982	Danbury, CN	Dr. Seltzer
17. Structural Control of Deployed Optical Systems • SPIE	January 20, 1983	Hughes Corp. Los Angeles, CA	Dr. Seltzer Dr. Worley
18. VCOSS - I Final Review Review • Lockheed	March 8, 1983	Wright- Patterson AFB, OH	Dr. Seltzer
19. VCOSS - I Final Review • TRW	March 9, 1983	"	"
20. Guidance and Control Conference • AIAA	August 15-17, 1983	Gatlinburg, TN	"
21. 9th Strategic Symposium • DARPA	October 4-7, 1983	Monterey, CA	"

## 2.4 Task 4 - Determination of Optimal Form for ACOSS Controller

2.4.1. Introduction. The determination of an optimal form for the ACOSS model is the subject of the work presented here. The structural model used was developed by Control Dynamics under the ACOSS/VCOSS program. The emphasis on the control system design was primarily one of simplicity. The idea was to keep the design as straightforward as possible and to increase the level of complexity of the design as well as the fidelity of the model as more knowledge of the control problem was determined.

The control scheme used here involves using the frequency domain design tools to design a two loop digital control system. The initial design of the inner loop is performed to design a tracking notch filter by phase stabilizing the unstable outer loop bending modes, and gain stabilizing all other modes. After the inner loop is closed and cascaded with the outer loop, compensation is then derived to stabilize the outer loop. This design technique has shown that it is possible to retain an appreciable bandwidth while suppressing vibrational modes and disturbances.

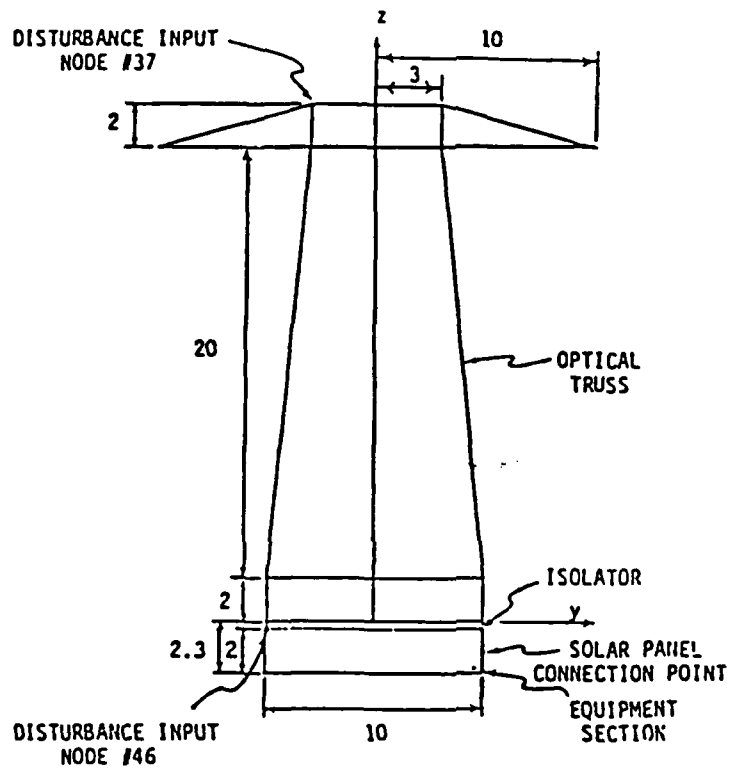
2.4.2 Control Law Formulation. The preliminary control law developed for ACOSS model #2 is based on one sensor actuator pair. For attitude control of the structure, a torque actuator was placed between the equipment section and the optical truss. An accelerometer package is needed at the equipment section to sense translational motion. Finally, a sensor is needed at the focal plane to detect errors in the line of sight (LOS). A planar model of the ACOSS model #2 in the y-z plane is shown in Figure 4-1. The input actuator in the model is a torque actuator located along the z-axis midway between the optical truss and the equipment section. The accelerometer measurement will be used to construct the inner loop notch filter.

The block diagram of the control system for the planar model shown in Figure 4-2 includes one disturbance input and one control input. The sensors are an accelerometer at node 46 in the equipment section (inner loop) and the focal plane error (outer loop).

The multi-loop control scheme has been applied in the design of control systems for large flexible structures of the DARPA type. In the next section the design technique is illustrated by way of an example.

2.4.3. Multi-loop Design Technique. The multi-loop design technique developed for DARPA is illustrated here with an example. The block diagram of Figure 4-2 will be used where the modal data is given in Table 4-1 (Figure 4-3).

The design procedure is initiated by computing the outer loop frequency response and determining which modes are significant. Using block diagram algebra and Mason's Gain Formula the uncompensated outer loop transfer function is given by



ALL DIMENSIONS IN METERS  
 NODE #37 (-4,-3,24)  
 NODE #46 (-4,-5,-.3)

Figure 4-1. Y-Z Planar Projection of ACOSS Model #2 (Solar Panels Omitted).

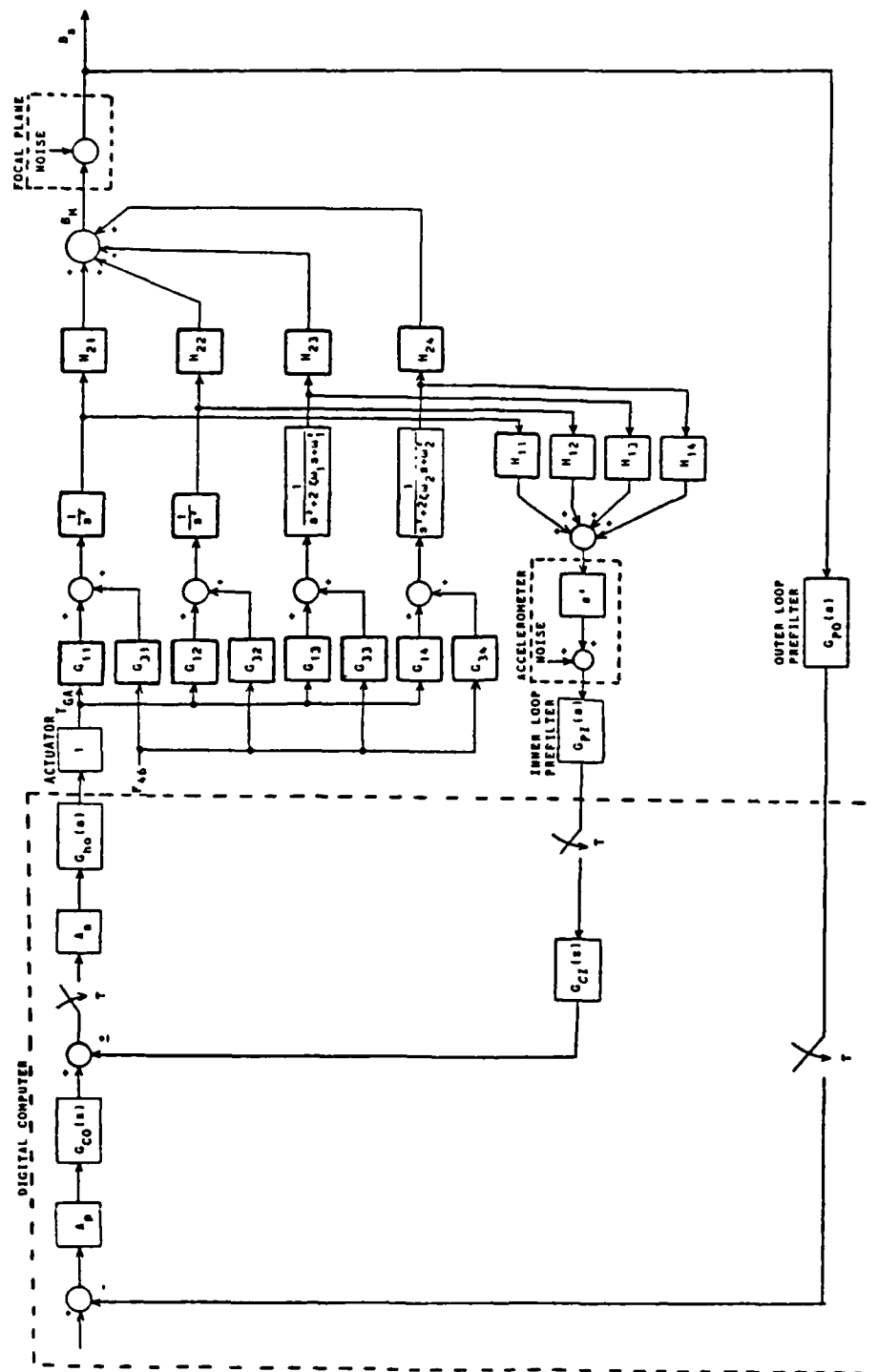


Figure 4-2. Block Diagram of Control System for ACROSS Model #2

Table 4-1. Modal Data Used in Design Example

Mode	Freq. (rad/sec)	Freq. (Hz)	INNER LOOP MODAL GAIN	OUTER LOOP MODAL GAIN
RIGID BODY	0	0	0	0
RIGID BODY	0	0	$6.298 \times 10^{-6}$	$3.1145 \times 10^{-4}$
1	56.495	8.997	$1.64815 \times 10^{-3}$	$3.11022 \times 10^{-3}$
2	59.709	9.503	$1.1362 \times 10^{-5}$	$4.97848 \times 10^{-5}$
3	64.955	10.338	$4.05327 \times 10^{-6}$	$3.41787 \times 10^{-5}$
4	118.526	18.864	$2.67517 \times 10^{-7}$	$6.06852 \times 10^{-6}$
5	198.554	31.100	$-5.30946 \times 10^{-3}$	$4.35723 \times 10^{-5}$

Figure 4-3. Modal Data for Plant Shown in Figure 4-2.

$$\mathcal{Z}[G_{OL}(s)] = A_p A_a G_{IC}(z) \mathcal{Z}\{G_{PO}(s) G_{HO}(s) F(s)\} \quad (4-1)$$

where

$$F(s) = \left[ \frac{G_{11}H_{21}}{s^2} + \frac{G_{12}H_{22}}{s^2} + \sum_{i=1}^N \frac{G_{1i+2}H_{2i+2}}{s^2 + 2\zeta\omega_{ni}s + \omega_{ni}^2} \right]$$

where  $G_{HO}(s)$  is the transfer function for a zero order hold,  $A_p$  is the outer loop gain constant,  $A_a$  is the inner loop gain constant,  $G_{IC}(z)$  is the z-domain closed loop transfer function of the inner loop between the output of the outer loop compensator  $G_{CO}(z)$  and the input to the block labeled  $A_a$ ,  $\zeta$  is the modal damping ratio for each mode and is assumed to be 0.5%,  $\omega_{ni}$  is the undamped natural frequency of the  $i$ th mode,  $G_{11}H_{21}$  and  $G_{12}H_{22}$  are the rigid body modal gains for the outer loop,  $G_{1i+2}H_{2i+2}$  is the modal gain of the  $i$ th bending mode of the outer loop where  $i=1, 2, \dots, N$ . The closed loop transfer function of the inner loop is given by

$$G_{IC}(z) = \frac{1}{1 - G_{CI}(z) \mathcal{Z}[G_{IO}(s)]} \quad (4-2)$$

where  $G_{IO}(s)$  is the uncompensated open loop transfer function of the inner loop, given by

$$\mathcal{Z}[G_{IO}(s)] = A_a \mathcal{Z}\{G_{PI}(s) G_{HO}(s) \left[ \frac{G_{11}H_{11}}{s^2} + \frac{G_{12}H_{12}}{s^2} + \sum_{i=1}^N \frac{G_{1i+2}H_{1i+2}}{s^2 + 2\zeta\omega_{ni}s + \omega_{ni}^2} \right]\} \quad (4-3)$$

and  $G_{CI}(z)$  is the inner loop digital compensation. The frequency response of the uncompensated outer loop in Equation (4-1) was computed using the sampled-data frequency domain computer-aided design tools and is shown in Figure 4-4. The response shows that only the first bending mode (56.495 rad/sec) is significant. Hence, the inner loop will be designed such that a notch occurs at the frequency corresponding to the first bending mode.

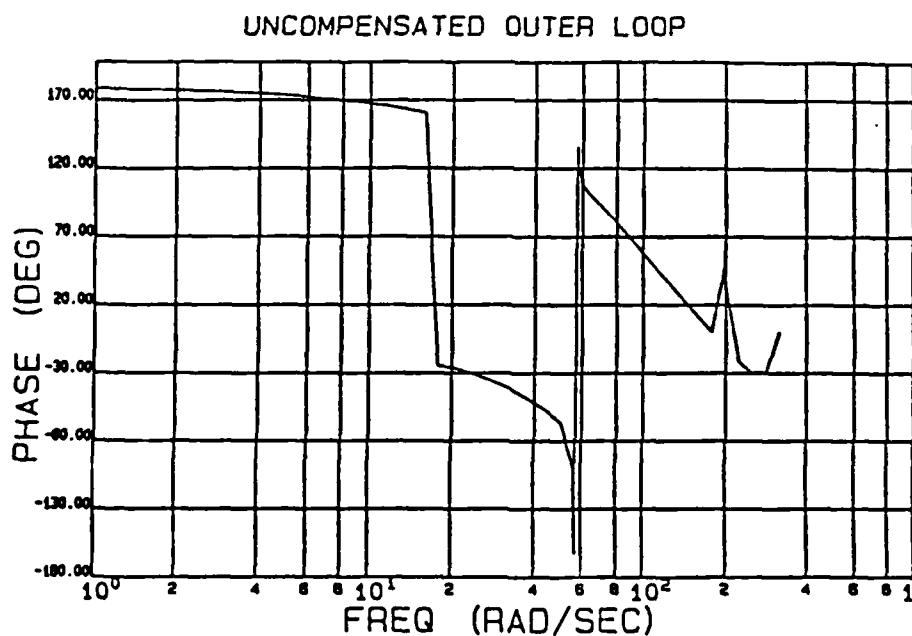
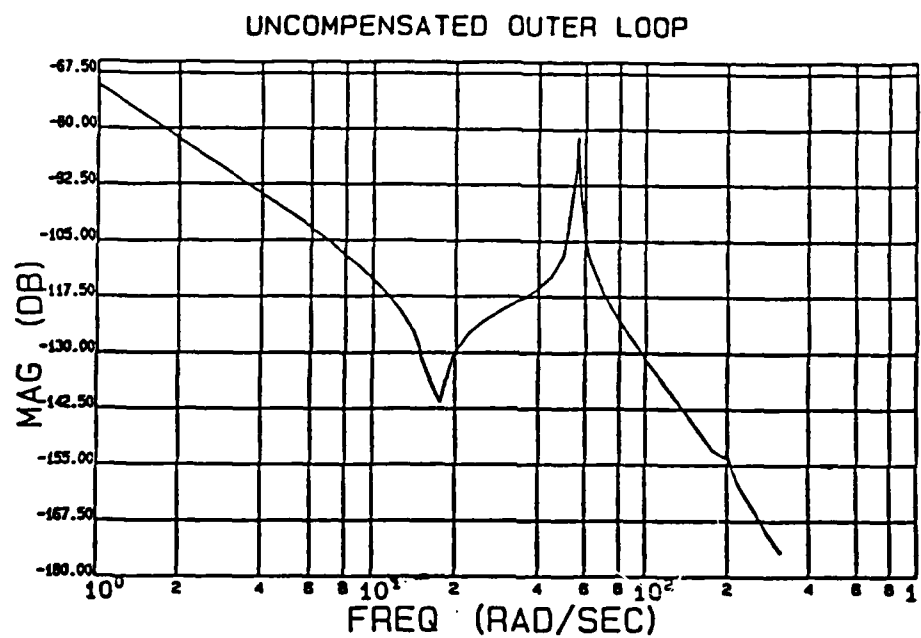


Figure 4-4. Frequency Response of the Uncompensated Outer Loop (Inner Loop Open)

2.4.3.1 Inner Loop Design. The frequency response of the uncompensated inner loop is shown in Figure 4-5. The response shows that the first and fifth bending mode basically determine the stability of this loop. The outer loop response has shown that only the first bending mode is significant in that loop. Therefore, the compensation for the inner loop will be designed to phase stabilize the first bending mode to preserve the peak so that when it is closed a notch will occur at this frequency. The fifth bending mode will then be gain stabilized. A two stage digital compensator that will achieve these specifications was designed using the direct z-domain analytical design technique. The compensator is given by

$$G_{CI}(z) = G_{C11}(z) \cdot G_{C12}(z)$$

where

$$G_{C11}(z) = \frac{(z + 1)^2}{31.25581 z^2 - 46.67205z + 19.41624} \quad (4-4)$$

and

$$G_{C12}(z) = \frac{6.0085z - 4.0085}{8.9159z - 6.9159} \quad (4-5)$$

The first stage is an underdamped second-order dominant pole compensator with a damping ratio of 0.6 and a break frequency of 40 rad/sec. It was designed to phase stabilize the first bending mode by contributing -120 degrees at a frequency of 56.495 rad/sec (the frequency of the first bending mode). At higher frequencies the gain of this compensator continues to decrease and therefore serves to gain stabilize the fifth bending mode (198.554 rad/sec). The second stage is a digital lag compensator designed to provide sufficient gain margin at a frequency of 31 rad/sec. The frequency response of the compensated inner loop, magnitude and phase, is shown in Figure 4-6. The response shows that the loop has two gain and two phase margins:

$$\begin{aligned} GM_1 &= 6 \text{ dB} @ 32 \text{ rad/sec} \\ GM_2 &= 31 \text{ dB} @ 130 \text{ rad/sec} \\ PMA &= 50^\circ @ 45 \text{ rad/sec} \\ PMB &= 80^\circ @ 62 \text{ rad/sec} \end{aligned}$$

Further observation indicates that the magnitude and phase of the compensated inner loop response at the frequency of the first bending mode are

$$\begin{aligned} M_{u1} &= 28 \text{ dB} \\ P_{u1} &= -10^\circ \end{aligned}$$

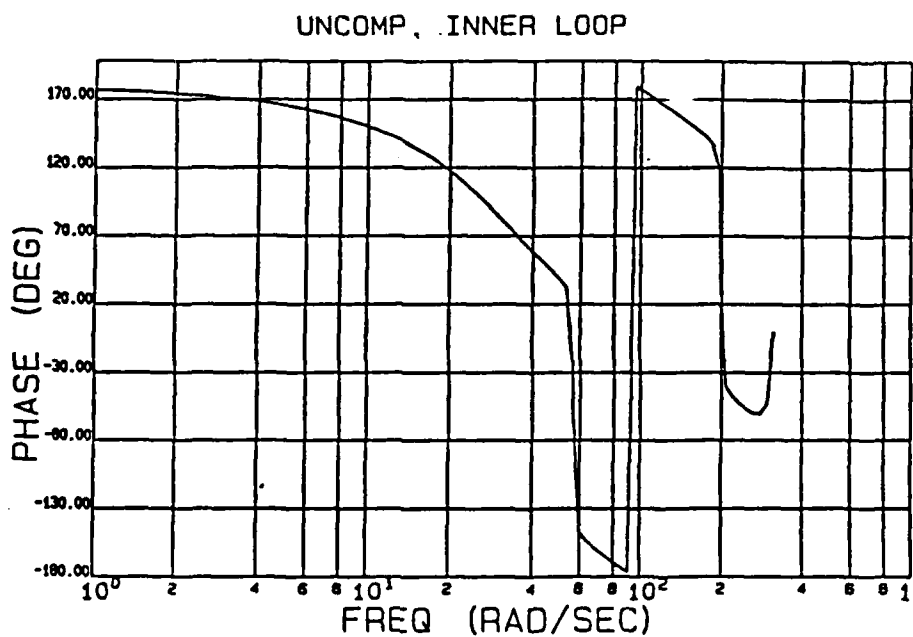
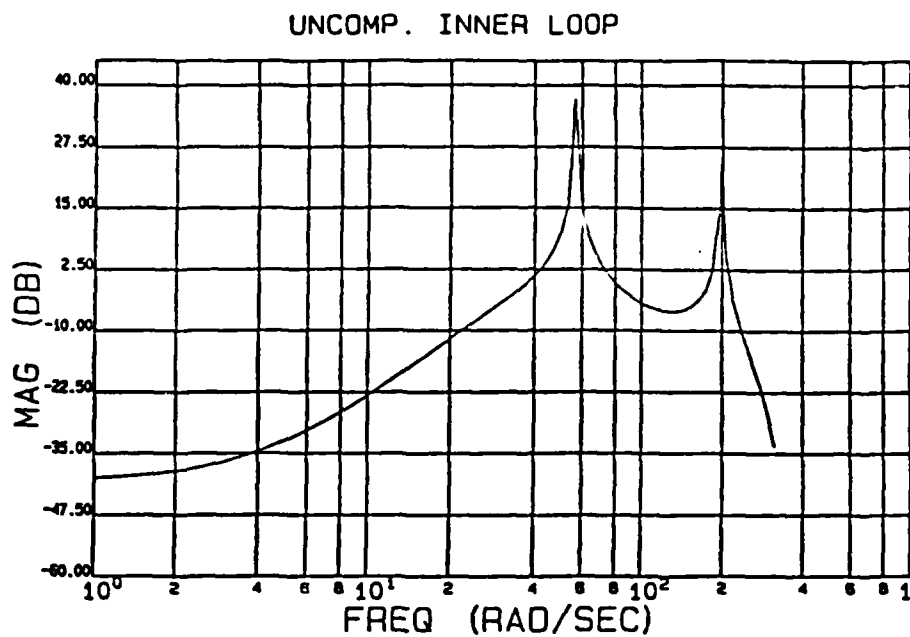


Figure 4-5. Frequency Response of the Uncompensated Inner Loop

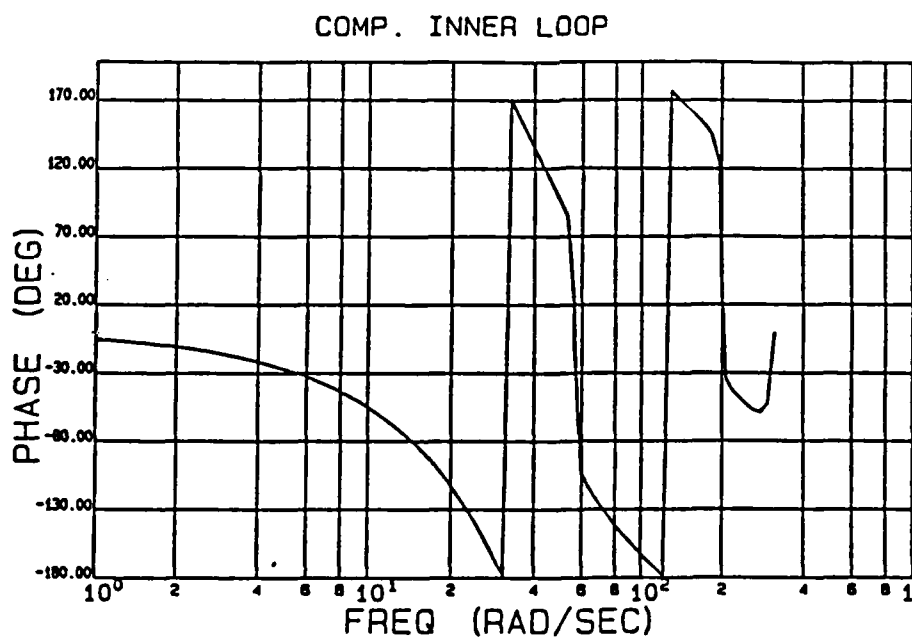
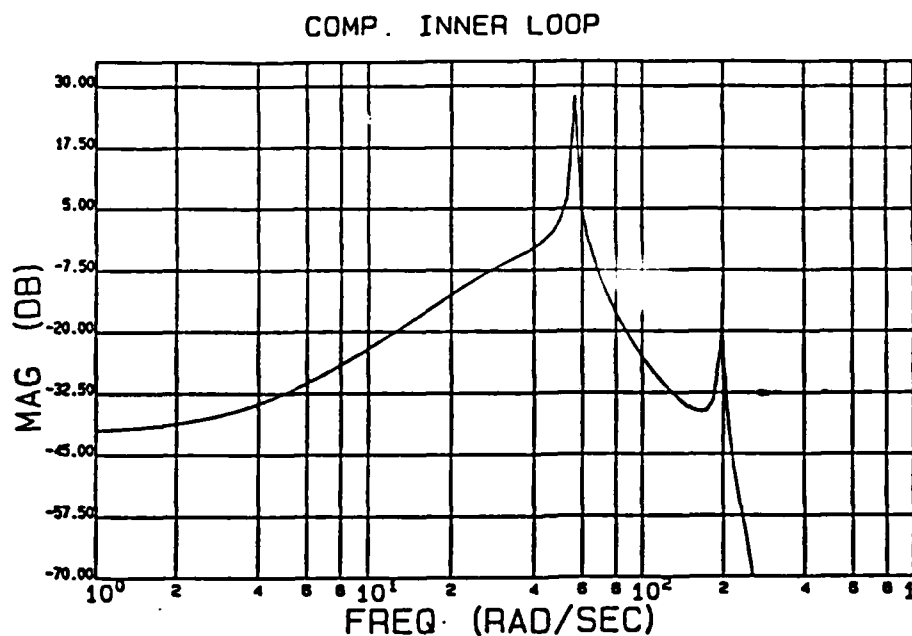


Figure 4-6. Frequency Response of the Compensated Inner Loop

which shows that this mode is in fact phase stabilized. The magnitude of the response at the fifth mode is

$$P_{\omega 5} = -10 \text{ dB}$$

which also shows the fifth bending mode to be gain stabilized. Finally, the closed loop response for the compensated inner loop is given in Figure 4-7. This response shows a notch occurring at the frequency of the first bending mode. With the inner loop compensated and closed, the design of the outer loop follows.

2.4.3.2 Outer Loop Design. The frequency response of the outer loop with the compensated inner loop closed is illustrated in Figure 4-8. Comparison of Figure 4-8 and Figure 4-4 shows that the inner loop notch has provided some desirable attenuation of the first bending mode.

Sketching the Nyquist plot of the outer loop shows the loop to be unstable. Analysis of this response shows that phase lead will stabilize the system. Thus, compensation for the outer loop will be designed to stabilize the system, and maximize closed loop bandwidth. Again using the analytical frequency domain compensator design technique, the compensation necessary to stabilize the outer loop was determined to be:

$$G_{C0}(z) = G_{C21}(z) \cdot G_{C22}(z)$$

where

$$G_{C21}(z) = \frac{(200.9983z - 198.9983)(z + 1)}{132.6555z^2 - 243.58133z + 114.92579} \quad (4-6)$$

$$G_{C22}(z) = \frac{(z + 1)}{8.36235z - 6.36235} \quad (4-7)$$

where the first stage is a lead-lag compensator and the second stage is a lag type compensator. The Bode plot for the compensated outer loop is shown in Figure 4-9. The response shows that with the compensation previously derived the following stability margins were achieved:

$$PM_1 = 33^\circ \quad @ \quad 8.2 \text{ rad/sec}$$

$$GM_A = 7.5 \text{ dB} \quad @ \quad 12.6 \text{ rad/sec}$$

$$GM_B = 5.2 \text{ dB} \quad @ \quad 34 \text{ rad/sec.}$$

The computer-aided design tools make it a relatively simple task to compute the closed loop frequency response of the system. This response is shown in Figure 4-10. The plot shows the bandwidth to be approximately 12.6 rad/sec.

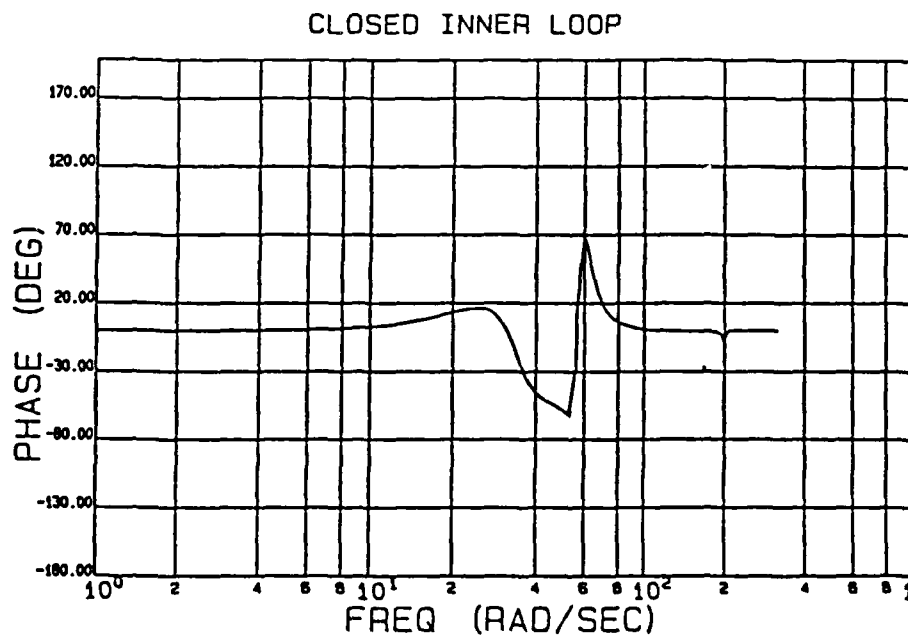
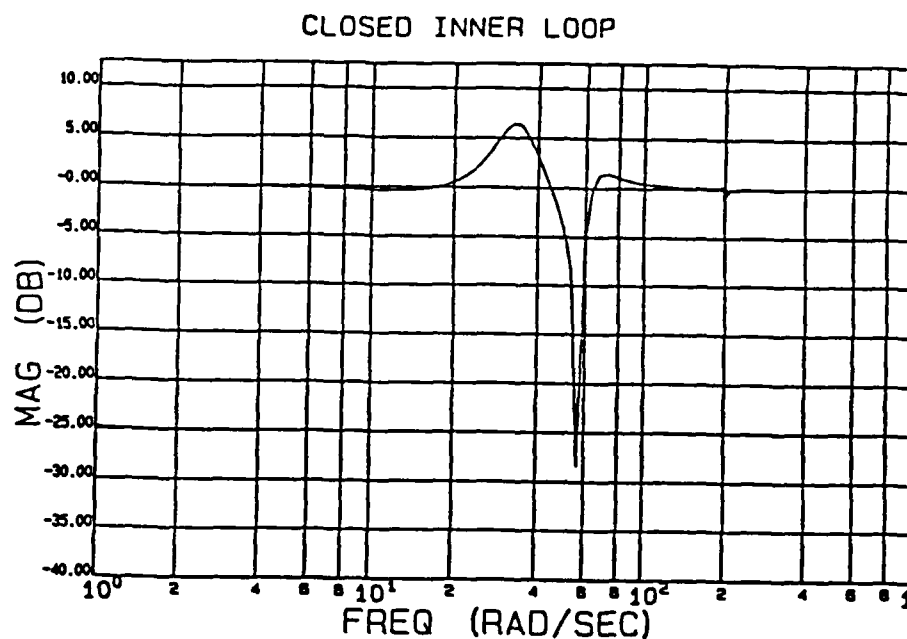


Figure 4-7. Closed Loop Frequency Response of the Compensated Inner Loop

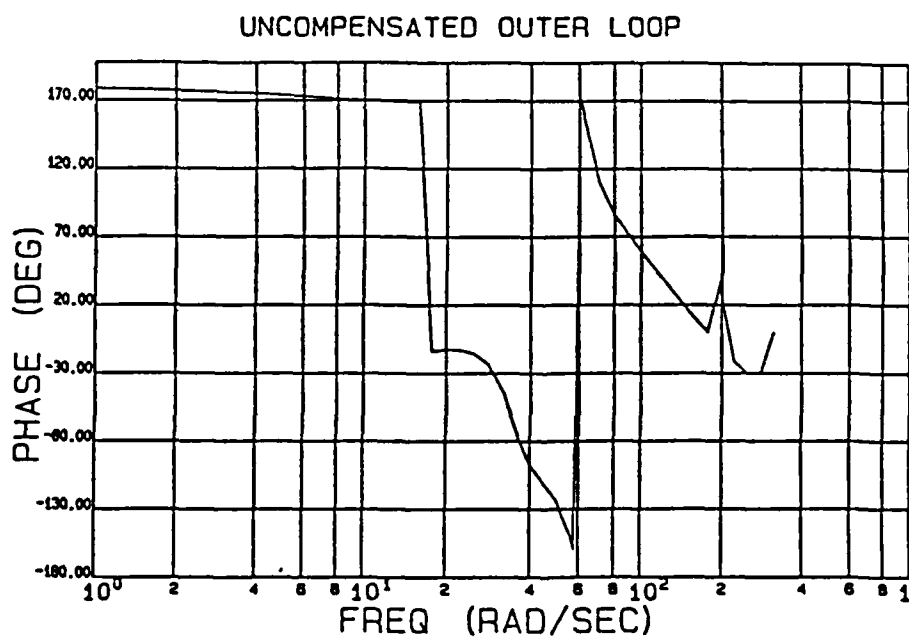
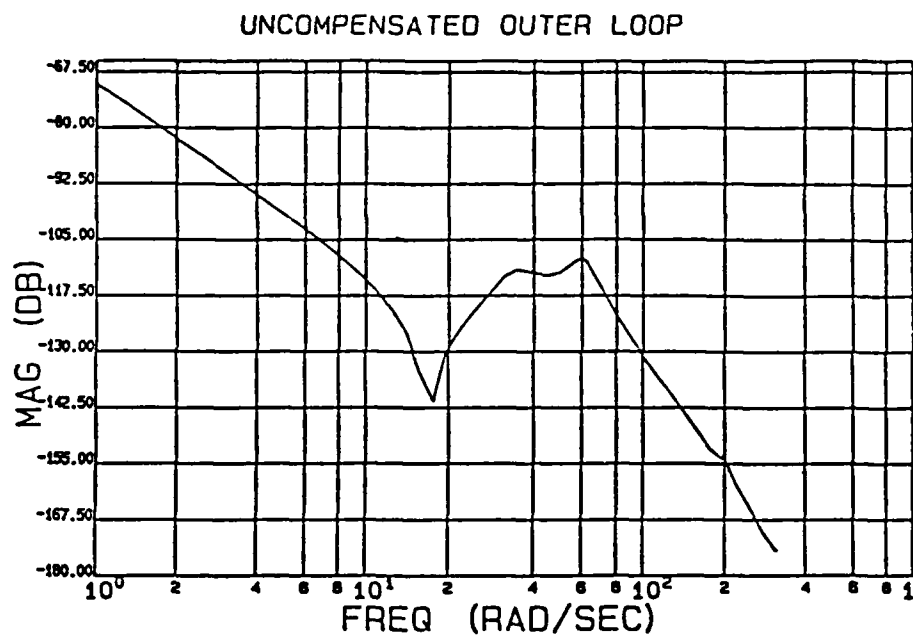


Figure 4-8. Frequency Response of the Uncompensated Outer Loop (Inner Loop Closed)

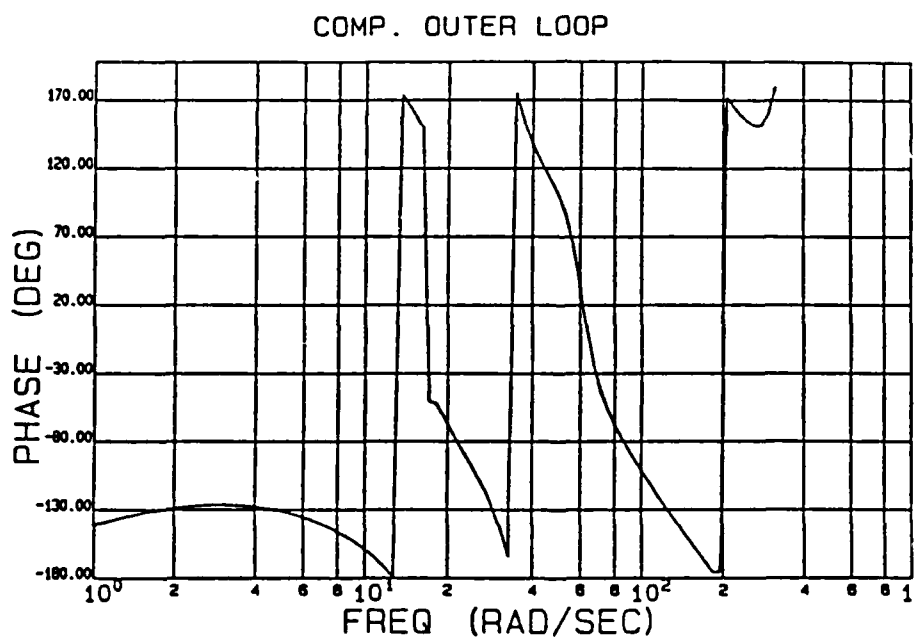
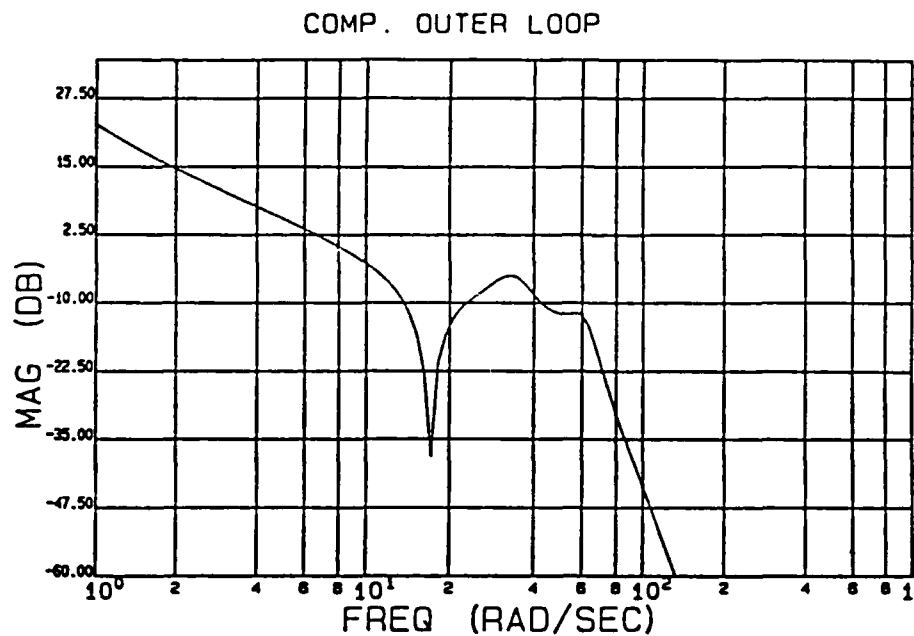


Figure 4-9. Frequency Response of the Compensated Outer Loop (Inner Loop Closed)

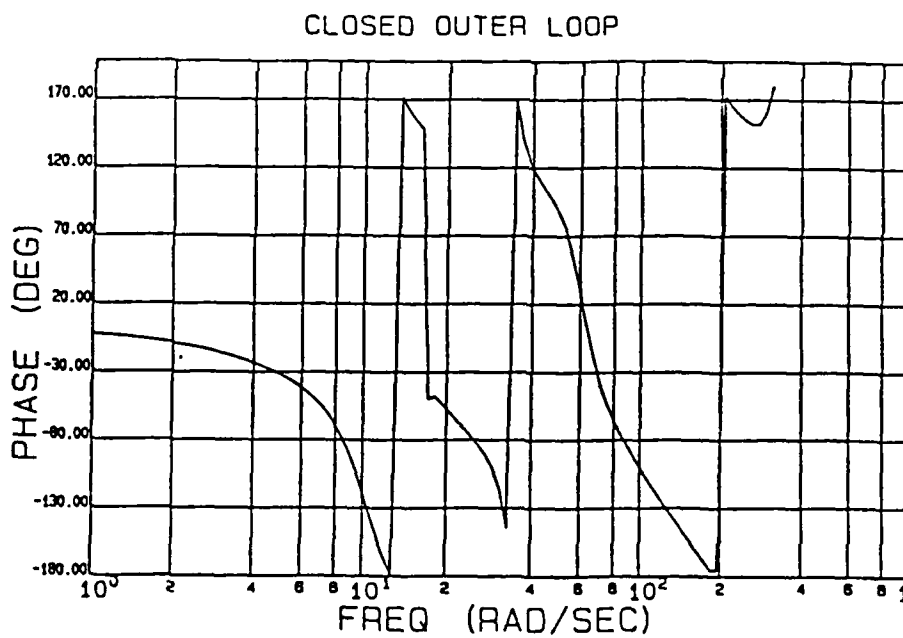
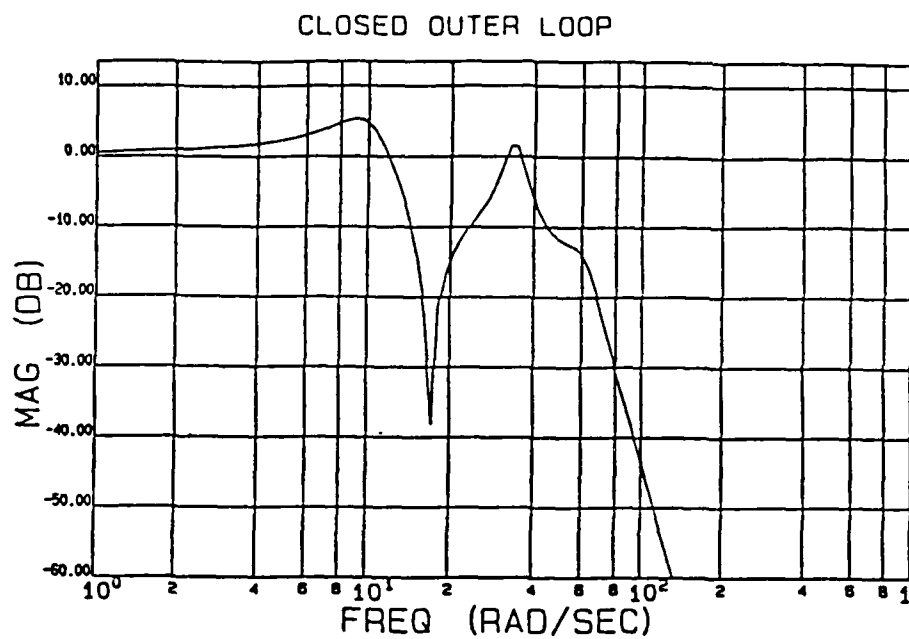


Figure 4-10. Closed Loop Frequency Response of the Outer Loop

2.4.4. Summary of Design Technique/Tools. The application of the computer aided-design tools to design a digital control system for a class of Large Space Structures has been demonstrated. It has been shown that the design tools reduce the computational burden associated with the design process. The tools have been designed such that the model can assume as many bending modes as necessary.

The form of the control system for the DARPA Structure has been developed. The preliminary analyses show that it is possible to design the system with a bandwidth that actually extends beyond the frequency of the significant bending modes. Sensitivity studies indicate that the multi-loop design technique is also "robust" relative to variations in modal data. In the example given in Section 2.4.3, modal frequencies were varied from  $\pm 10\%$  and  $\pm 20\%$  of their nominal values. The results showed that the system response was reasonably stable up to  $\pm 20\%$ .

2.5 Task 5 - Investigation of Structural Damping Models. Early in the performance of this task, it became obvious that the work and results were so closely related to that of Task 2 - Extensions of Modeling Techniques, that it was considered appropriate to report the monthly progress made in the two tasks under the Task 2 heading. To provide the reader and potential user of the results a comprehensive presentation and discussion of the work in the area of LSS modeling techniques and structural damping models, the work and results relative to this task are contained in the Task 2 section (2.2) in this report.

## 2.6 Task 6 - Implementation of Component Cost Analysis.

2.6.1. Introduction. The mathematical models of physical systems which are to be controlled are usually reducible to a linear form. The standard methods of control design assume this as a starting point. These models are frequently of very large dimension such that it becomes impractical to employ them directly in the design process. Because of this, analysts and designers usually work with a truncated or reduced order model. The methods for reducing the order of a high order system model are a part of the folklore of the designers' art in the field. Thus, each individual analyst may well have his own pet technique for accomplishing reduction. Of course, in the final analysis it is the performance that is the proof of any design, and the analytical exercises become merely the means for establishing the preliminary design which is then confirmed only after an extensive test program involving as much of the actual hardware as can be obtained. However, the lighter weight aerospace structures are becoming less amenable to ground based testing prior to flight due to the reduced tolerance to the 1 G earth environment. These factors have motivated this look at two of the techniques that are currently being used to guide the modal truncation process.

2.6.2 Discussion. The typical mechanical system can be modeled by a 2nd order, vector-matrix differential equation. Using a vector  $\underline{q}$  of generalized coordinates to represent the system configuration, we can write

$$M\ddot{\underline{q}} + C\dot{\underline{q}} + K\underline{q} = \underline{B}w \quad (6-1)$$

$$\underline{y} = \underline{P}'\dot{\underline{q}} + \underline{P}\underline{q} \quad (n \times 1)$$

$$M^T = M;$$

$$K^T = K;$$

M and K are symmetric matrices,  
M is positive definite,  
and K is nonnegative definite.

We have used the vector  $\underline{y}$  to represent the set of variables subject to measurement and assumed that they are linear functions of system coordinates or velocities which are not otherwise observable in the physical system. Matching physical measurements with analysis results consists of comparing values of  $\underline{y}$ . Acceptability of this match depends on whether the values fall within the required tolerances. If we let  $\tilde{\underline{y}}$  represent the measured values and  $\underline{y}$  the analytical values, then we can write the requirements as

$$|y_i - \tilde{y}_i| < r_i \quad (6-2)$$

These requirements represent the degree to which we desire the physical model to match the mathematical model. Frequently, the mathematical model is too large at this stage to be used conveniently or economically. For this reason, truncation procedures which can be applied to the mathematical model

to reduce it to a more convenient size while giving a measure of the degree of error incurred in the process are desirable. Several methods exist for doing this. We shall discuss two of them. The first method which we shall discuss is called Modal Cost Analysis (MCA) and is taken from "Modal Cost Analysis for Linear Matrix-Second-Order Systems," R. E. Skelton and P. C. Hughes, Journal of Dynamic Systems, Measurement and Control, September 1980, Vol. 102-pp. 151).[12] This method treats the problem of truncation from either of two viewpoints which result in the same truncation criteria. The second method does not have a name but, for convenience, let us refer to it as Old Tried and True (OT<sup>2</sup>). Both approaches (MCA and OT<sup>2</sup>) begin with a cost function defined in terms of the system measurement vector  $y$ . The term cost function is used here in the mathematical sense and arises from its similarity to such usage in the theory of extremization as in the Calculus of Variations. For MCA, the cost function is for the analyst to define within the usual restrictions for cost functions, i.e., it must be positive definite. It is desirable to select a cost function that provides a "good" description of model error. The meaning of "good" must be left for the analyst to define. For OT<sup>2</sup>, the term cost function is used simply for comparison with MCA. It should more appropriately be called the "modal peak function" since the values are the modal peak amplitudes on the output response curve. The MCA approach is statistical in nature and requires that certain assumptions be made concerning the nature of the disturbance vector  $w$ . First, any deterministic disturbances are assumed to be absorbed into the differential equation so that the remaining disturbance  $w$  is stochastic in nature. Second,  $w$  is uncorrelated in time and has zero mean. Thus,

$$E \{w\} = 0 \quad (6-3)$$

$$E \{w(t)w(\tau)^T\} = \sigma\delta(t - \tau) \quad (6-4)$$

The system equations given in Equation 6-1 can be transformed to modal variables, coordinates such that

$$\underline{q} = \underline{\phi}\eta \quad (6-5)$$

$$\underline{\phi}^T M \underline{\phi} = 1 \quad (6-6)$$

$$\underline{\phi}^T K \underline{\phi} = \Lambda^2 = \text{diag} (\omega_1^2, \omega_2^2, \dots, \omega_n^2). \quad (6-7)$$

Under this same transformation the damping matrix  $C$  is transformed to the matrix  $D$ .

$$\underline{\phi}^T C \underline{\phi} = D. \quad (6-8)$$

Frequently, for mechanical systems such as aerospace structures which are lightly damped, it is sufficient to approximate the matrix  $D$  by a diagonal

- 
12. Skelton, R.E. and Hughes, P.C., "Modal Cost Analysis for Linear Matrix Second Order Systems," Journal of Dynamics Systems, Measurements and Control, September 1980, Vol. 102 - pp. 151.

matrix. Thus, we shall henceforth treat  $D$  as a diagonal matrix. It is convenient to express this diagonal  $D$  matrix in terms of the fraction of critical damping, the diagonal matrix  $\zeta$

$$D = 2\zeta\Lambda \quad (6-9)$$

Using Equation 6-1 together with 6-5 through 6-9, we obtain the so-called modal equations

$$\begin{aligned} \ddot{\underline{n}} + 2\zeta\Lambda\dot{\underline{n}} + \Lambda^2\underline{n} &= \underline{Q}\underline{w} \\ \underline{y} &= \underline{C}\dot{\underline{n}} + \underline{n} \end{aligned} \quad (6-10)$$

These equations then become the working equations for modal cost analysis. We must now construct a useful cost function which shall become the basis of our modal truncation considerations. Ideally, we desire a cost function based on the model error components as in Equation 6-2. It is tempting to define a modeling error "cost" function  $V$  in terms of the difference  $\underline{y} - \hat{\underline{y}}$ , where  $\underline{y}$  is computed from the original, large dimensional system model as given in Equation 6-10, and  $\hat{\underline{y}}$  is computed using a truncated version of Equation 6-10 in which certain modal coordinates are dropped from consideration as being relatively unimportant in their effect on  $\underline{y}$ . The determination of this relative importance is what this study is all about. For now, we shall define the cost function in terms of the measurement vector  $\underline{y}$  only

$$V = \lim_{t \rightarrow \infty} E \{ \underline{y}^T Q \underline{y} \} ; \quad (6-11)$$

$$Q^T = Q \text{ and } Q \text{ is positive definite.}$$

We shall show later that maximizing the cost  $V$  of the truncated system has the effect of minimizing the model error introduced by truncation. In Appendix B it is shown that for lightly damped, mechanical systems such as described by Equation 6-10, the cost function  $V$  can be separated into a sum of terms each of which depends only on a single mode. These terms are referred to as modal costs. Thus,

$$V = \sum V_\alpha; V_\alpha \text{ depends only on mode } \alpha \text{ and } V_\alpha \geq 0. \quad (6-12)$$

These modal costs then become indicators of the relative importance of the particular mode in  $V$  and hence in the model error. The differential equations shown in Equation 6-10 which determine the model displacements  $\underline{n}$  are an uncoupled set of  $n$  2nd order differential equations driven by time-dependent disturbances. This implies that the individual modal responses are unaffected by truncation. Since this is the case and since the cost function is decomposed into modal costs depending only on the modes separately, the effect of truncation is to reduce the total cost by the sum of the modal costs over the truncated modes. This sum, then, is indicative of model truncation error. If the modes are arranged in descending order of the modal costs such that the lowest order modes have the largest effect on the cost  $V$ ,

then it is the high order modes that become the candidates for truncation from the reduced order model. It is possible that some modes have zero costs and can be safely truncated from the model with no ill effect on the cost. This is not to say that there are no effects on the model results, but only that the effects of such truncation do not noticeably change the system measurement or output vector  $\underline{y}$ . Or in other words the physically measurable parameters are not significantly changed as a result of this truncation. Perhaps this can be viewed in a different light if we consider that the system configuration requires  $n$  coordinates for its specification, but we are only measuring  $n$  quantities in  $\underline{y}$  and thus there is insufficient information to uniquely specify the system state from the measured data. The modeling philosophy being employed in the modal cost analysis technique holds that the only important model parameters are the mathematical counterparts to the physical measurements, i. e., the outputs  $\underline{y}$ .

In order to gain insight into this method let us consider its application to a relatively simple example. At the George C. Marshall Space Flight Center in Huntsville, AL, personnel from NASA and Control Dynamics are developing a large space structure ground-based pointing control experiment and related facility. We have developed a model of this which will serve us here. The system is illustrated in Figure 6-1.

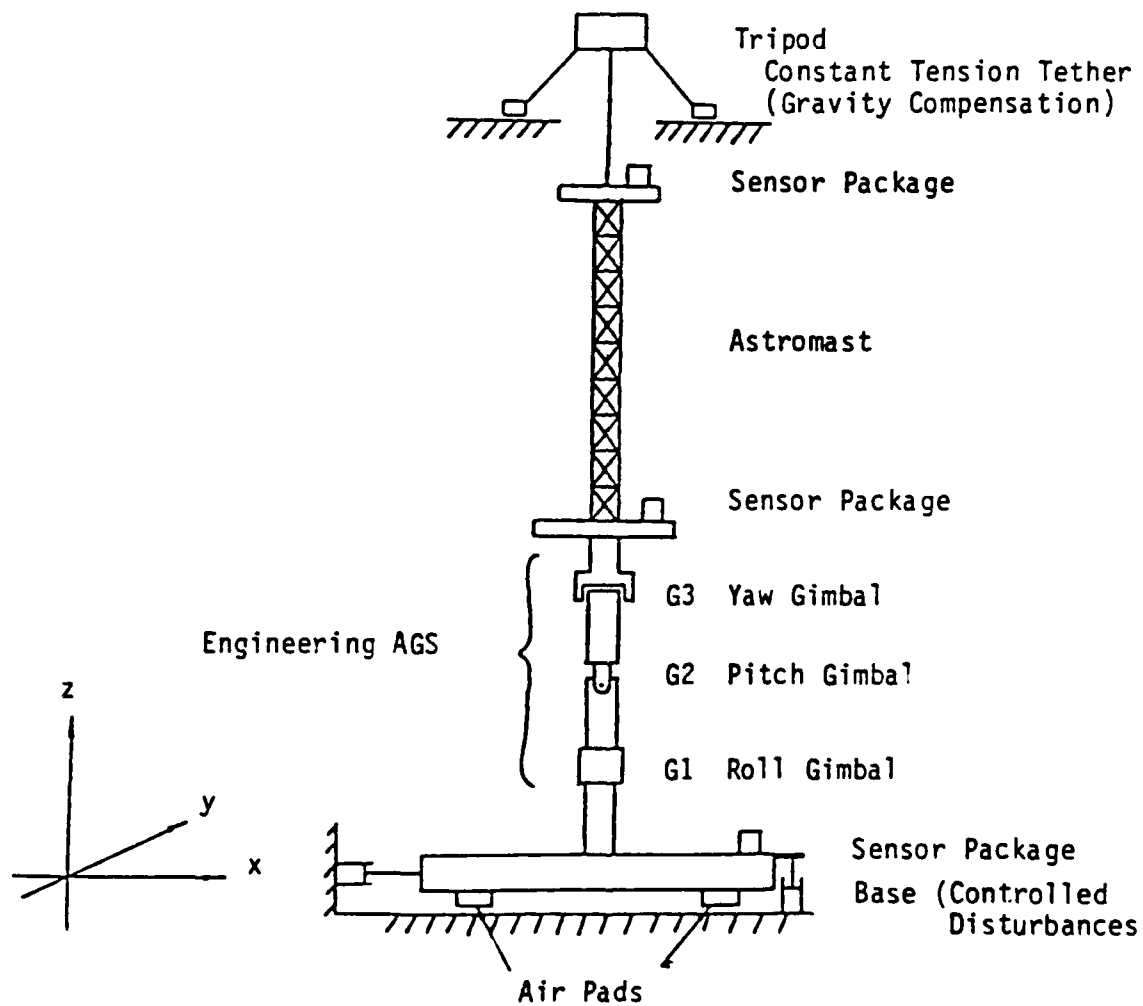


Figure 6-1. Illustration of NASA/MSFC Large Space Structure Ground Based Pointing Control Experiment.

The simplified, planar model of this system consists of the x-translation of the base, y axis gimbal rotation at G2, the first 3 cantilever modes of the astromast treated as a simple beam and the x-translation of the gravity compensation mechanism. This yields a 6 degree-of-freedom model. The choice of three cantilever modes to represent the beam was the result of an intuitive truncation process in which it was felt that the modal frequencies of the higher beam modes were not likely to be excited. This truncation process should probably be revisited but for purposes of this example it is not required. Since we are currently refining our model of this system we have refrained from any refinements of this simple model. The modal version of this model is given below.

$$\ddot{n}_1 + 0n_1 + 0n_1 = [.09451, -.006146]w \quad (6-13)$$

$$\ddot{n}_2 + 0\dot{n}_2 + 0n_2 = [-.8976, .001778]w$$

$$\ddot{n}_3 + .020469\dot{n}_3 + 4.1897n_3 = [-.1379, .007640]w$$

$$\ddot{n}_4 + .05885\dot{n}_4 + 34.64n_4 = [-.6993, .040155]w$$

$$\ddot{n}_5 + .2266\dot{n}_5 + 513.3n_5 = [-.2475, .01613]w$$

$$\ddot{n}_6 + .6825\dot{n}_6 + 4658n_6 = [-.06957, .005251]w$$

$$y = [-.006152, .001776, .005918, -.02791, .1022, -.1773]n$$

$$E \{ \underline{w} \underline{w}^T \} = \begin{bmatrix} 100 & 0 \\ 0 & 1 \end{bmatrix} \delta(t - \tau) = \sigma \delta(t - \tau)$$

For this case we have only a single output so we let  $Q = 1$ . In Appendix B, it is shown that the modal cost function is

$$V_\alpha = \frac{\underline{p}'_\alpha T Q \underline{p}'_\alpha \omega_\alpha^2 + \underline{p}_\alpha T Q \underline{p}_\alpha}{4 \zeta_\alpha \omega_\alpha^3} \underline{\hat{p}}_\alpha T \underline{\hat{p}}_\alpha \quad (6-14)$$

Using Equation 6-1, we compute a modal cost vector (column MCA of Table 6-1) and suppose we choose to select the three most significant modes with which to analyze this system. First, we note that the two zero frequency modes have an infinite modal cost and thus must be included in the reduced model. Thus, we are left with selecting an additional mode from the remaining four.

Under the MCA selection criteria, we select mode 4 to keep since it has the largest modal cost of the remaining modes. Thus, using MCA we have selected modes 1, 2, and 4 as the three "best" modes to model our system. Let us now look at the other technique which we call OT<sup>2</sup>. The selection criteria are discussed in Appendix C and result in a modal factor which is similar in appearance to the modal cost. Thus, let us call this factor  $V_o$ . Then from Appendix C (using the notation above) we have

$$V_{0\alpha} = \sum_{\beta, \rho} \left| \frac{\phi_{\beta\alpha} + i\omega_{\alpha} \phi'_{\beta\alpha}}{2\zeta_{\alpha}\omega_{\alpha}^2} \right|_{\alpha\rho\omega_{\rho}}^2 \quad (6-15)$$

To use this technique, we must estimate expected amplitudes for the driving force  $w$ . We assume here that the force at the base has a magnitude 10 and at the gimbal a magnitude 1. Using these assumptions, we obtain the vector shown under the  $OT^2$  column of Table 6-1.

TABLE 6-1

MCA AND  $OT^2$  SELECTION CRITERIA VALUES

Mode	MCA	$OT^2$
1	$\infty$	$\infty$
2	$\infty$	$\infty$
3	0.00388	0.727
4	0.00934	0.0106
5	0.000275	0.000048
6	0.0000024	$5.88 \times 10^{-7}$

From these results, we see that we should select modes 1, 2, and 3. This conclusion conflicts a bit with MCA. That this should be so is not surprising since the selection criteria are very different from those used under MCA. It is unknown whether there is any equivalence between the two methods.

These methods can be applied to more complex, flexible systems. Appendix D contains a brief discussion of the application of the modal cost analysis method to a continuous, uniform beam model. This model can also be analyzed using the  $OT^2$  technique. With this technique we can proceed in analogous fashion for the first eleven steps. The truncation criteria for  $OT^2$  are based on keeping modes which have the highest response amplitudes as explained in Appendix D. Starting from Appendix D Step 12, we can calculate

$$V_{0\alpha} = \frac{\phi_{\alpha}^2(x_0) \phi_{\alpha}^2(x_a)}{4\zeta_{\alpha}^2 \omega_{\alpha}^4 m_b^2} \quad (6-16)$$

This can be compared with Appendix D Step 16 and reveals that the two truncation methods yield nearly the same results except that  $OT^2$  contains the extra factor  $2\zeta_{\alpha}\omega_{\alpha}$  which tends to reduce emphasis on the higher order modes. This result is similar to that which was noted before for the simple 6 degree-of-freedom model where modes 1, 2, and 4 were retained using MCA while  $OT^2$  procedures suggested 1, 2, and 3 should be retained. Results for the 1st 10 beam modes are shown in Table 6-2.

TABLE 6-2

COMPARISON OF MODAL IMPORTANCE AS DETERMINED BY THE MCA AND OT<sup>2</sup> METHODS

Mode	x 10 <sup>-10</sup> MCA	x 10 <sup>-10</sup> OT <sup>2</sup>	MCA Rank	OT <sup>2</sup> Rank	Parameters
1	100.666	161.27	1	1	$EI = 10^6$ $L = 10$ $M_6 = 1$ $X_0 = L/2$ $X_a = L/4$
2	$1.35 \times 10^{-12}$	$5.39 \times 10^{-14}$	7	7	
3	10.4822	.18659	2	2	
4	$2.59 \times 10^{-13}$	$2.60 \times 10^{-15}$	8	8	
5	.94791	.00607435	3	3	
6	$1.99 \times 10^{-15}$	$8.88 \times 10^{-19}$	6	6	
7	.13535	$4.425 \times 10^{-4}$	4	4	
8	$1.89 \times 10^{-14}$	$4.74 \times 10^{-17}$	9	9	
9	.018735	$3.705 \times 10^{-5}$	5	5	
10	$4.56 \times 10^{-16}$	$7.3 \times 10^{-19}$	10	10	

These results point up the fact that modal truncation is not entirely scientific. The accuracy of the truncated model depends on the disturbances as well as the accuracy of the original model. It appears to be impossible to remove the analyst's subjectivity entirely from the analysis process. It enters into the construction of the system model and thus affects the large dimensional system model. Judgement must be exercised to select the disturbances to be included. This judgement is necessarily based on subjective assessments. Since analysis is always subjective, one can only assess how "good" the analysis was by observing how well the analyst's predictions match experimental reality. Any other kind of assessment is probably unrealistic at best and an exercise in obfuscation at worst.

These two methods (MCA and OT<sup>2</sup>) can be compared on the basis of ease of understanding and application. The application of each method appears to be about equally difficult. However, since the OT<sup>2</sup> method is more pictorially appealing, it seems to be more readily understandable and perhaps from that standpoint better. What remains to be assessed is the effect on overall stability of the control system designs based on MCA vs. OT<sup>2</sup> truncated models. In any event, such proofs are probably academic unless some element of physical reality is injected. The real world will tell if the system is stable. Analysis can only make well-educated but uncertain predictions. Finally, then, the Modal Cost Analysis technique offers a very nice formal way of

treating modal truncation and should appeal to those of mathematical bent and offers greater potential for extension to more general systems and to the problem of modal truncation in general. It would take an exhaustive study to conclude superiority of either technique or of any technique and, until this is done, the analyst's judgement must necessarily continue to be involved in modal simplification.

2.6.3 Conclusion. The Modal Cost Analysis (MCA) method for the truncation of linear system models is a versatile method. It provides a formalism for reducing the order of a large variety of problems. It is oriented toward the optimal control problem and consequently may be somewhat less useful for other applications. Also, it does not seem to take into account questions of stability. It is not clear that the modes selected through the MCA criteria include the ones that are most potentially destabilizing. Also, it appears that there is too much freedom for the analyst to select the reduction criteria, in that much judgment must be exercised for the determination of the statistical behavior of the disturbances and for the selection of the weights to be used in the cost function. This freedom means that it is possible and indeed likely that different analysts working the same problem will arrive at different models and results. Thus, it appears that less formal, more intuitive methods for modal truncation are just as good as the MCA method and perhaps better since they may provide the analyst with more intuitive insights into his particular problem and certainly require less effort in learning a new formalism. The use of formal methods for modal truncation or for model reduction in general is an area in which much more work is needed and methods along the lines of modal cost analysis are desirable. We have outlined what we feel are some of the difficulties of MCA and it appears that there are ways to overcome at least some of them. This effort should be continued to reach a more generally usable and understandable technique or techniques.

2.6.4 Modal Cost Analysis. The work performed by Dr. Robert E. Skelton on this task under a subcontract is described in Appendix E, "Case Studies of Model Reduction of Flexible Structures by Modal Cost Analysis."

### 3. CONCLUSIONS

3.1 Task 1 - Digital Implementation of Control Techniques. Software routines have been written that allow systems of the DARPA type to be analyzed quickly and efficiently. Frequently domain design programs have been developed that allow digital compensators to be designed rather simply. A design technique has also been developed that extends the application of Seltzer's Digital Parameter Space technique to the design of digital controllers for large flexible structures characterized by an arbitrary number of bending modes.

#### 3.2 Task 2 - Extensions of Modeling Techniques, and

Task 5 - Investigation of Structural Damping Models. Because the work on these two tasks was so closely related, the conclusion is drawn from the consolidated results.

The modeling techniques developed for the LSS/GTV were given important corroboration by modal testing done on the ASTROMAST beam at MSFC. These results indicated accuracies in the lower modes of 11% or better. Thus, we have developed a dynamic model of the LSS/GTV and it has been verified, to the extent it can be currently, with the data available and we are confident our techniques represent the structures.

3.3 Task 3 - Evaluation of ACOSS Control Methodologies. The LSS control techniques discussed include Lockheed's LAC/HAC, TRW's Positivity, and General Dynamic's MESS. Although each approach is observedly different, each technique employs the same objective, optimal performance when presented with an inaccurate plant model. Each technique addressed the problem of the destabilizing effect of uncontrolled modes on the system. TRW concludes that application of the positivity theorem to LSS assures stability (i.e. system will not become unstable due to observation and control spillover effects). In addition, positivity more indepthly (than LAC/HAC or MESS) examines the problem of noncolocation and inclusion of actuator and sensor dynamics. Lockheed concludes that LAC/HAC algorithm eliminates spillover instabilities through the application of frequency shaping. General Dynamics concludes that MESS solves the problem of known truncation through restructuring of the performance index.

3.4 Task 4 - Determination of Optimal Form for ACOSS Controller. The application of the computer aided-design tools to design a digital control system for a class of Large Space Structures has been demonstrated. It has been shown that the design tools reduce the computational burden associated with the design process. The tools have been designed such that the model can assume as many bending modes as necessary.

The form of the control system for the DARPA Structure has been developed. The preliminary analyses show that it is possible to design the system with a bandwidth that actually extends beyond the frequency of the significant bending modes. Sensitivity studies indicate that the multi-loop design

technique is also "robust" relative to variations in modal data. In the example given in Section 2.4.3, modal frequencies were varied from  $\pm 10\%$  and  $\pm 20\%$  of their nominal values. The results showed that the system response was reasonably stable up to  $\pm 20\%$ .

### 3.5 Task 5 (See 3.2 above.)

3.6 Task 6 - Implementation of Component Cost Analysis. The Modal Cost Analysis (MCA) method for the truncation of linear system models is a versatile method. It provides a formalism for reducing the order of a large variety of problems. It is oriented toward the optimal control problem and consequently may be somewhat less useful for other applications. Also, it does not seem to take into account questions of stability. It is not clear that the modes selected through the MCA criteria include the ones that are most potentially destabilizing. Also, it appears that there is too much freedom for the analyst to select the reduction criteria, in that much judgment must be exercised for the determination of the statistical behavior of the disturbances and for the selection of the weights to be used in the cost function. This freedom means that it is possible and indeed likely that different analysts working the same problem will arrive at different models and results. Thus, it appears that less formal, more intuitive methods for modal truncation are just as good as the MCA method and perhaps better since they may provide the analyst with more intuitive insights into his particular problem and certainly require less effort in learning a new formalism. The use of formal methods for modal truncation or for model reduction in general is an area in which much more work is needed and methods along the lines of modal cost analysis are desirable. We have outlined what we feel are some of the difficulties of MCA and it appears that there are ways to overcome at least some of them. This effort should be continued to reach a more generally usable and understandable technique or techniques.

3.7 Application of Results of ACOSS SEVENTEEN. The results of this two year contract were considered by DARPA to be of such significance that a follow-on contract was established and effort was initiated in December 1983. The new effort is called Advanced Structural Control Techniques (ASCOT) and will be for a period of twelve months.

#### 3.7.1 Objective of ASCOT.

3.7.1.1 To develop, evaluate, and prepare to test and implement Advanced Structural Control Techniques (ASCOT) that are applicable to future large flexible military spacecraft.

3.7.1.2 To develop and integrate a Simplified Systematic Digital Design (S2D2) which meets anticipated structural and attitude control system performance requirements.

3.7.1.3 To develop an ASCOT Technical/Management Program Development Plan and to select, evaluate and compare candidate control system techniques including S2D2.

APPENDICES TO FINAL TECHNICAL REPORT FOR  
ACOSS SEVENTEEN  
(ACTIVE CONTROL OF LARGE SPACE STRUCTURES)

APPENDIX A  
EXTENSION OF THE PARAMETER SPACE METHOD TO  
LARGE FLEXIBLE STRUCTURES

S. M. Seltzer, H. E. Worley, R. J. York

Control Dynamics Company

Huntsville, Alabama

Abstract

The application of the parameter space method is extended to a significant class of digital control problems associated with large flexible structures. The control problem considered was to develop a proportional-derivative form of a control law that would keep a sensor inertially fixed that was mounted on a large flexible structure which is represented in modal coordinates by a rigid mode and an arbitrary number of bending modes. An algorithm was developed that would accept as input an arbitrary number of bending modes and would return as output the form of the characteristic equation needed for the parameter space method. Values of the control gains would then be determined from stability considerations and desired damping.

I. Background

This paper extends the application of the parameter space method to a significant class of digital control problems associated with large flexible structures, problems that were previously intractable when the designer wished to include several bending modes in the plant representation. The control problem considered was to develop a proportional/derivative form of a control law that would keep a sensor inertially fixed that was mounted on a large flexible structure which is represented by a rigid mode and an arbitrary number of bending modes. The goal was to develop an algorithm that would accept as input from the designer an arbitrary number of bending modes for the plant representation and would return to him the form of the characteristic equation needed for the parameter space method. Based upon stability considerations and the desired damping, values of the control gains would then be determined by this method. The ability to handle a digital proportional/derivative controller for an arbitrarily large number of bending modes is the main contribution of this work.

Before proceeding, a quick review of the parameter space method is in order, including its foundation and the previous work to extend it to higher order systems. Based primarily on the work of D. D. Siljak[A-1] the parameter space method is an analytical tool developed for use in control system analysis and synthesis. Briefly, the method as developed by S. M. Seltzer[A-2] permits one to map the location of the roots of the system's characteristic equation onto a plane (or three-space if desired) whose coordinates are the system's free parameters. The parameter plane is readily divided into regions identified with system stability and instability.

Once the parameters of interest,  $k_0$  and  $k_1$ , are chosen, the characteristic equation of the closed-loop control system is written in the needed form:

$$\text{C.E.} = \sum_{i=1}^M [a_i k_0 + b_i k_1 + f_i] z^i \quad (\text{A-1})$$

The free parameters need not be gains but just as well could be other system parameters. In addition to the characteristic root locations, other factors of interest such as constant damping ratios and specified exponential time constants may be portrayed as contours on the parameter space. Thus in a manner somewhat reminiscent of the classical root locus method, a portrait may be presented of all pertinent aspects of the system's transient response as functions of several parameters (rather than the single parameter, open-loop gain), and as a function of the independent argument,  $\omega T$ , where  $\omega$  is the system damped frequency and  $T$  is the digital sampling period.

The parameter space approach may be employed in either the continuous or discrete domain. Techniques such as the Simplified Analytic Method have been developed for the purpose of generating the needed arrays A, B, and F for the characteristic equation, and are satisfactory for lower order systems. When  $N$  becomes large (i.e.  $N > 3$ ), the problem becomes intractable. The extension of the method to handle arbitrarily high order systems for the continuous case has been accomplished by Seltzer and B. A. Asner.[A-3] This work addresses the sampled data or discrete control case.

---

A-1. Siljak, D.D., Nonlinear Systems, Wiley, New York, 1969.

A-2. Seltzer, S.M., "Sampled-Data Control System Design in the Parameter Plane," Proc. of Eight Annual Allerton Conferences on Circuit System Theory, Monticello, ILL., 1970, pp. 454-463.

A-3. Asner, B.A. and Seltzer, S.M., "Parameter Plane Analysis for Large Flexible Spacecraft," Journal of Guidance and Control, Vol. 4, No. 3, May-June, 1981, pp. 284-290.

## II. Plant Representation

### Modal Coordinates

It is assumed that the plant representation of the large scale space structure is in modal coordinates. If the original system is defined by the vector matrix equation

$$[m] \ddot{\underline{X}} + [k] \underline{X} = \underline{F} \quad (A-2)$$

where

$[m]$  is the mass matrix  
 $[k]$  is the stiffness matrix  
 $\underline{F}$  is the force/torque vector,

then the transformation

$$\underline{X} = Q \underline{n} \quad (A-3)$$

where  $Q$  is the modal matrix composed of the normalized eigenvectors will yield the desired representation

$$\ddot{\underline{n}} + [\omega^2] \underline{n} = Q^T \underline{F} = \underline{I}_c \quad (A-4)$$

The plant transfer function is expressed as

$$G_p(s) = \sum_{i=1}^N \frac{\phi_i \gamma_i s}{s^2 + 2\zeta_i \omega_i s + \omega_i^2} \quad (A-5)$$

where  $\gamma_i, \phi_i$  denote the slope of the  $i$ th mode at the torquer, sensor respectively.

$\zeta_i, \omega_i$  denote the damping ratio, natural frequency of the  $i$ th mode respectively.

(See Fig. A-1) Note that modal damping has been introduced here.

### Form of the Control Law

The sensed angular rate,  $\dot{\theta}$ , is measured directly,

$$\dot{\theta} = \sum_{j=1}^N \phi_j \dot{n}_j . \quad (A-6)$$

The commanded torque employs  $\dot{\theta}$  and its integrated value,  $\theta$ , (see Fig. A-2),

$$T_c = K_p \theta + K_D \dot{\theta} . \quad (A-7)$$

### Assumptions

- a) The digital onboard controller will be of the position/derivative (PD) form.
- b) One has knowledge of the damping ratio,  $\zeta_j$ , and frequency,  $\omega_j$ , of each mode used.
- c) Only one sensor, torquer pair is used, but colocation is not assumed.
- d) No torquer-sensor dynamics are included.

The selected parameters for portrayal on the parameter plane are related to the control gains, namely for the algorithm developed,

$$k_0 = K_D \quad k_1 = K_p T/2. \quad (A-8)$$

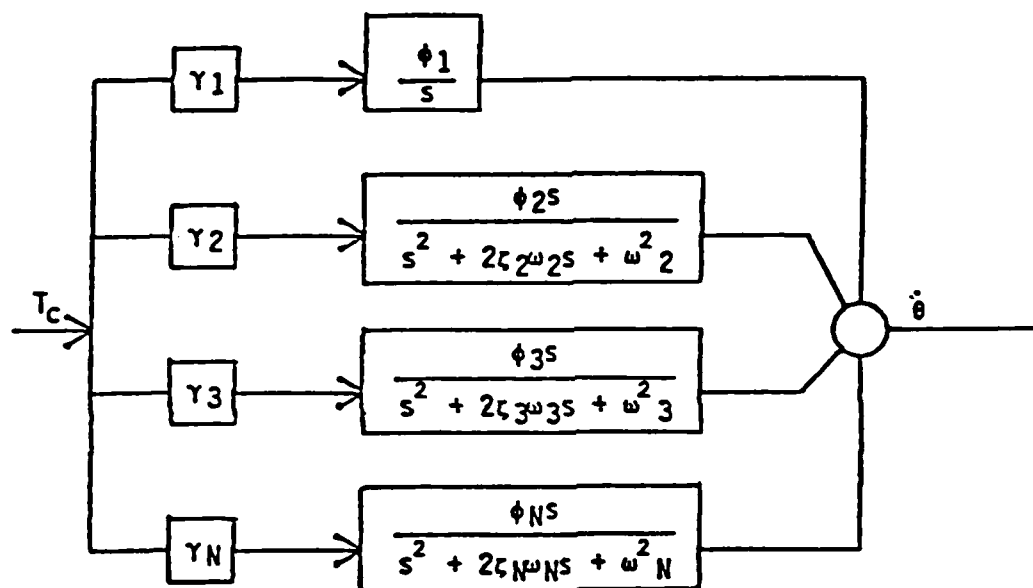


Figure A-1. Plant representation.

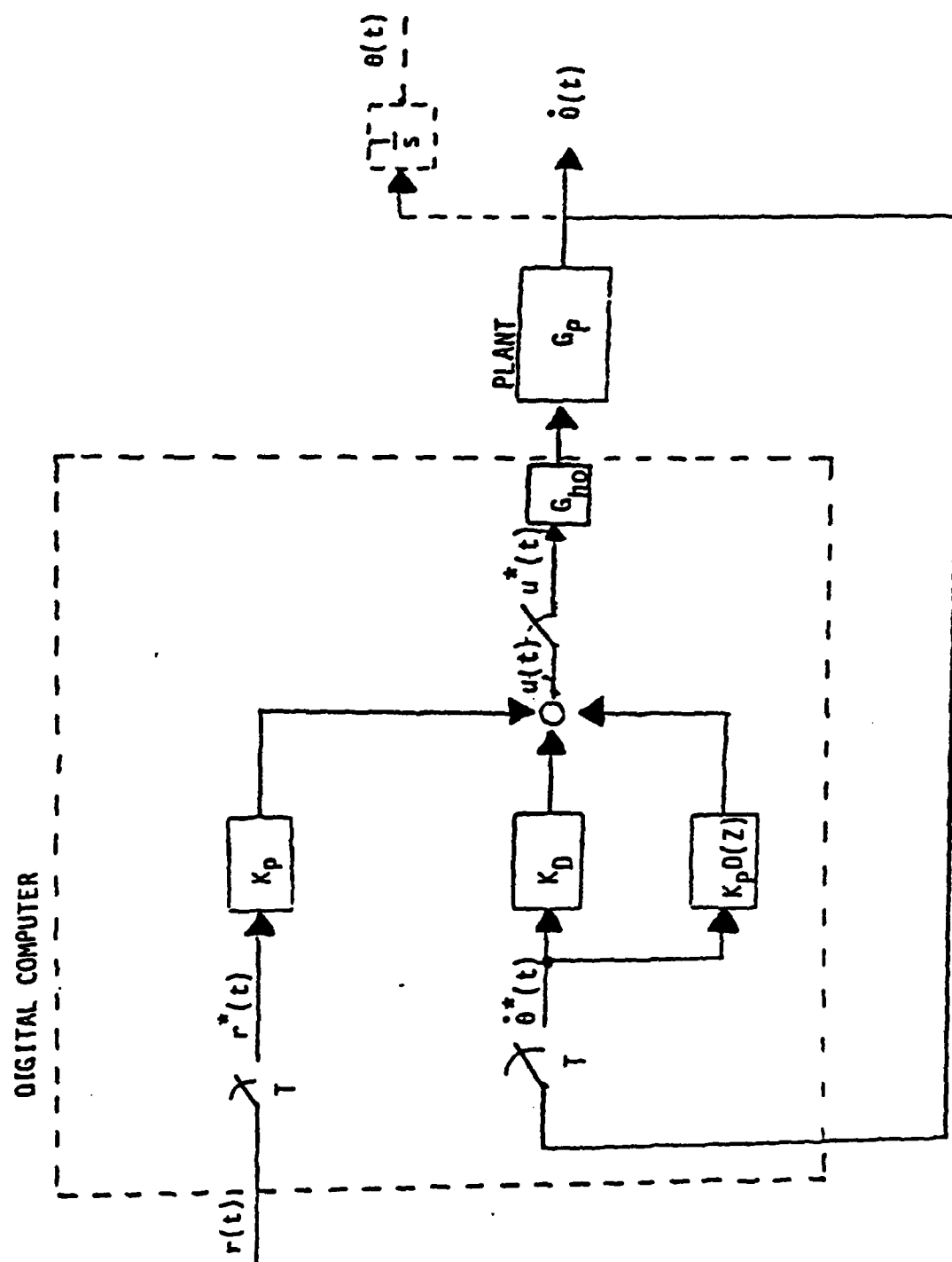


Figure A-2. Proportional ( $\theta$ ) - derivative ( $\dot{\theta}$ ) control law

### III. CHARACTERISTIC EQUATION

Using standard feedback control simplifying techniques, the transfer function corresponding to the control system in Fig. A-2 is given by

$$\frac{\theta^*}{r^*} = \frac{K_p Z[G_{ho}(s)G_p(s)]}{1 + [K_D + K_p D_f(z)]Z[G_{ho}(s)G_p(s)]} \quad (A-9)$$

where

$$G_p(s) = \sum_{i=1}^N \frac{\phi_i \gamma_i s}{s^2 + 2\zeta_i \omega_i s + \omega_i^2} \quad (A-10)$$

$$G_{ho}(s) = \frac{1 - e^{-Ts}}{s}, \quad D_f(z) = \frac{T(z+1)}{2(z-1)}, \quad (A-11)$$

with  $\gamma_i$ ,  $\phi_i$  denoting the slope of the  $i$ th mode at torquer, sensor (respectively), and  $\zeta_i$ ,  $\omega_i$  denoting the damping ratio, natural frequency of the  $i$ th mode. The sample time is  $T$ , and  $D_f(z)$  represents the trapezoidal integration rule.

The following, frequently appearing quantities in the derivation are represented by the given symbol:

$$\begin{aligned} \alpha_i &\equiv \zeta_i \omega_i & c_i &\equiv \cos \beta_i T \\ \beta_i &\equiv \omega_i [1 - \zeta_i^2]^{1/2} & s_i &\equiv \sin \beta_i T \\ e_i &\equiv e^{-\alpha_i T} \end{aligned} \quad (A-12)$$

Three lemmas which simplify the derivation follow[A-4]

Lemma 1.

$$Z[G_{ho}(s)G(s)] = (1-z^{-1}) Z \left[ \frac{G(s)}{s} \right]. \quad (A-13)$$

---

A-4. Kuo, C.K., Digital Control Systems, SRL Publishing, ILL., 1977.

Lemma 2. If  $\omega \neq 0$ , then

$$Z \left[ \frac{1}{s^2 + 2\zeta\omega s + \omega^2} \right] = \frac{1}{\omega(1-\zeta^2)^{1/2}} \cdot \frac{ze^{-\zeta\omega T} \cdot \sin[\omega(1-\zeta^2)^{1/2}T]}{z^2 - 2ze^{-\zeta\omega T} \cos[\omega(1-\zeta^2)^{1/2}T] + e^{-2\zeta\omega T}} \quad (A-14)$$

Restating Lemma 2 using the notation in Equation (A-12) yields

$$Z \left[ \frac{1}{s^2 + 2\zeta\omega s + \omega^2} \right] = \frac{1}{\beta} \cdot \frac{esz}{z^2 - 2ecz + e^2} \quad (A-15)$$

Finally, if  $\omega=0$ , then

Lemma 3.

$$Z \left[ \frac{1}{s^2} \right] = \frac{Tz}{(z-1)^2} \quad (A-16)$$

With the above limits, the characteristic equation can now be derived. Equation (A-11) will replace  $D_f(z)$ , but one must calculate

$$Z[G_{ho}(s)G_p(s)] = \left[ \frac{z-1}{z} \phi_1 \gamma_1 \frac{Tz}{(z-1)^2} + \sum_{i=2}^N \frac{\phi_i \gamma_i}{\beta_i} \frac{e_i c_i z}{z^2 - 2e_i c_i z + e_i^2} \right] \quad (A-17)$$

Next, substitute into the denominator of the  $\theta^*/r^*$ , i.e. Equation (A-9), to obtain

$$1 + \left[ K_D + K_P \cdot \frac{T}{2} \cdot \frac{z+1}{z-1} \right] \cdot \frac{z-1}{z} \cdot \left[ \phi_1 \gamma_1 \frac{Tz}{(z-1)^2} + \sum_{i=2}^N \frac{\phi_i \gamma_i}{\beta_i} \cdot \frac{e_i s_i z}{z^2 - 2e_i c_i z + e_i^2} \right] = 0. \quad (A-18)$$

Multiplying through by the common denominator

$$(z-1)^2 \prod_{i=2}^N (z^2 - 2e_i c_i z + e_i^2) \quad (A-19)$$

yields for the characteristic equation

$$\begin{aligned} & (z-1)^2 \prod_{i=2}^N (z^2 - 2e_i c_i z + e_i^2) + \left[ K_D(z-1) + K_P \frac{T}{2}(z+1) \right] \\ & \left[ \phi_1 \gamma_1 T \prod_{i=2}^N (z^2 - 2e_i c_i z + e_i^2) \right. \\ & \left. + \sum_{k=2}^N \left[ \frac{\phi_k \gamma_k e_k s_k}{\beta_k} (z-1)^2 \prod_{\substack{i=2 \\ i \neq k}}^N (z^2 - 2e_i c_i z + e_i^2) \right] \right] = 0. \end{aligned} \quad (A-20)$$

#### IV. Algorithmic Development of Parameter Plane Form of C.E.

For the parameter plane analysis, the characteristic equation must be in the form

$$\text{C.E.} = \sum_{i=0}^{2N} (A_i k_0 + B_i k_1 + F_i) z^i. \quad (A-21)$$

The objective then will be to develop a programmable algorithm to transform the characteristic equation of Equation (A-20) into that of Equation (A-21), that is, generate the arrays A, B, and F.

The following algorithm for multiplying polynomials will be instrumental in achieving the above goal. As can be seen from Equation (A-20), polynomial products of the form

$$P_{2N} = \prod_{i=1}^N (z^2 + a_i z + b_i) \quad (A-22)$$

occur often. Notation: In  $p_m(z)$ , let  $p_{m,j}$  denote the coefficient of the  $z^j$  term of this polynomial. For example,

$$p_2(z) = p_{2,2}z^2 + p_{2,1}z + p_{2,0}, \quad (A-23)$$

where

$$p_{2,2} = 1, \quad p_{2,1} = a_1, \quad p_{2,0} = b_1. \quad (A-24)$$

ALGORITHM P: Let  $N \geq 2$  be specified. Then the coefficient of the polynomial,

$$p_{2N}(z) = \prod_{i=1}^N (z^2 + a_i z + b_i) \quad (A-25)$$

can be determined recursively by

$$p_{2m,0} = p_{2m-2,0} b_m$$

$$p_{2m,1} = p_{2m-2,1} b_m + p_{2m-2,0} a_m$$

$$p_{2m,i} = p_{2m-2,1} b_m + p_{2m-2,i-1} a_m + p_{2m-2,i-2} b_m$$

for  $i=2, 3, \dots, 2m-2$ .

$$p_{2m,2m-1} = p_{2m-2,2m-2} a_m + p_{2m-2,2m-3} b_m$$

$$p_{2m,2m} = p_{2m-2,2m-2} b_m$$

where  $m = 2, 3, \dots, N$

Proof: (Method of mathematical induction)

Notes: 1. Calculation order is  $p_2(z)$  given, then  $p_4(z)$ ,  $p_6(z)$ , ...,  $p_{2n}(z)$ .

2. The above recursive approach is more accurate computationally than closed form expressions.

To obtain the desired form of the characteristic equation, Equation (A-21), one can generate polynomials  $D(z)$  and  $H(z)$  so that the characteristic polynomial becomes

$$D(z) + \left[ K_D(z-1) + K_P \frac{T}{2} (z+1) \right] H(z). \quad (A-27)$$

The general procedure is outlined in Figure A-3. Note that  $D(z)$  and  $H(z)$  have degree  $2N$  and  $2N-2$ , respectively.

Each step in the procedure is discussed with computational efficiency in mind.

Step 1. The polynomial  $D(z)$  can be obtained using Algorithm P with initial values of

$$d_2 = 1, \quad d_1 = -2, \quad d_0 = 1. \quad (A-28)$$

Notation: Let  $c_i$  denote the coefficient of  $z^i$  in polynomial  $C(z)$ , i.e. for  $D(z)$

$$D(z) = d_{2N} z^{2N} + d_{2N-1} z^{2N-1} + \dots + d_2 z^2 + d_1 z + d_0 \quad (A-29)$$

Step 2. Obtain the coefficients of  $G(z)$  from those of the previously calculated  $D(z)$ . Since

$$D(z) = (z^2 - 2z + 1) \cdot G(z), \quad (A-30)$$

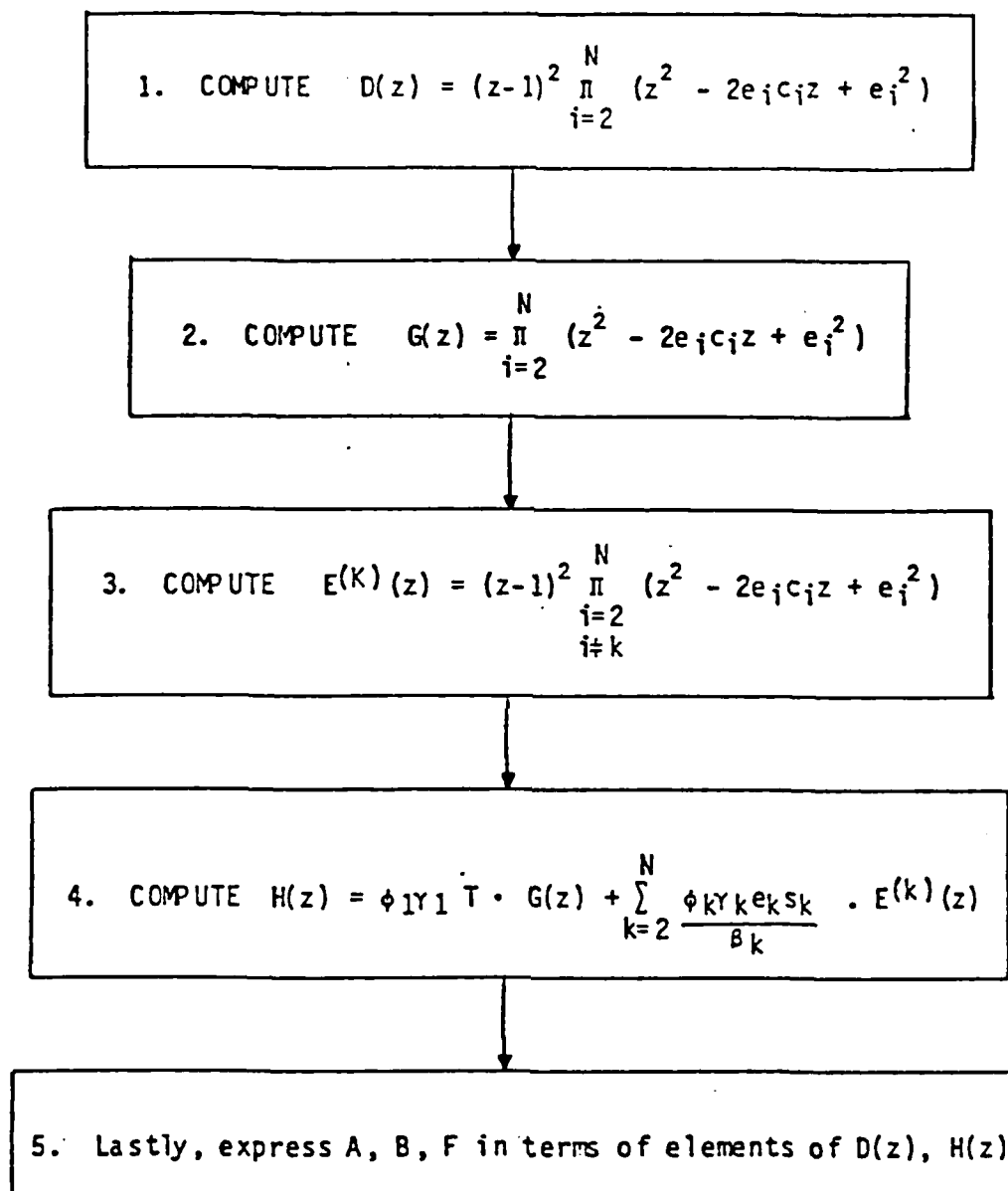


Figure A-3. Procedure for obtaining arrays A, B, and F.

multiply out the right-hand side, equate coefficients, and solve for the coefficients  $g_i$ ,  $i=0, 1, 2, \dots, 2N-2$  to obtain

$$\begin{aligned} g_{2N-2} &= d_{2N} \\ g_{2N-3} &= d_{2N-1} + 2g_{2N-2} \\ g_{2N-2-i} &= d_{2N-1} + 2g_{2N-1-i} - g_{2N-i} \end{aligned} \quad (A-31)$$

for  $i = 2, 3, \dots, 2N-2$ .

Step 3. Express the coefficients of  $E^{(k)}(z)$  in terms of those of  $D(z)$ ,  $K$  given. To do this, note that

$$D(z) = (z^2 + a_k z + b_k) \cdot E^{(k)}(z) \quad (A-32)$$

where (referring to Equation (A-20)),

$$a_i = -2e_i c_i, \quad b_i = e_i^2 \quad (A-33)$$

As done above in Step 2, one can obtain

$$\begin{aligned} e^{(k)}_{2N-2} &= d_{2N} \\ e^{(k)}_{2N-3} &= d_{2N-1} - a_k e^{(k)}_{2N-2} \\ e^{(k)}_{2N-2-i} &= d_{2N-i} - b_k e^{(k)}_{2N-i} - a_k e^{(k)}_{2N-1-i} \end{aligned} \quad (A-34)$$

for  $i=2, 3, \dots, 2N-2$ .

Step 4. Just element by element addition.

Step 5. With  $k_0, k_1$  being the two parameters of interest as given in Equation (A-22), the arrays  $A, B$ , and  $F$  can be obtained. For example, the coefficient of  $z^2$  is given by

$$d_2 + K_D \cdot h_1 + K_P \cdot \frac{T}{2} h_1 - h_2 \cdot K_D + K_P \cdot \frac{T}{2} h_2 \quad (A-35)$$

Collecting the appropriate terms as shown in Equation (A-21) yields

$$A_2 = h_1 - h_2, B_2 = h_1 + h_2, F_2 = d_2 \quad (A-36)$$

The complete arrays are given in the following Table A-1.

TABLE A-1. TWO PARAMETER FORM OF CHARACTERISTIC EQUATION (ARRAYS A, B, AND F)

$z^i$	$A_i$	$B_i$	$F_i$
$z^{2N}$	0	0	$d_{2N}$
$z^{2N-1}$	$h_{2N-2}$	$h_{2N-2}$	$d_{2N-1}$
$z^{2N-2}$	$h_{2N-3} - h_{2N-2}$	$h_{2N-3} + h_{2N-2}$	$d_{2N-2}$
$z^{2N-3}$	$h_{2N-4} - h_{2N-3}$	$h_{2N-4} + h_{2N-3}$	$d_{2N-3}$
$\vdots$	$\vdots$	$\vdots$	$\vdots$
$z^2$	$h_1 - h_2$	$h_1 + h_2$	$d_2$
$z^1$	$h_0 - h_1$	$h_0 + h_1$	$d_1$
$z^0$	$-h_0$	$+h_0$	$d_0$

## V. VERIFICATION

In previous contractual work on large space structures, the parameter space approach was employed with one bending mode. Subsequently, a second bending mode was added. The results obtained with the new algorithm that is designed to handle an arbitrary number of bending modes are in agreement with those of the previous work.

## VI. CONCLUSIONS AND RECOMMENDATIONS FOR FUTURE STUDY

The development of this algorithm removes a serious drawback in the application of the parameter plane approach to the problem of discrete control of large space structures. Previously, the number of desired bending modes exceeded two, then the task of obtaining the necessary form of the characteristic equation was quite complex. Now, once the modal representation is available, this drawback is eliminated by the automated generation of the needed arrays A, B, F. It is anticipated that this algorithm will now be employed in conjunction with the modal representation of the DARPA type large scale flexible space structure as developed by Control Dynamics.

Several areas of possible extension of this work follow:

- 1) Include sensor, torquer dynamics.
- 2) Allow for more than one sensor, torquer pair.
- 3) Include structural damping at the start, rather than introducing it later into the modal representation.
- 4) Introduce a second integrator into the feedback loop with a corresponding control gain. Preliminary work indicates that the same line of development can be used and that the needed arrays A, B, C, F can be generated by the computer.

## APPENDIX B

### Derivation of Modal Cost Function

The modal cost analysis technique (MCA) is a method based on statistics for selecting a reduced set of coordinates for modeling a linear system. The method starts with a cost function and proceeds to select a subset of the modal coordinates of a specified size such that the reduction in the cost function resulting from dropping the coordinates not in the subset is minimized. Let us consider a linearized system

$$\begin{aligned} \dot{\underline{x}} &= \underline{A}\underline{x} + \underline{B}\underline{d}, \\ \underline{y} &= \underline{P}\underline{x}. \end{aligned} \quad (B-1)$$

There exists a transformation  $T$  which transforms this equation to modal coordinates  $\underline{x} = T\underline{\eta}$ .

$$\begin{aligned} \dot{\underline{\eta}} &= \underline{\Lambda}\underline{\eta} + \underline{B}\underline{d} \\ \underline{y} &= \underline{P}\underline{\eta} \\ \underline{B} &= T^{-1}\underline{B}; \underline{P} = \underline{P}T \end{aligned} \quad (B-2)$$

The modal coordinates  $\underline{\eta}$  diagonalize the matrix  $A$  to  $\Lambda$ . Rewriting the component equations

$$\begin{aligned} \dot{\eta}_\alpha &= \lambda_\alpha \eta_\alpha + \bar{B}_{\alpha\beta} d_\beta, \quad (\alpha \text{ not summed}) \\ y_\mu &= P_{\mu\alpha} \eta_\alpha. \end{aligned} \quad (B-3)$$

Here we have used the convention that repeated indices are summed except as noted. Let us define a cost function  $V$

$$\begin{aligned} V &= \lim_{t \rightarrow \infty} \epsilon \{ \underline{y}^+ Q \underline{y} \}; \quad \underline{y}^+ = \underline{y}^T{}^*; \text{ where } * \text{ denotes complex conjugate} \\ &= \lim_{t \rightarrow \infty} \epsilon \{ Q_{\mu\nu} y_\mu^* y_\nu \} \\ &= \lim_{t \rightarrow \infty} \epsilon \{ Q_{\mu\nu} P_{\mu\alpha}^* P_{\nu\gamma} \eta_\alpha^* \eta_\gamma \} \\ &= \epsilon \lim_{t \rightarrow \infty} \{ Q_{\mu\nu} P_{\mu\alpha}^* P_{\nu\gamma} \eta_\alpha^* \eta_\gamma \} \\ &= \epsilon \{ Q_{\mu\nu} P_{\mu\alpha}^* P_{\nu\gamma} \eta_\alpha^* \eta_\gamma^\infty \} \\ &= Q_{\mu\nu} P_{\mu\alpha}^* P_{\nu\gamma} \epsilon \{ \eta_\alpha^* \eta_\gamma^\infty \} \end{aligned}$$

Now Equation B-3 can be integrated in closed form

$$\eta_\alpha = e^{\lambda_\alpha t} \eta_{\alpha 0} + \int_0^t dt' e^{\lambda_\alpha(t-t')} \bar{B}_{\alpha\beta} d_\beta(t') \quad (\alpha \text{ not summed})$$

$$n_{\alpha}^{\infty} = \lim_{t \rightarrow \infty} \int_0^t dt' e^{\lambda_{\alpha}(t-t')} \overline{B}_{\alpha\beta} d_{\beta}(t') \quad (B-4)$$

Equation B-4 only holds if the linear system is stable asymptotically. Now

$$\begin{aligned} \epsilon \{n_{\alpha}^{\infty} n_{\gamma}^{\infty}\} &= \lim_{t \rightarrow \infty} \epsilon \left\{ \int_0^t \int_0^t dt' dt'' e^{\lambda_{\alpha}^*(t-t')} e^{\lambda_{\gamma}(t-t'')} \right. \\ &\quad \left. \overline{B}_{\alpha\beta}^* \overline{B}_{\gamma\delta} d_{\beta}^*(t') d_{\delta}(t'') \right\} \\ &= \lim_{t \rightarrow \infty} \left( \overline{B}_{\alpha\beta}^* \overline{B}_{\gamma\delta} \int_0^t \int_0^t dt' dt'' e^{\lambda_{\alpha}^*(t-t')} e^{\lambda_{\gamma}(t-t'')} \right. \\ &\quad \left. \epsilon [d_{\beta}^*(t') d_{\delta}(t'')] \right) \end{aligned} \quad (B-5)$$

At this point it is reasonable to assume that the disturbances  $d_{\beta}(t')$  and  $d_{\delta}(t'')$  are uncorrelated for  $t' \neq t''$  so that

$$\epsilon \{d_{\beta}^*(t') d_{\delta}(t'')\} = \sigma_{\beta\delta}(t) \delta(t' - t'') \quad (B-6)$$

In addition, we assume the disturbance statistics are also independent of time so that  $\sigma_{\beta\delta}$  is constant. Thus

$$\epsilon \{d_{\beta}^*(t') d_{\delta}(t'')\} = \sigma_{\beta\delta} \delta(t' - t'') \quad (B-7)$$

Substituting Equation B-7 in Equation B-5 and integrating over  $t''$  we obtain

$$\begin{aligned} \epsilon \{n_{\alpha}^{\infty} n_{\gamma}^{\infty}\} &= \lim_{t \rightarrow \infty} \int_0^t dt' e^{(\lambda_{\alpha}^* + \lambda_{\gamma})(t-t')} \overline{B}_{\alpha\beta}^* \overline{B}_{\gamma\delta} \sigma_{\beta\delta} \\ &= \lim_{t \rightarrow \infty} \overline{B}_{\alpha\beta}^* \overline{B}_{\gamma\delta} \sigma_{\beta\delta} \int_0^t dt' e^{(\lambda_{\alpha}^* + \lambda_{\gamma})t'} \\ &= \overline{B}_{\alpha\beta}^* \overline{B}_{\gamma\delta} \sigma_{\beta\delta} \frac{1}{\lambda_{\alpha}^* + \lambda_{\gamma}} [e^{(\lambda_{\alpha}^* + \lambda_{\gamma})t} - 1] \\ &= \frac{\overline{B}_{\alpha\beta}^* \overline{B}_{\gamma\delta} \sigma_{\beta\delta}}{\lambda_{\alpha}^* + \lambda_{\gamma}} (-1) \\ &= - \frac{\overline{B}_{\alpha\beta}^* \overline{B}_{\gamma\delta}}{\lambda_{\alpha}^* + \lambda_{\gamma}} \sigma_{\beta\delta} \end{aligned} \quad (B-8)$$

Thus,

$$V = -Q_{\mu\nu} \overline{P}_{\mu\alpha} \overline{P}_{\nu\gamma} \frac{\overline{B}_{\alpha\beta}^* \overline{B}_{\gamma\delta}}{\lambda_{\alpha}^* + \lambda_{\gamma}} \sigma_{\beta\delta} \quad (B-9)$$

In virtually all problems of interest the system described in Equation B-1 was originally a mechanical system whose equations of motion were developed as a set of 2nd order linear equations

$$\begin{aligned} M\ddot{\underline{q}} + D\dot{\underline{q}} + K\underline{q} &= \underline{d} \\ \underline{y} &= \underline{q} + \dot{\underline{q}} \end{aligned} \quad (B-10)$$

The mass matrix  $M$  is normally positive definite and symmetric, and the stiffness matrix  $K$  is nonnegative definite and also symmetric. With these assumptions we are assured of the existence of a transformation matrix  $\phi$  such that

$$\begin{aligned} \phi^T M \phi &= 1 \text{ and} \\ \phi^T K \phi &= \Omega^2 = \text{diag}(\omega_1^2 \dots \omega_N^2). \end{aligned} \quad (B-11)$$

In general, the matrix  $\phi$  does not diagonalize the damping matrix  $D$ . However, for lightly damped systems it is assumed that  $\phi^T D \phi$  is approximately diagonal and the assumption is made that

$$\phi^T D \phi = 2\zeta\Omega; \zeta = \text{diag}\{\zeta_1 \dots \zeta_N\}. \quad (B-12)$$

The system in Equation B-9 is put in the form of Equation B-1 by writing

$$\begin{bmatrix} \ddot{\underline{q}} \\ \dot{\underline{q}} \\ \underline{q} \end{bmatrix} = \begin{bmatrix} -M^{-1}D & -M^{-1}K \\ 1 & 0 \end{bmatrix} \begin{bmatrix} \dot{\underline{q}} \\ \underline{q} \end{bmatrix} + \begin{bmatrix} -M^{-1} \\ 0 \end{bmatrix} \underline{d}. \quad (B-13)$$

Using the transformation  $\underline{q} = \phi \underline{n}$  we transform Equation B-12 to

$$\begin{bmatrix} \ddot{\underline{n}} \\ \dot{\underline{n}} \\ \underline{n} \end{bmatrix} = \begin{bmatrix} -2\zeta\Omega & -\Omega^2 \\ 1 & 0 \end{bmatrix} \begin{bmatrix} \dot{\underline{n}} \\ \underline{n} \end{bmatrix} + \begin{bmatrix} \phi^T M^{-1} \\ 0 \end{bmatrix} \underline{d} \quad (B-14)$$

The subsystem  $j$  corresponding to  $\eta_j$  can be written from Equation B-13 as

$$\begin{bmatrix} \ddot{\eta}_j \\ \dot{\eta}_j \\ \eta_j \end{bmatrix} = \begin{bmatrix} -2\zeta_j\omega_j & -\omega_j^2 \\ 1 & 0 \end{bmatrix} \begin{bmatrix} \dot{\eta}_j \\ \eta_j \end{bmatrix} + \begin{bmatrix} \phi_j^T M^{-1} \beta \\ 0 \end{bmatrix} \quad (B-15)$$

$$\phi = [\phi_1 \dots \phi_N] . \quad (B-16)$$

The eigenvalues arising from Equation F-14 are

$$\lambda_j = -\zeta_j\omega_j \pm i\omega_j \sqrt{1 - \zeta_j^2} \quad (B-17)$$

Looking back at Equation B-8 and using Equation B-16 for the eigenvalues, we note that the terms in which  $\alpha = \gamma$  are the dominant ones with  $\lambda_k^* + \lambda_k = -2\zeta_k\omega_k$  since  $\zeta_k$  is assumed to be small. Thus, we can write  $V = \sum_{\alpha} V_{\alpha}$  where

$$V_{\alpha} = \frac{(\bar{P}^* Q \bar{P})_{\alpha\alpha} \cdot (\bar{B}^* \sigma^T \bar{B})_{\alpha\alpha}}{2\zeta_{\alpha}\omega_{\alpha}} \quad (\text{no sum on } \alpha) \quad (B-18)$$

The system in Equation B-13 can be diagonalized by the matrix  $T$

$$T = \left[ \begin{array}{c|c} \Lambda & \Lambda^* \\ \hline 1 & 1 \end{array} \right] ; \quad \Lambda = \text{diag} (\lambda_1 \dots \lambda_N). \quad (B-19)$$

Also,

$$T^{-1} = \left[ \begin{array}{c|c} 1 & -\Lambda^* \\ \hline -1 & \Lambda \end{array} \right] \left[ \begin{array}{c|c} (\Lambda - \Lambda^*)^{-1} & 0 \\ \hline 0 & (\Lambda - \Lambda^*)^{-1} \end{array} \right] \quad (B-20)$$

Now, referring back to Equations B-1, B-9, and B-12, we see that for the 2nd order system

$$P = \left[ \begin{array}{c|c} \bar{P} & \bar{P} \end{array} \right] ; \quad B = \left[ \begin{array}{c} M^{-1} \beta \\ 0 \end{array} \right] . \quad (B-21)$$

In terms of the transformed system, Equation B-13, we have

$$\bar{P}' = \left[ \begin{array}{c|c} P' \Phi & P \Phi \end{array} \right]; \quad \bar{B} = \left[ \begin{array}{c} -\frac{\Phi M^{-1} B}{0} \end{array} \right] \quad (B-22)$$

Using Equation B-2 and the transformation T in Equations B-18 and B-19, we obtain

$$\bar{P} = \left[ \begin{array}{c|c} P' \Phi & P \Phi \end{array} \right] \left[ \begin{array}{c|c} \Lambda & \Lambda^* \\ \hline 1 & 1 \end{array} \right] \quad (B-23)$$

or,

$$\bar{P} = \left[ \begin{array}{c|c} P' \Phi \Lambda + P \Phi & P \Phi \Lambda^* + P \Phi \end{array} \right] \quad (B-24)$$

and

$$\bar{B} = \left[ \begin{array}{c} \frac{(\Lambda - \Lambda^*)^{-1} \Phi M^{-1} B}{-(\Lambda - \Lambda^*)^{-1} \Phi M^{-1} B} \end{array} \right] \quad (B-25)$$

Thus,

$$\bar{P}_{\mu\alpha} = P'_{\mu k} \Phi_{k\alpha} \lambda_{\alpha} + P_{\mu k} \Phi_{k\alpha}; \quad \alpha = 1 \dots N \quad (B-26)$$

and

$$\bar{P}_{\mu\alpha+N} = P_{\mu\alpha}^*,$$

Similarly,

$$\bar{B}_{\alpha\beta} = \frac{1}{2i\omega_{\alpha}} B'_{\alpha\beta} \quad (\alpha \text{ no sum}) \quad (B-27)$$

and

$$\bar{B}_{\alpha+N,\beta} = - \frac{1}{2i\omega_\alpha} \bar{B}'_{\alpha\beta}$$

Now, from these results, we have

$$(\bar{P}^+ Q \bar{P})_{\alpha\alpha} = \bar{P}_{\mu\alpha} Q_{\mu\nu} \bar{P}_{\nu\alpha} \quad (\alpha \text{ no sum}) \quad (B-28)$$

$$\begin{aligned} &= (\bar{P}'_{\mu k} \phi_{k\alpha} \lambda_\alpha^* + \bar{P}_{\mu k} \phi_{k\alpha}) Q_{\mu\nu} \\ &\quad (\bar{P}'_{\nu\rho} \phi_{\rho\alpha} \lambda_\alpha + \bar{P}_{\nu\rho} \phi_{\rho\alpha}) \\ &= \phi_{k\alpha} \phi_{\rho\alpha} [\bar{P}'_{\mu k} \bar{P}'_{\nu\rho} |\lambda_\alpha|^2 + \bar{P}_{\mu k} \bar{P}_{\nu\rho} \\ &\quad + (\bar{P}'_{\mu k} \bar{P}_{\nu\rho} \lambda_\alpha^* + \bar{P}_{\mu k} \bar{P}'_{\nu\rho} \lambda_\alpha)] Q_{\mu\nu} \end{aligned} \quad (B-29)$$

From the symmetry of Q and since  $\lambda_\alpha = -\zeta_\alpha \omega_\alpha \pm i\omega_\alpha \sqrt{1 - \zeta_\alpha^2}$

$$\begin{aligned} (\bar{P}^+ Q \bar{P})_{\alpha\alpha} &= \phi_{k\alpha} \phi_{\rho\alpha} Q_{\mu\nu} [\bar{P}'_{\mu k} \bar{P}_{\nu\rho} \omega_\alpha^2 + \bar{P}_{\mu k} \bar{P}_{\nu\rho}] \\ &\quad - 2\zeta_\alpha \omega_\alpha \phi_{k\alpha} \phi_{\rho\alpha} Q_{\mu\nu} \bar{P}'_{\mu k} \bar{P}_{\nu\rho} \quad (\text{no sum on } \alpha) \end{aligned} \quad (B-30)$$

From Equation F-26 and Equation F-18, we obtain

$$\begin{aligned} V_{0\alpha} = V_\alpha + V_{N+\alpha} &= \phi_{k\alpha} \phi_{\rho\alpha} Q_{\mu\nu} [\bar{P}'_{\mu k} \bar{P}_{\nu\rho} \omega_\alpha^2 + \bar{P}_{\mu k} \bar{P}_{\nu\rho}] \\ &\quad \times \frac{[\bar{B}'_{\alpha\beta} \sigma_{\beta\gamma} \bar{B}'_{\alpha\gamma}]}{4\zeta_\alpha \omega_\alpha^3} \end{aligned} \quad (B-31)$$

# APPENDIX C

## Derivation of $OT^2$ Modal Peak Function

$$\text{System: } \ddot{\eta}_\alpha + 2\zeta_\alpha \omega_\alpha \dot{\eta}_\alpha + \omega_\alpha^2 \eta_\alpha = \sum_{\rho} B_{\alpha\rho} w_\rho; \quad y_\beta = \sum_{\alpha} \rho_{\beta\alpha} \eta_\alpha + \rho'_{\beta\alpha} \dot{\eta}_\alpha$$

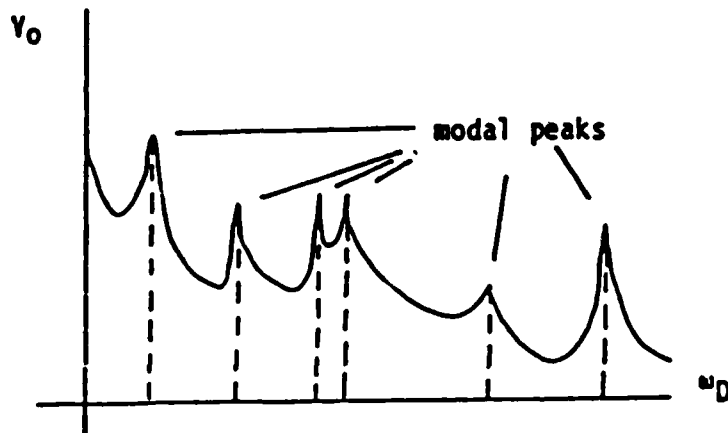
Steady State Solution:

$$\eta_\alpha = \frac{B_{\alpha\rho} w_\rho}{\omega_\alpha^2 - \omega_D^2 + 2i\zeta_\alpha \omega_\alpha \omega_D} e^{i\omega_D t}$$

$$y_\beta = \sum_{\alpha} (\rho_{\beta\alpha} \eta_\alpha + \rho'_{\beta\alpha} \dot{\eta}_\alpha)$$

$$= \frac{\rho_{\beta\alpha} + i\omega_D \rho'_{\beta\alpha}}{\omega_\alpha^2 - \omega_D^2 + 2i\zeta_\alpha \omega_\alpha \omega_D} B_{\alpha\rho} w_\rho e^{i\omega_D t}$$

$$V_0 = \sum_{\beta} |y_\beta|^2 = \sum_{\beta\alpha} \left| \left( \frac{\rho_{\beta\alpha} + i\omega_D \rho'_{\beta\alpha}}{\omega_\alpha^2 - \omega_D^2 + 2i\zeta_\alpha \omega_\alpha \omega_D} \right) B_{\alpha\rho} w_\rho \right|^2$$



As before, we assume  $\zeta_\alpha \ll 1$  so that the peaks in the  $V_0$  curve corresponding to the modes are due to coincidence between  $\omega_D$  and some  $\omega_\alpha$ . Thus,

$$V_0 = \sum_{\alpha} V_{0\alpha}; \quad V_{0\alpha} = \sum_{\beta, \rho} \left| \frac{\rho_{\beta\alpha} + i\omega_\alpha \rho'_{\beta\alpha}}{2\zeta_\alpha \omega_\alpha^2} \sum_{\rho} B_{\alpha\rho} w_\rho \right|^2$$

$$V_{0\alpha} = \sum_{\lambda\beta} \frac{\rho_{\lambda\alpha}^2 + \omega_\alpha^2 \rho'_{\lambda\alpha}^2}{4\zeta_\alpha^2 \omega_\alpha^4} B_{\alpha\beta}^2 w_\beta^2$$

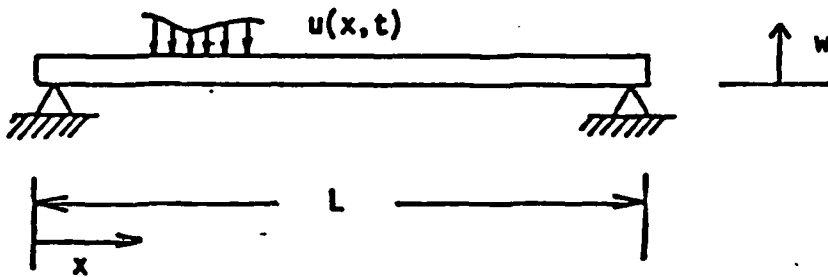
## APPENDIX D

### A Tutorial Example of Modal Cost Analysis

by Robert E. Skelton

Objective: Illustrate the features of Modal cost analysis with the minimum of detail.

Suggested model: A simply supported Euler-Bernouli beam.



Equations of Motion:

$$EI \frac{\partial^4 w(x, t)}{\partial x^4} + \rho A \frac{\partial^2 w(x, t)}{\partial t^2} = u(x, t) \quad (D-1)$$

$u(x, t)$ : force per unit length  
 $w(x, t)$ : vertical displacement  
 $\rho$ : uniform mass density per unit area  
 $A$ : cross-sectional area of beam

$$w(x, t) = \phi(x) \eta(t) = \sum_{i=1}^{\infty} \phi_i(x) \eta_i(t) \quad (D-2)$$

$$\phi_i(x) = \alpha_i \sin \frac{i\pi x}{L}, \quad i = 1, 2, \dots \quad (D-3)$$

$$\omega_i^2 = \frac{i^2 \pi^4}{L^4} \frac{EI}{\rho A}, \quad i = 1, 2, \dots \quad (D-4)$$

normalize  $\phi_i(x)$ :

$$\int_0^L \rho A \phi_i^2(x) dx = \rho AL = m_b \text{ (determines } \alpha_i) \quad (D-5)$$

leads to

$$\ddot{n}_i(t) + 2\zeta_i \dot{n}_i(t) + \omega_i^2 n_i(t) = \frac{\int_0^L \phi_i(x) u(x, t) dx}{\int_0^L \rho A \phi_i^2(x) dx}; \quad (D-6)$$

Damping  $\zeta_i$  arbitrarily added to reflect presence of material damping; Point located actuator (force):

$$u(x, t) = u(t) \delta(x - x_0) \quad (D-7)$$

Output of interest:  $w(x_0, t) = y(t) =$  displacement at  $x_0$ .

$$y(t) = \sum_{i=1}^{\infty} \phi_i(x_0) n_i(t) \quad (D-8)$$

Hence (6) reduces to

$$\ddot{n}_i(t) + \omega_i^2 n_i(t) = b_i u(t) \quad (D-9)$$

$$y(t) = \sum_{i=1}^{\infty} \phi_i(x_0) n_i(t) \quad (D-10)$$

where

$$b_i = \frac{1}{m_b} \phi_i(x_a) \quad (D-11)$$

### Modal Cost Analysis

In the absence of any closed loop information about the control inputs  $u(t)$  we shall assume that the actuator device has some signal to noise ratio such that "at idle" (no control commands)  $u(t)$  is simply the zero mean white noise emanating from electronic noise within the device power system.

$$\epsilon u(t) = 0, \quad \epsilon u(\tau) u(\tau) = \delta(t - \tau) \quad (D-12)$$

Under these conditions the performance metric

$$V = \lim_{T \rightarrow \infty} \frac{1}{T} \int_0^T y^2(t) dt \quad (D-13)$$

measures the response of the system at the location  $x$  of interest, and the contribution that each mode makes in  $V$  is

$$V_i = \frac{1}{2\zeta_i \omega_i^3} \phi_i^2(x_0) b_i^2 \quad (D-14)$$

and the total response is the sum of the modal responses

$$V = \sum_{i=1}^{\infty} V_i \quad (D-15)$$

$V_i$  is called the modal cost.

From a variety of substitutions of (3), (4), (11) into (14) the following equivalent expressions of modal cost are obtained.

$$V_i = \frac{1}{2\zeta_i \omega_i^3 m_b^2} \phi_i^2(x_0) \phi_i^2(x_a) \quad (D-16)$$

$$V_i = k_1 \frac{1}{\zeta_i i^6} \phi_i^2(x_0) \phi_i^2(x_a) \quad (D-17)$$

$$k_1 = L^4 [(EI)^{3/2} (\rho A)^{1/2} \pi^6]^{-1} \quad (D-18)$$

$$V_i = k \frac{1}{\zeta_i i^6} \sin^2 \frac{i\pi x_0}{L} \sin^2 \frac{i\pi x_a}{L} \left[ \int_0^L \sin^2 \frac{i\pi x}{L} dx \right]^{-4} \quad (D-19)$$

$$k_0 = k_1 L^4$$

### Conclusions:

1. The modal cost  $V_i$  tends toward zero as  $i$  tends toward  $\infty$ , but not monotonically!
2. Explicit analytical formulas can be developed for any continuum model of a structure for which mode shapes are known.
3. The value of a mode (with respect to a quadratic performance measure) is related to the product of the mode shape at the input output locations (D-16).

APPENDIX E

CASE STUDIES OF MODEL REDUCTION OF FLEXIBLE  
STRUCTURES BY MODAL COST ANALYSIS

Prepared by

R. Skelton, Principal Investigator

A. Yousuff, Research Assistant

M. Dornseif, Research Assistant

Prepared for

Control Dynamics Company  
Huntsville, Alabama

February 1983

## Abstract

The purpose of this report is to present a detailed account of the application of modal cost analysis for lightly damped flexible structures. The report presents detailed data for model reduction and control design for two different structures and two different model reduction methods.

The first structure is the simply-supported Euler-Bernoulli beam, chosen for minimum complexity to gain insight into the methods. The second structure is a truss structure for a solar optical space telescope, chosen for more practical applications. The finite element model for the telescope was provided by C. Draper Laboratories.

The first model reduction method is called modal cost analysis, (MCA), a technique which most readily applies to lightly damped structures. This technique decomposes the mean-squared outputs as a sum of contributions from each mode of the structure, and retains the modes making the largest contribution. The second model reduction method is called cost-equivalent realizations (CER), a technique which matches the overall mean-squared value of the outputs.

For lightly damped structures, the modal cost analysis is computationally simpler and performs just as well as the more sophisticated cost-equivalent models. For systems which are not lightly damped the cost-equivalent models have advantages.

## 1.0 INTRODUCTION

When compared to other large scale systems, flexible spacecrafts have some peculiarities which can make control more difficult. In this discussion emphasis is placed upon the time domain and suboptimal Linear Quadratic Gaussian (LQG) methods, with special attention given to the effects of modeling errors. These effects are discussed in light of the model reduction problem, stability, and control design.

Flexible structures and their dynamics have been studied well over a century. However, only recently has there been an interest in the active control of flexible structures. Such interest was piqued in the 1960's by a flexibility-induced instability in USA's first satellite [1], and more recently by sophisticated requirements for precision controlled structures in space for astronomy, communication networks, near-earth scientific studies, and space solar power alternatives, [2]. The rapid development of computers and control theory in the 1960's has encouraged active control applications for other structures as well, such as flutter suppression in aircraft [3], and active damping of bridges and tall buildings [4]. This is not to say that active control is needed in every structure, however, and there is no clear means to make the decision of when and how much control effort is needed in a structure. There is a need to study the dynamical properties of the mechanical system with a view toward discerning what improvements in performance can easily be made by redesigning the structure and what improvements must be left for active control functions. This *beneficial* interaction of the dynamics and control disciplines in the

development of a rational design methodology has not yet occurred to any mature degree. Usually the structure designs and the control designs occur sequentially. This luxury cannot be afforded in the future, as stringent requirements force us to provide better coordination between structure design, control design, and controller software design.

Some of the reasons that the control of flexible spacecraft can be a difficult task are briefly described by the following three problems.

(i) The Model Error Problem

The space structure is usually constructed of lightweight materials, and thus the assembled structure is very lightly damped. This uniqueness of light damping for the space structure makes the control design extremely sensitive to modeling errors, since the slightest perturbation of truncated modes by control action can shift these eigenvalues into the right half plane. Also there is the usual uncertainty in the computation of the modal data. This problem is especially critical for spacecraft since modal data uncertainties cannot be removed before flight, due to the difficulty of testing the extremely lightweight structure in a 1-g environment.

(ii) The Limited Controller Software Problem

The practical limitations of memory and speed of on-board computers mean that only controllers of constrained dimension can be considered.

These constraints can severely reduce the performance capabilities of the controlled system due again to the effect of modeling errors imposed by the controller order constraints. (An infinite dimensional system controlled by finite controllers immediately suggests that "optimal" state feedback solutions are not going to be realized). Thus, limited software serves only to compound the model error problem by constraining the order of the controller and by adding delays in the feedback loop.

#### (iii) The Performance Requirement Problem

Of course the model error problem and the limitations of software pose no serious threat to the mission if the performance requirements are quite lenient. Thus, the degree to which (i) and (ii) pose problems is directly related to the severity of the performance requirements. Therefore, early researches on the subject have sought to help with the tradeoffs between performance and modeling errors (including those induced by controller software limitations).

The report is organized as follows. Section 2.0 derives the equations of motion for a simply-supported beam. Section 3.0 describes the model reduction methods to be used. Section 4.0 designs controllers using the reduced models and evaluates them using the full evaluation model. Section 5.0 describes the solar optical telescope application, and Section 6.0 summarizes the report. All proofs of theorems are contained in Appendices so as not to impede the tutorial nature of the text.

## 2.0 EXAMPLES OF DYNAMIC SYSTEMS

The purpose of this chapter is to develop models for several dynamic systems. These models will be used throughout the report to illustrate various control concepts. It is hoped that repeated use of the same examples will further enhance the educational process. By using examples which have *physical* significance and by using the *same* examples to illustrate each new control concept, the bridge between mathematics and control engineering is to be built.

For decades control theory has been treated as a discipline to be applied *after* the model is developed. This point of view must necessarily be changed for the simple reason that the mathematical models never describe the physical phenomena exactly. There are many different models that could be developed for a given physical phenomena, and persons developing the models could make appropriate modeling decisions if only they knew the particular purpose the model is intended to serve. If the purpose of the model is to develop a control policy then the conclusion is that *the modeling problem and the control problem are not independent*. This leads to the following discomforting reality: The particular control policy cannot be developed without prior knowledge of the model, and the best model for the situation cannot be developed without prior knowledge of the control policy. This "chicken and egg" dilemma occupies much of the current research on control theory. For introductory purposes, however, we shall present in this chapter simple models of physical dynamical systems and we shall pretend that these models are correct and hence that their accuracy is not dependent upon the control policy. In other words, we shall momentarily invoke a "separation principle" between the modeling and control problems.

## 2.1 A Flexible Structure

In many applications of control and estimation theories the physical process is described by a set of partial differential equations. Examples include flexible structures, fluid dynamics, electromagnetic fields, etc. This Section develops the partial differential equations for the elastic structure of Fig. 2.1

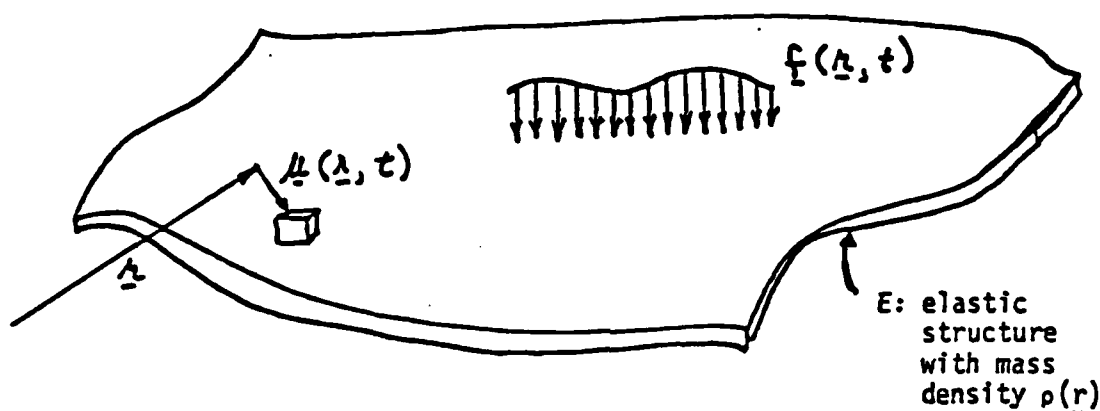


Fig. 2.1 An Elastic Structure

The reference in which the generic position vector  $\underline{r}$  is described is inertially fixed; and the constant vector  $\underline{r}$  is chosen so that  $\underline{u}(\underline{r}, t)$  is a vector of *short* length to the elemental volume. In this way the equations of motion can later be linearized in the small variable  $\underline{u}$ .

Hamilton's principle states that the first variation of the "action"  $L$  is zero along the actual time-varying path of  $\underline{u}(\underline{r}, t)$ , where the "action"  $L$  is the difference between the kinetic energy  $T$  and the potential energy  $U$ , plus the nonworking constraint forces  $W$ . Thus, from Hamilton's principle

$$\delta \int_{t_1}^{t_2} L(\underline{u}, \dot{\underline{u}}, t) dt = 0, \quad L \stackrel{\Delta}{=} T - U + W \quad (2.1.1)$$

The kinetic energy is the norm of the velocity vector  $\dot{\underline{u}}(\underline{r}, t)$  over the entire structure, weighted with  $\frac{1}{2} \rho(\underline{r})$ . We shall now assume that all vectors  $\underline{u}$  and  $\underline{r}$  are described in the same given reference frame, and we shall drop the basis vectors. Hence we denote  $\underline{u}$  and  $\underline{r}$

$$\begin{aligned} \underline{r} &= \underline{e}^T \underline{r} = \underline{e}_1 r_1 + \underline{e}_2 r_2 + \underline{e}_3 r_3 \\ \underline{u} &= \underline{e}^T \underline{u} = \underline{e}_1 u_1 + \underline{e}_2 u_2 + \underline{e}_3 u_3 \end{aligned} \quad (2.1.2)$$

simply by  $u \in R^3$  and  $r \in R^3$  with the basis  $\underline{e}$  understood. The kinetic energy may be written

$$T = \|\dot{\underline{u}}(r, t)\|_{\frac{1}{2} \rho(r)}^2 = \frac{1}{2} \int_E \dot{\underline{u}}^T(r, t) \rho(r) \dot{\underline{u}}(r, t) dr \quad (2.1.3)$$

where  $dr$  denotes a volume increment. The potential energy is the norm of the displacement vector  $\underline{u}(r, t)$  over the entire structure, weighted with  $\frac{1}{2} \bar{K}$  where  $\bar{K}$  is a symmetric matrix operator defined to include the boundary conditions. We will not pause here to elaborate on this definition of  $\bar{K}$ . Instead, we shall construct  $\bar{K}$  for an example. Now write the potential energy

$$U = \|\dot{u}(r, t)\|_{\frac{1}{2} \bar{K}}^2 = \frac{1}{2} \int_E u^T(r, t) \bar{K} u(r, t) dr \quad (2.1.4)$$

The first variation of (2.1.1) is given from the calculus of variations by

$$\begin{aligned} \delta \int_{t_1}^{t_2} L(u, \dot{u}, t) dt &= \left. \frac{\partial L}{\partial \dot{u}} \delta u \right|_{t_1}^{t_2} + \left( L - \frac{\partial L}{\partial \dot{u}} \dot{u} \right) \Delta t \Big|_{t_1}^{t_2} + \\ &\int_{t_1}^{t_2} \left( \frac{\partial L}{\partial u} - \frac{d}{dt} \frac{\partial L}{\partial \dot{u}} \right) \Delta u dt \end{aligned} \quad (2.1.5)$$

where

$$L = \frac{1}{2} \int_E \dot{u}^T \dot{u} \rho dr - \frac{1}{2} \int_E u^T \bar{K} u dr + \int_E f^T u dr \quad (2.1.6)$$

Hence, from the rules of differentiation

$$\frac{\partial L}{\partial \dot{u}} = \int_E \rho \dot{u} dr \quad (2.1.7)$$

$$\frac{\partial L}{\partial u} = - \int_E \bar{K} u dr + \int_E f dr \quad (2.1.8)$$

See from (2.1.5) that for variations which satisfy  $\left. \frac{\partial L}{\partial \dot{u}} \delta u \right|_{t_1}^{t_2} = 0$ ,  $(L - \frac{\partial L}{\partial \dot{u}} \dot{u}) \Delta t \Big|_{t_1}^{t_2} = 0$ , and for arbitrary variations  $\Delta u$  between  $t_1$  and  $t_2$  the requirement (2.1.1) dictates that

$$\frac{\partial L}{\partial u} - \frac{d}{dt} \frac{\partial L}{\partial \dot{u}} = 0 \quad (2.1.9)$$

which leads to (using (2.1.6)-(2.1.8))

$$-\int_E \bar{k}_u dr + \int_E f dr - \int_E \rho \ddot{u} dr = 0 \quad (2.1.10)$$

or equivalently,

$$\rho(r) \ddot{u}(r,t) + \bar{k}_u(r,t) = f(r,t) \quad (2.1.11)$$

with initial conditions,  $u(r,0) = u_0(r)$ ,  $\dot{u}(r,0) = \dot{u}_0(r)$ .

This is the partial differential equation describing the dynamics of the elastic structure of Fig. 2.1.

The Ritz method [5] is now illustrated to convert the partial differential equation (2.1.11) to an ordinary differential equation. Let the set of admissible basis functions  $\varphi_i(r)$ ,  $i = 1, 2, \dots$ , be *complete* (in the sense for arbitrary "square-integrable"  $u$ ,  $\min_{\{q_1, q_2, \dots\}} \|u - \psi q\|^2 = 0$ ). Then

$$u(r) \triangleq [\varphi_1(r), \varphi_2(r), \dots, \varphi_n(r)] \quad (2.1.12)$$

and in the mean squared-sense

$$u(r,t) = \varphi(r) q(t) \quad (2.1.13)$$

Substitution of (2.1.12)-(2.1.13) into (2.1.11) yields

$$\rho(r) \varphi(r) \ddot{q} + \bar{k} \varphi(r) q = f(r,t) \quad (2.1.14)$$

Multiply (2.1.14) from the left by  $\varphi^T(r)$  and integrate (2.1.14) with respect to the volume of the structure  $E$  to obtain

$$\left[ \int_E \varphi^T(r) \rho(r) \varphi(r) dr \right] \ddot{q} + \left[ \int_E \varphi^T(r) \bar{k} \varphi(r) dr \right] q = \int_E \varphi^T(r) f(r,t) dr \quad (2.1.15)$$

or, simply

$$M\ddot{q} + Kq = \delta(t) \quad (2.1.16a)$$

$$M \triangleq \int_E \psi^T(r) \rho(r) \psi(r) dr \quad (2.1.16b)$$

$$K \triangleq \int_E \psi^T(r) \bar{k}\psi(r) dr \quad (2.1.16c)$$

$$\delta(t) = \int_E \psi^T(r) f(r,t) dr \quad (2.1.16d)$$

where  $M$  is commonly referred to as the "mass matrix" of the structure and  $K$  is referred to as the "stiffness matrix" of the structure. If the forces  $f(r,t)$  are applied only at discrete points ( $r_1, r_2, \dots, r_m$ ) on the structure then

$$f(r,t) = \sum_{i=1}^m f_i \delta(r-r_i), \quad \underline{f}_i = f_i \underline{n}_i \quad (2.1.17)$$

where  $f_i$  is the force applied in the  $\underline{n}_i$  direction at the spatial location  $\underline{r}_i$ . Now (2.1.16) becomes

$$M\ddot{q} + Kq = Bu \quad (2.1.18a)$$

where

$$u^T = [f_1^T, f_2^T, \dots, f_m^T] \quad (2.1.18b)$$

$$B = [\psi^T(r_1), \psi^T(r_2), \dots, \psi^T(r_m)] \quad (2.1.18c)$$

Note that if torques rather than forces are applied to the structure, the right hand side of (2.1.18a) is changed as follows. Let the torque  $T$ , applied at  $r_1$  be described in the limit as  $\Delta r \rightarrow 0$  as a couple applied at  $r_1 + \frac{1}{2} \Delta r$  (that is, equal and opposite forces of magnitude  $f_1$  are separated by the small distance  $\Delta r$ , hence  $T = f_1 \Delta r$ ). Thus, for this couple the right

hand side of (2.1.18a) becomes

$$\begin{aligned}
 \delta u &= \lim_{\Delta r \rightarrow 0} [\psi^T(r_1)f_1 + \psi^T(r_2)f_2] & f_1 &= -f_2, & r_2 &= r_1 + \Delta r \\
 & & T &= f_1 \Delta r \\
 &= \lim_{\Delta r \rightarrow 0} \{[\psi^T(r_1 + \Delta r) - \psi^T(r_1)] \frac{T}{\Delta r}\} \\
 &= \frac{\partial \psi^T}{\partial r}(r_1) T(r_1, t) = \phi^T(r_1) T(r_1, t) = \phi^T(r_1) T_1
 \end{aligned} \tag{2.1.19}$$

where  $\phi \triangleq \partial \psi / \partial r$ . Therefore, we shall interpret the right hand side of (2.1.18a) as applying to either forces or torques simply by substituting  $T_i$  for  $f_i$  and  $\phi_i$  for  $\psi_i$  where a torque is applied.

## 2.2 The pinned elastic beam

The above equations of motion will be illustrated for the simply supported beam of Fig. 2.2. The beam has deflection  $u(r, t)$  only in the plane of the paper, where  $r$  is the position from the left end of the beam. The kinetic energy of such beams is given by (2.1.3)

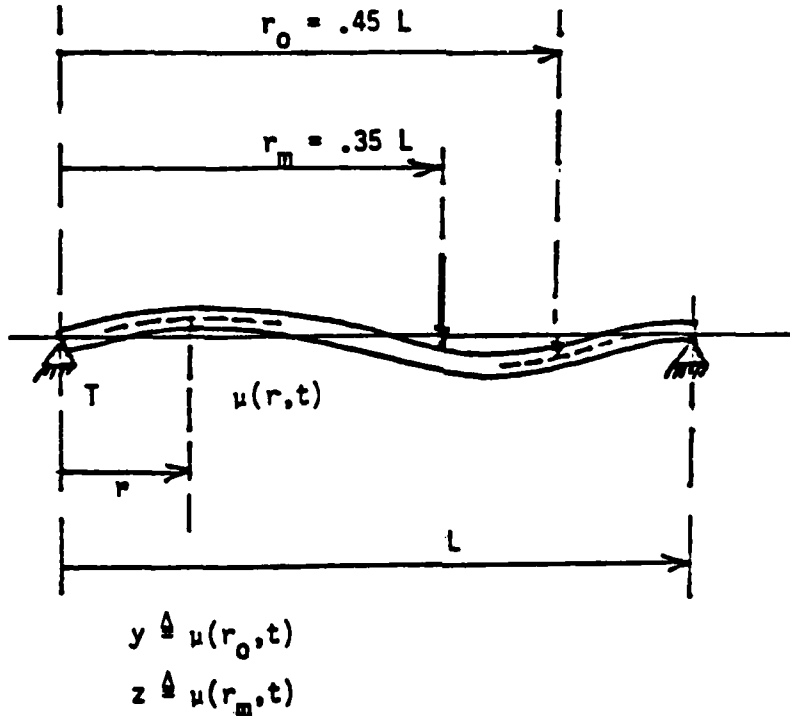


Fig. 2.2 Simply Supported Beam

$$T = \frac{1}{2} \int_0^L \rho(r) \dot{u}^2(r,t) \rho \, dr \quad (2.2.1)$$

A uniform mass density will be assumed so that  $\rho(r) = \rho = \text{const.}$  The potential energy for the beam is<sup>†</sup>

$$U = \frac{1}{2} \int_0^L EI \left[ \frac{\partial^2 u(r,t)}{\partial r^2} \right]^2 dr \quad (2.2.2)$$

where  $EI$ , the modulus of elasticity, will also be assumed constant.

Integrating (2.2.2) by parts twice leads to

$$U = \left\{ \left[ \frac{\partial u(r,t)}{\partial r} \frac{\partial^2 u(r,t)}{\partial r^2} \right] \Big|_0^L - \left[ u(r,t) \frac{\partial^3 u(r,t)}{\partial r^3} \right] \Big|_0^L \right. \\ \left. + \int_0^L u(r,t) \frac{\partial^4 u(r,t)}{\partial r^4} dr \right\} \frac{1}{2} EI \quad (2.2.3)$$

But since the beam in Fig. 2.2 has the boundary conditions

$$\frac{\partial^2 u(L,t)}{\partial r^2} = \frac{\partial^2 u(0,t)}{\partial r^2} = 0 \quad (2.2.4a)$$

$$u(L,t) = u(0,t) = 0 \quad (2.2.4b)$$

(2.2.3) reduces to

$$U = \frac{1}{2} EI \int_0^L u(r,t) \frac{\partial^4 u(r,t)}{\partial r^4} dr \quad (2.2.5)$$

Thus, comparison of (2.1.4) with (2.2.5) leads to the conclusion that the operator  $\bar{K}$  for the beam of Fig. 2.2 is

---

<sup>†</sup>The assumptions made here are that both the shear deformation and rotary inertia effects are negligible. This is the so-called Euler-Bernouli beam [6].

$$\bar{K} = EI \frac{\partial^4}{\partial r^4} \quad (2.2.6)$$

By comparing (2.1.4) with (2.2.3) it is now clearer what is meant by the earlier statement that the definition of the operator  $\bar{K}$  must include the boundary conditions.

Now the equation of motion (2.1.1) can be written using (2.2.6) and the notation  $[ ]^{(4)} = \frac{\partial^4 [ ]}{\partial r^4}$ ,

$$\rho \ddot{u}(r,t) + EI u^{(4)}(r,t) = f(r,t) = f(r_c,t) \delta(r-r_c) \quad (2.2.7)$$

$$y = u(r_0,t)$$

where  $f(r_c,t)$  is the applied force at location  $r_c$  in Fig. 2.2 and  $y \triangleq u(r_0,t)$  is the displacement at point  $r_0$ . The boundary conditions for (2.2.7) are given by (2.2.4).

Using the Ritz method (2.1.13) we shall investigate the solution of (2.2.7). Consider first the homogeneous solution,

$$\rho \ddot{v}(r) \bar{q}(t) + EI v^{(4)}(r) q(t) = 0 \quad (2.2.8)$$

For convenience, define the scalar  $\omega_i^2$  by

$$\rho \omega_i^2 v_i(r) = EI v_i^{(4)}(r), \quad v_i(L) = v_i(0) = v_i''(L) = v_i''(0) = 0 \quad (2.2.9)$$

where the boundary conditions on the  $v_i$  satisfy the physical constraints (2.2.4). The matrix  $\Omega^2$  will be defined by

$$\Omega^2 = \begin{bmatrix} \omega_1^2 & & \\ & \omega_2^2 & \\ & & \ddots \end{bmatrix} \quad (2.2.10)$$

Now (2.2.8) may be written

$$\rho \Psi(r) [\ddot{q}(t) + \Omega^2 q(t)] = 0 = \rho \sum_{i=1}^{\infty} \Psi_i(r) [\ddot{q}_i + \omega_i^2 q_i] = 0 \quad (2.2.11)$$

But since the  $\Psi_i(r)$  are linearly independent, (2.2.11) requires that for all  $i = 1, 2, \dots$ ,

$$\ddot{q}_i(t) + \omega_i^2 q_i(t) = 0 \quad (q_i(0), \dot{q}_i(0) \text{ specified}) . \quad (2.2.12)$$

Our first trial solution for (2.2.9) is

$$\Psi_i(r) = A_i \cosh \beta_i r + B_i \sinh \beta_i r + C_i \cos \beta_i r + D_i \sin \beta_i r$$

where  $\beta_i^4 \triangleq \rho \omega_i^2 / EI$ . Now to check to see if this is an admissible solution we must satisfy (2.2.9). The four boundary conditions require

$$\begin{aligned} \Psi_i(0) = 0 &= A_i \cosh 0 + B_i \sinh 0 + C_i \cos 0 + D_i \sin 0 \\ &= A_i + C_i \end{aligned}$$

Likewise,

$$\Psi_i''(0) = 0 = A_i - C_i$$

Hence  $A_i = C_i = 0$ . Now,

$$\Psi_i(L) = 0 = B_i \sinh \beta_i L + D_i \sin \beta_i L$$

$$\Psi_i''(L) = 0 = B_i \sinh \beta_i L - D_i \sin \beta_i L .$$

Add these two eqns. to get  $2B_i \sinh \beta_i L = 0, \Rightarrow B_i = 0$ . Hence,  $D_i \sin \beta_i L = 0$  also, the nontrivial solution of which is  $\sin \beta_i L = 0$  or

$$\beta_i = \frac{i\pi}{L}, \quad i = 1, 2, 3, \dots \quad (2.2.13)$$

Hence,

$$\psi_i(r) = D_i \sin \frac{i\pi}{L} r \quad (2.2.14)$$

$$\Psi(r) = [\psi_1(r), \dots, \psi_\infty(r)] ,$$

and from (2.2.9)

$$\omega_i = \sqrt{\frac{EI}{\rho}} \beta_i^2 = \sqrt{\frac{EI}{\rho}} \left(\frac{i\pi}{L}\right)^2 , \quad i = 1, 2, \dots, \infty \quad (2.2.15)$$

which establishes the frequencies of vibration of the simply supported beam of Fig. 2.2..

We shall make the columns of  $\Psi(r)$  orthogonal. That is, the columns of  $\Psi(r)$  are orthogonal on  $r \in E$  ( $r$  ranges throughout the elastic structure  $E$ ) subject to the weight  $g(r)$  if

$$\Lambda = \int_E \Psi^T(r) g(r) \Psi(r) dr \quad (2.2.16)$$

is a diagonal matrix. Note from (2.1.16b) that (2.2.16) is simply the *mass* matrix of the structure if we choose the weight  $g(r) = \rho(r)$ , and (2.2.16) is the *stiffness* matrix if we choose the weight  $g(r) = \bar{K}$ . We shall choose  $g(r) = \rho(r)$  so that  $\Lambda$  is the mass matrix. For the present example  $\psi_i(r)$  is given by (2.2.14) for some unspecified  $D_i$ . Substituting (2.2.14) into (2.2.16) yields

$$\Lambda_{ij} = \int_0^L \rho D_i^2 \sin \frac{i\pi}{L} r \sin \frac{j\pi}{L} r dr = \rho \frac{D_i^2 L}{2} \delta_{ij} \quad (2.2.17)$$

If we choose  $\Lambda_{ii} = 1$  (i.e. normalize the mass matrix to identity  $M = I$ ), then (2.2.17) yields

$$D_i = \sqrt{\frac{E}{\rho L}} \quad , \quad i = 1, 2, \dots \quad (2.2.18)$$

Hence, from (2.2.15), (2.2.18) the  $i^{\text{th}}$  "mode shape" is

$$\Psi_i(r) = \sqrt{\frac{E}{\rho L}} \sin \frac{i\pi}{L} r \quad , \quad i = 1, 2, \dots \quad (2.2.19)$$

The homogeneous solution of (2.2.9) is now completed.

The homogeneous solution of (2.2.12) is

$$q_i(t) = Q_i \sin(\omega_i t + \phi_i) \quad (2.2.20)$$

as can easily be checked by substituting into (2.2.12) if  $Q_i$  and  $\phi_i$  are chosen to satisfy the initial conditions,  $Q_i \sin \phi_i = q_{i0}$ ,  $\omega_i Q_i \cos \phi_i = \dot{q}_{i0}$ . That is,

$$Q_i = \sqrt{q_{i0}^2 + \dot{q}_{i0}^2 / \omega_i^2} \quad , \quad \phi_i = \tan^{-1} q_{i0} \omega_i / \dot{q}_{i0} \quad (2.2.21)$$

Thus, the complete homogeneous solution of (2.2.7) is

$$\begin{aligned} u(r, t) &= \Psi(r)q(t) = \sum_{i=1}^{\infty} \Psi_i(r) q_i(t) \\ &= \sum_{i=1}^{\infty} \sqrt{\frac{E}{\rho L}} \sin \frac{i\pi r}{L} Q_i \sin(\omega_i t + \phi_i) \end{aligned} \quad (2.2.22)$$

The first 5 mode shapes (2.2.19) are plotted in Fig. 2.3.

Models are constructed for a specific purpose. No single model is adequate for all purposes. Now suppose one is interested in using the model of the beam to study the RMS or mean-squared deflections and their rates over the surface of the beam, during the interval  $t \in [0, t_f]$ . That is, suppose one is particularly interested in computing

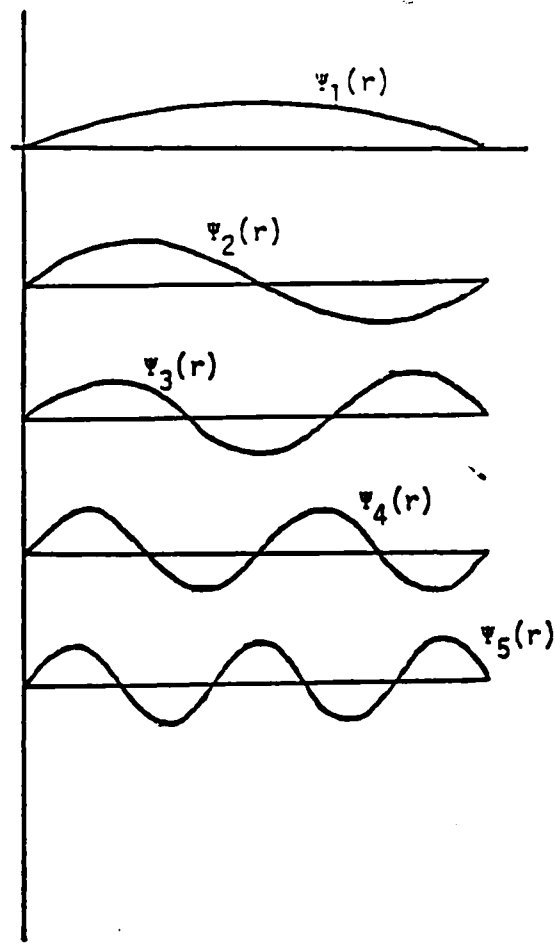


Fig. 2.3 Mode shapes for pinned elastic beam

$$V \triangleq \int_0^{t_f} (\|u(r,t)\|_{g_1(r)}^2 + \|\dot{u}(r,t)\|_{g_2(r)}^2) dt \quad (2.2.23)$$

for some weights  $g_1(r)$ ,  $g_2(r)$ , where the norm of  $u(r,t)$  on the domain of  $r$  is defined by

$$\|u(r,t)\|_{g_1(r)}^2 \triangleq \int_E u^T(r,t) g_1(r) u(r,t) dr \quad (2.2.24)$$

From (2.1.3), (2.1.4) note that the choices  $g_1(r) = \frac{1}{2} \bar{K}$ ,  $g_2(r) = \frac{1}{2} \rho(r)$  yields  $V = \int_0^{t_f} (T+U) dt$ , (although we do not have to restrict  $g_1(r)$ ,  $g_2(r)$  to these choices). Now substitute  $u(r,t) = \Psi(r) q(t)$  to get

$$V = \int_0^{t_f} \int_E [q^T(t) \Psi^T(r) q_1(r) \Psi(r) q(t) + \dot{q}^T(t) \Psi^T(r) g_2(r) \Psi(r) \dot{q}(t)] dr dt \quad (2.2.25)$$

For  $g_1(r) = \frac{1}{2} \bar{K}$ ,  $g_2(r) = \frac{1}{2} \rho(r)$ ,  $V$  becomes

$$V = \int_0^{t_f} [q^T(t) K q(t) + \dot{q}^T(t) M \dot{q}(t)] dt \quad (2.2.26)$$

Now if  $\Psi(r)$  is normalized so that

$$M = I, \quad K = \Omega^2 = \text{diag}\{\omega_1^2, \dots, \omega_N^2\} \quad (2.2.27)$$

then

$$V = \int_0^{t_f} \sum_{i=1}^N (q_i^2(t) \omega_i^2 + \dot{q}_i^2(t)) dt = \sum_{i=1}^N V_i \quad (2.2.28)$$

where

$$V_i = \int_0^{t_f} (q_i^2(t) \omega_i^2 + \dot{q}_i^2(t)) dt \quad (2.2.29)$$

From (2.2.20) integration in (2.2.28) yields

$$V_i = \omega_i^2 Q_i^2 t_f \quad (2.2.30)$$

But since  $Q_i^2 = q_i^2(0) + \dot{q}_i^2(0)/\omega_i^2$ ,

$$V_i = [\omega_i^2 q_i^2(0) + \dot{q}_i^2(0)] t_f \quad (2.2.31)$$

Hence, the energy in each mode  $T(0) + U(0) = \dot{q}_i^2(0) + \omega_i^2 q_i^2(0)$  stays constant and this magnitude determines the critical modes of the structure with respect to the performance measure (2.2.23). Due to the special structure assumed for the mass and stiffness (matrices) in (2.2.27), the  $q_i$  are *modal* coordinates and  $V_i$  in (2.2.31) are referred to as *modal costs*. More about modal cost analysis later.

Now suppose a different performance measure is of interest. Suppose one is interested only in the deflections and rates at the location  $r_0$  (Fig. 2.2), rather than in the distribution of the deflections over the entire structure as in the previous example. For this new performance measure choose  $g_1(r)$ , and  $g_2(r)$  in (2.2.23) such that

$$g_1(r) = g_1(r_0) \delta(r-r_0), \quad g_2(r) = g_2(r_0) \delta(r-r_0) \quad (2.2.32)$$

Now (2.2.25) becomes

$$V = \int_0^{t_f} [\dot{q}^T(t) \Psi^T(r_0) g_1(r_0) \Psi(r_0) q(t) + \dot{q}^T(t) \Psi^T(r_0) g_2(r_0) \Psi(r_0) \dot{q}(t)] dt \quad (2.2.33)$$

In order to examine the *modal* contributions in  $V$  the transformation to modal coordinates is made

$$q = E \eta \quad (2.2.34)$$

where  $E$  is chosen such that

$$\begin{aligned} E^T M E &= I \\ E^T K E &= \Omega^2 = \text{diag. } \{\omega_1^2 \dots \omega_N^2\} \end{aligned} \quad (2.2.35)$$

Define

$$Q_1 \triangleq E^T \Psi^T(r_0) g_1(r_0) \psi(r_0) E \quad (2.2.36)$$

$$Q_2 \triangleq E^T \Psi^T(r_0) g_2(r_0) \psi(r_0) E$$

then

$$V = \int_0^{t_f} (\dot{n}^T Q_1 \dot{n} + \dot{n}^T Q_2 \dot{n}) dt = \sum_{i,j=1}^N \int_0^{t_f} (\dot{n}_i \dot{n}_j Q_{1ij} + \dot{n}_i \dot{n}_j Q_{2ij}) dt \quad (2.2.37)$$

where  $\ddot{n}_i + \omega_i^2 n_i = 0$ ,  $i = 1, \dots, N$ . The contribution from  $n_i$ ,  $\dot{n}_i$  is

$$V_i = \int_0^{t_f} (\dot{n}^T Q_{1i} \dot{n}_i + \dot{n}^T Q_{2i} \dot{n}_i) dt \quad (Q_{1i} = i^{\text{th}} \text{ col. of } Q_1) \quad (2.2.38)$$

where the modal cost  $V_i$  satisfies the cost-decomposition property

$$V = \sum_{i=1}^N V_i \quad (2.2.39)$$

To simplify the expressions in this illustrative example we assume  $n_i(0) = 0$ ,  $\dot{n}_i(0) \neq 0$ . Then the integral becomes

$$V_i = \left[ \frac{\dot{n}_i^2(0)}{2\omega_i^2} Q_{1ii} + \frac{\dot{n}_i^2(0)}{2} Q_{2ii} \right] t_f \quad (2.2.40)$$

$$V_i = \frac{1}{2} \dot{n}_i^2(0) t_f [Q_{1ii}/\omega_i^2 + Q_{2ii}] \quad (2.2.41)$$

for any  $t_f$  satisfying

$$\begin{aligned} 2\omega_i t_f &= \alpha\pi \\ (\omega_i - \omega_j) t_f &= \beta\pi \\ (\omega_i + \omega_j) t_f &= \gamma\pi \end{aligned} \quad (2.2.42)$$

for any integers  $\alpha$ ,  $\beta$ ,  $\gamma$ . This condition on  $t_f$  allows the crossproduct terms between  $V_i$  and  $V_j$  to be zero. Thus  $V_i$  in (2.2.38) is presented as an example and not a general result in order to discuss the *concept* of modal

cost analysis. The general theory is presented in a latter section. Note that the importance of mode  $i$  is measured by the magnitude of  $V_i$ .

To investigate the forced solution of (2.2.7), first assume a solution of the form

$$u(r,t) = \psi(r)q(t) \quad (2.2.43)$$

where  $\psi(r)$  is given as before (2.2.19), and  $q(t)$  is unknown. Since the  $\psi_i(r)$ ,  $i = 1, 2, \dots$  form a complete set they may be used as basis functions for the forced response as well. Multiplying (2.2.7) by  $\psi^T(r)$  and integrating with respect to  $r$  yields the earlier result (2.1.15) repeated here for the beam example with a torque applied at  $r = r_c = 0$ . (see Fig. 2.2 and Eqs. (2.1.18), (2.1.19)).

$$M\ddot{q} + Kq = \phi^T(r_c)T(r_c,t) \quad (2.2.44)$$

The unit normalization of the mode shapes (2.2.16) yields  $M = I$ . Hence,

$$\ddot{q}_i(t) + \omega_i^2 q_i(t) = \phi_i^T(r_c)T(r_c,t) \quad (2.2.45)$$

where the definition of  $\omega_i^2$  is given by (2.2.9), (2.2.15). Note that the  $i^{\text{th}}$  mode shape at the point of application  $r_c$  of the force

$$\phi_i(r_c) \triangleq \left. \frac{\partial \psi_i}{\partial r} \right|_{r=r_c} = \frac{i\pi}{L} \sqrt{\frac{2}{\rho L}} \cos \frac{i\pi}{L} r_c \quad (2.2.46)$$

is zero if  $r_c = \frac{kL}{2i}$  for any integer  $k$ . These points are called "nodes" of the  $i^{\text{th}}$  mode slope. Thus, if a torque is applied at a node of mode  $i$ , then the torque cannot excite mode  $i$ . A systematic way to deal with these events will be developed in the next chapter.

### 2.3 State Equations

The equations of motion are now summarized by

$$\ddot{q}_i + \omega_i^2 q_i = \phi_i^T(r_c) T(r_c, t) \quad , \quad i = 1, 2, \dots \quad (2.3.1)$$

$$y \triangleq u(r_o, t) = \psi(r_o) q(t) = \sum_{i=1}^n \psi_i(r_o) q_i(t)$$

$$z \triangleq u(r_m, t) = \psi(r_c) q(t) = \sum_{i=1}^n \psi_i(r_m) q_i(t)$$

A set of first order differential eqs. can be generated from (2.3.1) as follows

$$\frac{d}{dt} \begin{pmatrix} q_1 \\ \dot{q}_1 \\ q_2 \\ \dot{q}_2 \\ \vdots \\ \vdots \\ \vdots \end{pmatrix} = \begin{bmatrix} 0 & 1 & & \\ -\omega_1^2 & 0 & & \\ & & 0 & 1 \\ & & -\omega_2^2 & 0 \\ & & & & \ddots & \ddots \end{bmatrix} \begin{pmatrix} q_1 \\ \dot{q}_1 \\ q_2 \\ \dot{q}_2 \\ \vdots \\ \vdots \\ \vdots \end{pmatrix} + \begin{bmatrix} 0 \\ b_1^T \\ 0 \\ b_2^T \\ \vdots \\ \vdots \\ \vdots \end{bmatrix} f(r_o, t) \quad (2.3.2)$$

$$\begin{pmatrix} u(r_o, t) \\ u(r_m, t) \end{pmatrix} = \begin{bmatrix} p_1 & 0 & p_2 & 0 & \dots & \dots \\ m_1 & 0 & m_2 & 0 & & \end{bmatrix} \begin{pmatrix} q_1 \\ \dot{q}_1 \\ q_2 \\ \dot{q}_2 \\ \vdots \\ \vdots \end{pmatrix}$$

where

$$b_i^T = \phi_i^T(r_c)$$

$$p_i = \psi_i(r_o)$$

$$m_i = \psi_i(r_m)$$

The parameters for the beam example is given by

$$L = \pi, \quad \rho = 2/L, \quad EI = \rho, \quad r_o = .45L, \quad r_c = 0,$$

$$r_m = .35L$$

and for the choices

$$\omega_i = i^2, \quad p_i = \sin(.45\pi i), \quad m_i = \sin(.35\pi i), \quad b_i = i.$$

Note from (2.2.44) or (2.3.1) that the number of variables  $(q_1, q_2, \dots, q_N)$  required to *write* the differential equations is  $N$ , whereas, the number of pieces of information required to *solve* the differential equations (2.2.44) or (2.3.1) is  $2N$  (both  $\dot{q}_i(0)$  and  $\ddot{q}_i(0)$  must be specified). That is, the *order* of the system of eqs. (2.2.44); (2.3.1) is  $2N$  if  $q \in R^N$ , and the order of the system dictates the number of necessary initial conditions required to solve the equations (2.3.2). The variables  $q_i$  in (2.2.44) are called *configuration variables* in dynamics [ 7 ]. If the system (2.3.1) is put into the first order form (2.3.2), then the variables  $(q_1, \dot{q}_1, q_2, \dot{q}_2, \dots, q_N, \dot{q}_N) = x^T$  are called the *state* variables.

For the simply supported beam (2.3.2) the state equations are

$$\begin{aligned} \dot{x} &= Ax + Bu, & x &\in R^{2N}, \quad \bar{T}(r_c, t) = u \in R^1 \\ y &= Cx, & u(r_o, t) &= y \in R^1 \\ z &= Mx, & u(r_m, t) &= z \in R^1 \end{aligned} \quad (2.3.3)$$

where

$$A = \begin{bmatrix} 0 & 1 & & \\ -\omega_1^2 & 0 & & \\ & & 0 & 1 \\ & & -\omega_2^2 & 0 \\ & & & & \ddots & \ddots \end{bmatrix}, \quad B = \begin{bmatrix} 0 \\ b_1^T \\ 0 \\ b_2^T \\ \vdots \end{bmatrix}, \quad x = \begin{pmatrix} q_1 \\ \dot{q}_1 \\ q_2 \\ \dot{q}_2 \\ \vdots \end{pmatrix} \quad (2.3.3)$$

$$C = [p_1 \ 0 \ p_2 \ 0 \ p_3 \ \dots], \quad M = [m_1 \ 0 \ m_2 \ 0 \ m_3 \ \dots]$$

We now add noise to the actuators and sensors to make the model (2.3.3) more realistic. Define  $w(t)$  as a zero-mean white noise with intensity  $W$ . That is,

$$E w(t) = 0 \quad (2.3.4a)$$

$$E w(t)w^T(\tau) = W\delta(t-\tau) \quad (2.3.4b)$$

$$E w(t)x^T(0) = 0, \quad t \geq 0 \quad (2.3.4c)$$

where  $E$  is the expectation operator

$$E [\cdot] \triangleq \int_{-\infty}^{\infty} [\cdot] f(\xi) d\xi \quad (2.3.5)$$

where  $f(\xi)$  is the probability density function of the random variable  $[\cdot]$ , as the sample space ranges over  $-\infty \leq \xi \leq \infty$ . The torque actuator which produces the desired control torque  $T(r_c, t)$  in (2.3.3) also produces the

undesired "noisy" torque  $w(t)$ . Hence  $T(r_c, t)$  is replaced by  $T(r_c, t) + w(t)$ . That is,  $Bu$  is replaced by  $Bu + Dw$  where  $D = B$  in our special case, although disturbances from other sources would call for a more general  $D \neq B$ .

The noisy measurements are described by

$$E v(t) = 0 \quad (2.3.6a)$$

$$E v(t) v^T(\tau) = V\delta(t-\tau) \quad (2.3.6b)$$

$$E v(t) x^T(0) = 0 \quad (2.3.6c)$$

$$E v(t) w^T(\tau) = 0 \quad (2.3.6d)$$

Equations (2.3.4c), (2.3.6c), and (2.3.6d) result from the assumption that the random vectors  $x(0)$ ,  $w(t)$ ,  $v(t)$  are assumed to be independent. The complete system description is now given by

$$\begin{aligned} \dot{x} &= Ax + Bu + Dw \\ y &= Cx \\ z &= Mx + v \end{aligned} \quad (2.3.7)$$

where  $w$  and  $v$  are described by (2.3.4) and (2.3.6). Models of the form (2.3.7) will be used throughout the sequel. The performance of the system (2.3.7) will be measured by

$$J \triangleq \lim_{t \rightarrow \infty} E \frac{1}{t} \int_0^t (y^T Q y + u^T R u) dt \quad (2.3.8)$$

where the notation  $\|y\|_Q^2 = y^T Q y$  will often be used to illustrate that the norm of the vector  $y$  is of primary interest in the control objective. The term  $\|u\|_R^2 = u^T R u$  measures the amount of control effort being used to keep  $\|y\|_Q^2$  small. In the first of our studies we shall set  $u = 0$  in order to study the open-loop situation - the behavior of the structure without feedback control. Our great difficulties begin with the recognition

that the model (2.3.7) is of order  $2N$  and even for the simply supported beam example  $N \rightarrow \infty$ . In order to make our analysis and control design tractable we are forced to consider the topic of model reduction.

### 3.0 MODEL REDUCTION BY COMPONENT COST ANALYSIS

#### 3.1 Introduction

Numerous schemes for model reduction exist in the literature. Many of these schemes are not applicable to the model reduction of flexible space structures, due to the large dimension of these models. Modal Cost Analysis (MCA) is one method which can be easily applied to such systems. MCA is a special case of Component Cost Analysis (CCA), which also offers a theory of 'Cost Equivalent Realizations' (CER).

After a brief introduction to component cost analysis, we present the MCA, and the CER-theory and compare these two methods with the aid of the pinned beam example.

#### 3.2 Brief Description of CCA

Basically, CCA considers any system as an interaction of different *components* constituting the system. The definition of these components is up to the analyst: they may have physical significance, or they may be defined for mathematical convenience. For *any* choice of components CCA assigns a metric called *component cost* to each component. These component costs measure the significance (contribution) of each component to a predefined quadratic cost function. Then, a reduced model of the given system is obtained by deleting those components that have the smallest component costs.

Mathematically, the concepts of CCA are explained as follows:  
Let a state space description of a time-invariant system driven by

zero mean gaussian white noise process  $w$ , with intensity  $\omega$  be given as

$$\begin{aligned} \dot{x} &= Ax + Dw; \quad x \in R^n, w \in R^m \\ y &= Cx \quad ; \quad y \in R^k \end{aligned} \quad (3.2.1a)$$

(one may specify appropriate initial conditions on the states  $x$ ; however, for the infinite-time problems considered herein, these initial conditions become irrelevant). The system (3.2.1a) can be equivalently expressed in its 'component' form as

$$\begin{aligned} \dot{x}_i &= \sum_{j=1}^p A_{ij} x_j + D_i w; \quad x_i \in R^{n_i}, \quad \sum_{i=1}^p n_i = n \\ y &= \sum_{j=1}^p C_j x_j \end{aligned} \quad (3.2.1b)$$

where the states  $x_i$  define the  $i$ -th 'component'.

Now, let a cost function associated with (3.2.1) be given as

$$V = \lim_{t \rightarrow \infty} E \{V(t)\}; \quad V(t) \triangleq \frac{1}{t} \int_0^t \|y(\sigma)\|_Q^2 d\sigma \quad (3.2.2)$$

where  $Q > 0$  is a weighting matrix and where  $\|\cdot\|_Q^2$  is the weighted Euclidian norm. The component costs  $\hat{V}_i$ , associated with each component  $x_i$  are defined by

$$\hat{V}_i \triangleq \frac{1}{2} \lim_{t \rightarrow \infty} E \left\{ \frac{\partial V(t)}{\partial x_i} x_i \right\}, \quad i = 1, 2, \dots, p \quad (3.2.3)$$

and are calculated according to the following component cost formula.

*Component Cost Formula*

$$\hat{V}_i = \text{Tr} [C^T Q C]_{ii}, \quad i = 1, 2, \dots, p \quad (3.2.4a)$$

where  $X$ , the steady state covariance of the states, satisfies

$$XA^T + AX + DWD^T = 0 \quad (3.2.4b)$$

Clearly, since  $V = \text{Tr} [C^T Q C X]$ , [8], the component costs  $\hat{v}_i$  satisfy the *cost decomposition property*

$$V = \sum_{i=1}^p \hat{v}_i. \quad (3.2.5)$$

(Note: in Section II, this property was shown to hold for the special case of *modal* costs, (ref. eqn. (2.2.39)).

For certain definitions of components, it is possible for a component cost  $\hat{v}_i$  to be negative. However, for the components defined in this report, these component costs are non-negative. Hence, we will assume for clarity, that  $\hat{v}_i \geq 0$ .

Based upon the definition of component costs, the CCA algorithm for model reduction is therefore characterized by these two steps.

#### *The Basic CCA Model Reduction Algorithm*

- I. Compute the component costs  $\hat{v}_i$  by (3.2.4) and reorder the components  $x_i$  in (3.2.1b) so that

$$\hat{v}_1 \geq \hat{v}_2 \geq \dots \geq \hat{v}_r \geq \hat{v}_{r+1} \geq \dots \geq \hat{v}_p \quad (3.2.6)$$

- II. To obtain a reduced model retaining only  $r$  components, delete the  $(p-r)$  components associated with the  $(p-r)$  smallest component costs from (3.2.1b). The reduced model can then be written as

$$\dot{x}_R = A_R x_R + D_R w; \quad x_R \in R^{n_r}, \quad n_r \triangleq \sum_{i=1}^r n_i \quad (3.2.7a)$$

$$\hat{y} = C_R x_R$$

where

$$A_R \triangleq \begin{bmatrix} A_{11} & A_{12} & : & A_{1r} \\ A_{21} & A_{22} & : & A_{2r} \\ : & : & : & : \\ A_{r1} & A_{r2} & : & A_{rr} \end{bmatrix} \quad D_R \triangleq \begin{bmatrix} D_1 \\ D_2 \\ : \\ D_r \end{bmatrix} \quad (3.2.7b)$$

$$C_R \triangleq [C_1, C_2, : C_r]$$

*Cost Perturbation Indices:*

When comparing the reduced model (3.2.7) with the original model (3.2.1), a convenient measure of 'model error' is defined and calculated as follows.

*Definition 3.1* The error associated with the model (3.2.7) produced by the CCA algorithm is measured by the *Cost Perturbation Index*,  $q$

$$q \triangleq \frac{1}{V} |V - V_R| \quad (3.2.8a)$$

where  $V_R$  is the cost associated with (3.2.7) defined as

$$V_R \triangleq \lim_{t \rightarrow \infty} E(V_R(t)); \quad V_R(t) = \frac{1}{t} \int_0^t \|\hat{y}(\sigma)\|_Q^2 d\sigma \quad (3.2.8b)$$

If the disturbance subspace of (3.2.7) is asymptotically stable, then

$$V_R = \text{Tr}[C_R^T Q C_R X_R] \quad (3.2.9a)$$

where  $X_R$ , the steady state covariance of  $x_R$ , satisfies

$$X_R A_R^T + A_R X_R + D_R \omega D_R^T = 0. \quad (3.2.9b)$$

Remark: The cost perturbation index  $q$  measures the difference in the overall mean-squared values of the outputs.

Of course,  $V_R$  ( and hence  $q$  ) can be computed only *after* model reduction. The information available *a priori* can be used to compute only the predicted cost perturbation index  $\hat{q}$ , defined below.

*Definition 3.2* The predicted cost perturbation index  $\hat{q}$  is defined by

$$\hat{q} \triangleq \frac{1}{V} (V - \hat{V}_R) \quad (3.2.10a)$$

where  $\hat{V}_R \triangleq \sum_{i=1}^r \hat{V}_i. \quad (3.2.10b)$

Thus, CCA offers a simple way of 'pricing' each 'component' of a system, thereby identifying components that can be deleted to form a reduced model. It also offers convenient indices for the evaluation of the 'errors' in these reduced models.

### 3.3 Modal Cost Analysis (MCA)

#### 3.3.1 General Formulation:

In the context of model reduction, there may be considerable freedom in the definition of 'components' before model reduction begins. That is to say that the definition of components is up to the analyst.

For mechanical systems described in matrix second order form, it is customary to obtain its reduced model by ignoring high-frequency modes, without regards to the performance objective (cost function). Modal Cost Analysis (MCA) was introduced to systematically identify those modes that have the least significance in the cost function. MCA is a special case of Component Cost Analysis. In MCA, a mechanical system described by  $N$ -modes, is decomposed into  $N$ -components  $x_i$ ,  $i = 1, 2, \dots, N$ , where each component  $x_i$  is defined by

$$x_i \triangleq \begin{bmatrix} \eta_i \\ \dot{\eta}_i \end{bmatrix} \in \mathbb{R}^2, \quad i = 1, 2, \dots, N \quad (3.3.1)$$

where the  $i$ -th modal displacement is  $\eta_i$  and the corresponding rate is  $\dot{\eta}_i$ . (Refer to (2.2.34) and (2.2.38)). The CCA of these components  $x_i$  is called MCA. The matrices in the 'component-descriptions' (3.2.1b) of the system take the form

$$A_{ii} = \begin{bmatrix} 0 & 1 \\ -\omega_i^2 & -2\zeta_i\omega_i \end{bmatrix} \in \mathbb{R}^{2 \times 2} \quad (3.3.2a)$$

$$A_{ij} = 0 \quad j \neq i$$

$$D_i = \begin{bmatrix} 0 \\ b_i^T \end{bmatrix} \in \mathbb{R}^{2 \times m}, \quad u = u \quad (3.3.2b)$$

$$C_i = [p_i \quad p_i'] \in \mathbb{R}^{k \times 2} \quad (3.3.2c)$$

where the output  $y$  is related to the modes by

$$y = \sum_{i=1}^N p_i n_i + \sum_{i=1}^N p_i' \dot{n}_i. \quad (3.3.3)$$

In order to compute the modal costs  $\hat{v}_i$ , one would then use the equations (3.2.4a) and (3.2.4b). It is possible to obtain closed form expression for modal costs  $\hat{v}_i$  in terms of the modal data. And, this expression greatly simplifies under certain conditions on the system, as given below.

*Theorem 3.1*

If either (a), (b), or (c) holds:

$$(a) \quad b_i^T u b_j = 0, \quad i \neq j \quad (\text{input decoupled modes})$$

$$(b) \quad c_i^T Q c_j = 0, \quad i \neq j \quad (\text{output decoupled modes})$$

$$(c) \quad \zeta_i \rightarrow 0, \quad i = 1, 2, \dots, N \quad (\text{lightly damped modes})$$

$$\text{with } \omega_i^2 \neq \omega_j^2 \text{ and } p_i^T Q p_j = p_i^T Q p_i'; \quad j \neq i$$

then the model costs are given by

$$\hat{v}_i = \frac{1}{4\zeta_i\omega_i^3} \{ \|P_i\|_Q^2 + \omega_i^2 \|P_i'\|_Q^2 \} \|b_i\|_U^2 \geq 0 \quad (3.3.4)$$

#### Remarks

- 1) Since the modes, by definition, are dynamically uncoupled, mode  $i$  is uncontrollable (unobservable) if and only if  $b_i \equiv 0$  ( $P_i \equiv 0$  and  $P_i' \equiv 0$ ). Hence,  $\hat{v}_i = 0$ , if and only if that mode is either uncontrollable and/or unobservable. Note from the definitions of  $b_i$  in (2.3.2), and  $\varphi_i(r_c)$  in (2.2.46) that if a force is applied at a mode of mode  $i$ , then  $b_i \neq 0$ , i.e., mode  $i$  is uncontrollable and hence  $\hat{v}_i \neq 0$ . Similar argument applies to unobservability of mode  $i$ . Thus MCA offers a systematic way to deal with these events.
- 2) Since the rigid body modes have zero frequencies ( $\omega_i = 0$ ), by (3.3.4) they have infinite modal costs if they are both observable and controllable.
- 4) The computations of the modal costs  $\hat{v}_i$  are obviously simple and can be carried out for any number of modes.
- 4) Almost all of the flexible space structures have very low damping (typically  $\zeta_i = .005$ ) and in most of the applications  $P_i^T Q P_j = 0$ ,  $i \neq j$ . Hence, for such structures, the condition (c) of Theorem 3.1 always holds. In the sequel, therefore, we will assume that this condition is satisfied.

The CCA algorithm for model reduction would then delete those modes that have the smallest  $\hat{v}_i$  to yield a reduced model. The cost perturbation indices associated with such a reduced model satisfy the following.

*Theorem 3.2*

For lightly damped structures, the cost perturbation indices associated with the reduced models produced by the CCA algorithm satisfy

$$q = \hat{q} = \sum_{i \in T} \hat{v}_i / V \quad (3.3.5)$$

where the set  $T$  corresponds to the deleted modes.

Remarks:

- 1) The predicted cost perturbation index is exact (i.e.  $\hat{q} = q$ ) and is calculated by (3.3.5)
- 2) The cost perturbation indices ( $q$  and  $\hat{q}$ ) are evaluated with respect to the cost functions (3.2.2).

We have assumed the definition of the output  $y$  in (3.3.3), (i.e.  $P_i$  and  $P_i'$ ), and the weighting matrix  $Q$  in (3.2.2) to be arbitrary (without enforcing any relation to the performance objective (2.3.8)). Different choices of  $y$  offer different interpretations of the cost function  $V$ . For instance, by proper choice of  $P_i$  and  $P_i'$ ,  $V$  can be made to reflect either potential energy and/or kinetic energy of the system. Now since the model reduction decisions in MCA are based upon  $V$ , different choices of  $V$  will therefore yield different reduced models.

In the following subsections we will present two cost functions  $V$  related to the performance objective (2.3.8) and study their merits. The cost functions considered are

$$3.3.2) \quad V = V_c \stackrel{\Delta}{=} V_y + \rho V_u \quad (3.3.6a)$$

$$3.3.3) \quad V = V_o \stackrel{\Delta}{=} V_y + \beta V_z \quad (3.3.6b)$$

where

$$V_y \stackrel{\Delta}{=} \lim_{t \rightarrow \infty} \frac{1}{t} E \int_0^t \|y(\sigma)\|_Q^2 d\sigma \quad (3.3.6c)$$

$$V_u \stackrel{\Delta}{=} \lim_{t \rightarrow \infty} \frac{1}{t} E \int_0^t \|u(\sigma)\|_R^2 d\sigma \quad (3.3.6d)$$

$$V_z \stackrel{\Delta}{=} \lim_{t \rightarrow \infty} \frac{1}{t} E \int_0^t \|z(\sigma)\|_{Q_2}^2 d\sigma \quad (3.3.6e)$$

and where  $y$ ,  $u$  and  $z$  are the output, input and measurements (2.3.3) respectively,  $Q$  and  $R$  are the output and input weighting matrices in the performance objective (2.3.8), and  $Q_2$  is a positive-definite matrix.

### 3.3.2 Closed Loop Formulation

Note from (3.3.6) that, since

$$V_c = V_y + \rho V_u = \lim_{t \rightarrow \infty} \frac{1}{t} E \int_0^t \{ \|y(\sigma)\|_Q^2 + \rho \|u(\sigma)\|_R^2 \} d\sigma \quad (3.3.7)$$

the cost function  $V = V_c$  is identical to the performance objective (2.3.8) that we wish to minimize by a proper design of a controller. Hence, the definition (3.3.7) for the cost function is most appropriate.

To write (3.3.7) in the form of (3.2.2) and (3.3.3) requires the following

$$y = \begin{bmatrix} y \\ u \end{bmatrix} \quad (3.3.8a)$$

and

$$Q = \text{diag} \{Q, \rho R\} . \quad (3.3.8b)$$

Now, unless a relation between the input and the modes is known in the form

$$u = - \sum_{i=1}^N g_i \eta_i - \sum_{i=1}^N g'_i \dot{\eta}_i \quad (3.3.9)$$

(3.3.8a) cannot be expressed as (3.3.3). Since the MCA assumes the representation (3.3.3), the relation (3.3.9) becomes essential for the application of MCA (with respect to (3.3.7)).

Note that the control law (3.3.9) assumes that the modal displacements  $\eta_i$  and the rates  $\dot{\eta}_i$  are available for feedback - in general, this assumption is not valid. Furthermore, in order to calculate the modal gains  $g_i$  and  $g'_i$  one needs to solve the following Riccati equation [8] for the full order system containing N-modes, (a formidable task when N is large).

$$KA + A^T K - \frac{1}{\rho} KBR^{-1}B^T K + C^T QC = 0 \quad (3.3.10)$$

where the system matrices {A, B, C} are as defined in (2.3.3). Assume, for the present, that (3.3.10) can be solved and that the expression (3.3.9) can be obtained. With this control law in 'action', the following representation results for the closed loop system.

$$\begin{aligned} \ddot{\eta}_i + (2\zeta_i \omega_i + b_i^T g'_i) \dot{\eta}_i + (\omega_i^2 + b_i^T g_i) \eta_i \\ + b_i^T \sum_{\substack{j=1 \\ j \neq i}}^N (g_j \eta_j + g'_j \dot{\eta}_j) = b_i^T w \end{aligned} \quad (3.3.11)$$

$$i = 1, 2, \dots, N.$$

Clearly, the modes  $\eta_i$  are no longer decoupled which leads to the inapplicability of MCA formula (3.3.4) to the closed loop system (3.3.11). However, under certain

assumptions, one can solve the equation (3.3.10) analytically and obtain the modal gains  $g_i$  and  $g'_i$  so that the resulting closed loop system can be expressed in modal form. We now enumerate these assumptions and discuss them briefly.

*Assumptions for closed loop MCA*

(A1) All modal displacements  $n_i$  and the rates  $\dot{n}_i$  are available for feedback.

$$(A2) \quad b_i = r_i e_i, \quad i = 1, 2, \dots, N \quad (3.3.11a)$$

where  $e_i$  is the  $i^{\text{th}}$  unit vector, i.e.

$$e_i^T = [0, 0, \dots, 0, 1, 0, \dots, 0] \quad (3.3.11b)$$

with 1 at  $i^{\text{th}}$  position,  $r_i$  is a scalar, and

$$R = I_N$$

$$U = \text{diag} \{W_{11}, W_{22}, \dots, W_{NN}\} \quad (3.3.11c)$$

$$(A3) \quad y = \begin{bmatrix} y_p \\ y_r \end{bmatrix} \in \mathbb{R}^{2N}; \quad (3.3.12a)$$

$$\text{where } y_p = \sum_{i=1}^N e_i n_i, \quad (3.3.12b)$$

$$y_r = \sum_{i=1}^N e_i \dot{n}_i,$$

$$\text{and } Q = \text{diag} \{\omega_1^2, \dots, \omega_N^2, 1, 1, \dots, 1\}, \quad (3.3.12c)$$

so that

$$V_y = \sum_{i=1}^N \omega_i^2 n_i^2 + \sum_{i=1}^N \dot{n}_i^2 \quad (3.3.12d)$$

now represents potential and kinetic energy.

### Discussions

- 1) (A1) implies that  $n_i$  and  $\dot{n}_i$  are measured directly and accurately.
- 2) Clearly, from the structure of  $b_i$  in (3.3.11), assumption (A2) requires as many inputs as the modes, i.e.,  $m = N$ . This may not happen in general. However, when one has not decided on the location of the  $m$  actuators, one may consider  $N(N > m)$  possible locations for the actuators (so that (A3) is satisfied) and use the subsequent MCA to determine (if possible) the best, desired ( $m$ ) number of locations. Hence (A2) may be interpreted as "the admissible set of actuator locations."
- 3) Since the cost function (3.3.7) is the closed loop cost function, when (A3) holds, the modal costs  $\hat{v}_i$  represent the contributions of mode  $i$  to the *closed loop* potential and kinetic energy of the structure. Hence, (A3) implies the evaluation of the participation of the modes in the total energy of the closed-loop structure.

### *Theorem 3.3*

When the assumptions (A1)-(A3) hold, the closed loop model costs are given by

$$\hat{v}_{c_i} = \frac{1}{4 \bar{\zeta}_i \bar{\omega}_i^3} \{ \omega_i^2 + \frac{1}{\rho} r_i^2 k_{i2}^2 + \bar{\omega}_i^2 (1 + \frac{1}{\rho} r_i^2 k_{i3}^2) \} r_i^2 w_{ii} \quad (3.3.13a)$$

$i = 1, 2, \dots, N$

where

$$\bar{\omega}_i^2 \triangleq (\omega_i^4 + \frac{1}{\rho} r_i^2 \omega_i^2)^{1/2} \quad (3.3.13b)$$

$$\bar{\zeta}_i \triangleq \frac{1}{2\bar{\omega}_i} \{ 2(\bar{\omega}_i^2 - \omega_i^2) + 4\bar{\zeta}_i^2 \omega_i^2 + \frac{1}{\rho} r_i^2 \}^{1/2} \quad (3.3.13c)$$

$$k_{i2} \triangleq \frac{p}{r_i} (\bar{\omega}_i^2 - \omega_i^2) \quad (3.3.13d)$$

$$k_{i3} \triangleq \frac{2\sigma}{r_i} (\bar{z}_i \bar{\omega}_i - z_i \omega_i) \quad (3.3.13e)$$

Remark

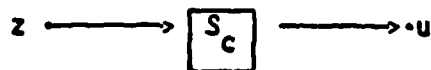
$\bar{\omega}_i$  and  $\bar{z}_i$  are respectively the closed loop frequency and the closed loop damping factor of mode  $i$ .

With the expressions (3.3.13a - 3.3.13e) available, we are now in a position to evaluate the *closed loop* modal costs. Thus, the reduced models obtained by the CCA algorithm is now based upon *closed loop* information.

### 3.3.3 Open Loop Formulation

Even though (3.3.7) is the most appropriate cost function to use for obtaining reduced models, a number of assumptions (A1-A3) are needed to arrive at closed form expression for the closed loop modal costs as in (3.3.13). These assumptions, in general, may not hold. Hence, by enforcing these assumptions one is *changing* the definition of the problem. One is therefore forced to consider an alternate cost function which reflects the closed loop information, at least approximately if not exactly.

In order to present such a cost function, consider briefly the subsequent controller design process; (the controller design is treated in detail in section 4). A controller (dynamic or static) operates on the measurements  $z$  to generate the input signals  $u$ , as shown in the block diagram below.



Now, the controllers that are designed based upon reduced models assume that the measurement signals available from the reduced models are exact. In other words, if  $\hat{z}$  is the measurement resulting from the reduced model, then the controllers are designed with the assumption that  $\hat{z}(t) = z(t)$ . Furthermore, these controllers are designed to minimize not the actual performance objective (2.3.8) but only its approximation  $\hat{V}$ ,

$$\hat{V} = \lim_{t \rightarrow \infty} \frac{1}{t} E \int_0^t \{ \|\hat{y}(\sigma)\|_Q^2 + \rho \|u(\sigma)\|_R^2 \} d\sigma \quad (3.3.14)$$

where  $\hat{y}$  is the output from the reduced model.

Hence, the reduced models should reproduce *both* the outputs and the measurements fairly accurately. Therefore, for model reduction purposes, one should consider not only  $V_y$  (defined in (3.3.6c)) but also  $V_z$  (defined in (3.3.6e)) in the cost function. The weighting matrix  $Q_2$  in (3.3.6e) can be selected as follows. It is well known that, in Kalman's optimal filters [8], the magnitude of the filter gain on a measurement is inversely related to the intensity of the noise on the measurement. This implies that the filter gain on a noise-free measurement is high and hence this measurement should be modeled fairly accurately by the reduced model. Therefore, an appropriate choice for the weighting matrix  $Q_2$  is  $V^{-1}$ , where  $V$  is the intensity of the noise on the measurements.

With this consideration, an alternate cost function to (3.3.7) is the following

$$V_0 = V_y + \beta V_z \quad (3.3.15)$$

where

$$V_y \triangleq \lim_{t \rightarrow \infty} \frac{1}{t} E \int_0^t \|y(\sigma)\|_Q^2 d\sigma, \quad (3.3.16a)$$

$$V_z \triangleq \lim_{t \rightarrow \infty} \frac{1}{t} E \int_0^t \|z(\sigma)\|_{V^{-1}}^2 d\sigma, \quad (3.3.16b)$$

and where  $\beta$  is an arbitrary weighting parameter. The following theorem results from the application of the modal cost expression (3.3.4).

*Theorem 3.4*

For the open loop cost function, defined in (3.3.15), the modal costs are given by

$$\hat{V}_{o_i} = \frac{1}{4\zeta_i \omega_i^3} \{ \|p_i\|_Q^2 + \beta \|m_i\|_{V^{-1}}^2 + \omega_i^2 (\|p_i'\|_Q^2 + \beta \|m_i'\|_{V^{-1}}^2) \} \|b_i\|_U^2 \quad (3.3.17)$$

$i = 1, 2, \dots, N$

with

$$z = \sum_{i=1}^N m_i \eta_i + \sum_{i=1}^N m_i' \dot{\eta}_i + v \quad (3.3.18)$$

where  $v$  is assumed to be a zero mean gaussian white noise process with intensity  $V$ .

Remarks

- 1) Unlike the closed loop MCA, there has been no necessity to make any special assumptions concerning the system, (except, of course, that the damping is small).
- 2) The definition for  $y$  and  $Q$  which permits the representation of (3.3.15) in the form of (3.3.3) and (3.2.2) is the following

$$y = \begin{bmatrix} y \\ z \end{bmatrix}, \quad Q = \text{diag} \{Q, sV^{-1}\} \quad (3.3.19a)$$

and

$$P_i = \begin{bmatrix} p_i \\ m_i \end{bmatrix}, \quad P_i' = \begin{bmatrix} p_i' \\ m_i' \end{bmatrix} \quad (3.3.19b)$$

The proof of this theorem follows from substitution of (3.3.19) in (3.3.4)

- 3) Since the expression (3.3.17) for the open loop modal costs depends on  $\beta$ , the reduced models will also depend on  $\beta$ .

Note in (3.3.15) that the weighting parameter  $\beta$  reflects the importance of reproducing the measurements accurately by the reduced model. For instance, if a high bandwidth controller is used, then any error in the measurement produced by the reduced model will be amplified by the high gains of the controller, resulting in degradation of the performance (if not instability) of the closed loop system. Therefore, one would choose a large  $\beta$  for a high bandwidth controller. But, since the controller bandwidths (or equivalently, the values of  $\rho$ ) are not known before the model reduction, there seems to be no easy 'rule-of-thumb' to pick an appropriate value of  $\beta$  before the initiation of model reduction. A reasonable choice for  $\beta$  seems to be

$$\beta = \frac{1}{\rho} \left\| \frac{W}{V} \right\| \cdot \left\| \frac{0}{R} \right\|.$$

However, in many situations, it seems reasonable to take

$$V = V_y = \lim_{t \rightarrow \infty} \frac{1}{t} \int_0^t \|y(\sigma)\|_Q^2 d\sigma. \quad (3.3.20)$$

Note that this cost function is equivalent to assuming that  $u = 0$  in (3.3.7), which corresponds to the open loop operation of the system. If one knows *a priori* that only a low bandwidth controller will be subsequently used, then (3.3.20) serves as a sufficiently good cost function for model reduction purposes. That is, in the case of low bandwidth controllers, the effect of errors present in the approximate measurements  $\hat{z}$  will not be very serious. Hence, one may set  $\beta = 0$  in (3.3.15). This yields the same cost function (3.3.20).

As a corollary to theorem 3.4, we have (by setting  $\beta = 0$  in (3.3.17))

*Corollary 3.1*

For the cost function defined in (3.3.20), the modal costs are given by

$$\hat{V}_{y_i} = \frac{1}{4\zeta_i\omega_i^3} \{ \|p_i\|_Q^2 + \omega_i^2 \|p_i'\|_Q^2 \} \|b_i\|_u^2 \quad (3.3.21)$$

$$i = 1, 2, \dots, N.$$

Remark

By defining

$$\hat{V}_{z_i} \triangleq \frac{1}{4\zeta_i\omega_i^3} \{ \|m_i\|_{V^{-1}}^2 + \omega_i^2 \|m_i'\|_{V^{-1}}^2 \} \|b_i\|_u^2 \quad (3.3.22a)$$

the modal costs in (3.3.17) can be expressed as

$$\hat{V}_{o_i} = \hat{V}_{y_i} + \beta \hat{V}_{z_i}, \quad i = 1, 2, \dots, N. \quad (3.3.22b)$$

Note that if the ordering of the modes according to the CCA algorithm does not depend on  $\beta$ , (this happens, for example, when  $\hat{V}_{z_i} = \hat{V}_{y_i}$ ,  $i = 1, 2, \dots, N$ ), then the reduced models too are independent of  $\beta$ . In this case we say that the modeling-problem and the control-problem are *separable*. That is, when the modeling and control problems are *separable*, one may design a controller based upon *one* reduced model for *all* bandwidth controllers.

*Theorem 3.5*

The modeling-problem and the control-problem are *separable* if the measurements and the outputs are related by

$$z = Ty + v; \quad T \in \mathbb{R}^{l \times k} \quad (3.3.23a)$$

with  $T$  satisfying

$$T^T V^{-1} T = \alpha Q \quad (3.3.23b)$$

for some positive scalar  $\alpha$ .

Remark

If  $z = y$  and  $V^{-1} = \alpha Q$ , then obviously the conditions (3.3.23a,b) hold. This implies that if the outputs are directly measured ( $z = y+v$ ) and if the noise statistics satisfy  $V^{-1} = \alpha Q$ , then the modeling-problem and the control problem are separable.

### 3.3.4 Example

For the beam example considered in Section 2, the following expressions hold.

$$\omega_i = i^2, \quad \zeta = .005$$

$$b_i = i, \quad p_i = \sin(.45 \pi i), \quad m_i = \sin(.35 \pi i)$$

$$p'_i = m'_i = 0$$

$$i = 1, 2, \dots, 10.$$

$$V = Q = U = R = 1.$$

The closed loop MCA formula (3.3.13) is not applicable, since the assumptions (A2) and (A3) do not hold.

The expressions for open loop modal costs  $\hat{v}_{y_i}$  (3.3.21) and  $\hat{v}_{z_i}$  (3.3.22a) greatly simplify to yield

$$\hat{v}_{y_i} = \frac{1}{.02 i^4} \sin^2(.45 \pi i) \quad (3.3.24a)$$

$$\hat{v}_{z_i} = \frac{1}{.02 i^4} \sin^2(.35 \pi i). \quad (3.3.24b)$$

The expression (3.3.17) correspondingly simplifies to

$$\hat{v}_{o_i} = \frac{1}{.02 i^4} [\sin^2(.45 \pi i) + \beta \sin^2(.35 \pi i)] \quad (3.3.24c)$$

Now, we apply the basic CCA algorithm for model reduction, using the open loop cost function of Section 3.3.3 for different values of  $\beta$ .

# STEP I

a) Compute the modal costs:

Since both  $\hat{v}_{y_i}$  and  $\hat{v}_{z_i}$  are independent of  $\beta$ , we will first compute  $\hat{v}_{y_i}$  and  $\hat{v}_{z_i}$  independently. These are tabulated below.

MODE #(i)	$\hat{v}_{y_i}$	$\hat{v}_{z_i}$
1	4.8777 e+1	3.9699 e+1
2	2.9841 e-1	2.0454 e+0
3	4.9006 e-1	1.5106 e-2
4	6.7480 e-2	1.7666 e-1
5	4.0000 e-2	4.0000 e-2
6	2.5250 e-2	3.8841 e-3
7	4.2921 e-3	2.0315 e-2
8	1.1042 e-2	4.2174 e-3
9	1.8699 e-4	1.5707 e-3
10	5.0000 e-3	5.0000 e-3

$$v_y = \sum_{i=1}^{10} \hat{v}_{y_i} = 4.9718 \text{ e+1}$$

$$v_z = \sum_{i=1}^{10} \hat{v}_{z_i} = 4.2007 \text{ e+1}$$

Note that the modal costs do not decrease monotonically as  $i \rightarrow 10$ . Hence one should not arbitrarily delete the high frequency modes, as is traditionally done.

Figs. 3.1a and 3.1b display the effect of  $\beta$  on modal costs and, as a consequence, on the modal sequence. In these figures the *normalized* modal costs are defined as

$$\hat{q}_i \triangleq \hat{v}_{o_i} / v_o, \quad i = 1, 2, \dots, N \quad (3.3.25a)$$

so that

$$\sum_{i=1}^N \hat{q}_i = 1 \quad (3.3.25b)$$

Fig. 3.1a illustrates that mode-1 dominates over all the other modes, for all values of  $\beta$ . This mode has been suppressed in Fig. 3.1b to exhibit the behavior of the other modal costs as  $\beta$  changes. Clearly, the significance of modes 2 and 3 changes as  $\beta$  goes from 0 to 100.

b) Rank the modes in the descending order of their modal costs,  $\hat{v}_{o_i}$

We will illustrate this only for  $\beta = 0$  and  $\beta \rightarrow \infty$ , as shown in the following table.

$\beta$	RANKING OF MODES
0	{1, 3, 2, 4, 5, 6, 8, 10, 7, 9}
$\rightarrow \infty$ *	{1, 2, 4, 5, 7, 3, 10, 8, 6, 9}

\*  $\beta \rightarrow \infty$  is equivalent to omitting  $v_y$  in the open loop cost function  $v_o$ .

STEP II. Construct the reduced models of order  $n_r = 2r$ , where  $r$  is the number of modes to be retained in the reduced models.

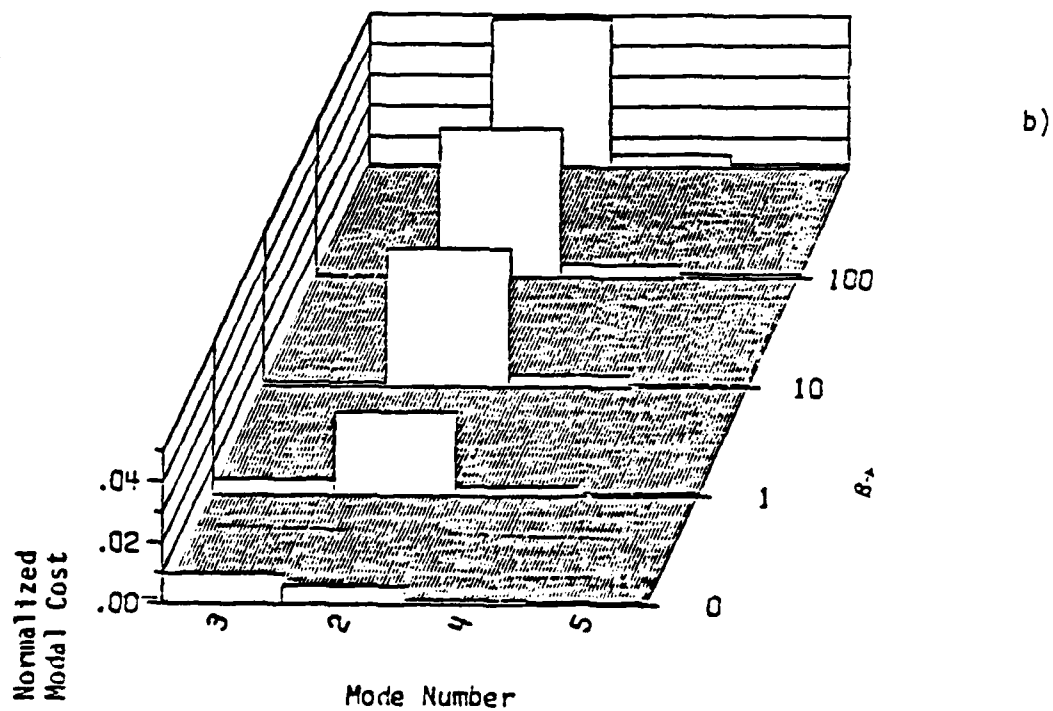
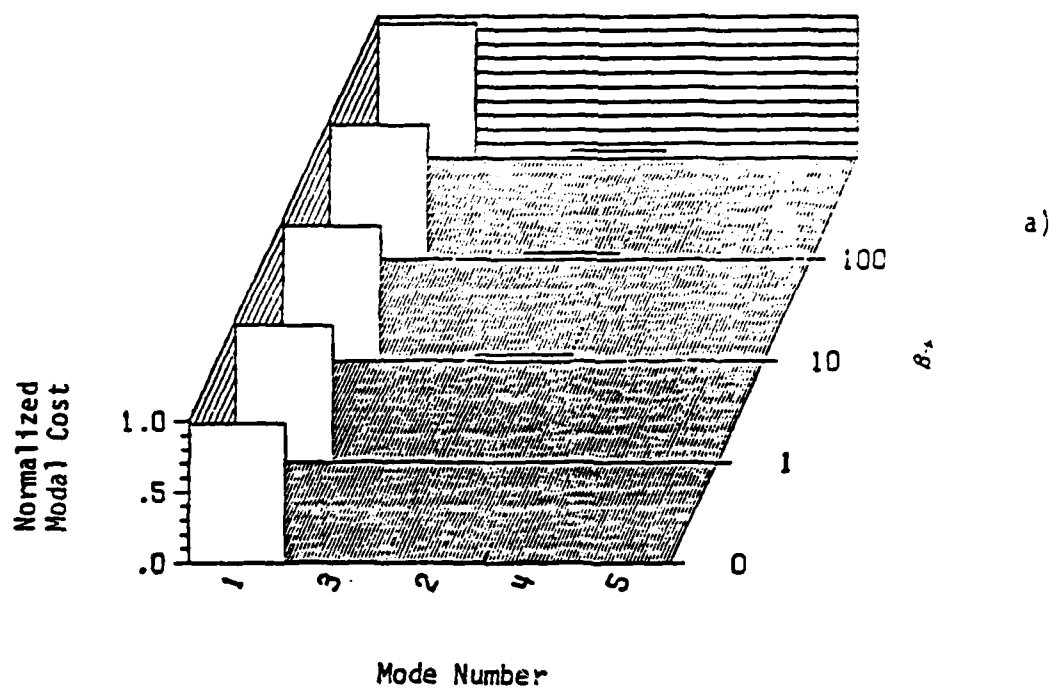


Fig. 3.1 Normalized Modal Costs vs. Beta

TABLE 3.1 DEPENDENCE OF REDUCED MODELS ON  $\beta$

r	$\beta = 0$		$\beta = 2$		$\beta \rightarrow \infty$	
	MODES RETAINED	q	MODES RETAINED	q	MODES RETAINED	q
1	1	.1094 e-1	1	.4300 e-1	1	.5504 e-1
2	1,3	.9085 e-2	1,2	.0543 e-2	1,2	.6346 e-2
3	1,3,2	.3240 e-2	1,2,3	.5018 e-2	1,2,4	.2140 e-2
4	1,3,2,4	.1725 e-2	1,2,3,4,	.8590 e-3	1,2,4,5,	.7042 e-3
5	1,3,2,4,5	.9206 e-3	1,2,3,4,5	.8590 e-3	1,2,4,5,7	.7042 e-3
6	1,3,2,4,5,6	.4128 e-3	1,2,3,4,5,7	.5078 e-3	1,2,4,5,7,3	.3446 e-3
7	1,3,2,4,5,6,8	.1907 e-3	1,2,3,4,5,7,6	.2800 e-3	1,2,4,5,7,3,10	.2256 e-3
8	1,3,2,4,5,6,8,10	.9011 e-4	1,2,3,4,5,7,6,8	.1391 e-3	1,2,4,5,7,3,10,8	.1252 e-3
9	1,3,2,4,5,6,8,10,7	.3777 e-5	1,2,3,4,5,7,6,8,10	.2619 e-4	1,2,4,5,7,3,10,8,6	.3746 e-4
10	1,3,2,4,5,6,8,10,7,9	0	1,2,3,4,5,7,6,8,10,9	0	1,2,4,5,7,3,10,8,6,9	0

Clearly, for  $2 \leq r \leq 8$ , we get different reduced models, depending on the values of  $\beta$ . Table 3.1 illustrates the dependence of the reduced models on  $\beta$ .

Observe that if one can tolerate a reduced model with a cost perturbation index of 60%, then a reduced model containing only one mode is sufficient. Furthermore, this model retains the first mode for any value of  $\beta$ . Hence, for this example, for a reduced model with  $q = .6$ , the modeling-problem and the control-problem are separable. However, for  $q \leq .05$ , they are not separable since the reduced models now depend on  $\beta$ , (except when  $r \geq 9$ ).

For comparison purposes (in section 3.5), we will choose two reduced models, both containing 3 modes; one corresponding to  $\beta = 0$ ,  $\{1,3,2\}$  with a  $q = .00324$ , and the other corresponding to  $\beta \rightarrow \infty$ ,  $\{1,2,4\}$ , with a  $q = .00214$ . Denoting these models respectively by  $S_1$  and  $S_2$ , their state-space representation are given below.

$$S_1 : \quad \dot{x}_1 = A_1 x_1 + B_1 u$$

$$y_1 = C_1 x_1$$

$$z_1 = M_1 x_1 + v$$

where

$$x_1 \triangleq \{n_1, n_3, n_2, \dot{n}_1, \dot{n}_3, \dot{n}_2\}^T$$

$$A_1 = \begin{bmatrix} 0 & 0 & 0 & 1 & 0 & 0 \\ 0 & 0 & 0 & 0 & 1 & 1 \\ 0 & 0 & 0 & 0 & 0 & 0 \\ -1 & 0 & 0 & -.01 & 0 & 0 \\ 0 & -.81 & 0 & 0 & -.09 & 0 \\ 0 & 0 & -.16 & 0 & 0 & -.04 \end{bmatrix} \quad B_1 = \begin{bmatrix} 0 \\ 0 \\ 0 \\ 1 \\ 3 \\ 2 \end{bmatrix}$$

$$C_1 = [.9877, -.8910, .3090, 0, 0, 0]$$

$$M_1 = [.8910, -.1564, .8090, 0, 0, 0]$$

$$S_2: \dot{x}_2 = A_2 x_2 + B_2 u$$

$$y_2 = C_2 x_2$$

$$z_2 = M_2 x_2$$

where

$$x_2 \stackrel{\Delta}{=} \{n_1, n_2, n_4, \dot{n}_1, \dot{n}_2, \dot{n}_4\}^T$$

$$A_2 = \begin{bmatrix} 0 & 0 & 0 & 1 & 0 & 0 \\ 0 & 0 & 0 & 0 & 0 & 0 \\ 0 & 0 & 0 & 0 & 0 & 1 \\ -1 & 0 & 0 & -.01 & 0 & 0 \\ 0 & -16 & 0 & 0 & -.04 & 0 \\ 0 & 0 & -256 & 0 & 0 & -.16 \end{bmatrix}; \quad B_2 = \begin{bmatrix} 0 \\ 0 \\ 0 \\ 1 \\ 2 \\ 4 \end{bmatrix}$$

$$C_2 = [.9877, .3090, -.5878, 0, 0, 0]$$

$$M_2 = [.8910, .8090, -.9511, 0, 0, 0]$$

These reduced models will be compared with the cost equivalent realizations to be generated in Section 3.4.

### 3.4 Cost Equivalent Realization (CER)

#### 3.4.1 Definition.

Modal Cost Analysis, a special case of component cost analysis (CCA), offers a convenient model reduction algorithm for mechanical systems described in second order matrix form. These reduced models satisfy

$q = \hat{q}$ . There exists another special set of coordinates in which the reduced models obtained by the CCA algorithm also satisfy this property. Additionally, these reduced models yield zero cost perturbation index, i.e.,  $q = 0$ . This implies, from the definition of cost perturbation index, that these reduced models are equivalent to the original model with respect to the cost function, i.e.,  $V_R = V$ . Hence, these are called Cost Equivalent Realizations (CERs).

*Definition 3.3* A Cost Equivalent Realization (CER) is defined to be a reduced model with the property

$$V_R = V. \quad (3.4.1)$$

Note from (3.3.5), (3.3.4) and (3.2.10) that in MCA

$$V - V_R = \sum_{i \in T} \hat{v}_i \geq 0,$$

with the equality holding only if the truncated modes ( $i \in T$ ) are either unobservable and/or uncontrollable. Hence, in general, the reduced models obtained by MCA do not satisfy the cost equivalence property (3.4.1).

In this Section we present a set of coordinates, called normalized Hessenberg coordinates, in which the CCA yields reduced models which are cost equivalent. Presenting the properties of the CERs, we conclude this Section by illustrating the numerical procedure with the aid of the beam example.

#### 3.4.2 Normalized Hessenberg Coordinates

The generalized Hessenberg coordinates have received considerable attention in the context of model reduction, [9-13]. These coordinates are used to identify the least observable states of a given system, which can then be deleted to yield an acceptable reduced model. However, these

least observable states may be highly controllable. But, this 'controllability-information' is not taken into account in either of these references. Hence, we enforce a normalization of these coordinates to include the controllability of the states also in the model reduction decisions.

*Definition 3.4* Normalized Hessenberg coordinates are defined to be those coordinates in which the given model (3.2.1) has the following properties.

$$a) \quad X \stackrel{\Delta}{=} \lim_{t \rightarrow \infty} E \{x(t) x^T(t)\} = I_n. \quad (3.4.2)$$

$$b) \quad A_{ij} \stackrel{\Delta}{=} 0, \quad j > i+1, \quad i = 1, 2, \dots, p$$

$$\text{rank} [A_{i,i+1}] = n_{i+1}, \quad i = 1, 2, \dots, p-1 \quad (3.4.3)$$

where  $x_i \in \mathbb{R}^{n_i}$

$$c) \quad y = C_1 x_1,$$

$$\text{with } C_1^T Q C_1 = \text{diag} \{\alpha_1^2, \alpha_2^2, \dots, \alpha_{n_1}^2\} \quad (3.4.4)$$

$$\alpha_1^2 \geq \alpha_2^2 \geq \dots \geq \alpha_{n_1}^2 > 0$$

Remarks

1) (3.4.3) and (3.4.4) imply the following structure to (3.2.1a)

$$\begin{bmatrix} \dot{x}_1 \\ \dot{x}_2 \\ \dot{x}_3 \\ \vdots \\ \dot{x}_{p-1} \\ \dot{x}_p \end{bmatrix} = \begin{bmatrix} A_{11} & A_{12} & 0 & \dots & 0 \\ A_{21} & A_{22} & A_{23} & \dots & 0 \\ A_{31} & A_{32} & A_{33} & \dots & 0 \\ \vdots & \vdots & \vdots & \ddots & \vdots \\ A_{p-1,1} & A_{p-1,2} & A_{p-1,3} & \dots & A_{p-1,p} \\ A_{p1} & A_{p2} & A_{p3} & \dots & A_{pp} \end{bmatrix} \begin{bmatrix} x_1 \\ x_2 \\ x_3 \\ \vdots \\ x_{p-1} \\ x_p \end{bmatrix} + \begin{bmatrix} d_1 \\ d_2 \\ d_3 \\ \vdots \\ d_{p-1} \\ d_p \end{bmatrix} \quad w \quad (3.4.5a)$$

$$y = Cx \stackrel{\Delta}{=} [c_1 \quad 0 \quad 0 \quad \dots \quad 0] x \quad (3.4.5b)$$

- 2) The model is naturally divided into  $p$  'components'  $x_i$ ,  $i = 1, 2, \dots, p$  of which only the first component  $x_1$  is directly observable in  $y$ . We will call these components the 'normalized Hessenberg components'.
- 3) The following relation holds

$$n_i \geq n_{i+1}, \quad i = 1, 2, \dots, p-1. \quad (3.4.5c)$$

(proof can be found in [11]).

- 4) Clearly, if  $A_{i,i+1} = 0$ , for some  $i$ , then the components  $\{x_{i+1}, x_{i+2}, \dots, x_p\}$  are unobservable.
- 5) At steady state, by definition (3.4.2), the normalized Hessenberg coordinates (and hence the components) are uncorrelated.
- 6) The algorithm to transform any given system to the normalized Hessenberg coordinates is included in the CER algorithm of Section 3.4.3.

We will now present some of the properties of normalized Hessenberg coordinates in the following theorems.

*Theorem 3.6*

The component costs of the normalized Hessenberg coordinates are given by

$$\hat{v}_i = \begin{cases} \alpha_i^2 & i = 1, 2, \dots, n_1 \\ 0 & i > n_1 \end{cases} \quad (3.4.5)$$

#### Remark

It follows from theorem 3.6 that the only 'component' that contributes to the cost function is the first normalized Hessenberg component  $x_1 \in \mathbb{R}^{n_1}$ , and that the remaining components  $x_i$ ,  $i = 2, 3, \dots, p$  do not contribute to the cost function.

#### *Theorem 3.7*

The component costs associated with the normalized Hessenberg coordinates are minimally sensitive to perturbations in the state weighting matrix  $C^T Q C$  in the cost function.

#### Remark

Consider the case when the state weighting matrix  $C^T Q C$  in the cost function is subject to perturbation - this may happen, for example, when the output matrix  $C$  is not known exactly, or when the model is used for the subsequent modification of the output weighting matrix  $Q$ , as in [3.7]. Theorem 3.7 implies that, in this situation, the choice of the reduced models in normalized Hessenberg coordinates is minimally sensitive to these perturbances, since in CCA the model reduction decisions are based upon the component costs.

#### 3.4.3 CER-Algorithm and Properties.

In this Section we present an algorithm for transforming a system to normalized Hessenberg coordinates and to extract cost equivalent realizations by CCA. We also present the properties of CERs thus generated.

*CER-Algorithm*

STEP I. Read the system matrices  $\{A, D, C, W\}$  and the weighting matrix  $Q$  in the cost function.

STEP II.

2a). Compute  $X$  by solving

$$XA^T + AX + DW D^T = 0 \quad (3.4.7a)$$

2b). Compute  $\theta_x$ , the square root of  $X$ ;

$$X = \theta_x \theta_x^T \quad (3.4.7b)$$

2c). Compute  $\theta_y$ , the orthonormal modal matrix of

$$\theta_x^T C^T Q C \theta_x \text{ such that}$$

$$\theta_y^T \cdot \theta_x^T C^T Q C \theta_x \cdot \theta_y = \text{diag} \{ \alpha_1^2, \alpha_2^2, \dots, \alpha_{n_1}^2, 0, \dots, 0 \} \quad (3.4.7c)$$

$$\text{where } \alpha_1^2 \geq \alpha_2^2 \geq \dots \geq \alpha_{n_1}^2 > 0 \quad (3.4.7d)$$

STEP III.

3a). Define  $T_1 \triangleq \theta_x \theta_y$  (3.4.8)

3b). Define

$$\begin{bmatrix} A_{11} & A_{12} \\ A_{21} & A_{22} \end{bmatrix} = T_1^{-1} A T_1 ; \quad \begin{matrix} A_{11} \in R^{n_1 \times n_1} \\ A_{22} \in R^{(n-n_1) \times (n-n_1)} \end{matrix} \quad (3.4.9)$$

$$\begin{bmatrix} D_1 \\ D_2 \end{bmatrix} = T_1^{-1} D, \quad D_1 \in R^{n_1 \times m}$$

3c). Set  $i = 2$ ,  $p = 2$  and  $n_r = n_1$ .

STEP IV.

4a). Obtain the Singular Value Decomposition of  $A'_{i-1,i}$  as

$$A'_{i-1,i} = U^i \begin{bmatrix} \sigma_i & 0 \\ 0 & 0 \end{bmatrix} \begin{bmatrix} V_1^{iT} \\ V_2^{iT} \end{bmatrix} \quad (3.4.10a)$$

where  $\sigma^i = \text{diag} \{ \sigma_1^i, \sigma_2^i, \dots, \sigma_{n_i}^i \}$ ,  $\sigma_j^i \geq \sigma_{j+1}^i > 0$  (3.4.10b)

and  $V_1^i \in R^{(n-n_r) \times n_i}$ .

4b). Define

$$T_i \triangleq \begin{bmatrix} I_{n_r} & 0 \\ 0 & V^i \end{bmatrix}; \quad V^i \triangleq [V_1^i, V_2^i] \quad (3.4.10c)$$

4c). Set  $n_r = n_r + n_i$ . If  $n_r = n$ , go to step V.

4d). Define  $A'_{i,i+1} \triangleq V_1^{iT} A'_{ii} V_2^i$  (3.4.11a)

and  $A'_{i+1,i+1} \triangleq V_2^{iT} A'_{ii} V_2^i$ . (3.4.11b)

4e). Set  $i = i+1$  and  $p = p+1$  and repeat step IV.

STEP V.

$$\text{Define } T = \prod_{i=1}^p T_i. \quad (3.4.12)$$

STEP VI.

Apply the transformation

$$x = Tx \quad (3.4.13a)$$

to obtain the model in normalized Hessenberg coordinates, i.e.,  
the model

$$\begin{aligned}\dot{x} &= Ax + Dw \\ y &= Cx\end{aligned}\tag{3.4.13b}$$

where

$$\begin{aligned}A &= T^{-1}AT \\ D &= T^{-1}D \\ C &= CT\end{aligned}\tag{3.4.13c}$$

satisfies the specification (3.4.2-3.4.4).

#### STEP VII.

To obtain a reduced model, retaining  $r$  normalized Hessenberg components, (of order  $n_r = \sum_{i=1}^r n_i$ ), delete the last  $(p-r)$  components  $\{x_i, i = r+1, \dots, p\}$  from (3.4.13), where  $x$  is partitioned as

$$x^T = [x_1^T, x_2^T, \dots, x_p^T]; \quad x_i \in \mathbb{R}^{n_i}.$$

This reduced model of order  $n_r$  is given by

$$\begin{aligned}\dot{x}_R &= A_R x_R + D_R w \\ \hat{y} &= C_R x_R\end{aligned}\tag{3.4.14a}$$

where

$$A_R = \begin{bmatrix} A_{11} & A_{12} & \dots & 0 \\ A_{21} & A_{22} & \dots & 0 \\ \vdots & \vdots & \ddots & \vdots \\ A_{r1} & A_{r2} & \dots & A_{rr} \end{bmatrix}, \quad D_R = \begin{bmatrix} D_1 \\ D_2 \\ \vdots \\ D_r \end{bmatrix}\tag{3.4.14b}$$

$$C_R \stackrel{\Delta}{=} [C_1, 0, \dots, 0].$$

If (3.4.14) is controllable, then it is a CER.

### Remark

This algorithm does not guarantee that the resulting reduced model (3.4.14) is asymptotically stable. The following theorem includes the stability properties of (3.4.14).

### *Theorem 3.8* (stability properties of (3.4.14))

- i)  $\text{Re} \{ \lambda_i(A_R) \} \leq 0, i = 1, 2, \dots, n_r$   
where  $\text{Re} \{ \cdot \}$  denotes the real part of  $(\cdot)$  and  $\lambda_i(A_R)$  denotes the  $i$ -th eigenvalue of  $A_R$ .
- ii)  $\text{Re} \{ \lambda_i(A_R) \} < 0, i = 1, 2, \dots, n_r$ , if and only if the matrix pair  $(A_R, D_R)$  is controllable.
- iii) If  $J_z(p) = 0, z = 1, 2, \dots, i$  for some  $i$ , then for any

$$n_r \leq \sum_{j=1}^i n_j .$$

(3.4.14) is not asymptotically stable, where  $J_j(p) \triangleq CA^{j-1}D$  is the  $j$ -th Markov Parameter of the full order model.

### Remarks

- 1) From (i) note that none of the eigenvalues of the reduced model lie in the open right half plane.
- 2) From (iii) observe that the Markov Parameters of the full order model dictate the asymptotic stability of the reduced models. For single input single output systems the same observation can be made in the original version of model reduction by Routh Approximations [15].
- 3) (iii) also implies that, if  $J_z(p) = 0, z = 1, 2, \dots, i$ , then for (3.4.14) to be a CER, the number of components  $r$  retained in the model, must satisfy

$$r > i.$$

The cost equivalent realizations obtained by the CER-algorithm have the following properties.

*Theorem 3.9*

i) The CERs match the steady state output covariances:

$$\lim_{t \rightarrow \infty} E\{\hat{y}(t)\hat{y}^T(t)\} = \lim_{t \rightarrow \infty} E\{y(t)y^T(t)\} \quad (3.4.15a)$$

and

$$\lim_{t \rightarrow \infty} E\{\dot{\hat{y}}(t)\hat{y}^T(t)\} = \lim_{t \rightarrow \infty} E\{\dot{y}(t)y^T(t)\}. \quad (3.4.15b)$$

ii) For

$$n_r = \sum_{j=1}^i n_j,$$

$$J_j(i) = J_j(p), \quad j = 1, 2, \dots, i \quad (3.4.16)$$

where  $J_j(i) \triangleq C_R \Lambda_R^{j-1} p_R$  is the  $j$ -th Markov Parameter of the reduced model retaining  $i$  components.

Remarks

1) Since

$$V = \lim_{t \rightarrow \infty} \text{Tr}[E\{y(t)y^T(t)\}],$$

(3.4.15a) clearly implies that  $V_R = V$  (cost equivalence).

2) Consider  $y_i$ ,  $i = 1, 2, \dots, k$ , the  $i$ -th component of  $y$ . The RMS value of  $y_i$ , defined as

$$v^{1/2}(y_i) \triangleq \left[ \lim_{t \rightarrow \infty} \frac{1}{t} \int_0^t y_i^2(\sigma) d\sigma \right]^{1/2}$$

is a fundamental input-output property of a system and is independent of any coordinate transformation. It is, therefore, encouraging to observe from (3.4.15a) that, this fundamental property is preserved by CERs.

- 3) Since matching of Markov Parameters reflects the matching of the transient response of  $\hat{y}$  and  $y$  [16], (3.4.16) implies that, by increasing the order of the reduced model, better matching between the transient response can be achieved.

*A note on the cost function:*

As pointed out in Section 3.3, one may either consider the open loop cost function  $V_y$ , (defined in (3.3.20)), or an augmented cost function  $V_o$ , (3.3.15), for the model reduction purposes. Either cost function can be handled equally well by the CER algorithm, by properly defining the 'outputs'  $y$  and the weighting matrix  $Q$  in the cost function. This can be achieved as follows.

- 1) For  $V = V_y$ ,

set  $y = y$ , the actual output

and  $Q = Q$ , the weighting matrix in (2.3.8).

- 2) For  $V = V_o$ ,

set  $y^T = [y^T, z^T]$

and  $Q = \text{diag} \{Q, \beta V^{-1}\}$

where  $V$  is the intensity of the measurement noise.

#### 3.4.4 Example

We will illustrate the application of the CER-algorithm with the aid of the beam example. For illustration, consider the case  $\beta = 0$ . The  $A$  matrix of the model in normalized coordinates is given in Table 3.2.

Note, that since the first Markov Parameter,

$$J_1(20) = CD = 0 ,$$

we have  $D_1 = 0$ , in the input matrix, and consequently  $\lambda_1(A_{11}) = A_{11} = 0$ . Hence, the reduced model retaining the first state (coordinate) is not asymptotically stable and therefore it cannot be a CER.

Also, note that since  $y \in R^1$ ,  $n_1 = 1$ . And, hence from (3.4.5c)  $n_i = 1$ ,  $i = 1, 2, \dots, p$  and thus  $p = 20$ . In other words, for this example, the normalized Hessenberg 'components' are 'coordinates' themselves.

In order to determine the desirable order of the reduced model, we have Table 3.3. The quantity  $\|A_{RT}\|/\|A_R\|$  measures the observability of the truncated normalized Hessenberg coordinates. Since none of the entries of the fourth column of Table 3.3 is small (of the order of 0.1), it warns us that the CER-algorithm may not yield a 'good' reduced model.

For comparison purposes, we select the reduced model of order 6. We generate two reduced models, one corresponding to  $\beta = 0$  and the other,  $\beta \rightarrow \infty$ . These are respectively denoted by  $S_1$  and  $S_2$ , and their describing matrices are given in Tables 3.4a and 3.4b.

TABLE 3.2 REPRESENTATION OF THE BEAM MODEL IN  
NORMALIZED HESSENBERG COORDINATES

Table 3.2 Representation of the Beam Model in  
Normalized Hessenberg Coordinates

Columns 1-10 of the A Matrix

The AA-CER A Matrix (20x20)

	1	2	3	4	5	6
1	-1.041E-16	1.019E+01	-8.059E-14	2.427E-14	-3.502E-14	1.169E-16
2	-1.019E+01	-9.166E-01	9.773E+01	-2.196E-13	1.149E-12	-9.594E-14
3	8.254E-14	-9.773E+01	-5.716E-07	-1.766E+01	1.849E-14	6.903E-14
4	-2.566E-14	-3.841E-01	1.766E+01	-4.023E-02	2.870E+01	-3.178E-14
5	3.115E-14	2.654E-02	-2.096E-05	-2.869E+01	-1.921E-04	4.440E+01
6	-1.607E-15	1.230E+00	-9.714E-04	2.577E-01	-4.442E+01	-4.128E-01
7	2.202E-14	-3.810E-02	3.008E-05	-7.981E-03	5.515E-04	-3.355E+01
8	-1.797E-14	4.895E-01	-3.865E-04	1.025E-01	-7.086E-03	-3.284E-01
9	-1.032E-14	8.131E-02	-6.421E-05	1.704E-02	-1.177E-03	-5.457E-02
10	1.593E-14	-2.593E+00	2.047E-03	-5.432E-01	3.753E-02	1.740E+00
11	-2.341E-14	-1.986E-02	1.568E-05	-4.161E-03	2.875E-04	1.333E-02
12	-1.801E-14	2.953E-01	-2.332E-04	6.187E-02	-4.275E-03	-1.982E-01
13	-4.222E-15	9.834E-02	-7.766E-05	2.060E-02	-1.424E-03	-6.599E-02
14	4.945E-16	5.538E-01	-7.531E-04	1.998E-01	-1.381E-02	-6.400E-01
15	-1.609E-14	-9.541E-03	7.534E-06	-1.999E-03	1.381E-04	6.403E-03
16	-1.603E-16	-6.881E-01	5.434E-04	-1.442E-01	9.962E-03	4.618E-01
17	4.693E-14	-4.369E-02	3.450E-05	-9.154E-03	6.326E-04	2.932E-02
18	-1.129E-15	7.837E-01	-6.189E-04	1.642E-01	-1.135E-02	-5.259E-01
19	4.353E-14	2.241E-02	-1.770E-05	4.696E-03	-3.245E-04	-1.504E-02
20	5.975E-16	1.646E-01	-1.300E-04	3.449E-02	-2.384E-03	-1.105E-01

	7	8	9	10
1	-1.916E-14	-7.614E-16	1.186E-14	1.755E-15
2	1.032E-12	1.732E-15	-1.192E-12	-1.278E-14
3	-6.973E-15	-1.881E-14	6.905E-15	6.582E-15
4	-1.843E-13	-1.211E-14	-8.628E-14	3.581E-15
5	-1.595E-14	9.422E-14	6.078E-14	-6.037E-14
6	3.358E+01	1.227E-14	-1.034E-14	-8.506E-15
7	-3.958E-04	-3.630E+01	8.010E-15	-8.522E-14
8	3.631E+01	-6.534E-02	3.016E+01	-6.236E-14
9	1.690E-03	-3.018E+01	-1.803E-03	-5.456E+01
10	-5.388E-02	6.922E-01	5.468E+01	-1.833E+00
11	-4.127E-04	5.303E-03	8.810E-04	4.565E+01
12	6.136E-03	-7.884E-02	-1.310E-02	4.176E-01
13	2.044E-03	-2.625E-02	-4.362E-03	1.391E-01
14	1.982E-02	-2.546E-01	-4.230E-02	1.349E+00
15	-1.983E-04	2.548E-03	4.232E-04	-1.349E-02
16	-1.430E-02	1.837E-01	3.052E-02	-9.732E-01
17	-9.080E-04	1.167E-02	1.938E-03	-6.179E-02
18	1.629E-02	-2.092E-01	-3.476E-02	1.108E+00
19	4.658E-04	-5.985E-03	-9.942E-04	3.170E-02
20	3.421E-03	-4.396E-02	-7.303E-03	2.328E-01

Table 3.2 (cont'd)

Columns 10-20 of the A Matrix

	11	12	13	14	15	16
1	2.105E-14	-2.603E-15	2.729E-15	2.749E-15	1.299E-14	-6.390E-15
2	-1.224E-12	6.063E-14	3.979E-13	-1.728E-14	-5.115E-13	8.934E-15
3	9.925E-15	-1.001E-14	-2.995E-14	5.532E-14	2.837E-14	2.061E-15
4	1.772E-14	4.215E-15	-4.354E-14	-3.952E-15	-3.165E-14	7.745E-15
5	6.245E-14	3.744E-14	1.601E-13	-1.237E-14	-1.425E-13	1.071E-14
6	-5.806E-14	-5.397E-16	-8.749E-15	-6.713E-15	1.818E-13	1.206E-15
7	1.513E-14	2.304E-14	-6.048E-14	-8.795E-04	-1.996E-13	1.280E-13
8	8.875E-14	3.428E-14	1.644E-13	-1.511E-14	-3.347E-15	-.2322E-15
9	-1.242E-13	-2.023E-13	-1.093E-14	9.185E-14	1.594E-13	-2.225E-14
10	-4.668E+01	-1.239E-13	-3.509E-13	1.144E-13	3.217E-13	-1.668E-13
11	-1.076E-04	3.638E+01	-8.698E-15	2.988E-14	4.832E-14	8.995E-14
12	-3.638E+01	-2.378E-02	-3.138E+01	7.253E-14	3.534E-14	-2.187E-14
13	1.065E-03	3.136E+01	-2.638E-03	2.627E+01	-1.908E-14	2.210E-13
14	1.033E-02	-1.536E-01	-2.632E+01	-2.481E-01	-2.432E+01	6.678E-15
15	-1.034E-04	1.537E-03	5.118E-04	2.433E+01	-2.433E-05	1.380E+01
16	-7.455E-03	1.108E-01	3.691E-02	3.580E-01	-1.380E+01	-1.292E-01
17	-4.734E-04	7.038E-03	2.344E-03	2.273E-02	-2.274E-04	2.286E+00
18	8.491E-03	-1.262E-01	-4.204E-02	-4.077E-01	4.079E-03	2.942E-01
19	2.428E-04	-3.611E-03	-1.202E-03	-1.166E-02	1.167E-04	8.414E-03
20	1.784E-03	-2.652E-02	-8.832E-03	-8.566E-02	8.569E-04	6.180E-02

	17	18	19	20
1	-4.692E-14	-1.568E-15	-4.167E-14	-2.129E-15
2	1.265E-12	1.631E-14	9.986E-13	5.580E-14
3	4.026E-14	-5.907E-15	3.341E-14	-9.462E-15
4	1.055E-13	-1.363E-16	2.972E-14	-3.744E-16
5	-8.858E-14	-9.849E-15	-9.141E-14	-4.219E-14
6	-1.097E-13	1.545E-15	-2.396E-13	-4.629E-15
7	-9.056E-15	1.504E-14	-1.138E-13	7.441E-16
8	3.076E-13	7.694E-15	-2.680E-14	-7.462E-16
9	1.208E-13	2.708E-15	-1.204E-13	-1.028E-14
10	-3.504E-13	1.665E-14	-3.470E-13	1.338E-13
11	1.506E-15	4.107E-15	6.375E-14	-4.483E-14
12	3.507E-14	2.459E-13	3.256E-14	-3.790E-14
13	3.570E-14	-.1686E-14	-6.993E-14	1.160E-14
14	-9.134E-14	-2.507E-14	-9.050E-14	-1.273E-14
15	1.734E-14	3.077E-14	-2.500E-14	-1.401E-14
16	-2.302E-00	1.898E-15	1.416E-14	9.511E-16
17	-5.207E-04	-1.078E-01	1.099E-15	1.425E-14
18	1.080E-01	-1.675E-01	-1.091E-01	3.553E-15
19	5.342E-04	1.090E-01	-1.370E-04	-5.323E+00
20	3.924E-03	-7.039E-02	5.826E+00	-7.394E-03

Table 3.2 (cont'd)  
The D and C Matrices

The DD-CER Vector (20x1)

	1
1	0.
2	-1.354E+00
3	1.069E-03
4	-2.837E-01
5	1.960E-02
6	9.086E-01
7	-2.814E-02
8	3.615E-01
9	6.006E-02
10	-1.915E+00
11	-1.467E-02
12	2.181E-01
13	7.263E-02
14	7.044E-01
15	-7.047E-03
16	-5.082E-01
17	-3.227E-02
18	5.788E-01
19	1.655E-02
20	1.216E-01

The CC-Cer Vector (1x20)

1	2	3	4	5	6
-7.081E+00	6.226E-18	-3.485E-15	-1.446E-16	7.010E-15	6.260E-19
7	8	9	10	11	12
5.397E-15	7.958E-17	-5.537E-15	-1.633E-16	-4.310E-15	1.608E-16
17	18	19	20		
1.155E-14	1.022E-16	1.000E-14	2.587E-16		

TABLE 3.3

$n_r$	$\ A_R\ ^\dagger$	$\ A_{RT}\ ^\ddagger$	$\ A_{RT}\ /\ A_R\ $
2	10.2	97.73	9.5785
4	1.803	28.70	15.9236
6	1.521	33.58	22.0751
8	1.362	30.16	83.3333
10	1.323	46.68	35.3357
12	1.264	31.38	24.8139
14	1.193	24.32	20.3666
16	1.028	23.02	22.3714
18	1.021	10.91	10.6838

$$^\dagger \|A_R\| \triangleq \min_i \{|\lambda_i(A_R)|\}$$

$$^\ddagger \|A_{RT}\| \triangleq \max_i \{\lambda_i(A_{RT}^T A_{RT})\}.$$

TABLE 3.4a  
REDUCED MODEL,  $S_1$

THE PLANT MATRIX, $A_R$ (6 by 6)						
	1	2	3	4	5	7
1	-1.041 e-16	1.019 e+01	-8.059 e-14	2.487 e-14	-3.502 e-14	1.169 e-16
2	-1.019 e+01	-9.166 e-01	9.773 e+01	-2.196 e-13	1.149 e-12	-9.594 e-14
3	9.254 e-14	-9.773 e+01	-5.718 e-07	-1.766 e+01	1.849 e-14	6.903 e-14
4	-2.666 e-14	-3.841 e-01	1.766 e+01	-4.023 e-02	2.870 e+01	-3.178 e-14
5	3.115 e-14	2.654 e-02	-2.096 e-05	-2.869 e+01	-1.921 e-04	4.440 e+01
6	-1.607 e-15	1.230 e+00	-9.714 e-04	2.577 e-01	-4.442 e+01	-4.128 e-01

THE INPUT MATRIX,  $D_R$  (6 by 1)

	1
1	0.
2	-1.354 e+00
3	1.069 e-03
4	-2.837 e-01
5	1.960 e-02
6	9.086 e-01

THE OUTPUT MATRIX,  $C_R$  (1 by 6)

	1	2	3	4	5	6
1	-7.381 e+00	6.226 e-18	-3.485 e-15	-1.446 e-16	7.010 e-15	6.250 e-19

TABLE 3.4b

REDUCED MODEL,  $S_2$ THE PLANT MATRIX,  $A_R$  (6 by 6)

	1	2	3	4	5	6
1	2.082 e-17	-1.109 e+01	1.856 e-14	-2.300 e-14	-1.056 e-14	-6.632 e-17
2	1.109 e+01	-8.803 e-01	9.748 e+01	-6.445 e-14	-2.694 e-13	9.011 e-14
3	-1.966 e-14	-9.748 e+01	-1.774 e-06	-1.851 e+01	-1.157 e-13	-8.282 e-14
4	-3.572 e-14	-6.976 e-01	1.851 e+01	-1.382 e-01	-2.754 e+01	-4.179 e-14
5	1.493 e-14	-1.997 e-02	2.835 e-05	2.753 e+01	-1.133 e-04	4.288 e+01
6	2.711 e-15	-1.058 e+00	1.502 e-03	-4.191 e-01	-4.289 e+01	-3.177 e-01

THE INPUT MATRIX,  $D_R$  (6 by 1)

	1
1	0.
2	-1.327 e+00
3	1.884 e-03
4	-5.258 e-01
5	-1.505 e-02
6	-7.972 e-01

THE OUTPUT MATRIX,  $C_R$  (1 by 6)

	1	2	3	4	5	6
1	-6.519 e+00	4.257 e-17	-5.902 e-15	1.750 e-17	-4.935 e-15	-1.337 e-16

### 3.5 Comparison and Discussions

#### 3.5.1 Spectral Analysis.

Fundamental to every model is its modal properties, the eigenvalues and eigenvectors. In this section, we compare the eigenvalues of the reduced model obtained by MCA and CER-algorithms.

Since, in MCA, a subset of the original modes are retained in the reduced model, the eigenvalues of the reduced models are also a subset of the eigenvalues of the original full order model. This information is provided in Table 3.5, where  $n_r = 20$  denotes the full order model. Observe that for  $n_r = 2, 20$ , both  $S_1(\beta=0)$  and  $S_2(\beta \rightarrow \infty)$  retain the same modes, and hence as mentioned previously, the modeling-problem and the control-problem are separable in this case, (for  $n_r = 2, 20$ ).

For cost-equivalent realizations obtained by the CER-algorithm, it is not necessary that the eigenvalues of the CERs be a subset of the original eigenvalues. Depending upon the order of the CER, some or none of their eigenvalues may be contained in the set of the original eigenvalues. Nevertheless, by theorem 3.8, none of these eigenvalues lie in the open right half (unstable) complex plane. In Fig. 3.2a and Fig. 3.2b, the modal frequencies ( $\omega$ ) and their damping factors are plotted for the cost equivalent realizations of orders  $n_r = 20, 18, \dots, 2$ . Figs. 3.2a and 3.2b correspond respectively to  $\beta = 0$  and  $\beta \rightarrow \infty$ . Also provided in these figures are the corresponding modal cost sequence of the modes (of the full order model) - this is indicated by the numbers within parenthesis in the first column.

Observe that the changes in the damping ratio occur mostly at the low frequency range, and gradually extend to high frequency range as the order of the CER reduces. Furthermore, for both the cases  $\beta = 0$  and

TABLE 3.5. EIGENVALUES OF THE REDUCED MODELS - MCA

$n_r$	FREQUENCY, (RAD. SEC <sup>-1</sup> ) <sup>†</sup>	
	$S_1(\beta = 0)$	$S_2(\beta \rightarrow \infty)$
20	1,9,4,16,25,36,64,100,49,81 <sup>‡</sup>	1,4,16,25,49,9,100,64,36,81
18	1,9,4,16,25,36,64,100,49	1,4,16,25,49,9,100,64,36
16	1,9,4,16,25,36,64,100	1,4,16,25,49,9,100,64
14	1,9,4,16,25,36,64	1,4,16,25,49,9,100
12	1,9,4,16,25,36,64	1,4,16,25,49,9
10	1,9,4,16,25	1,4,16,25,49
8	1,9,4,16	1,4,16,25
6	1,9,4	1,4,16
4	1,9	1,4
2	1	1

<sup>†</sup> All these modes have the same damping factor of .005

<sup>‡</sup> The frequencies are ordered in the decreasing magnitudes of their modal costs.

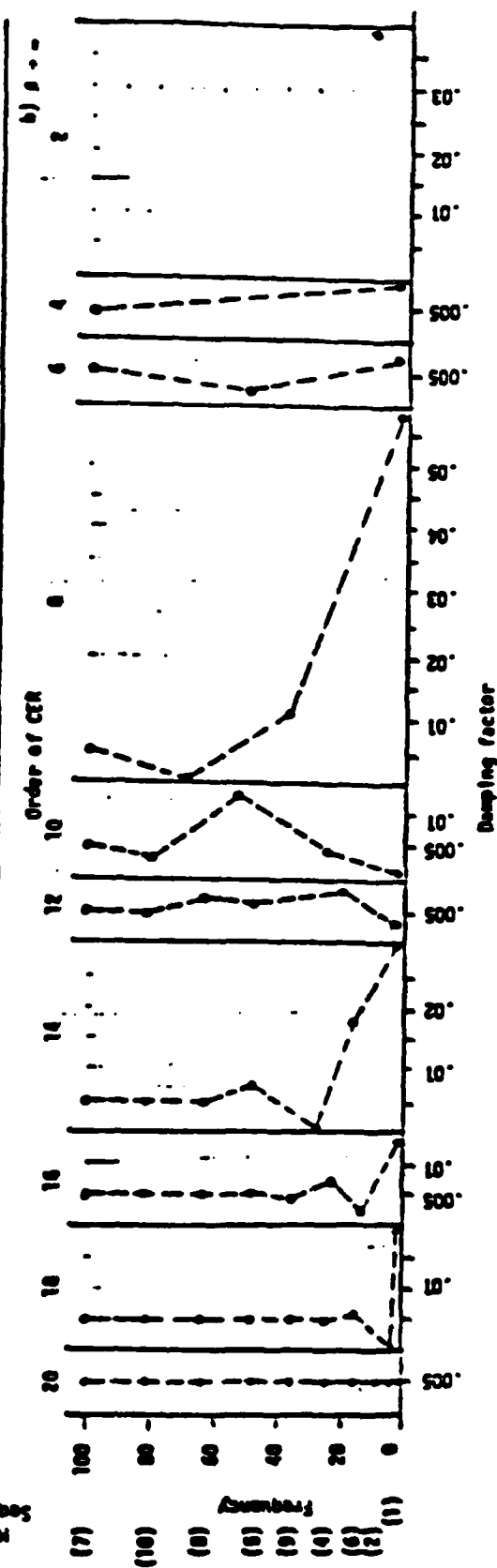
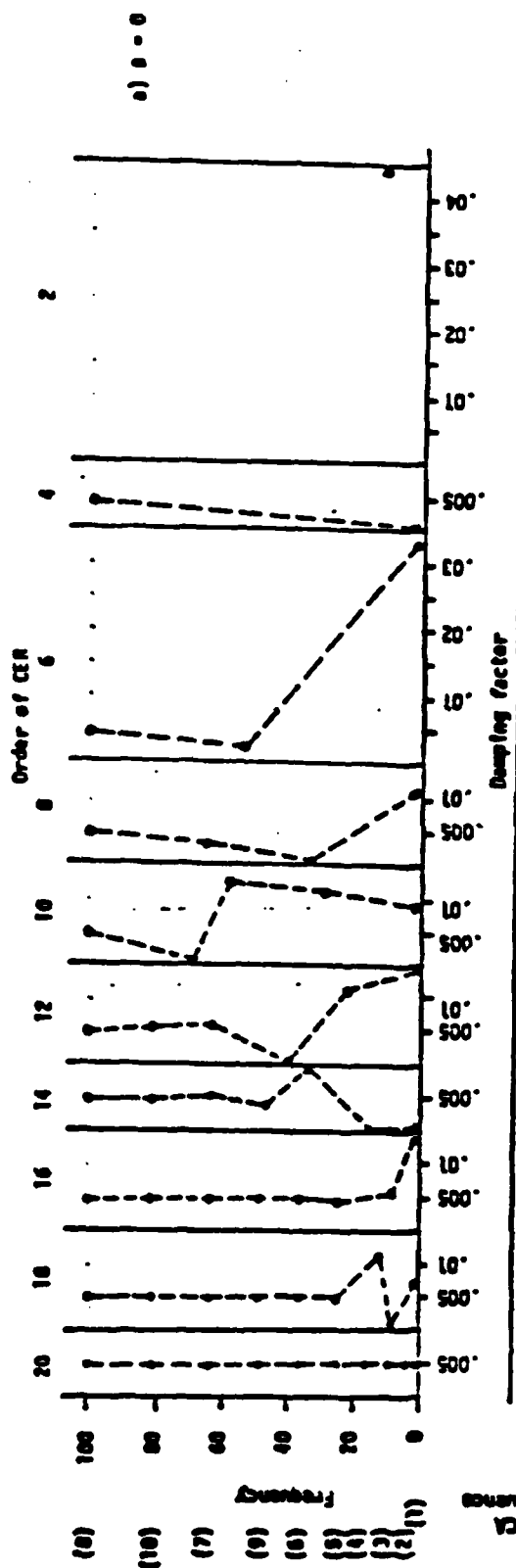


Fig. 3.2. Spectrum of Cost Equivalent Realizations

$\beta \rightarrow \infty$ , the CERS tend to retain the high frequencies, which is also a tendency observed in Routh Approximation methods [3.8].

Hence, in this example, the CERS tend to retain the high frequency spectrum, whereas the reduced models obtained by MCA retain the low frequency spectrum. The effect of this difference clearly shows up in the time response analysis of the reduced models in the following section.

### 3.5.2 Time Response.

This section compares the time response of the reduced models of order 6 (generated in sections 3.3 and 3.4) with that of the full model containing 10 modes. The input signals used are an impulse with unit strength, and a step with unit magnitude. Figs. 3.3a, b and Figs 3.4a, b display the results.

The 'system differences' plotted in these figures (i) ((ii)) are the differences between the output (measurement) generated by the reduced models and the full order model. Figs. (a) correspond to impulse response and Figs. (b) correspond to step response.

Observe, from Figs. 3.3a and 3.3b, that the system differences have high frequency oscillations. This is due to the fact that the MCA-models tended to retain the lower frequencies, and hence the error (difference) is predominantly due to high frequency modes. Also note that the model  $S_1$ , which corresponds to  $\beta = 0$ , generates the output more accurately than  $S_2$ . This is to be expected since  $S_1$  was generated with emphasis on the output ( $\beta = 0$ ). This observation is reversed in the case of measurement errors, which is again expected.

The same trend is observed in Figs. 3.3b (i) and (ii). These reduced models, do not retain the d.c. gain of the full model, except model  $S_1$  in Fig. 3.3b (i).

FIG.3.3a. REDUCED SYSTEM DIFFERENCES - IMPULSE

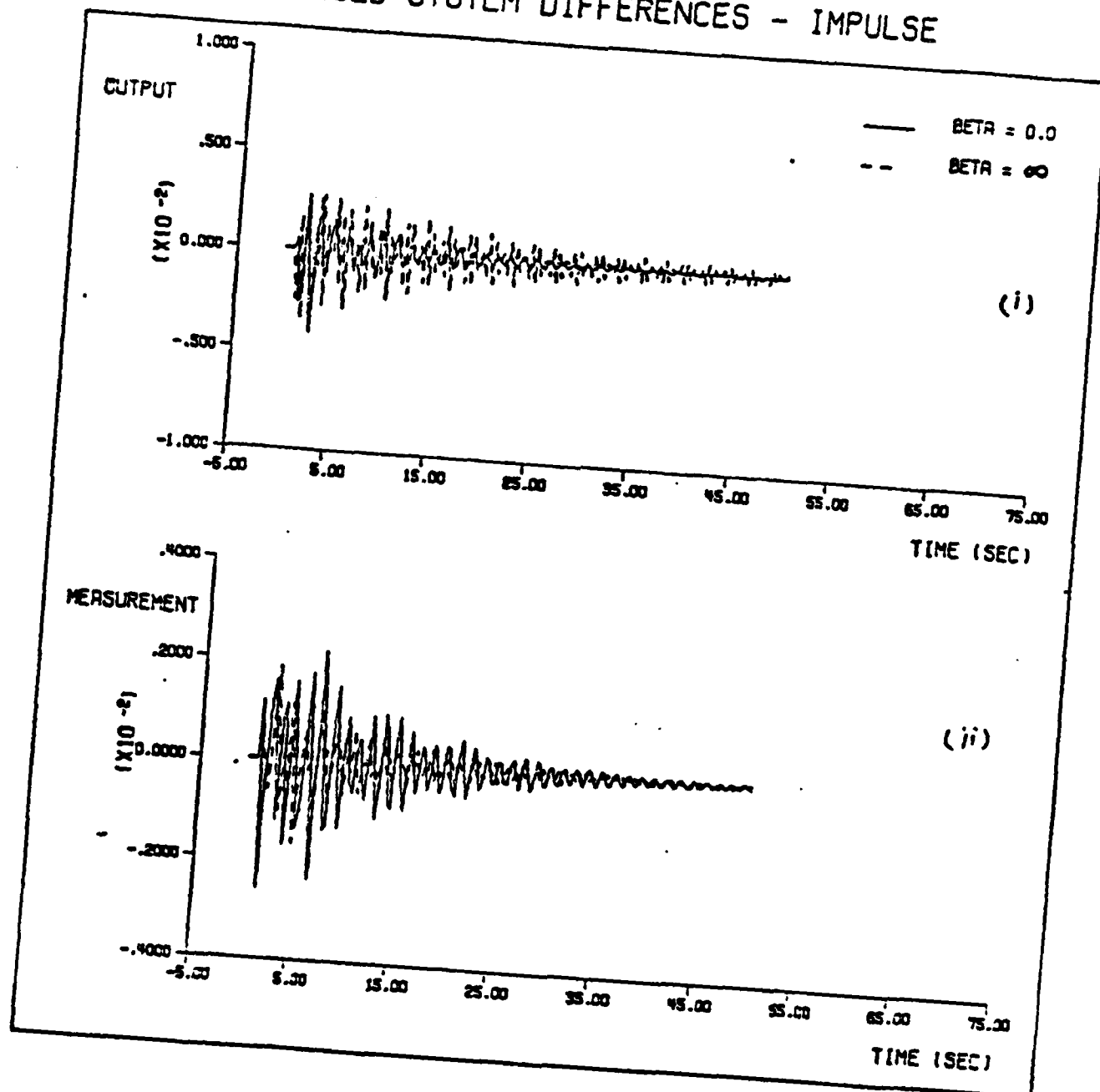


FIG. 3.3b REDUCED SYSTEM DIFFERENCES - STEP

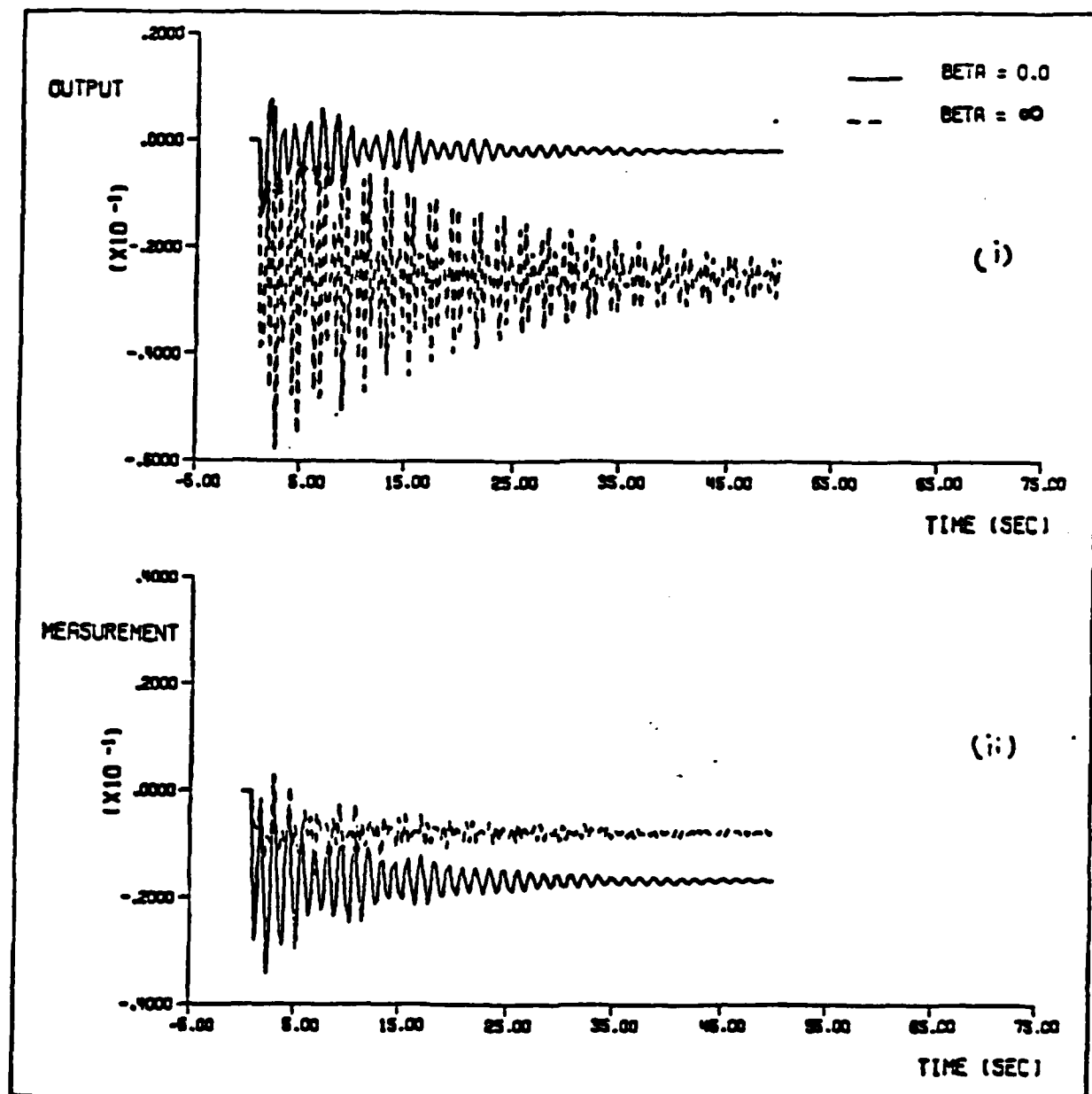


FIG. 3.4a. CER REDUCED SYSTEM DIFFERENCES - IMPULSE

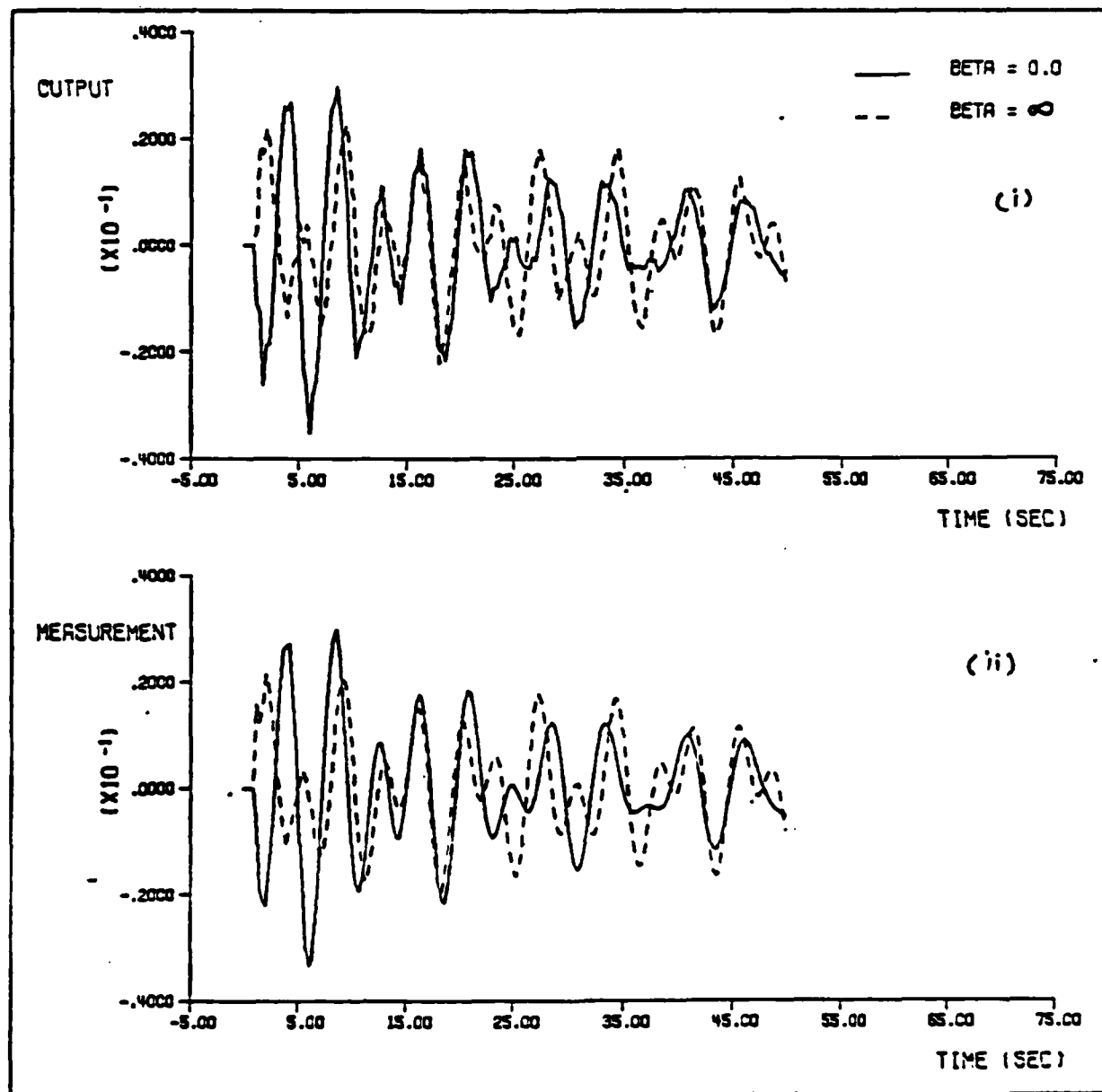
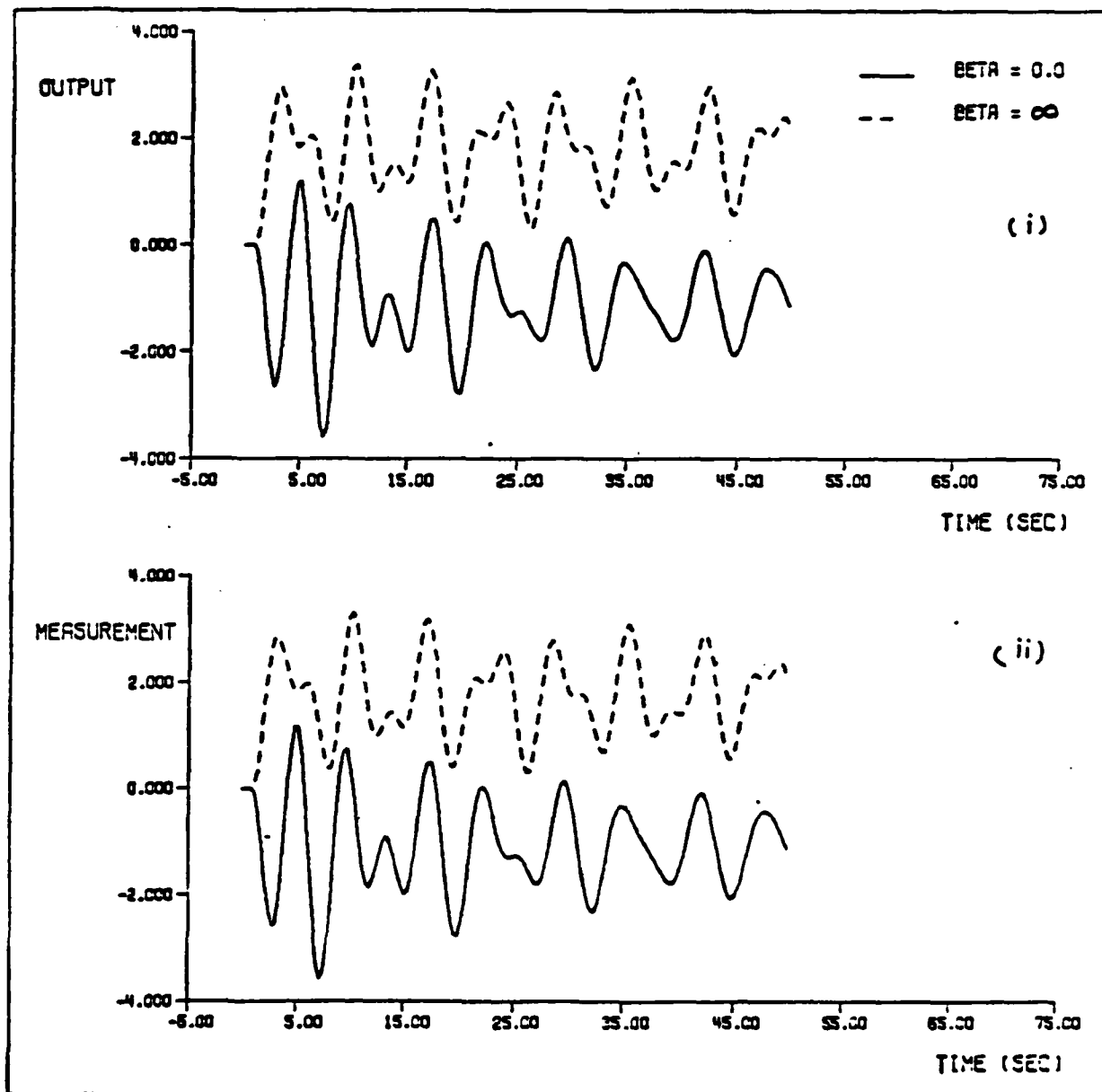


FIG.3.4b. CER REDUCED SYSTEM DIFFERENCES - STEP



The time response errors of the CERs to impulse and step inputs are plotted in Figs. 3.4a and 3.4b. The oscillations in these figures are of lower frequencies (than those in Figs. 3.3) since the CERs had eigenvalues with higher frequencies. Both the output error plot (Figs. 3.4a (i) and Fig. 3.4b(i) and the measurement error plot (Figs. 3.4a (ii) and Fig. 3.4b (ii)) exhibit identical behavior. None of these models retain the d.c. gain of the full model.

In comparison, based upon the time responses, the reduced models of order 6 produced by MCA, seem to be superior to the CERs of order 6.

### 3.6 Conclusion

This Section has presented and analyzed two model reduction schemes:

- (1) Modal Cost Analysis, and
- (2) Cost Equivalent Realizations.

Both these schemes are shown to yield reduced models whose cost perturbation indices can be predicted exactly, i.e.  $q = \hat{q}$ . In addition CERs have (in fact they are defined by) the property  $q = 0$ . However, for mechanical systems, for which modal data is available, MCA is much simpler to implement than the CER-algorithm.

Both these schemes are special cases of Component Cost Analysis, which generates reduced models based upon a quadratic cost function. The role of this cost function has been studied and different cost functions have been presented in this section.

The simply supported beam of Section 2 has been used as a numerical example to compare the above two model reduction schemes, and also to study the effect of different cost functions on the reduced models. For this example, it turns out that the reduced models by MCA are superior

to the CERs. It has also been observed that the CERs tend to contain high frequencies, while the reduced models produced by MCA retain low frequencies. As a result, it is shown by simulation, that the trajectory errors associated with CERs are smoother than the errors associated with the MCA-reduced models. However, the magnitude of the errors is larger for CERs.

#### 4.0 DESIGN AND EVALUATION OF CONTROLLERS

##### 4.1 Introduction

As mentioned in the beginning of this report, the purpose of the reduced models obtained in the previous section is to design a low-order controller based upon the approximate models. The situation at hand can be explained with the following diagram.

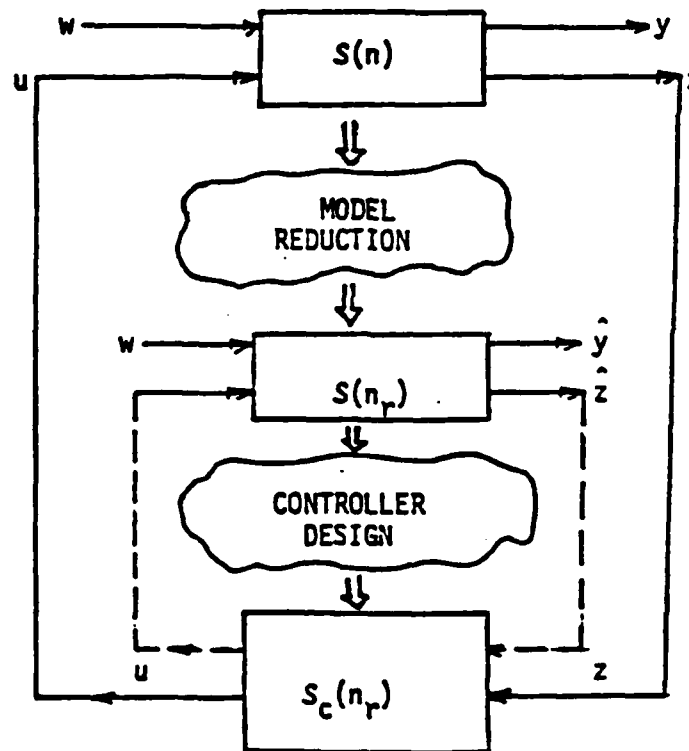


Fig. 4.1. Representation of Controller Design  
Based Upon Reduced Models

The process illustrated in Fig. 4.1 consists of two steps:

(1) Model reduction (this was the subject of Section 3), and (2) controller design (subject of the current section). In Step (1), the given model of order  $n$  is reduced to an approximate model of order  $n_r < n$ . The output and the measurement signals (which are now only approximate) are indicated respectively by  $\hat{y}$  and  $\hat{z}$ . Step (2), now assumes that this reduced model is exact and designs a controller to minimize the following cost function.

$$\hat{V} = \lim_{t \rightarrow \infty} \frac{1}{t} \mathbb{E} \int_0^t \{ \|\hat{y}(\sigma)\|_Q^2 + \rho \|\hat{u}(\sigma)\|_R^2 \} d\sigma. \quad (4.1.1)$$

In other words, step (2) assumes that  $\hat{y}$  and  $\hat{z}$  are exact and not approximations. (This is indicated by the dashed lines in Fig. 4.1.) But in reality, the controller  $S_c(n_r)$  receives the signals  $z$  and not  $\hat{z}$ , and drives the actual 'model'  $S(n)$  and not  $S(n_r)$ , (as indicated by the solid line). Furthermore, the cost function (performance objective) one is interested in is

$$V = \lim_{t \rightarrow \infty} \frac{1}{t} \mathbb{E} \int_0^t \{ \|y(\sigma)\|_Q^2 + \rho \|u(\sigma)\|_R^2 \} d\sigma \quad (4.1.2)$$

and not (4.1.1). Naturally then, the errors in  $\hat{z}$  and  $\hat{y}$  dictate the *actual* performance of the controller.

The purpose of this section is to present this design and evaluation procedure and to illustrate the effect of errors in the reduced model on the performance of the controller. We will use the four models generated in the previous section as the reduced models.

In Section 4.2, we present the standard controller design techniques by Linear Quadratic Gaussian Theory, and present the evaluation procedure in Section 4.3. Section 4.4 applies these techniques to the beam example.

## 4.2 LQG-Controller Design

The Linear Quadratic Gaussian (LQG) approach [8] to control system design for stochastic models has gained increasing acceptance as a practical design tool. Some of the reasons for the wide acceptance of LQG approach are due to easily derived analytical results, mathematical tractability and some guaranteed robustness properties in terms of gain and phase margins.

Since this is a standard text book theory (Ref. [8], for example), we only summarize the steps needed for controller design, for completeness.

We assume that a stabilizable and detectable<sup>†</sup> model is available in the following state space form.

$$\begin{aligned}\dot{x}_R &= A_R x_R + B_R u + D_R w \\ \hat{y} &= C_R x_R \\ \hat{z} &= M_R x_R + v\end{aligned}\tag{4.2.1}$$

with the vectors  $x_R \in \mathbb{R}^{n_r}$ ,  $u \in \mathbb{R}^m$ ,  $w \in \mathbb{R}^q$ ,  $\hat{y} \in \mathbb{R}^k$ , and  $\hat{z}, v \in \mathbb{R}^l$ . The process noise  $w$  and the measurement noise  $v$  are assumed to be uncorrelated zero-mean gaussian white noise processes, with intensities  $W$  and  $V$  respectively. (If needed, we can assume random initial conditions for the states  $x_R$  but, for the infinite-time design problem considered herein, this becomes unnecessary). We wish to design a controller of order  $n_c$ , which minimizes the cost function

$$\hat{J} = \lim_{t \rightarrow \infty} \frac{1}{t} E \int_0^t \{ \|\hat{y}(\sigma)\|_Q^2 + \rho \|u(\sigma)\|_R^2 \} d\sigma\tag{4.2.2}$$

<sup>†</sup>both the uncontrollable subspace and the unobservable subspace are asymptotically stable.

For this problem, the LQG-theory yields the following optimal controller.

$$\begin{aligned}\dot{x}_c &= A_c x_c + F \hat{z} ; & x_c &\in \mathbb{R}^{n_r} \\ u &= G x_c\end{aligned}\quad (4.2.3a)$$

where

$$A_c \triangleq (A_R + B_R G - F M_R) \quad (4.2.3b)$$

and where the control gain  $G \in \mathbb{R}^{m \times n_r}$  and the filter gains  $F \in \mathbb{R}^{n_r \times \ell}$  are given by

$$G = -\frac{1}{\rho} R^{-1} B_R^T K \quad (4.2.4a)$$

$$F = P M_R^T V^{-1} \quad (4.2.4b)$$

with  $K$  satisfying the control Riccati equation

$$K A_R + A_R^T K - \frac{1}{\rho} K B_R R^{-1} B_R^T K + C_R^T Q C_R = 0 \quad (4.2.4c)$$

and  $P$  satisfying the filter Riccati equation

$$P A_R^T + A_R P - P M_R^T V^{-1} M_R P + D_R W D_R^T = 0 \quad (4.2.4d)$$

Thus, to obtain the optimal controller, the following steps are needed.

*Algorithm for LQG controller design.*

- Step 1. Compute  $K$  and  $P$  by solving the Riccati equations (4.2.4c) and (4.2.4d).
- Step 2. Compute the controller parameters according to (4.2.3b), (4.2.4a) and (4.2.4b).

The controller (4.2.3), obtained by the LQG-theory minimizes the cost function (4.2.2) which is only an approximation of the actual cost

function (4.1.2). The following section describes the evaluation of this controller with respect to (4.1.2) and the full model  $S(n)$ .

### 4.3 Evaluation

Note that in (4.2.3a) we have indicated that the controller is driven by  $\hat{z}$  which is what the LQG-theory assumes. However, when the controller is used to drive the full order model, the following representations result.

$$\begin{aligned}\dot{x}_c &= A_c x_c + Fz \quad ; \quad x_c \in \mathbb{R}^{n_r} \\ u &= Gx_c\end{aligned}\tag{4.3.1}$$

$$\begin{aligned}\dot{x} &= Ax + Bu + Dw \quad ; \quad x \in \mathbb{R}^n \\ y &= Cx \\ z &= Mx + v.\end{aligned}\tag{4.3.2}$$

For the evaluation purposes, we wish now to compute the following quantities, which are defined as shown.

$$\text{Regulation Cost, } V(y) \triangleq \left[ \lim_{t \rightarrow \infty} \frac{1}{t} \int_0^t \|y(\sigma)\|_Q^2 d\sigma \right]\tag{4.3.3}$$

$$\text{Control Energy, } V(u) \triangleq \left[ \lim_{t \rightarrow \infty} \frac{1}{t} \int_0^t \|u(\sigma)\|^2 d\sigma \right]\tag{4.3.4}$$

RMS value of the  $i$ -th output ( $i = 1, 2, \dots, k$ )

$$v^{1/2}(y_i) \triangleq \left[ \lim_{t \rightarrow \infty} \frac{1}{t} \int_0^t y_i^2(\sigma) d\sigma \right]^{1/2}\tag{4.3.5}$$

RMS value of the input energy at the  $i$ -th actuator ( $i = 1, 2, \dots, m$ )

$$v^{1/2}(u_i) \triangleq \left[ \lim_{t \rightarrow \infty} \frac{1}{t} \int_0^t u_i^2(\sigma) d\sigma \right]^{1/2}\tag{4.3.6}$$

The first two quantities, regulation cost and the control energy, offer a macroscopic evaluation of the closed loop system. The RMS values  $v^{1/2}(y_i)$  and  $v^{1/2}(u_i)$ , however, are of more importance, since in general, the mission requirements are given only in terms of the RMS values of the outputs and the RMS values of the maximum allowable control energy at each input channel. Moreover, violation of any of these specifications does not always reflect in  $V(y)$  and/or  $V(u)$ .

We now present expressions for the computation of these quantities, based upon the following 'augmented' representation of the closed loop system.

$$\begin{aligned}\dot{x}_a &= A_a x_a + D_a w_a \\ y_a &= C_a x_a\end{aligned}\tag{4.3.7a}$$

where

$$\begin{aligned}x_a^T &\triangleq [x^T, x_c^T] ; \quad x_a \in R^{n+n_r} \\ w_a^T &\triangleq [w^T, v^T] ; \quad w_a \in R^{q+l} \\ y_a^T &\triangleq [y^T, u^T] ; \quad y_a \in R^{k+m}\end{aligned}\tag{4.3.7b}$$

$$\begin{aligned}A_a &\triangleq \begin{bmatrix} A & BG \\ FM & A_c \end{bmatrix} \\ D_a &\triangleq \begin{bmatrix} D & 0 \\ 0 & F \end{bmatrix} \\ C_a &\triangleq \begin{bmatrix} C & 0 \\ 0 & G \end{bmatrix} .\end{aligned}\tag{4.3.7c}$$

*Theorem 4.1*

The quantities (4.3.3 - 4.3.6) are calculated as follows.

$$V(y) = \text{Tr}[C^T Q C X_{11}] \quad (4.3.8a)$$

$$V(u) = \text{Tr}[G^T G X_{22}] \quad (4.3.8b)$$

$$V^{1/2}(y_i) = [c_i^T X_{11} c_i]^{1/2}; \quad i = 1, 2, \dots, k \quad (4.3.8c)$$

$$V^{1/2}(u_i) = [g_i^T X_{22} g_i]^{1/2}; \quad i = 1, 2, \dots, m \quad (4.3.8d)$$

where

$$c_i^T \triangleq \text{i-th row of } C \quad (4.3.9a)$$

$$g_i^T \triangleq \text{i-th row of } G \quad (4.3.9b)$$

and where

$$X_{11} \triangleq \lim_{t \rightarrow \infty} E \{x(t) x^T(t)\} \quad (4.3.10a)$$

$$X_{22} \triangleq \lim_{t \rightarrow \infty} E \{x_c(t) x_c^T(t)\} \quad (4.3.10b)$$

are obtained from partitioning

$$X_a \triangleq \lim_{t \rightarrow \infty} E \{x_a(t) x_a^T(t)\} \quad (4.3.10c)$$

as 
$$X_a = \begin{bmatrix} X_{11} & X_{12} \\ X_{12}^T & X_{22} \end{bmatrix} \quad (4.3.10d)$$

which satisfies,

$$X_a A_a^T + A_a X_a + D_a W_a D_a^T = 0 \quad (4.3.10e)$$

where

$$W_a \triangleq \text{diag} \{W, V\} \quad (4.3.10f)$$

For the evaluation and comparison purposes, one follows these steps.

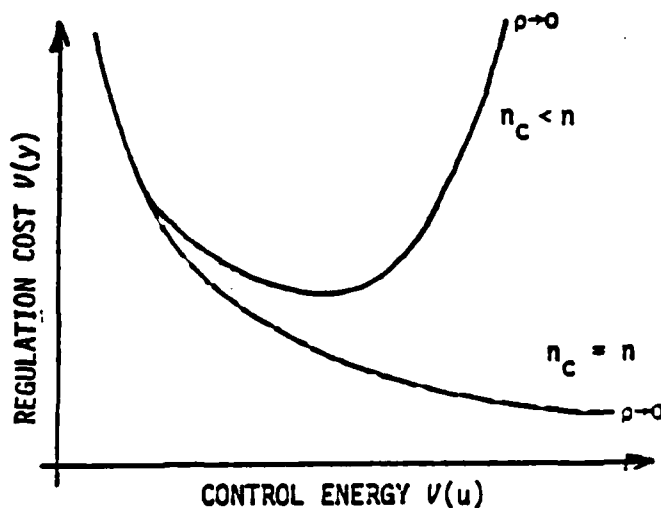
Step 1: Select a value of  $\rho$  and design an optimal LQG-controller of order  $n_c = n_r$ , the order of the reduced model (i.e. use the algorithm for LQG-controller design, for a specific value of  $\rho$ ).

Step 2: Evaluate the quantities  $v(y)$ ,  $v(u)$ ,  $v^{1/2}(y_i)$  and  $v^{1/2}(u_i)$ , according to Theorem 4.1.

Step 3: Repeat Step 1 and Step 2 for different values of  $\rho$ , until sufficient data is collected.

Step 4: Draw the 'performance-plot', as shown in Fig. 4.2.

Fig. 4.2 Performance Plot



Note that when  $n_c = n_r = n$  (i.e., when  $S_c(n_c = n)$  is designed based upon  $S(n)$ ), the LQG theory promises that the performance curve will asymptotically decrease (dotted line). However, for  $n_c < n$ , the effect of model errors (due to  $\hat{y}(t) \neq y(t)$  and  $\hat{z}(t) \neq z(t)$ ) deteriorates the performance with increasing control effort, and eventually drives the closed loop system to instability. Moreover, since the effect of model errors on the performance increases with increasing control energy, the difference between these performance curves (for  $n_c = n$  and  $n_c < n$ ) also increases, as shown in Fig. 4.2.

Such performance plots can be generated to compare different reduced models (and/or different model reduction schemes) in the closed loop situation, as is done in the following sections where the reduced models generated in Section 3 are used for numerical simulation.

#### 4.4 Example

The following four reduced models of the simply supported beam are compared.

1. S1-MCA: The reduced model generated by MCA, for  $\beta = 0$ , of order  $n_r = 6$ .
2. S2-MCA: The reduced model generated by MCA, for  $\beta \rightarrow \infty$ , of order  $n_r = 6$ .
3. S1-CER: Cost-Equivalent Realizations of order  $n_r = 6$ , for  $\beta = 0$ .
4. S2-CER: CER of order  $n_r = 6$ , for  $\beta \rightarrow \infty$ .

The order of the controllers designed from all these reduced models is  $n_c = 6$ , and the evaluation model  $S(n)$ , used for the evaluation purposes is the full 10-mode model with  $n = 20$ .

Since the example considered is a single input single output system ( $k = 1, m = 1$ ), the RMS values of the inputs and outputs are given by

$$V(y_1) = V(y) \quad (4.4.1a)$$

and

$$V(u_1) = V(u) \quad (4.4.1b)$$

Hence, only the plot of  $V(y)$  vs.  $V(u)$  is presented in Figs. 4.3a and 4.3b.

Also compared in the plots are the following models.

5. FULL ORDER: The full order evaluation model, i.e.  $n_r = n = 20$ .
6. S1-MCA;  $n_c=2$ : MCA-reduced model of order 2, for  $\beta = 0$ .
7. S1-CER;  $n_c=2$ : CER of order 2, for  $\beta = 0$ .

The curve corresponding to the full order model serves as a reference, since by LQG-theory, there exists no other controller (of any order) that can perform better than the LQG-optimal controller of order 20.

Observe from Fig. 4.3 that for low control energy, neither the choice of the reduced models nor the schemes of model reduction, influence the performance of the controllers. This is expected since in low bandwidth controllers the effect of model errors is attenuated by the low control gains. However, for high bandwidth controllers, the choice of the reduced model does play a significant role.

Of the four reduced models, S1-MCA, S2-MCA, S1-CER and S2-CER, all of order 6, the controllers designed based upon S2-CER yield the worst result, driving the closed loop system unstable for a control energy larger than  $1.0E-03$  units. For the comparison of the remaining three models, a magnification of Fig. 4.3a is presented in Fig. 4.3b. An obvious conclusion from Fig. 4.3b is that for the design of controllers of order 6, the reduced models generated by MCA are preferable.

FIG 4.3. PERFORMANCE PLOT

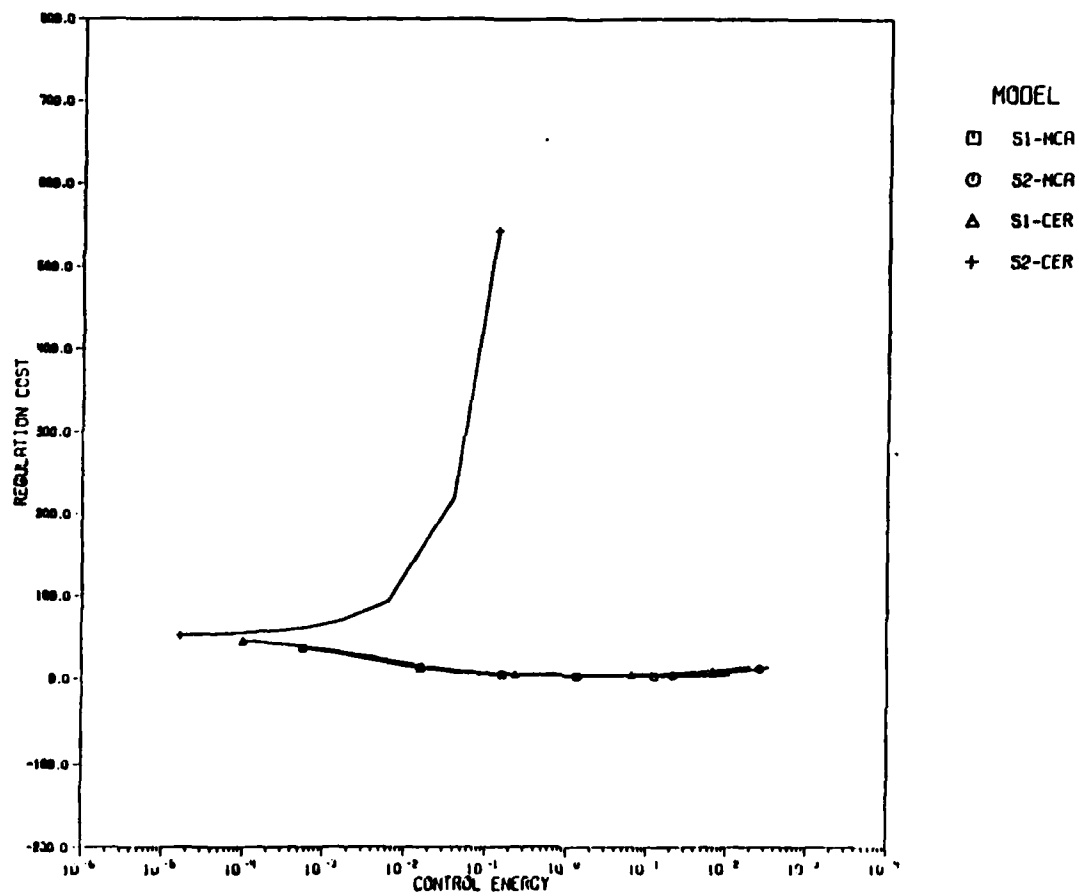
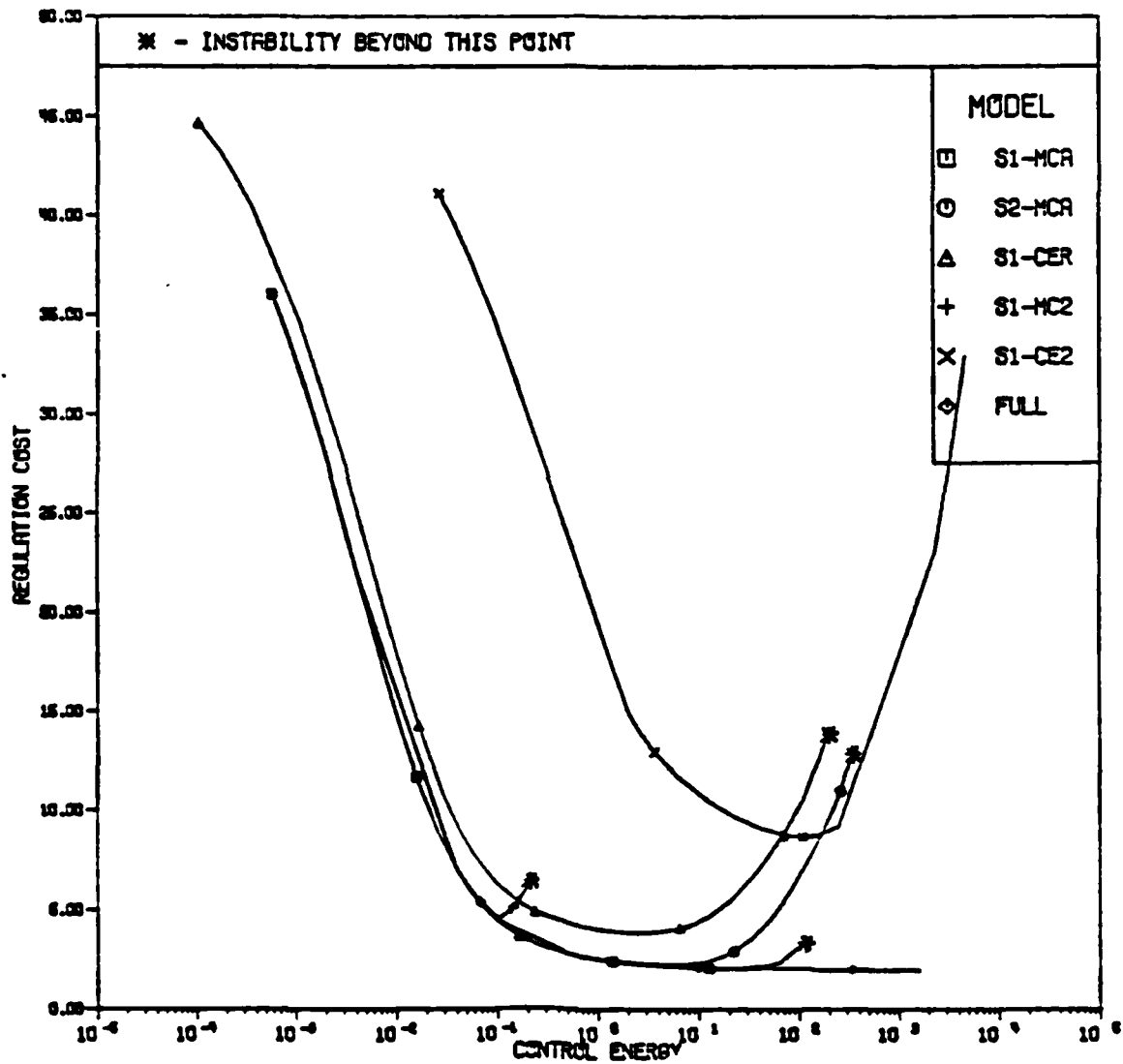


FIG 4.3b PERFORMANCE PLOT



Furthermore, the models generated by both MCA and CER-algorithm corresponding to  $\beta = 0$ , consistently yield better controller designs, than those for  $\beta \neq 0$ , contrary to the expectation that the ' $\beta \neq 0$ ' models would yield better designs at high control energy levels. This contradiction may be attributed to the fact that the filter gains (the measurement gains in the controller) are small, thereby attenuating the errors in the measurement signals generated by the reduced model. The spectrum of the filter, given in Table 4.1, reflects this 'small' filter gain, since the spectrum is essentially the open-loop spectrum.

Table 4.1 Spectrum of the Full Order Filter

Spectral Decomposition of Filter				
Real Part	Imaginary Part	Frequency (Hertz)	Damping Ratio	Time Const. (Sec/Rad)
-4.00233E-01	1.11204E+00	1.88101E-01	.33864260	2.49854E+00
-2.03656E-01	3.98795E+00	6.35528E-01	.05100151	4.91023E+00
-1.43274E-01	1.60017E+01	2.54686E+00	.00895327	6.97965E+00
-1.43620E-01	2.49988E+01	3.97876E+00	.00574496	6.96283E+00
-5.19468E-02	9.00149E+00	1.43266E+00	.00577081	1.92505E+01
-1.81831E-01	3.59999E+01	5.72964E+00	.00505081	6.49961E+00
-2.54960E-01	4.89996E+01	7.79863E+00	.00520324	6.92219E+00
-3.22104E-01	6.39990E+01	1.01859E+01	.00503290	6.10458E+00
-4.05784E-01	8.09991E+01	1.28916E+01	.00500968	2.46436E+00
-5.02495E-01	9.99988E+01	1.59155E+01	.00502495	1.99007E+00

To study the effect of the order of the controller, the curves corresponding to S1-MCA ( $n_c = 6$ ) and S1-MCA ( $n_c = 2$ ) can be compared.

Due to the smaller order of SI-MCA ( $n_c = 2$ ), the effect of errors on the controllers is more pronounced. This can be observed from the fact that the controllers designed based upon SI-MCA ( $n_c = 6$ ) remain stable over a wider range of bandwidth.

However, the controllers (based upon SI-CER,  $n_c = 2$ ) remained stable for all values of bandwidth attempted in this simulation. This is due to the fact that, for this beam example, the dimensions of the 'most' observable and 'most' controllable subspace is only 2. Now, since in CER-algorithm, the controllability is normalized by making  $X = I_n$  (3.4.2), the dimension of the above subspace is indicated by that  $n_r$  for which the ratio  $\|A_{RT}\| / \|A_R\|$  in Table (3.3) is the smallest. Note, from this table that the entry  $\|A_{RT}\| / \|A_R\|$  is the smallest for  $n_r = 2$ . Thus the CER of order 2 deletes the 'nearly' unobservable and uncontrollable subspace, thereby reducing the model errors. Hence, the controllers designed based upon this model remains stable for a wider range of bandwidth.

In conclusion, then, if the specifications on the RMS values

$$\begin{aligned} v^{1/2}(y_1) &\leq 3, \quad \text{and} \\ v^{1/2}(u_1) &\leq 15 \end{aligned}$$

is acceptable, then one would pick the controller corresponding to the minimum point of the curve SI-CER,  $n_c = 2$ , at which point,  $V(y) = 8.6962$  and  $V(u) = 108.13$ . This controller not only meets the specifications but also is more robust and requires less hardware, since the order of the controller is only two.

#### 4.5 Conclusion

This section has presented the controller design technique based upon reduced models and has also offered physically motivated metrics, and expressions for calculating them, for the evaluation of the controllers.

The comparison of different controllers has been presented with the following points in mind.

- 1) The influence of model-reduction scheme,
- 2) Effect of order of the model, and
- 3) The role of cost function for the model reduction process.

The conclusions based upon the beam example are:

- 1) At low bandwidth of the controllers, the influence of model reduction schemes is not significant. But at high bandwidth, the performance of the controllers depend, remarkably, on the model reduction scheme adopted. For the sixth order controller, of the MCA and CER-algorithm used for model reduction, MCA is more reliable.
- 2) The effect of the order of the reduced model is significant only at high bandwidth. In general, in the case of MCA, the smaller the order of the model, the worse is the performance of the controller which is designed based upon this model. However, in the case of CER this observation does not seem to hold, as is evidenced by SI-CER,  $n_c = 2$  curve. The metric that dictates the performance of the controller seems to be the term  $\|A_{RT}\|/\|A_R\|$  of Table 3.3, which reflects the observability and controllability of the subspace that is deleted from the full order model.

- 3) We expected the ' $\beta \rightarrow \infty$ ' models to yield better high bandwidth controllers. But none of the ' $\beta \rightarrow \infty$ ' controllers performed better than the ' $\beta = 0$ ' controllers. We conjecture that this could be due to the low filter gains.

## 5. APPLICATION: SOLAR OPTICAL TELESCOPE

### 5.1 Description

The Solar Optical Telescope (SOT) considered is schematically represented by Fig. 5.1. The SOT is modeled by finite element methods as follows.

$$\ddot{n}_i + 2\zeta_i\omega_i\dot{n}_i + \omega_i^2 n_i = b_i^T(u+w) \quad (5.1.1)$$

$$i = 1, 2, \dots, 44,$$

where  $\omega_i$  is the natural frequency and  $\zeta_i$  is the damping factor of mode  $i$ , ( $n_1, n_2$  and  $n_3$  represent the rigid body modes;  $\omega_1 = \omega_2 = \omega_3 = 0$ ). There are eight 'noisy' force actuators whose control forces  $u_1, \dots, u_8$  act in the  $z$ -direction, located as shown in Fig. 5.1. The actuator noise (assumed to be white) is denoted by  $w$  and has intensity  $W = 10^{-4} I_8 \text{ New}^2$ . The frequencies  $\omega_i$  are given in Table 5.1, and the damping ratios are taken as  $\zeta_i = .001, i = 4, 5, \dots, 44$ , and  $\zeta_i = 0, i = 1, 2, 3$ , corresponding to the rigid body modes.

The variables to be controlled are  $\text{LOS}(x)$ ,  $\text{LOS}(y)$  and defocus, where  $\text{LOS}(x)$  ( $\text{LOS}(y)$ ) is the angular displacement error of the optical line of sight in  $x$ - ( $y$ -) direction, and defocus is caused by changes in the length of the optical axis (deflections in the  $z$ -direction). These variables are related to the modes  $n_i$  by

$$y = \sum_{i=1}^{44} c_i n_i \quad (5.1.2)$$

where  $y^T = \{\text{LOS}(x), \text{LOS}(y), \text{defocus}\}$ . The control objective is then written as

$$V = \lim_{t \rightarrow \infty} \frac{1}{t} E \int_0^t \{ \|y(\sigma)\|_Q^2 + \rho \|u(\sigma)\|_R^2 \} d\sigma \quad (5.1.3)$$

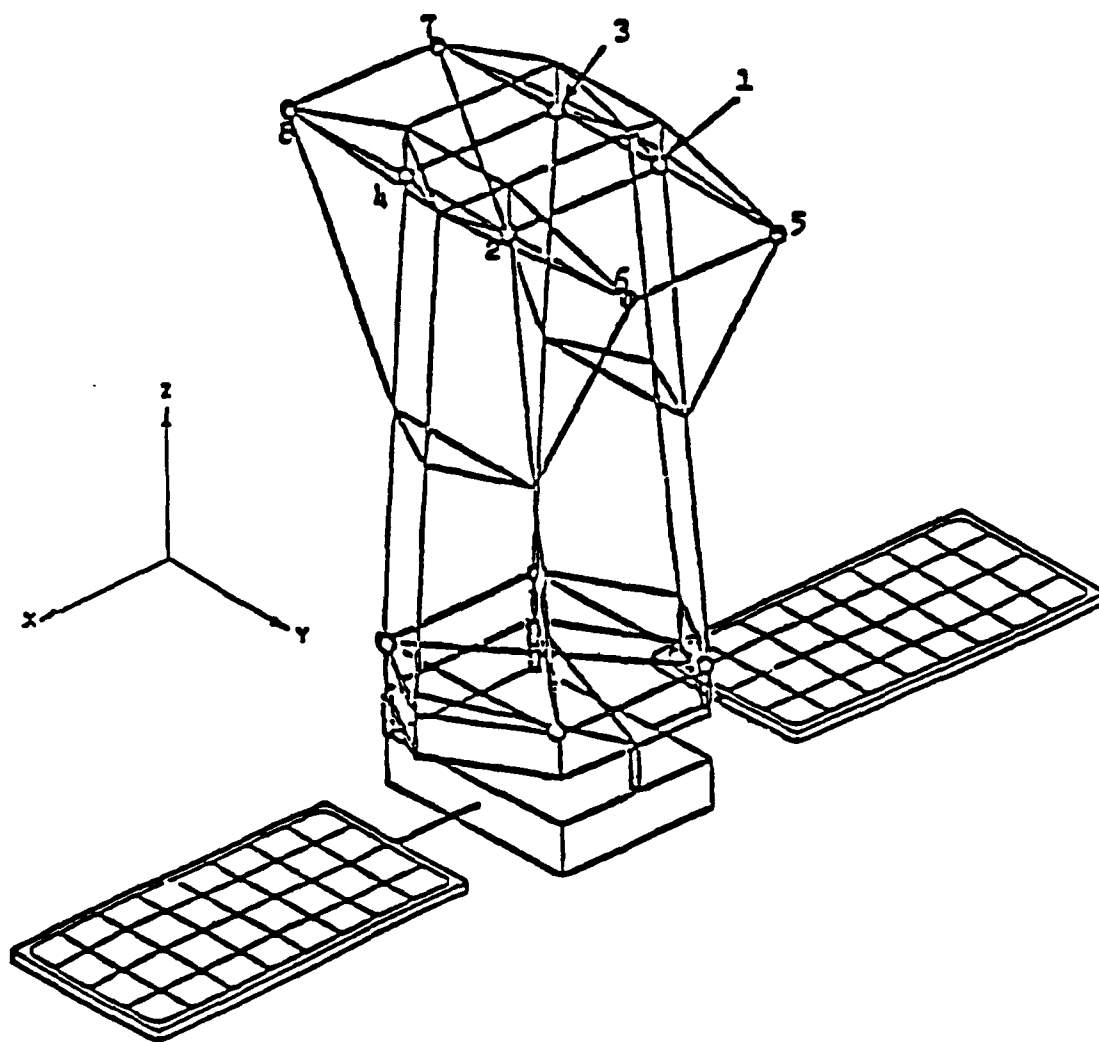


FIG. 5.1 SOLAR OPTICAL TELESCOPE STRUCTURE

TABLE 5.1 MODAL FREQUENCIES

Mode #	Freq(Hz)
1	0
2	0
3	0
4	.9136e+0
5	.1654e+1
6	.1993e+1
7	.2092e+1
8	.2783e+1
9	.3630e+1
10	.3652e+1
11	.7688e+1
12	.8171e+1
13	.8466e+1
14	.1081e+2
15	.1142e+2
16	.1143e+2
17	.1485e+2
18	.1878e+2
19	.1995e+2
20	.2128e+2
21	.3243e+2
22	.3305e+2
23	.4948e+2
24	.5101e+2
25	.5250e+2
26	.5386e+2
27	.5520e+2
28	.5532e+2
29	.7225e+2
30	.7997e+2
31	.8498e+2
32	.8618e+2
33	.8898e+2
34	.9836e+2
35	.1010e+3
36	.1039e+3
37	.1052e+3
38	.1078e+3
39	.1120e+3
40	.1198e+3
41	.1494e+3
42	.1534e+3
43	.1628e+3
44	.1657e+3

where the output weighting matrix  $Q$  is chosen as  $Q = \text{diag} \{1, 10, 10^{-3}\}$  to indicate that the LOS-errors about the  $y$ -axis are most critical to the experiments, and the control weighting matrix  $R$  is chosen as  $R = I_8$ , to reflect that all the actuators are equally weighted.

The available measurements for the control law implementation are

$$z = y + v, \quad z \in R^3 \quad (5.1.4)$$

where the disturbance  $v$  is assumed to be a zero mean Gaussian white noise process with intensity

$$V = \text{diag} \{10^{-13}, 10^{-13}, 10^{-15}\},$$

to reflect the uncertainties in the measurements.

The modal data  $b_i, c_i, i = 1, 2, \dots, 44$  is provided in Table 5.2.\*

To summarize, the SOT is modeled in its modal coordinates as follows.

$$\begin{aligned} \ddot{\eta}_i + 2\zeta_i \omega_i \dot{\eta}_i + \omega_i^2 \eta_i &= b_i^T (u+w); \quad i = 1, \dots, 44 \\ y &= \sum_{i=1}^{44} c_i \eta_i \\ z &= y + v \end{aligned} \quad (5.1.5)$$

with the performance objective given by (5.1.3).

Now, in state-space formulation, the order of the model (5.1.5) is 88. The LQG-optimal controller for this problem would also be of order 88, which is too large for practical purposes. Hence, the design of a feasible (of acceptable dimension) controller requires a reduced order controller design technique. We will adopt the MCA and CER-theory for such controller design in this Section.

---

\*Table 5.2 is available from the author.

## 5.2 Reduced Models

### 5.2.1 Modal Cost Analysis.

We use the following open loop cost function for obtaining reduced models of the SOT.

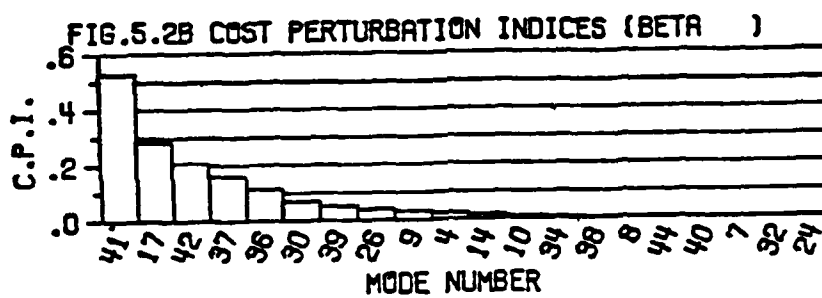
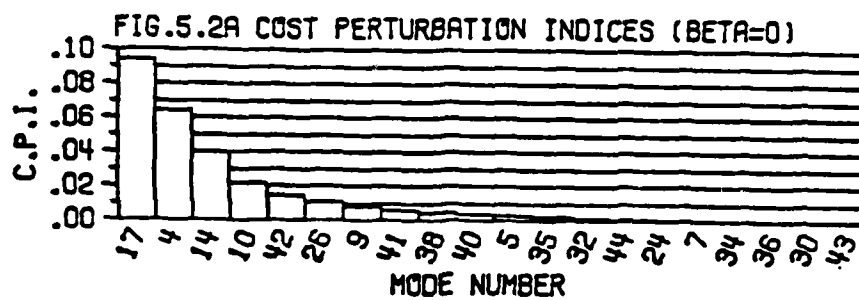
$$V_0 = V_y + \beta V_z$$

where  $V_y$  and  $V_z$  are defined in (3.3.16a) and (3.3.16b) respectively. Two reduced models are generated, one for  $\beta = 0$  and the other for  $\beta \rightarrow \infty$ . The results are presented in Fig. 5.2a and Fig. 5.2b.

Since both the first two rigid body modes ( $\eta_1, \eta_2$ ) are observable and controllable, and have zero frequencies ( $\omega_1 = \omega_2 = 0$ ), by the modal cost formula they have infinite costs. Hence, by modal cost rule these are the most significant modes and are thus retained in the reduced models. On the other hand the third rigid body mode ( $\eta_3$ ; rotation about z-axis) is not observable, and, hence has zero modal cost. Therefore  $\eta_3$  will not be retained in the reduced models. Due to the infinite costs associated with  $\eta_1$  and  $\eta_2$ , these modes are omitted in Fig. 5.2.

Observe that if the order  $n_c$  of the desired controller is four, then for any value of  $\beta$  in  $V_0$ , one would obtain the same reduced model (namely retaining the first two second-order rigid body modes,  $\eta_1$  and  $\eta_2$ ) and hence get the same controller. Thus, for  $n_c = 4$ , the modeling problem and the control problem are separable. However, this separation does not hold for  $n_c > 4$ , which can be observed from the change in the modal sequence for  $\beta = 0$  and  $\beta \rightarrow \infty$  - this change occurs due to the fact that (3.3.23b) is not satisfied.

The following two reduced models of order  $n_r = 10$  are generated for the subsequent controller design:



→ ONLY THE 20 MOST SIGNIFICANT MODES ARE SHOWN

- 1) S1-MCA: retaining the first five most significant modes  
(2 rigid and 3 elastic) corresponding to  $\beta = 0$ .  
This constitutes the set  $\{\eta_i: i \in 1, 2, 17, 4, 14\}$ .
- 2) S2-MCA: retaining the first five most significant modes  
corresponding to  $\beta \rightarrow \infty$ . This constitutes the set  
 $\{\eta_i: i \in 1, 2, 41, 17, 42\}$ .

The cost perturbation indices  $q$  of these reduced models, evaluated with respect to only the elastic modes (since the rigid body modes have infinite modal costs, they are not included in the calculation of these indices) are given below

$$q = \begin{cases} .0395 & \text{for S1-MCA} \\ .1592 & \text{for S2-MCA} \end{cases}$$

#### Choice of an Evaluation Model

At this point we point out that the full model with 44 modes is too large even for the purposes of evaluating the subsequent controllers. Hence, the 'evaluation model' should also be of lower order. This situation is illustrated in Fig. 5.3. The dashed lines in Fig. 5.3 indicate that the controller is designed based upon the reduced model. The solid lines indicate that the controller is evaluated with respect to the evaluation model. The only place where the full model is used is to generate the reduced model and the evaluation model. After the generation of these models, the evaluation model is treated as the 'true' model of the system.

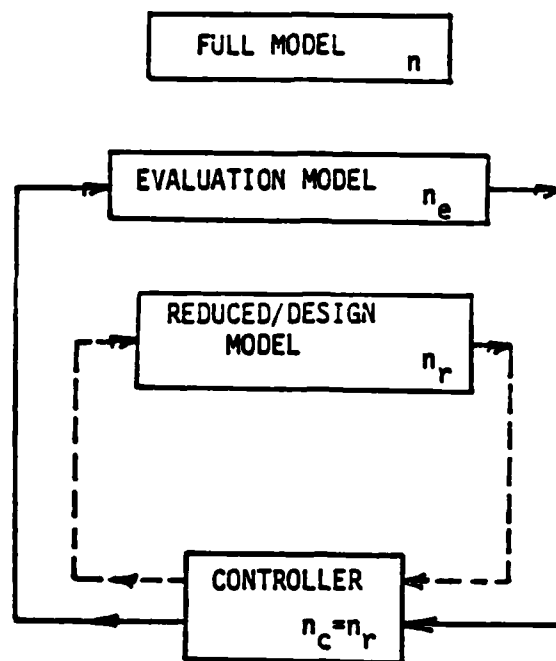


FIG. 5.3 The role of an evaluation model

A proper choice of the evaluation model is a research topic by itself, and we do not attempt to answer it herein. For the present, we shall select the order of the evaluation model to be  $n_e = 20$ , for convenience. This requires 10 second order modes to be retained, two of which must be rigid body modes  $n_1$  and  $n_2$ . The remaining 8 modes (elastic) are selected to be the union of the first 5 modes from Figs. 5.2a and 5.2b, so that the evaluation model will not be 'biased' toward either of the reduced models S1-MCA and S2-MCA. This results in the following evaluation model.

S-EVAL:  $\{n_i: i \in \{1, 2, 4, 10, 14, 17, 36, 37, 41, 42\}\}$

The cost perturbation index associated with S-EVAL is

$$q = \begin{cases} .0121 & \text{for } \beta = 0 \\ .0933 & \text{for } \beta \rightarrow \infty \end{cases}$$

Now, note from the modal cost formula (3.3.4) that the  $i$ -th modal cost  $\hat{v}_i$  is independent of all the other modes; in particular it is independent of the number of modes in the model. Consequently, if the modes retained in the evaluation model are to be ordered according to their modal costs, the sequence of these modes remains the same independent of the model (full or evaluation) used for the calculations. Thus, the modal cost analysis of S-EVAL would also yield the same reduced models S1-MCA (for  $\beta = 0$ ) and S2-MCA (for  $\beta \rightarrow \infty$ ).

### 5.2.2 Cost Equivalent Realizations.

Note from the CER-algorithm that, unlike the reduced models obtained by MCA, the cost equivalent realizations are not independent of the model (full or evaluation) which is reduced. Therefore, since the subsequent controllers are to be evaluated with respect to the evaluation model, we use the evaluation model as the 'true' model and generate its CER, so that the ensuing comparisons will be consistent.

In order to apply the CER-algorithm, we write the evaluation model in its state-space form as follows.

$$\begin{aligned}\dot{x} &= Ax + Bu + Dw, \quad x \in \mathbb{R}^{20} \\ y &= Cx \\ z &= Mx + v\end{aligned}\tag{5.2.1a}$$

where

$$\begin{aligned}x^T &= \{x_r^T, x_e^T\}, \quad x_r^T \triangleq \{n_1, n_2, \dot{n}_1, \dot{n}_2\} \\ x_e^T &\triangleq \{n_4, n_{10}, \dots, n_{42}, \dot{n}_4, \dot{n}_{10}, \dots, \dot{n}_{42}\} \\ A &= \begin{bmatrix} A_r & 0 \\ 0 & A_e \end{bmatrix}; \quad A_r \triangleq \begin{bmatrix} 0 & I_2 \\ 0 & 0 \end{bmatrix} \in \mathbb{R}^4 \times 4 \\ A_e &\triangleq \begin{bmatrix} 0 & I_{16} \\ -\omega^2 & -2\zeta\omega \end{bmatrix} \\ B = D &= \begin{bmatrix} B_r \\ B_e \end{bmatrix}; \quad B_r \triangleq \begin{bmatrix} 0 \\ B_r \end{bmatrix}, \quad B_e \triangleq \begin{bmatrix} 0 \\ B_e \end{bmatrix} \\ C = M &= [C_r \quad C_e], \quad C_r \triangleq [C_r \quad 0], \quad C_e \triangleq [C_e, 0],\end{aligned}\tag{5.2.1b}$$

and where

$$\omega^{\Delta} = \text{diag} \{ \omega_4, \omega_{10}, \dots, \omega_{42} \}; \quad \tau = .001$$

$$g_r^T \Delta = [b_1 \quad b_2]$$

$$g_e^T \Delta = [b_4, b_{10}, \dots, b_{42}] \quad (5.2.1c)$$

$$c_r^{\Delta} = [c_1, c_2]$$

$$c_e^{\Delta} = [c_4, c_{10}, \dots, c_{42}] .$$

Now, the CER-algorithm requires the solution of the Lyapunov equation (3.4.7a). Since the evaluation model (5.2.1) contains unstable subspace (corresponding to the rigid body modes), we need to factor out this unstable subspace, and compute the CER of the stable part (corresponding to elastic modes  $\{n_4, n_{10}, \dots, n_{42}\}$ ). Once this is achieved, then the unstable subsystem of (5.2.1) can be augmented to the resulting CER, to obtain the reduced model of (5.2.1). In order to do this, write the stable part of (5.2.1) as

$$\begin{aligned} \dot{x}_e &= A_e x_e + B_e u + D_e w, \quad x_e \in R^{16} \\ y_e &= C_e x_e \\ z_e &= M_e x_e + v \end{aligned} \quad (5.2.2a)$$

where

$$D_e = B_e \text{ and } M_e = C_e. \quad (5.2.2b)$$

The cost function considered in the CER-algorithm will then be

$$V_{oe} = V_{ye} + \beta V_{ze} \quad (5.2.3a)$$

where

$$v_{y_e} \triangleq \lim_{t \rightarrow \infty} \frac{1}{t} E \int_0^t \|y_e(\sigma)\|_Q^2 d\sigma \quad (5.2.3b)$$

$$v_{z_e} \triangleq \lim_{t \rightarrow \infty} \frac{1}{t} E \int_0^t \|z_e(\sigma)\|_{V^{-1}}^2 d\sigma \quad (5.2.3c)$$

With these modifications we are now in a position to apply the CER-algorithm to the model (5.2.2) with the cost function (5.2.3).

The following results are obtained for  $\beta = 0$ , in (5.2.3a).

- 1) From the structure of  $C_e$  and  $B_e$  in (5.2.1b), observe that the first Markov Parameter

$$C_e B_e = 0.$$

Since there are three outputs, from Theorem 3.8, the reduced model of order 3 obtained by the CER-algorithm is not asymptotically stable. (The same result holds for  $\beta \rightarrow \infty$ , since  $z = y + v$ .)

- 2) The CER-algorithm yields six normalized Hessenberg components of dimensions

$$\begin{aligned} n_i &= 3, \quad i = 1, 2, 3, 4, 5 \\ n_6 &= 1. \end{aligned} \quad \sum_{i=1}^6 n_i = 16$$

Thus there are 5 reduced models suggested by the CER-algorithm of order 15, 12, 9, 6 and 3. Table 5.3 compares these reduced models with respect to the metric  $\|A_{RT}\| / \|A_R\|$ .

TABLE 5.3 COMPARISON OF DIFFERENT REDUCED MODELS BY CER-ALGORITHM

$n_r$	$\ A_{RT}\ $	$\ A_R\ $	$\ A_{RT}\  / \ A_R\ $
15	1.513	$\sim e-9$	$\sim e+10$
12	8.812	8.835	.9974
9	109.9	$\sim e-5$	$\sim e+7$
6	103.3	19.64	5.26
3	144.8	0	-

Since the unstable subsystem  $x_r \in \mathbb{R}^4$  corresponding to the rigid body modes will be subsequently augmented to these reduced model, we select the reduced model of order 6, so that the final reduced model of (5.2.1) would be of order 10, (to be compatible with the reduced models generated by MCA).

For  $\beta \rightarrow \infty$ , identical results are observed and identical reduced models result, indicating that the modelling problem and the control problem, by the CER-algorithm are separable. This is due to the relation

$$z = y + v.$$

Thus, by CER-algorithm, there is only one conceivable reduced model of (5.2.1) of order 10. This reduced model is denoted by S-CER.

Also observe that the reduced model of order 4, obtained by either MCA or CER-algorithm, for any value of  $\beta$ , would be the same, namely the unstable subsystem  $x_r \in \mathbb{R}^4$  corresponding to the rigid body modes. We denote this model by S4.

In conclusion of this subsection, we have generated the following four reduced models.

- 1) S1-MCA: of order 10, for  $\beta = 0$
- 2) S2-MCA: of order 10, for  $\beta \rightarrow \infty$
- 3) S-CER: of order 10, for any  $\beta$
- 4) S4: Rigid-body model

The controllers designed based upon these four models are evaluated with respect to the evaluation model, in the following section.

### 5.3 Design and Evaluation of Controllers

The controllers designed and compared in this section are based upon the following four models of the SOT.

- 1) S1-MCA
- 2) S2-MCA
- 3) S-CER
- 4) S4
- 5) FULL: ie., the evaluation model S-EVAL.

All these controllers are compared with respect to the evaluation model S-EVAL.

Fig. 5.3 displays the Regulation cost  $V(y)$ , defined in (4.3.3), vs. the Control Energy, defined in (4.3.4), resulting from different controllers. There is hardly any perceptible difference between these curves. However, all controllers that are designed based upon any reduced models drive the evaluation model to instability beyond a control energy of  $.6E-4 \text{ N}^2$ . Hence, in view of the hardware involved, one would use a 4-th order controller, designed based upon S4. The corresponding RMS values of LOS(x) and LOS(y) can be read from Figs. 5.4a and 5.4b.

Figs. 5.4a and 5.4b display the RMS values of the LOS(x) and LOS(y) respectively as a function of the Control Effort, where the Control Effort, is defined as

$$\text{Control Effort} \triangleq v^{1/2}(u) ,$$

and where  $v(u)$  is defined in (4.3.4). Notice, once again from these Figures, that all the reduced order controllers ( $n_c=10, 4$ ) perform just as good as the full order controller ( $n_c=20$ ) until instability occurs,

FIG 5.3 REGULATION PLOT

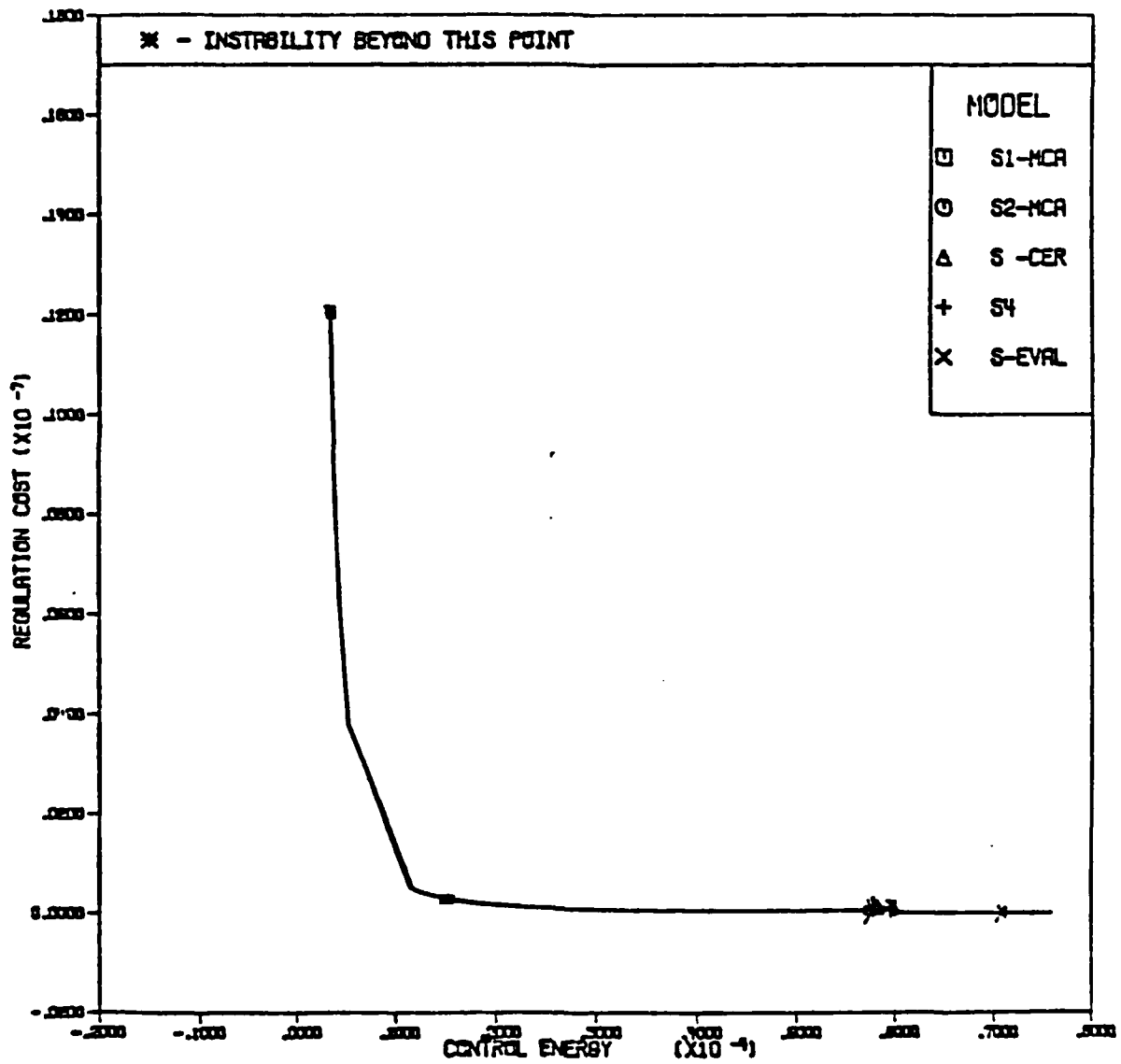


FIG 5.4A LOS(X) .VS. CONTROL

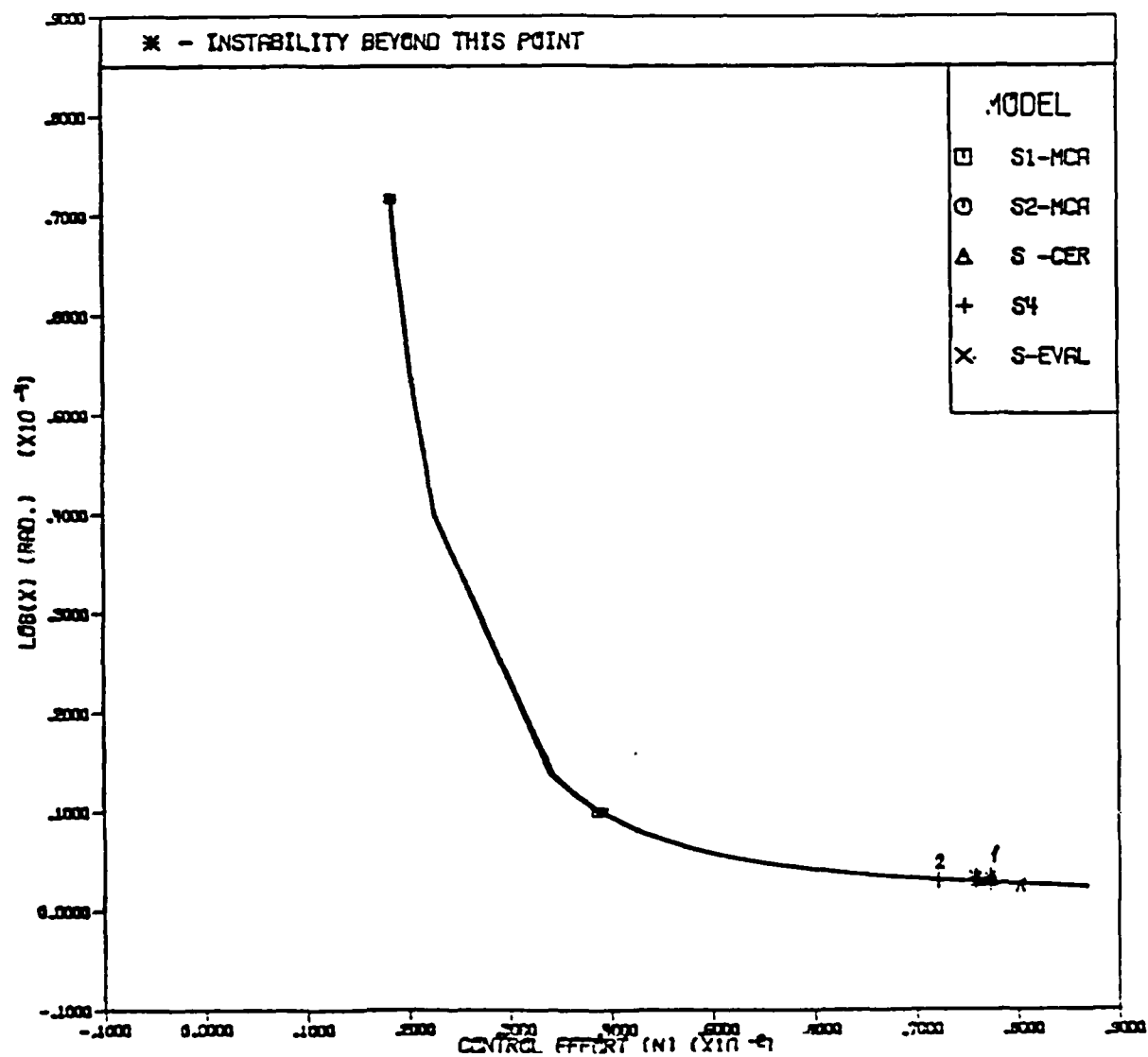
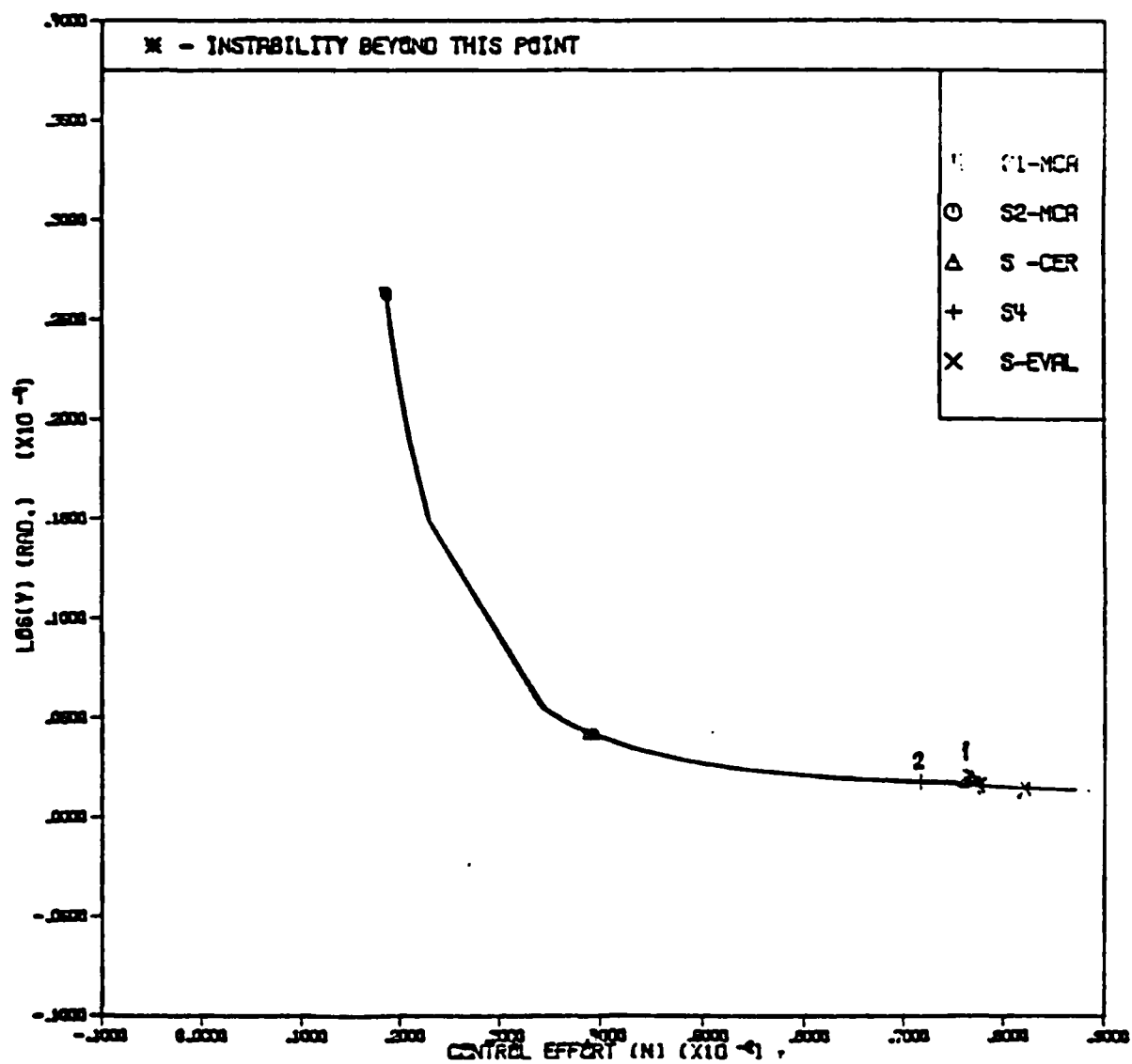


FIG 5.4B LOS(Y) .VS. CONTROL



(of course, by LQG-optimal control theory, the 20-th order controller remains stable over all bandwidth).

The smallest RMS values of the LOS(x) and LOS(y) obtained by different reduced order controllers is given in Table 5.5.

TABLE 5.5 REGULATION BY DIFFERENT CONTROLLERS

$n_c$	Reduced Model	LOS(x) (Rad.)	LOS(y) (Rad.)	$v^{1/2}(u)(N)$
10	S1-MCA	.2841 e-5	.1703 e-5	.7563 e-2
10	S2-MCA	.2841 e-5	.1676 e-5	.7738 e-2
10	S-CER	.2841 e-5	.1833 e-5	.7651 e-2
4	S4	.2841 e-5	.1833 e-5	.7639 e-2

Clearly then, if the mission specifications are

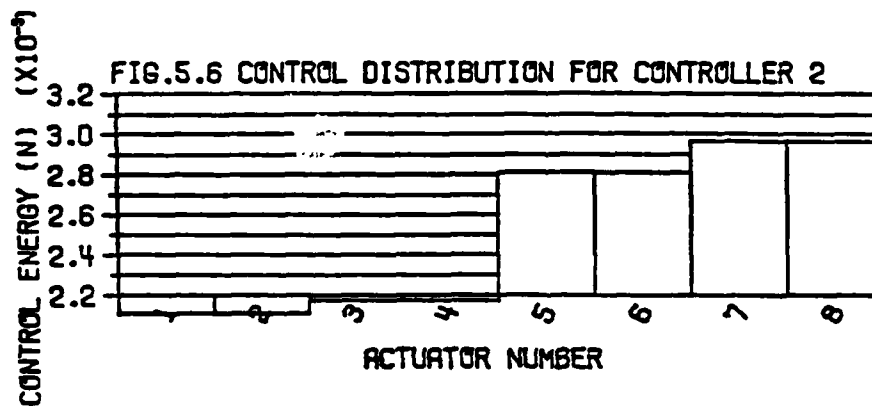
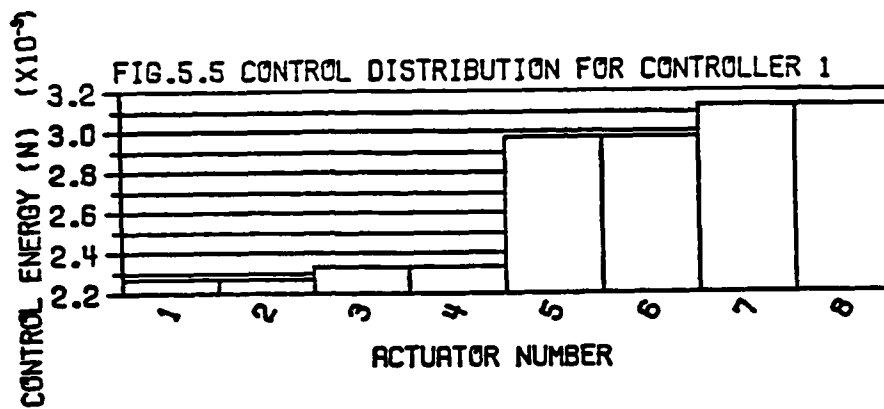
$$\text{LOS}(x) \leq .3 \text{ e-5 Rad.}$$

$$\text{LOS}(y) \leq .2 \text{ e-5 Rad.}$$

$$v^{1/2}(u) \leq .8 \text{ e-2 Newt.,}$$

one would pick the 4-th order controller (marked by '1' in Figs. 5.4a,b) instead of  $n_c > 4$  so that the performance specifications are met with the least amount of on-line controller hardware/software. Recall that the 4-th order controller is designed based upon the 4-th order rigid-body model, S4. Hence, for this SOT example, a rigid body model seems to be sufficient for the controller design.

Fig. 5.5 shows the RMS value of the input energy at the eight actuators, corresponding to the 4-th order controller. Observe that all the actuators are expending approximately the same amount of control energy, which is due to the symmetry of the structure and the equal penalty (i.e.  $R=I_8$ ) on all the actuators.



However, this choice of controller is prone to instability - even a little increase in the control effort (which may happen due to the variations of the plant parameters) may drive the closed loop system unstable. Hence, in order to ensure some stability margin, the choice of the 4-th order controller, marked by '2' in Figs. 5.4a, b, is preferable. The corresponding LOS(x), LOS(y) and the control effort is given below.

$$\text{LOS}(x) = .3036 \text{ e-5 Rad.}$$

$$\text{LOS}(y) = .1823 \text{ e-5 Rad.}$$

$$\text{CONTROL EFFORT} = .7186 \text{ e-2 Newt.}$$

The control energy distribution is displayed in Fig. 5.6. This choice of controller yields larger RMS value for LOS(x) than controller '1'. However note that, controller '1', which uses more control energy than controller '2', does not give a better RMS value for LOS(y) - this is due to the effect of the model errors, which are more pronounced for controllers with higher control energy.

#### 5.4 Conclusion

The model reduction schemes, namely MCA and CER-theory, presented in Section 3, have been applied, in this section, to a Solar Optical Telescope. Selecting four reduced models and an evaluation model, different controllers have been designed and evaluated.

Based upon the results obtained, it is concluded that the 4-th order rigid-body model is sufficient for the controller design. Two controller designs have been proposed, namely controllers '1' and '2'. Even though, controller '1' regulated LOS(x) better, it is prone to instability. In order to ensure some stability margin, controller '2' is preferred. This controller yields the following regulation and control effort.

$$\text{LOS}(x) = .3036 \text{ e-5 Rad.}$$

$$\text{LOS}(y) = .1823 \text{ e-5 Rad.}$$

$$\text{Control Effort} = .7186 \text{ e-2 Newt.}$$

To check if any of the actuators uses more control energy than allowable (by mission specifications), Fig. 5.6 has been presented which displays the control energy distribution for controller '2'.

## 6.0 CONCLUSION

This report has presented the design of reduced order controllers based upon reduced models of a given system. Considering the philosophy of such a design scheme, it is pointed out that the reduced models should reproduce accurately not only the output  $y$ , but also the measurement  $z$ .

The basic model reduction scheme used in this report is Component Cost Analysis (CCA). In particular the following two special cases of CCA have been adopted for the model reduction purposes.

- 1) Modal Cost Analysis, (MCA)
- 2) Cost Equivalent Realizations, (CERs).

Both these schemes are shown to yield reduced models whose cost perturbation indices can be predicted exactly, i.e.  $q = \hat{q}$ . In addition CERs have (in fact they are defined by) the property  $q = 0$ . However for mechanical systems for which modal data is available MCA is much simpler to implement than the CER-algorithm.

Section 4 has presented the controller design and evaluation strategy and has offered metrics for the evaluation and comparison of the controllers.

A simply supported beam example has been formulated in Section 2, and has been used as a numerical example for the illustration of the design procedure. For this example, it turns out that the reduced models by MCA are superior to the CERs. It has also been observed that the CERs tend to contain high frequencies, while the reduced models produced by MCA retain low frequencies. Consequently, it is shown by simulation, that the trajectory errors associated with CERs are smoother than the errors associated with the MCA-reduced models. Using the same example

in Section 4, it is pointed out that, at low bandwidth of the controllers, the influence of model reduction schemes is not significant. But at high bandwidth, the performance of the controllers depend, remarkably, on the model reduction scheme adopted. Also observed in Section 4 is that the effect of the order of the reduced model is significant only at high bandwidth.

Same techniques have been adopted for the controller design for a Solar Optical Telescope (SOT) in Section 5. It turns out that, for this SOT, it is sufficient to consider only the 4-th order rigid-body model of SOT for the controller design. Based upon the performance plots produced in Section 5, a 4-th order controller has been proposed as a suitable choice.

It must be pointed out that the observations and results presented in Section 5 are based upon the 10-mode evaluation model, S-EVAL. These observations *may* change for a different choice of the evaluation model. The question of the appropriate choice for the evaluation model remains unanswered.

## REFERENCES

1. Pilkington, W.C., "Vehicle Motions as Inferred From Radio Signal Strength Records," External Publication No. 551, Jet Propulsion Laboratory, Pasadena, CA, September 5, 1958.
2. AIAA/NASA Proceedings, Conference on Advanced Technology for Future Space Systems, Hampton, VA, May 8-10, 1979.
3. Nissim, E., "Flutter Suppression and Gust Alleviation Using Active Controls," NASA TN D-8212, 1976. Also see, J. Guidance and Control, Vol. 2, No. 5, September-October, 1979, pp. 395-401.
4. Nordell, W.J., "Active Systems for Blast-Resistant Structures," Technical Report R-611 Naval Civil Engineering Laboratory, Post Hueneme, CA, February 1969.
5. G. Strang and G.J. Fix, An Analysis of the Finite Element Method, Prentice-Hall, 1973.
6. Synge and Griffith, Principles of Mechanics, McGraw Hill, 1970.
7. L. Meirovitch, Methods of Analytical Dynamics, McGraw Hill, 1970.
8. W. Kwakernaak, R. Sivan, Linear Optimal Control Systems, Wiley, 1972.
9. E.C.Y. Tse, J.V. Medanic, W.R. Perkins, "Generalized Hessenberg Transformations for Reduced-order Modeling of Large Scale Systems," Int. J. Control, Vol. 27, No. 4, 1978, pp. 413-512.
10. W.R. Perkins, E.C.Y. Tse, J.V. Medanic, "Reduced Order Modeling using the QL Algorithm," in Proc. 21st Midwest Symp. Circuits and Systems, 1978, pp. 481-485.
11. R.V. Patel, "Computation of Minimal-order State-space Realizations and Observability Indices using Orthogonal Transformations," Int. J. Control, Vol. 33, No. 2, 1981, pp. 227-246.
12. C.P. Kwong, "Optimal Chained Aggregation for Reduced Order Modeling," Int. J. Control, Vol. 35, No. 6, 1982, pp. 965-982.
13. R.V. Patel, "Computation of Matrix Fraction Descriptions of Linear Time-Invariant Systems," IEEE Trans. Auto. Control, Vol. AC-26, No. 1, Feb. 1981, pp. 148-161.
14. R.E. Skelton, M. Delorenzo, "On the Selection of Weighting Matrices in the LQG Problem," Proc. 20th Allerton Conf. Comm. Contr. Comp., Monticello, Illinois, Oct. 1982.
15. M.F. Hutton, B. Fiedland, "Routh Approximations for Reducing Order of Linear, Time-Invariant Systems," IEEE Trans. Auto. Control, Vol. AC-20, No. 3, June 1975, pp. 329-337.

16. N.K. Sinha, I.El-Mahas, R.T.H. Alden, "Routh-Hurwitz Approximation of Multivariable Systems," *Proc. 19th Allerton Conference on Systems and Control*, Monticello, Illinois, Oct. 1980.
17. R.E. Skelton, D.A. Wagie, "Minimal Root Sensitivity in Linear Systems," submitted for publication.

# APPENDIX: PROOFS OF THEOREMS IN SECTION 3

## Proof of Theorem 3.1

Partition the covariance matrix  $X$  as

$$X = \begin{bmatrix} x_{11} & x_{12} & \dots & x_{1N} \\ x_{21} & x_{22} & \dots & x_{2N} \\ \vdots & \vdots & \ddots & \vdots \\ x_{N1} & x_{N2} & \dots & x_{NN} \end{bmatrix} \quad (A.1a)$$

where

$$x_{ij} \triangleq \lim_{t \rightarrow \infty} E \left\{ \begin{bmatrix} \eta_i(t) \\ \dot{\eta}_i(t) \end{bmatrix} [\eta_j(t), \dot{\eta}_j(t)] \right\}_{\epsilon R}^{2 \times 2} \quad (A.1b)$$

Using the special structure of the matrices in (3.3.2), the  $(i,j)$ -block partitioned equation of (3.2.4b) yields,

$$x_{ij} A_{jj}^T + A_{ii} x_{ij} + D_i \omega D_j^T = 0. \quad (A.2)$$

For  $j=i$ , the solution  $x_{ii}$  to (A.2) is given by,

$$x_{ii} = \frac{\|b_i\|_u^2}{4\zeta_i \omega_i^3} \begin{bmatrix} 1 & 0 \\ 0 & \omega_i^2 \end{bmatrix}. \quad (A.3)$$

Now, rewrite (3.2.4a) as

$$\hat{v}_i = \text{Tr}[C_i^T Q C X]_{ii} = \text{Tr}[C_i^T Q C_i x_{ii}] + \sum_{\substack{j=1 \\ j \neq i}}^N \text{Tr}[C_i^T Q C_j x_{ji}]. \quad (A.4)$$

Using (3.3.2c) and (A.3), the first term on the right hand side of (A.4) can be expressed as

$$\text{Tr}[C_i^T Q C_i X_{ii}] = \frac{1}{4\zeta_i \omega_i^3} \{ \|P_i\|_Q^2 + \omega_i^2 \|P_i'\|_Q^2 \} \|b_i\|_U^2. \quad (\text{A.5})$$

Hence, to complete the proof, we will now show that, under any of the three conditions of the theorem, the following relation holds.

$$\hat{v}_i = \text{Tr}[C_i^T Q C_i X_{ii}], \quad (\text{A.6a})$$

or equivalently,

$$\sum_{\substack{j=1 \\ j \neq i}}^N \text{Tr}[C_i^T Q C_j X_{ji}] = 0. \quad (\text{A.6b})$$

a)  $b_i^T U b_j = 0, \quad j \neq i.$

From the definition of  $D_i$  and  $\omega$  in (3.3.2), this implies that

$$D_i \omega D_j^T = 0, \quad j \neq i.$$

Hence, for non-zero damping,  $X_{ij} = 0$ , is the unique solution to (A.2), since both  $A_{ii}$  and  $A_{jj}$  are asymptotically stable. Clearly, then, (A.6b) holds.

b)  $C_i^T Q C_j = 0, \quad j \neq i,$

Obviously (A.6b) holds.

c)  $\zeta_i \rightarrow 0, \quad i = 1, 2, \dots, N,$

with  $\omega_i \neq \omega_j$  and  $P_i^T Q P_j' = P_i^T Q P_j; \quad j \neq i$

Partitioning  $x_{ij}$  as

$$x_{ij} = \begin{bmatrix} x_{ij}^{11} & x_{ij}^{12} \\ x_{ij}^{21} & x_{ij}^{22} \end{bmatrix} \quad (A.7a)$$

write (A.2) as

$$\begin{bmatrix} x_{ij}^{11} & x_{ij}^{12} \\ x_{ij}^{21} & x_{ij}^{22} \end{bmatrix} \begin{bmatrix} 0 & -\omega_j^2 \\ 1 & -2\zeta_j \omega_j \end{bmatrix} + \begin{bmatrix} 0 & 1 \\ -\omega_i^2 & -2\zeta_i \omega_i \end{bmatrix} \begin{bmatrix} x_{ij}^{11} & x_{ij}^{12} \\ x_{ij}^{21} & x_{ij}^{22} \end{bmatrix} + \begin{bmatrix} 0 & 0 \\ 0 & b_i^T u b_j \end{bmatrix} = 0 \quad (A.7b)$$

to obtain the following relations, (after some algebraic manipulations).

$$x_{ij}^{12} = \frac{b_i^T u b_j - \bar{\omega}_{ij}^2}{\bar{\omega}_{ij}^4 + \omega_i^2 \delta_{ij}^2 - 2\zeta_i \omega_i \delta_{ij} \bar{\omega}_{ij}^2} \quad (A.8a)$$

$$x_{ij}^{21} = -x_{ij}^{12} \quad (A.8b)$$

$$x_{ij}^{11} = \frac{\delta_{ij}}{\bar{\omega}_{ij}^2} x_{ij}^{12} \quad (A.8c)$$

$$x_{ij}^{22} = \frac{b_i^T u b_j}{\delta_{ij}} - \frac{\bar{\omega}_{ij}^2}{\delta_{ij}} x_{ij}^{12} \quad (A.8d)$$

where

$$\delta_{ij} \triangleq 2\zeta_i \omega_i + 2\zeta_j \omega_j \quad (A.8e)$$

$$\bar{\omega}_{ij} \triangleq \omega_i^2 - \omega_j^2.$$

Now, for  $\zeta_i \rightarrow 0, \forall i$ , the following occurs.

$$x_{ij}^{12} \rightarrow b_i^T u b_j / \bar{\omega}_{ij}^2 \quad (\text{A.9a})$$

$$x_{ij}^{11} \rightarrow 0, x_{ij}^{22} \rightarrow 0. \quad (\text{A.9b})$$

Therefore, substitution of (A.9) (A.7a) and (3.3.2a) yields,

$$\text{Tr}[C_i^T Q C_j x_{ji}] = (p_i^T Q p_j - p_i^T Q p_j) \frac{b_i^T u b_j}{\bar{\omega}_{ij}^2} = 0, j \neq i \quad (\text{A.10})$$

where the last equality follows by hypothesis.

Hence, in all the three cases, the equation (A.6a) is shown to be satisfied. In view of (A.5), this concludes the proof. #

### Proof of Theorem 3.2

Assume, without loss of generality, that the modes have been ranked according to (3.2.6), so that only the first  $r$  'components' (as defined in (3.3.1)) are retained in the reduced model. Now, from the definition of the cost perturbation indices, it suffices to show that

$$v_R = \hat{v}_R$$

to prove the theorem.

Recall from the previous proof that, under either of the three conditions of Theorem 3.1, we have

$$\hat{v}_R = \sum_{i=1}^r \hat{v}_i = \sum_{i=1}^r \text{Tr}[C_i^T Q C_i x_{ii}], \quad (\text{A.11a})$$

where  $x_{ii}$ ,  $i = 1, 2, \dots, r$ , satisfies

$$x_{ii} A_{ii}^T + A_{ii} x_{ii} + D_i \omega D_i^T = 0 \quad (\text{A.12b})$$

Note that the modal costs  $\hat{v}_i$  are independent of other modes,  $n_j$ ,  $j \neq i$ , and can be independently calculated by considering only the  $i$ -th modal data. Furthermore, this independence and the expressions (A.11) hold for any number of modes. Consequently, the cost  $V_R$  associated with the reduced model is given by

$$V_R = \sum_{i=1}^r v_i \quad (\text{A.12a})$$

where

$$v_i = \text{Tr}[C_i^T Q C_i \hat{x}_{ii}] , i = 1, 2, \dots, r \quad (\text{A.12b})$$

and where  $\hat{x}_{ii}$  satisfies

$$\hat{x}_{ii} A_{ii}^T + A_{ii} \hat{x}_{ii} + D_i W D_i^T = 0 . \quad (\text{A.12c})$$

Since  $A_{ii}$  is asymptotically stable, comparison of equations (A.12c) and (A.11b) reveals that

$$\hat{x}_{ii} = x_{ii} , i = 1, 2, \dots, r \quad (\text{A.13a})$$

and therefore

$$v_i = \hat{v}_i \quad (\text{A.13b})$$

and hence  $V_R = \hat{V}_R$  . #

### Proof of Theorem 3.3

In order to prove the theorem we will follow these three steps in sequel.

- 1) Establish the existence of a closed form, diagonal solution to the Riccati equation (3.3.10).
- 2) Show that the closed loop system can be expressed in the decoupled modal form.
- 3) Derive the expressions (3.3.14) from Theorem 3.1.

1) Defining the state vector  $x$  as

$$x^T \triangleq [\eta_1 \dot{\eta}_1 \eta_2 \dot{\eta}_2 \dots \eta_N \dot{\eta}_N], \quad (A.14a)$$

the system matrices take the following form.

$$A = \text{diag} \{A_{11}, A_{22}, \dots, A_{NN}\} \quad (A.14b)$$

$$A_{ii} = \begin{bmatrix} 0 & 1 \\ -\omega_i^2 & -2\zeta_i\omega_i \end{bmatrix} \quad (A.14b)$$

$$B = \begin{bmatrix} B_1 \\ B_2 \\ \vdots \\ B_N \end{bmatrix}, \quad B_i = \begin{bmatrix} 0 \\ b_i^T \end{bmatrix} \quad (A.14c)$$

Now, assumption (A2) implies that,

$$\frac{1}{\rho} B R^{-1} B^T = \frac{1}{\rho} \text{diag} \{0, r_1^2, 0, r_2^2, \dots, 0, r_N^2\}. \quad (A.15a)$$

and assumption (A3) implies that

$$C^T Q C = \text{diag}(\omega_1^2, 1, \omega_2^2, 1, \dots, \omega_N^2, 1). \quad (A.15b)$$

Hence, the Riccati equation (3.3.10) can be written in its partitioned form as

$$\begin{bmatrix} K_{11} & K_{12} & \dots & K_{1N} \\ K_{22}^T & K_{22} & \dots & K_{2N} \\ \vdots & \vdots & \ddots & \vdots \\ K_{1N}^T & K_{2N}^T & \dots & K_{NN} \end{bmatrix} \begin{bmatrix} A_{11} & 0 & \dots & 0 \\ 0 & A_{22} & & 0 \\ \vdots & \vdots & \ddots & \vdots \\ 0 & 0 & \dots & A_{NN} \end{bmatrix} + \begin{bmatrix} A_{11}^T & 0 & \dots & 0 \\ 0 & A_{22}^T & \dots & 0 \\ \vdots & \vdots & \ddots & \vdots \\ 0 & 0 & \dots & A_{NN}^T \end{bmatrix} \begin{bmatrix} K_{11} & K_{12} & \dots & K_{1N} \\ K_{12}^T & K_{22} & \dots & K_{2N} \\ \vdots & \vdots & \ddots & \vdots \\ K_{1N}^T & K_{2N}^T & \dots & K_{NN} \end{bmatrix}$$

$$-\frac{1}{\rho} \begin{bmatrix} K_{11} & \dots & K_{1N} \\ \vdots & \ddots & \vdots \\ K_{1N}^T & & K_{NN} \end{bmatrix} \begin{bmatrix} B_1 B_1^T & \dots & 0 \\ 0 & \ddots & \vdots \\ 0 & & B_N B_N^T \end{bmatrix} \begin{bmatrix} K_{11} & \dots & K_{1N} \\ \vdots & \ddots & \vdots \\ K_{1N}^T & & K_{NN} \end{bmatrix} + \begin{bmatrix} C_1^T Q C_1 & \dots & 0 \\ 0 & \ddots & \vdots \\ 0 & & C_N^T Q C_N \end{bmatrix} = 0 \quad (\text{A.16})$$

where  $C_i^T Q C_i \triangleq \text{diag} \{\omega_i^2, 1\}$ . Now from assumption (A2), the system is controllable (since every mode is now independently controllable). Therefore, the solution to (A.16) is unique [ 8 ].

We claim now that the solution  $K$  to (A.16) is

$$K = \text{diag} \{K_{11}, K_{22}, \dots, K_{NN}\} \quad (\text{A.17a})$$

where

$$K_{ii} \triangleq \begin{bmatrix} k_{i1} & k_{i2} \\ k_{i2} & k_{i3} \end{bmatrix} \quad (\text{A.17b})$$

and where  $k_{i2}$  and  $k_{i3}$  are defined in the theorem. To prove our claim, we show that (A.17) does solve (A.16) and hence by uniqueness, it is the solution to the Riccati equation (A.16). Substitution of (A.17) into (A.16) yields

$$K_{ii} A_{ii} + A_{ii}^T K_{ii} - \frac{1}{\rho} K_{ii} B_i B_i^T K_{ii} + C_i^T Q C_i = 0, \quad i = 1, 2, \dots, N \quad (\text{A.18})$$

which must now be satisfied by the  $K_{ii}$  defined in (A.17b). Substitution of (3.3.14b-e) verifies this.

Thus, a closed form solution to the Riccati equation (A.16) is obtained.

2) Now, the optimal control law is given by [8]

$$u = -\frac{1}{\rho} R^{-1} B^T K x \quad (A.19a)$$

which, in view of (A.14a), (A.14c) and (A.17) becomes

$$u = -\frac{1}{\rho} \sum_{i=1}^N b_i k_{i2} n_i - \frac{1}{\rho} \sum_{i=1}^N b_i k_{i3} \dot{n}_i \quad (A.19b)$$

Using (3.3.11), this expression can be rewritten as

$$u = -\sum_{i=1}^N g_i n_i - \sum_{i=1}^N g_i' \dot{n}_i \quad (A.19c)$$

where,  $g_i \triangleq \frac{r_i k_{i2}}{\rho} e_i \quad (A.19d)$

$$g_i' \triangleq \frac{r_i k_{i3}}{\rho} e_i \quad (A.19e)$$

and where  $e_i$  is the unit vector defined in (3.3.11b). Note that, since  $b_i = r_i e_i$ , from (A.19d) and (A.19e) we get

$$b_i^T g_j = 0 \quad \text{and} \quad b_i^T g_j' = 0, \quad j \neq i \quad (A.20)$$

Therefore the closed loop representation (3.3.11) simplifies to

$$\ddot{n}_i + 2\bar{\zeta}_i \bar{\omega}_i \dot{n}_i + \bar{\omega}_i^2 n_i = b_i^T \omega \quad (A.21a)$$

where  $\bar{\omega}_i^2 \triangleq \omega_i^2 + b_i^T g_i = \omega_i^2 + \frac{1}{\rho} r_i^2 k_{i2} \quad (A.21b)$

and  $2\bar{\zeta}_i \bar{\omega}_i \triangleq 2\zeta_i \omega_i + b_i^T g_i' = 2\zeta_i \omega_i + \frac{1}{\rho} r_i^2 k_{i3} \quad (A.21c)$

It is clear from (A.21a) that the modes  $n_i$  of the closed loop system are also decoupled.

3) To obtain the expression (3.3.14), note that the cost function

$$V = \lim_{t \rightarrow \infty} \frac{1}{t} E \int_0^t \{ \|y(\sigma)\|_Q^2 + \rho \|u(\sigma)\|_R^2 \} d\sigma \quad (A.22a)$$

can be written as

$$V = \lim_{t \rightarrow \infty} \frac{1}{t} E \int_0^t \|y(\sigma)\|_Q^2 d\sigma \quad (A.22b)$$

where

$$y^T \triangleq [y^T, u^T] \quad (A.22c)$$

$$\text{and } Q \triangleq \text{diag} \{Q, \rho R\} . \quad (A.22d)$$

Now from (3.3.12a,b) and (A.19), (A.22c) can be expressed in the required form as

$$y = \sum_{i=1}^N p_i \eta_i + \sum_{i=1}^N p_i' \dot{\eta}_i \quad (A.23a)$$

where,

$$p_i \triangleq \begin{bmatrix} e_i \\ 0_{N \times 1} \\ g_i \end{bmatrix} \in R^{3N} \quad (A.23b)$$

$$\text{and } p_i' \triangleq \begin{bmatrix} 0_{N \times 1} \\ e_i \\ g_i' \end{bmatrix} \in R^{3N} \quad (A.23c)$$

Now, since  $b_i^T u b_j = 0, j \neq i$ , Theorem 3.1 can be applied to the closed loop system (A.21), to get the closed-loop modal cost formula as

$$\hat{V}_{c_i} = \frac{1}{4\bar{\zeta}_i \bar{\omega}_i^3} \{ \|p_i\|_Q^2 + \bar{\omega}_i^2 \|p_i'\|_Q^2 \} \|b_i\|_u^2 \quad (A.24)$$

Substitution of (3.3.11), (3.3.12), and (A.23) in (A.24) results in (3.3.14), thereby completing the proof. #

#### Proof of Theorem 3.5

$$\text{Let } y = \sum_{i=1}^N p_i \eta_i + \sum_{i=1}^N p_i' \dot{\eta}_i$$

and

$$z = \sum_{i=1}^N m_i \eta_i + \sum_{i=1}^N m_i' \dot{\eta}_i + v.$$

Then (3.3.23a) implies that

$$m_i = T p_i \text{ and } m_i' = T p_i' \quad (\text{A.25})$$

Substitution of (A.25) in (3.3.22a) yields

$$\hat{v}_{z_i} = \frac{1}{4\epsilon_i \omega_i^3} \{ \|p_i\|_{T^{-1}V^{-1}T}^2 + \omega_i^2 \|p_i'\|_{T^{-1}V^{-1}T}^2 \} \|b_i\|_U^2 \quad (\text{A.26a})$$

which, in view of (3.3.23b) becomes

$$\hat{v}_{z_i} = \frac{\alpha}{4\epsilon_i \omega_i^3} \{ \|p_i\|_Q^2 + \omega_i^2 \|p_i'\|_Q^2 \} \|b_i\|_U^2 = \alpha \hat{v}_{y_i} \quad (\text{A.26b})$$

Therefore,

$$\hat{v}_{o_i} = \hat{v}_{y_i} + \beta \hat{v}_{z_i} = (1 + \alpha\beta) \hat{v}_{y_i} \quad (\text{A.27})$$

Since  $(1 + \alpha\beta)$  is positive constant, the ranking of the modes by the open loop modal cost  $\hat{v}_{o_i}$  is not affected by  $\alpha$  and  $\beta$ . Hence, for a fixed order  $r$  of the reduced model,  $\beta$  does not affect the modes retained in the reduced model. #

#### Proof of Theorem 3.6

Substitute the normalization condition (3.4.2) in the general expressions for component costs (3.2.4a) to get

$$\hat{v}_i = \text{Tr}[c^T Q C]_{ii} = [c^T Q C]_{ii}, \quad i = 1, 2, \dots, n. \quad (\text{A.28})$$

(Since the 'components' are individual coordinates,  $[c^T Q C]_{ii}$  is a scalar).

The proof now follows from the structure of the output matrix  $C$  in (3.4.5b) and from (3.4.4). #

#### Proof of Theorem 3.7

The proof relies on a result derived in [ 17], which is restated here.

Lemma 3.1, [ 17] Let  $\lambda_i$  be an eigenvalue of a matrix  $A$ . Then the sensitivity of  $\lambda_i$  to the perturbations in  $A$ , measured by

$$\Delta_i \triangleq \left\| \frac{\partial \lambda_i}{\partial A} \right\|^2$$

where  $\| [\cdot] \|^2 \triangleq \text{Tr} \{ [\cdot]^T [\cdot] \}$ , is minimized if and only if  $A$  is normal (i.e.,  $AA^T = A^T A$ ).

Now note from Theorem 3.6 and from (3.4.4) that the component costs are the eigenvalues of  $c^T Q C$ , i.e.,

$$\hat{v}_i = \lambda_i(c^T Q C), \quad i = 1, 2, \dots, n. \quad (\text{A.29})$$

Since,  $c^T Q C$  is symmetric (hence, normal), the proof follows from Lemma 3.1. #

#### Proof of Theorem 3.8

Partition the model (3.4.5) as

$$\begin{bmatrix} \dot{x}_R \\ \dot{x}_T \end{bmatrix} = \begin{bmatrix} A_R & A_{RT} \\ A_{TR} & A_T \end{bmatrix} \begin{bmatrix} x_R \\ x_T \end{bmatrix} + \begin{bmatrix} d_R \\ d_T \end{bmatrix} \quad \text{w} \quad (\text{A.30})$$

$$y = [C_R \ C_T] \begin{bmatrix} x_R \\ x_T \end{bmatrix}$$

where  $x_R \in R^{n_r}$  and  $x_T \in R^{n_t}$ .  $n_t + n_r = n$ . (Note from (3.4.5b) that for  $n_r \geq n_1$ ,  $C_T = 0$ .) Since the covariance  $X$  satisfies (3.2.4b), substitution of (3.4.2), and using the partitioned form (A.30) in (3.4.2) yields

$$\begin{bmatrix} A_R^T & A_{TR}^T \\ A_{RT}^T & A_T^T \end{bmatrix} + \begin{bmatrix} A_R & A_{RT} \\ A_{TR} & A_T \end{bmatrix} + \begin{bmatrix} D_R \\ D_T \end{bmatrix} \omega \begin{bmatrix} D_R^T & D_T^T \end{bmatrix} = 0. \quad (\text{A.31a})$$

The first partitioned equation of (A.31a) is written out as

$$A_R^T + A_R + D_R \omega D_R^T = 0. \quad (\text{A.31b})$$

(i) Now let  $\xi$  be a left eigenvector of  $A_R$  corresponding to the eigenvalue  $\lambda_1(A_R)$ , i.e.,  $\xi$  and  $\lambda_1(A_R)$  satisfy

$$\xi^* A_R = \lambda_1(A_R) \xi^*, \quad \xi \in C^{n_r} \quad (\text{A.32a})$$

$$\text{and} \quad A_R^T \xi = \overline{\lambda_1(A_R)} \xi, \quad (\text{A.32b})$$

where '\*' denotes the conjugate transposition and '-' denotes the conjugation. Pre- and post-multiply (A.31b) by  $\xi^*$  and  $\xi$  respectively to get

$$\xi^* A_R^T \xi + \xi^* A_R \xi + \xi^* D_R \omega D_R^T \xi = 0, \quad (\text{A.33a})$$

which upon substitution of (A.32) yields

$$2 \operatorname{Re}(\lambda_1(A_R)) = -\|D_R^T \xi\|_\omega^2 / \|\xi\|^2. \quad (\text{A.33b})$$

Since the right hand side of (A.33b) cannot be positive, part (i) is thus proved.

(ii) Now, from (A.33b) see that

$$\operatorname{Re}(\lambda_1(A_R)) = 0 \text{ if and only if } \xi^* D_R = 0. \quad (\text{A.34})$$

In this event ( $\text{Re}\{\lambda_i(A_R)\} = 0$ ) the right hand side of

$$\varepsilon^*[A_R^T + A_R = -D_R^T \omega D_R] A_R^\alpha D_R \quad , \quad \alpha = 1, 2, \dots, \quad (\text{A.35a})$$

is zero. Hence (3.7.35a) leads to

$$\varepsilon^* A_R^{\alpha+1} D_R = -\varepsilon^* A_R^T A_R^\alpha D_R = -\lambda_i(A_R) \varepsilon^* A_R^\alpha D_R \quad . \quad (\text{A.35b})$$

For each  $\{\alpha = 0, 1, 2, \dots, n_r-2\}$  the right hand side of (A.35b) becomes zero. Thus for  $\alpha = 0, 1, 2, \dots, n_r-2$ , the left hand side of (A.35a) leads to

$$\varepsilon^*[D_R, A_R D_R, \dots, A_R^{n_r-1} D_R] = 0 \text{ if and only if } \text{Re}\{\lambda_i(A_R)\} = 0 \quad (\text{A.36})$$

Thus from (A.34) and (A.36),  $\text{Re}\{\lambda_i(A_R)\} = 0$ , if and only if rank  $[D_R, A_R D_R, \dots, A_R^{n_r-1} D_R] \neq n_r$ , which implies that the matrix pair  $(A_R, D_R)$  is uncontrollable, [8]. This proves part (ii) of the theorem.

(iii) Let  $J_2(p) = 0$ ,  $\ell = 1, 2, \dots, i$ . Then,

$$J_1(p) = C D = C_1 D_1 = 0,$$

where the structure in (3.4.5) has been used. Notice from (3.4.4) that, for a positive definite  $Q$ , (3.4.4) is satisfied if and only if rank  $[C_1] = n_1$ . Hence,  $C_1 D_1 = 0$  if and only if  $D_1 = 0$ . Now, consider,

$$J_2(p) = C A D = C_1 A_{11} D_1 + C_1 A_{12} D_2 = C_1 A_{12} D_2 = 0.$$

Since  $|C_1| \neq 0$ , and  $A_{12}$  is monic by construction (i.e., rank  $[A_{12}] = n_2 \leq n_1$ , [3.6]),  $C_1 A_{12} D_2 = 0$  if and only if  $D_2 = 0$ . Proceeding similarly yields,  $J_2(p) = 0$ ,  $\ell = 1, 2, \dots, i$ ,  $D_j = 0$ ,  $j = 1, 2, \dots, i$ . Hence from the definition of  $D_R$  in (3.4.14b), it follows that

$$D_R = 0 \text{ for all } n_r \leq \sum_{j=1}^i n_j.$$

Clearly then the reduced model (3.4.14) is not controllable, and hence by (ii) it is not asymptotically stable for all

$$n_r \leq \sum_{j=1}^i n_j.$$

#

### Proof of Theorem 3.9

(i) The steady state output covariance can be written as

$$\lim_{t \rightarrow \infty} E \{ \hat{y}(t) \hat{y}^T(t) \} = \lim_{t \rightarrow \infty} E \{ C_R X_R(t) X_R^T(t) C_R^T \} = C_R X_R C_R^T \quad (\text{A.36})$$

where  $X_R$  is the steady state covariance of the states  $x_R$ . Now,  $X_R$  satisfies,

$$X_R A_R^T + A_R X_R + D_R W D_R^T = 0. \quad (\text{A.37})$$

Since all CERs are asymptotically stable, comparing (A.37) with (A.31b) shows that,

$$X_R = I_{n_r} \quad (\text{A.38})$$

Therefore,

$$\lim_{t \rightarrow \infty} E \{ \hat{y}(t) \hat{y}^T(t) \} = C_R C_R^T = C_1 C_1^T; \quad n_r \geq n_1$$

where the structure of  $C_R$  in (3.4.14) has been used. Furthermore, since  $X = I_n$ , from (3.4.2), we have

$$C_1 C_1^T = C C^T = C X C^T = \lim_{t \rightarrow \infty} E \{ y(t) y^T(t) \},$$

thus proving (3.4.15a).

To prove (3.4.15b), consider the trajectories  $x(t)$  and  $x_R(t)$ ,  
(assuming zero initial conditions):

$$x(t) = \int_0^t e^{A\sigma} \mathcal{D}w(\sigma) d\sigma \quad , \quad (\text{A.39a})$$

and

$$x_R(t) = \int_0^t e^{A_R\sigma} \mathcal{D}_R w(\sigma) d\sigma \quad . \quad (\text{A.39b})$$

Hence,

$$\begin{aligned} \lim_{t \rightarrow \infty} E\{\dot{\hat{y}}(t) \dot{\hat{y}}^T(t)\} &= \lim_{t \rightarrow \infty} C_R E\{\dot{x}_R(t) \dot{x}_R^T(t)\} C_R^T \\ &= \lim_{t \rightarrow \infty} C_R E\{[A_R x_R(t) + \mathcal{D}_R w(t)] \int_0^t w^T(\sigma) \mathcal{D}_R^T e^{A_R^T \sigma} d\sigma\} C_R^T \\ &= \lim_{t \rightarrow \infty} E\{C_R A_R \int_0^t x_R(t) w^T(\sigma) \mathcal{D}_R^T e^{A_R^T \sigma} d\sigma C_R^T\} \\ &\quad + \frac{1}{2} \lim_{t \rightarrow \infty} C_R \mathcal{D}_R w \mathcal{D}_R^T C_R^T \quad . \quad (\text{A.40a}) \end{aligned}$$

where the screening property of the delta function

$$E \int_0^t w(t) w^T(\sigma) d\sigma = \int_0^t w \delta(t-\sigma) d\sigma = w/2$$

has been used to obtain the second term in (A.40a). Since,  $x_R(t)$ , and  $w(\sigma)$ ,  $t \geq \sigma$ , are uncorrelated with each other, the first term in (A.40a) becomes zero resulting in

$$\begin{aligned} \lim_{t \rightarrow \infty} E\{\dot{\hat{y}}(t) \dot{\hat{y}}^T(t)\} &= \frac{1}{2} C_R \mathcal{D}_R w \mathcal{D}_R^T C_R^T \\ &= \frac{1}{2} C_1 \mathcal{D}_1 w \mathcal{D}_1^T C_1^T \quad . \quad (\text{A.40b}) \end{aligned}$$

Similarly,

$$\begin{aligned}\lim_{t \rightarrow \infty} E\{y(t)y^T(t)\} &= \frac{1}{2}CD\omega\omega^TC^T = \frac{1}{2}C_1\mathcal{D}_1\omega\omega^TC_1^T \\ &= \lim_{t \rightarrow \infty} E\{\hat{Y}(t)\hat{Y}^T(t)\}.\end{aligned}$$

(ii) Consider,

$$J_1(i) = C_R\mathcal{D}_R = C_1\mathcal{D}_1 = CD = J_1(p), \text{ for all } i = 1, 2, \dots, p,$$

and

$$J_2(i) = C_RA_R\mathcal{D}_R = C_1A_{11}\mathcal{D}_1 + C_2A_{12}\mathcal{D}_2 = CAD = J_2(p),$$

for all  $i = 2, 3, \dots, p$ .

Part (ii) is thus proved by extending this argument to  $J_j(i)$ ,  $j = 1, 2, \dots, i$ .

#

# DISTRIBUTION LIST

addresses	number of copies
Ricahrd W. Carman RADC/QCSP	5
RADC/TSTD GRIFFISS AFB NY 13441	1
RADC/DAP GRIFFISS AFB NY 13441	2
ADMINISTRATOR DEF TECH INF CTR ATTN: DTIC-DDA CAMERON STA BG 5 ALEXANDRIA VA 22314	12
Control Dynamics Company 555 Sparkman Drive, Suite 1414 Huntsville, Alabama 35805	5
Charles Stark Draper Lab Attn: Dr. Keto Soosaar 555 Technology Square M. S. -95 Cambridge, MA 02139	1
NASA Headquarters ATTN: Mr. J. B. Dahlgren Code RTH-6 Washington, DC 20546	1
Charles Stark Draper Lab Attn: Mr. R. Strunce 555 Technology Square M. S. -60 Cambridge, MA 02139	1

Charles Stark Draper Lab  
Attn: Dr. Daniel R. Hegg  
555 Technology Square  
M.S. -60  
Cambridge, MA 02139

1

ARPA/STO  
Attn: Lt Col A. Herzberg  
1400 Wilson Blvd  
Arlington, VA 22209

1

ARPA/STO  
Attn: Maj E. Dietz  
1400 Wilson Blvd  
Arlington, VA 22209

1

Riverside Research Institute  
Attn. Mr. A. DeVilliers  
1701 N. Ft. Myer Drive, Suite 711  
Arlington, VA 22209

2

Riverside Research  
Attn: HALO Library, Mr. Bob Passut  
1701 N. Ft. Myer Drive  
Arlington, VA 22209

1

Itek Corp  
Optical Systems Division  
10 Maguire Rd.  
Lexington, MA 02173.

1

Perkin Elmer Corp  
Attn: Mr. H. Levenstein  
Electro Optical Division  
Main Avenue  
Norwalk, CT 06856

1

Hughes Aircraft Company  
Attn: Mr. George Speak  
M.S. B\_156  
Culver City, CA 09230

1

Hughes Aircraft Company  
Attn: Mr. Ken Beale  
Centinela Teale Sts  
Culver City, CA 90230

1

Air Force Flight Dynamics Lab  
Attn: Dr. Lynn Rogers  
Wright Patterson AFB, OH 45433

1

AFWL/FIBQ  
Attn: Mr. Jerome Pearson  
Wright Patterson AFB, OH 45433

1

Air Force Wright Aero Lab. FIGC  
Attn: Siva S. Banda  
Wright Patterson AFB, OH 45433

1

Air Force Institute of Technology  
Attn: Prof. R. Calico/ENY  
Wright Patterson AFB, OH 45433

1

Aerospace Corp.  
Attn: Dr. G.T. Tseng  
2350 E. El Segundo Blvd  
El Segundo, CA 90245

2

Aerospace Corp.  
Attn: Mr. J. Mosich  
2350 E. El Segundo Blvd  
El Segundo, CA 90245

1

Aerospace Corp/Bldg 125/1054  
Attn: Mr. Steve Burrin  
Advanced Systems Tech Div.  
2400 E El Segundo Blvd  
El Segundo, CA 90245

1

SD/SD/YLVS  
Attn: Mr. Lawrence Weeks  
P.O. Box 92960  
Worldway Postal Center  
Los Angeles CA 90009

1

SD/YCD  
Attn: YCPT/Capt Gajewski  
P.O. Box 92960  
Worldway Postal Center  
Los Angeles, CA 90009

1

Grumman Aerospace Corp  
Attn: Dr. A. Mendelson  
South Oyster Bay Road  
Bethpage, NY 11714

1

OUSDR&E/DS  
Attn. Mr. A. Bertapelli  
Room 3D136  
Pentagon, Washington, DC 20301

1

Jet Propulsion Laboratory  
Dr. S. Szermay  
4800 Oak Grove Drive  
Pasadena, CA 91103

2

MIT/Lincoln Laboratory  
Attn: S. Wright  
P.O. Box 73  
Lexington, MA 02173

1

MIT/Lincoln Laboratory  
Attn: Dr. D. Hyland  
P.O. Box 73  
Lexington, MA 02173

1

MIT/Lincoln Laboratory  
Attn: Dr. N. Smith  
P.O. Box 73  
Lexington, MA 02173

1

Control Dynamics Co.  
Attn: Dr. Sherman Seltzer  
Suite 1414 Executive Plaza  
555 Sparkman Drive  
Huntsville, AL 35805

1

Lockheed Space Missile Corp. 5  
Attn: A. A. Woods, Jr., D/62-E6  
p.O. Box 504  
Sunnyvale, California 94088-3504

Lockheed Missiles Space Co. 1  
Attn: Mr. Paul Williamson  
3251 Hanover St.  
Palo Alto, CA 94304

General Dynamics 1  
Attn: Ray Halstenberg  
Convair Division  
5001 Kearny Villa Rd  
San Diego, CA 92123

STI 1  
Attn: Mr. R.C. Stroud  
20065 Stevens Creek Blvd.  
Cupertino, CA 95014

NASA Langley Research Ctr 2  
Attn: Dr. Earle K. Huckins III  
Dr. M. F. Card  
Langley Station, Bldg 1293B, MS 230  
Hampton, VA 23665

NASA Johnson Space Center 1  
Attn: Robert Piland  
Ms. EA  
Houston, TX 77058

McDonald Douglas Corp 1  
Attn: Mr. Read Johnson  
Douglas Missile Space Systems Div  
5301 Bolsa Ave  
Huntington Beach, CA 92607

Integrated Systems Inc. 2  
Attn: Dr. N. K. Gupta and M. G. Lyons  
151 University Avenue, Suite 400  
Palo Alto, California 94301

Boeing Aerospace Company 1  
Attn: Mr. Leo Cline  
P.O. Box 3999  
Seattle, WA 98124  
MS B W-23

TRW Defense Space Sys Group Inc. Attn: Ralph Iwens Bldg 82/2054 One Space Park Redondo Beach, CA 90278	1
TRW Attn: Mr. Len Pincus Bldg R-5, Room 2031 Redondo Beach, CA 90278	1
Department of the NAVY Attn: Dr. K. T. Alfrend Naval Research Laboratory Code 7920 Washington, DC 20375	1
Airesearch Manuf. Co. of Calif. Attn: Mr. Oscar Buchmann 2525 West 190th St. Torrance, CA 90509	1
Analytic Decisions, Inc. Attn: Mr. Gary Glaser 1401 Wilson Blv. Arlington, VA 22209	1
Ford Aerospace & Communications Corp. Drs. I. P. Leliakov and P. Barba, MS/C80 3939 Fabian way Palo Alto, California 94304	1
Center for Analysis Mr. James Justice 13 Corporate Plaza Newport Beach, CA 92660	1
W. J. Schafer Associates Dr. R. Kappesser Suite 800 1901 Fort Meyer Drive Arlington, VA 22209	1
General Research Corp Attn: Mr. Thomas Zakrzewski 7655 Old Springhouse Road McLean, VA 22101	1

Air Force Weapons Laboratory Attn: Lt Col D. Washburn ARAA Kirtland AFB, NM 87117	2
Karman Sciences Corp. Attn: Dr. Walter E. Ware 1500 Garden of the Gods Road P.O. Box 7463 Colorado Springs, CO 80933	1
MRJ, Inc. 10400 Eaton Place Suite 300 Fairfax, VA 22030	1
Photon Research Associates Attn: mr. Jim Myer P.O. Box 1318 La Jolla, CA 92038	1
Rockwell International Attn: Russell Loftman (Space Systems Group) (Mail Code - SL56) 12214 Lakewood Blvd. Downey, CA 90241	1
Science Applications, Inc. Attn: Mr. Richard Ryan 3 Preston Court Bedford, MA 01730	1
U.S. Army Missile Command Attn: DRSMI-RAS/Mr. Fred Haak Redstone Arsenal, AL	1
Naval Electronic Systems Command Attn: Mr. Charles Good PME_106-4 National Center I Washington, DC 20360	1
Lockheed Palo Alto Research Laboratory Attn: Dr. J. N. Aubrun, 0/52-56 3251 Hanover Street Palo Alto, California 94304-1187	2

U. S. Army/DARCOM  
Attn: Mr. Bernie Chasnov  
AMC Bldg  
5001 Eisenhower Ave  
Alexandria, VA 22333

1

Defense Documentation Center  
Cameron Station  
Alexandria, VA 22314

1

Honeywell Inc.  
Attn: Dr. Thomas B. Cunningham  
Attn: Dr. Michael F. Barrett  
2600 Ridgway Parkway MN 17-2375  
Minneapolis, MN 55413

2

NASA Marshall Space Flight Center  
Attn: Dr. J. C. Blair, ED01  
Henry B. Waites  
Marshall Space Flight Center, AL 35812  
q

2

TRW  
Attn: Robert Benhabib  
Bldg 82/2024  
One Space Park  
Redondo Beach, CA 90278

1

NASA Langley Research Center  
Attn: Dr. L. Pinson  
MS - 230  
Hampton, VA 23665

1

H. R. Textron  
Attn: Mr. Richard Quartararo  
2485 McCabe Way  
Irvine, CA 92714

1

Naval Research Lab  
Attn: W. Bennett  
Mail Code: 7926  
Washington, DC 20375

1

TOTAL COPIES REQUIRED

101

Engineer/LCN Signature

*Richard W. Carson* 25 Feb 90



## *MISSION of Rome Air Development Center*

RADC plans and executes research, development, test and selected acquisition programs in support of Command, Control Communications and Intelligence (C<sup>3</sup>I) activities. Technical and engineering support within areas of technical competence is provided to ESD Program Offices (POs) and other ESD elements. The principal technical mission areas are communications, electromagnetic guidance and control, surveillance of ground and aerospace objects, intelligence data collection and handling, information system technology, ionospheric propagation, solid state sciences, microwave physics and electronic reliability, maintainability and compatibility.